UNIVERSITY OF
BIRMINGHAM

THEORETICAL AND EXPERIMENTAL INVESTIGATION OF SILICA GEL / WATER ADSORPTION REFRIGERATION SYSTEMS

By

Ahmed Rezk Masoud Rezk

A thesis submitted to the
University of Birmingham
For the degree of

Doctor of Philosophy

School of Mechanical Engineering
College of Engineering and Physical Science
The University of Birmingham
July - 2012

ABSTRACT

This PhD project was set out to improve the performance of silica gel / water adsorption cooling systems using a number of investigation tools. A novel global lumped analytical simulation model has been constructed for a commercialised two-bed silica gel / water 450kW adsorption chiller. The model has been constructed based on the fundamental heat and mass transfer equations. It was integrated with a genetic algorithm (GA) optimisation toolbox to determine the optimum operating conditions to obtain the optimum chiller performance. The model was used to investigate the effect of physical and operating conditions including fin configuration, cycle times and secondary fluid flow rate on the chiller performance. The model was also used to investigate the effect of various adsorbent bed enhancement techniques that are presented in published literature. A proposed technique of pasting the first layer of adsorbent granules to the adsorbent bed heat exchanger surface showed enhancements of 8.9% and 4.9% for chiller cooling capacity and COP respectively. Adding aluminium metal particles and pasting the first layer of adsorbent / metal mixture, the observed enhancement in the cooling capacity is 25% at maximum fin spacing

An experimental test facility has been designed, constructed and commissioned to study the performance of scaled down adsorbent bed modules (heat driven compressor). It has been constructed to understand the effect of the operating conditions on adsorbent-bed heat and mass transfer performance.

A dynamic vapour sorption (DVS) gravimetric analyser has been used to characterise a new species of adsorbents named metal organic frameworks (MOFs) that have extraordinary adsorption behaviour and porosity structure. These adsorbents have strong potential towards water sorption and could replace the currently applied silica gel. The analyser directly measures the adsorbent mass using sensitive microbalance as it adsorbs controlled concentrations of condensable vapours. MOFs adsorbents have been characterised in terms of adsorption isotherms and kinetics, in addition to its cyclic analysis. It was found that HKUST-1 (copper based MOF) outperforms silica gel with 95.7% increase in the water uptake. Iron based MOF (MIL-100) was found to outperform silica gel for high evaporating temperature application.

Dedicated to the soul of my beloved father,

To my beloved mother and my family

ACKNOWLEDGEMENTS

First of all, I would like to express my gratitude to Allah Almighty for giving me ideas and strengths to make my dreams true and accomplish this thesis. I ask Allah that this thesis and the published works to be a useful guides to help other researchers towards a green world that is utilised by sustainable energy systems.

I have been indebted in the preparation of this thesis to my supervisor, Dr Raya Al-Dadah, whose patience and kindness, as well as his academic experience have been invaluable to me. I would like to express my deep and sincere gratitude to Mr Whitehouse (the head of Weatherite Holdings LTD) for supporting me financially as part of cooperation scheme between University of Birmingham and Weatherite Holdings LTD during my study and allowing me doing work in the factory.

I wish to express my warm and sincere thanks to the members of the adsorption chiller group at Weathrite Holdings LTD, Bill Boxford and Paul Griffiths for giving me all the information needed about their commercial adsorption chillers. I would like to thank Mr Rowan for helping me constructing my test facility. My warm thanks are due to Dr Bridson for teaching me how to use the DVS analyzer and I extend my thanks to Dr Bowen for helping me to use the analyzer and solving all the problems I have faced in science city lab. My warm thanks to Dr Saad Mahmoud for his help. The informal support and encouragement of many friends has been indispensable.

My parents have been a constant source of support – emotional and moral – during my postgraduate years, and this thesis would certainly not have existed without them. However, when my father died my mother continued the way. My sister, brother and fiancée have been always my pillar, my joy and my guiding light, and I thank them all.

TABLE OF CONTENTS

LIST OF FIGURES

LIST OF TABLES

ABBREVIATIONS

ABS-PD	Absolute percent deviation
AC	Activated carbon
ACF	Activated carbon fibre
APD	Average percent deviation
BC	Before Christ
CCHP	Combined cooling heating power
CFC	Chlorofluorocarbon
COP	Coefficient of performance
DVS	Dynamic vapour sorption
FSR	Fin spacing ratio
GA	Genetic algorithm
GHG	Greenhouse gas
GWP	Global warming potential
HCFC	Hydrochlorofluorocarbon
HCR	Heat capacity ratio
HD	High density
HFC	Hydrofluorocarbon
LMTD	Logarithmic mean temperature difference
LPM	Litre per minute
LPS	Litre per second
LTD	Limited Company
MOF	Metal organic frameworks
NTU	Number of transfer units
ODP	Ozone depletion potential
OPTIM	Optimum

RD	Regular density
RTD	Resistance temperature detector
SCE	Specific cooling energy
SCP	Specific cooling power
SEM	Scanning electron microscope
SWS	Selective water sorption

NOMENCLATURE

Symbol	Quantity	SI Unit
ΔH_{ads}	Isosteric heat of adsorption	J/kg
A_1	Coefficient in Eq. (2)	kg/(kg K)
A_2	Coefficient in Eq. (2)	kg/(kg K^2)
A_3	Coefficient in Eq. (2)	kg/(kg K^3)
A_o	Coefficient in Eq. (2)	kg/kg
B_1	Coefficient in Eq. (3)	K^{-1}
B_2	Coefficient in Eq. (3)	K^{-2}
B_3	Coefficient in Eq. (3)	K^{-3}
B_o	Coefficient in Eq. (3)	K
COP	Coefficient of performance	(-)
Cp	Specific heat	kJ/(kg K)
$C_{s,f}$	Boiling coefficient	(-)
Ct	Tóth constant	(-)
d/dt	Change rate	1/s
D_{so}	Pre-exponential constant	m^2/s
dT/dx	Average temperature gradient	K/m
E_a	Activation energy	J/mol
F	Friction factor	(-)
G	Gravitational acceleration	m/s^2
H	Specific enthalpy	kJ/(kg K)
h′	Modified specific enthalpy	kJ/kg
htc	Heat transfer coefficient	kW/(m^2 K)
Ja	Jacob number	(-)

K	Thermal conductivity	kW/(m K)
K_o	Tóth pre-exponential constant	(-)
$K_s a_v$	Overall mass transfer coefficient	(-)
L	Length	m
LMTD	Log mean temp difference	K
M	Mass	kg
$\dot{m}$	Mass flow rate	kg/s
N	Increment number	(-)
n	Metal additive shape factor	(-)
n_b	Boiling index	(-)
N_{bed}	Number of increment	(-)
N_{cond}	Number of tube rows	(-)
Nu	Nusselt number	(-)
P	Pressure	kPa
Pr	Prandtl number	(-)
Q	Heat	kW
$\overline{R}$	Universal gas constant	J/(mol K)
R	Thermal resistance	K/kW
R_{cont}	Contact thermal resistance	K/kW
Re	Reynolds number	(-)
R_p	Particle radius	m
SCP	Specific cooling power	kW/kg
T	Temperature	K
t	Time	s
UA	Overall conductance	kW/K
Vn	Volume ratio	m^3/m^3
W	Uptake value	kg_{water}/kg_{silica}

w*	Equilibrium uptake	kg_{water}/kg_{silica}
wt%	Percentage weight ratio	%

Greek symbols

Δ	Difference	
Σ	Summation	
Φ	Flag	
δ	Flag	
ξ	Flag	
γ	Flag	
μ	Fluid viscosity	Pa s
ϱ	Density	kg/m^3
σ	Surface tension	N/m
ε	Surface roughness	m
η	Efficiency	%

Subscripts

ads	Adsorbent
bed	Bed
chw	Chilled water
cond	Condenser
cw	Cooling water
eff	Effective
evap	Evaporator
f	Fin

g	Gas
Hex	Heat exchanger
heat recovery	Heat recovery time period
hw	Hot water
i	Inside
k	Increment index
l	Liquid
lg	Liquid-gas
met	Metal
o	Outside
ref	Refrigerant
s	Surface
sat	Saturation
t	Tube
w	Water

Superscript

•	Rate
_	Average

LIST OF PUBLICATIONS

Journal Publications

[1] ARM Rezk, RK Al-Dadah, Physical and operating conditions effects on silica gel/water adsorption chiller performance, Applied Energy, 2012. 89(1): p. 142-149. (Impact Factor: 3.915)

[2] A. Rezk, R.K. Al-Dadah, S. Mahmoud and A. Elsayed, Effects of contact resistance and metal additives in finned-tube adsorbent beds on the performance of silica gel/water adsorption chiller, Applied Thermal Engineering, In press, doi:10.1016/j.applthermaleng.2012.04.08. (Impact Factor: 1.823)

[3] A. Rezk, R.K. Al-Dadah, S. Mahmoud and A. Elsayed, Experimental Investigation of Metal Organic Frameworks Characteristics for Water Adsorption Chillers, , Journal of Mechanical Engineering Science, Accepted final manuscript. (Impact Factor: 0.451)

[4] A. Rezk, R.K. Al-Dadah, S. Mahmoud and A. Elsayed, Characterisation of metal organic frameworks for adsorption cooling, International Journal of Heat and Mass Transfer, Accepted final manuscript. (Impact Factor: 2.422)

Conference Publications

[1] RK Al-Dadah, ARM Rezk. Empirical simulation model of silica gel/water adsorption chiller. ASME-ATI-UIT, Thermal and Environmental Issues in Energy Systems. 2010. Sorrento, Italy.

[2] ARM Rezk, RK Al-Dadah. Physical and operating conditions effects on silica gel/water adsorption chiller performance. Sus TEM 2010. 2010. Newcastle upon Tyne.

[3] A Rezk, R Al-Dadah, A Elsayed. Study on the finned-tube bed and metal additives of adsorbent for the performance of silica gel/water adsorption chiller. Sus TEM 2011. 2011. Newcastle upon Tyne.

[4] A Rezk, R Al-Dadah, A Elsayed. Ethanol adsorption characteristics on metal organic frameworks for cooling applications. ICAE. 2012. Suzhou, China.

[5] A Rezk, R Al-Dadah, A Elsayed. Experimental investigation of silica gel granular packed rectangular finned tube adsorbent-bed. 2012. Heat Powered Cycles, Netherlands.

CHAPTER 1: INTRODUCTION

1.1 Introduction

Refrigeration systems are required for food and vaccines transportation, comfort cooling, cold storage applications, supermarket display and retails. Industry market research for business leaders, January 2011, statistically stated that the global demand for commercial refrigeration equipment is projected to rise 5.2% per year through 2014 to $29.7 billion [1]. The global industry analysts announced that the global market of air conditioning is expected to reach 78.8 million units in volume sales by 2015 and this global demand is significant in areas of warm climate and high capita income. Currently, most of the above demand is met by mechanical vapour compression systems driven by high grade electrical power input and utilises environmentally harmful refrigerants [2-4]. Refrigeration and air conditioning systems consumes around 30% of total worldwide energy consumption [5]. Based on the new environmental regulations (Kyoto protocol, Vienna Convention and Montreal Protocol) CFCs and HCFCs phase-out have been agreed. Moreover, HFCs were one of the six addressed greenhouse gases by Kyoto protocol and countries may seek to limit its use to meet its legally binding greenhouse gas emissions targets.

1.2 Aims and objectives

The main aim of this PhD project is to investigate the various means of improving the performance of two bed silica gel / water adsorption cooling systems utilized with heat and mass recovery schemes.

To achieve the above mentioned research aim, the project objectives are set out below.

1- Review of theoretical and experimental research work on adsorption refrigeration cycles.
2- Review of various adsorbents to understand their advantages and disadvantages and the parameters that are used in evaluating of new materials.
3- Develop a global simulation model flexible in changing both of physical parameters and operating conditions, using Matlab platform.
4- Use an optimisation tool that enables selecting the optimum operating conditions corresponding to the best performance.
5- Design and construct a test facility that helps understanding the effect of changing the operating conditions on chiller performance. This test facility is flexible in term of accommodating different bed designs.
6- Select appropriate test facility in order to investigate the adsorbent materials characteristics.
7- Study the capability of new species of adsorbent materials to replace the currently used silica gel.

1.3 Thesis outline

This thesis consists of eight chapters. Chapter one introduces the research topic covered by this thesis. It includes project aims, objectives and thesis outline.

Chapter two reviews the up to date research progress on adsorption refrigeration cycle improvement techniques. It statistically presents the increasing demand for the refrigeration

systems and the ability of adsorption refrigeration system to cover this demand and cope with the recent environmental restrictions.

Chapter three presents the development of novel lumped analytical simulation model that will be used as a performance evaluation tool to study the effect of various physical and operating conditions. The validation of the model was based on experimental data for a commercialised 450 kW silica gel/water adsorption chiller. The use of global optimisation genetic algorithm (GA) tool and the optimisation control parameters will also be presented.

Chapter four presents the design of a test facility that will be used to investigate the effect of operating conditions on the performance of scaled down adsorbent bed reactor. The instruments calibration and results of uncertainty analysis will also be presented.

Chapter five presents the effect of operating conditions on overall chiller performance theoretically and experimentally. These operating conditions are cycle time, generation temperature lift and secondary fluid flow rate. The GA optimisation tool will be used to determine the optimum operating conditions in order to achieve the best chiller performance.

Chapter six presents the effect of physical conditions on chiller performance. Based on the literature review that presents various adsorbent bed improvement techniques, some technique will be evaluated. The effect of fin spacing, gluing the first adsorbent layer and using metal additives on adsorbent reactor heat and mass transfer will be investigated.

Chapter seven presents the experimentally tested adsorbent materials that could replace the applied silica gel. A new species of adsorbents named metal organic framework MOFs were

identified and tested. These new species has extremely high porosity compared to the currently used silica gel. The feasibility of applying these materials in water adsorption chillers is discussed in this chapter. The adsorption characteristics of MOFs in terms of adsorption isotherms, adsorption kinetics and adsorption cycle analysis was discussed.

The study of adsorption refrigeration cycle improvement using water as refrigerant will be concluded in chapter eight. The major findings from the study are summarized and possible future research topics are suggested.

CHAPTER 2: LITERATURE REVIEW

2.1 Introduction

Adsorption refrigeration system is an environmentally friendly alternative for the vapour compression refrigeration system and it has to be enhanced to overcome the problem of its low efficiency. This chapter presents a comprehensive review of different adsorption cooling systems and their development techniques. The adsorption refrigeration system is developed by changing the working materials, the heat exchangers design to improve its heat and mass transfer performance and / or changing the operating cycle. The parameters that affect the system performance and limit the system enhancement are investigated. Each of the above mentioned points are extensively reviewed to conclude the optimum enhancement techniques for the adsorption refrigeration systems.

2.2 Sorption refrigeration systems

There is an increasing need to evolve the refrigeration technology by looking for new alternative technologies [6]. Sorption refrigeration systems appear to be an alternative to the vapour compression refrigeration systems, named green refrigeration technology [7]. Sorption refrigeration integrated with combined heating and power plants to produce cooling, heating and power (CCHP) as a trigeneration system can be employed in many industrial and commercial applications [8-11] and sustainable building acclimatisation using solar energy as heat source [12-19]. Sorption cooling technology is a promising solution for more environmentally friendly system in terms of refrigerant used and energy demand [20-22].

2.2.1 Sorption phenomena

The sorption phenomena could be absorption or adsorption, where absorption is the incorporation of a substance in one state in another of different state by dissolution of the molecules within a phase [23]. The adsorption is a surface phenomenon based on the physical adherence of molecules onto the surface of another phase mainly by Van der Waals force [24].

2.2.2 Sorption refrigeration cycle

The sorption refrigeration cycle is a thermodynamic cycle with two sources and two sinks, which operates using three temperature levels [25]. Two of them are used to drive the thermal compressor "Reactor" that replaces the mechanical compressor in a vapour compression refrigeration cycle, Figure 2-1. The sorption refrigeration cycle operates between two pressures and two refrigerant / sorbent concentration levels as shown in Figure 2-2. The sorption systems are classified into Adsorption and Absorption system, where table 2-1 compares between them. Due to the favourable features of adsorption refrigeration system over absorption refrigeration system, it makes the former system more preferable [26].

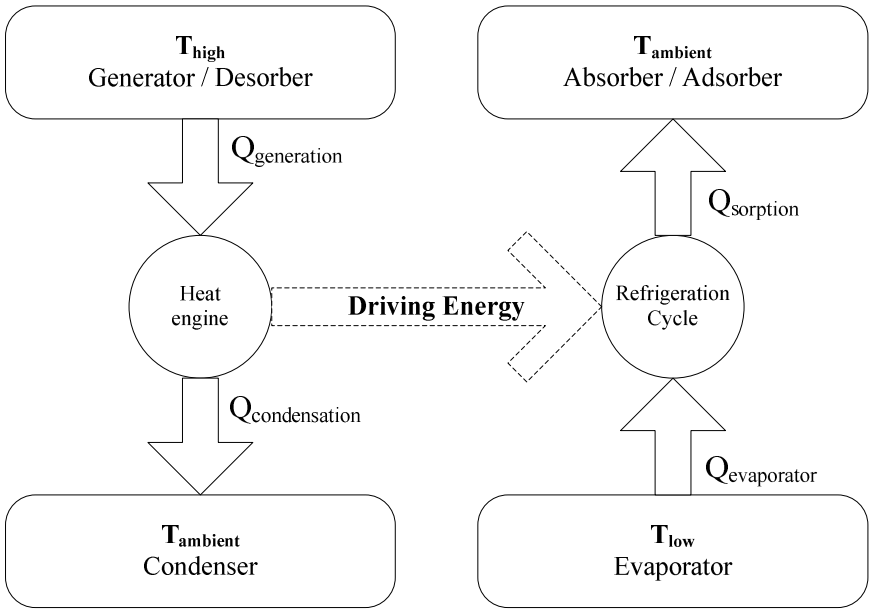

Figure 2-1, Sorption thermodynamic cycle

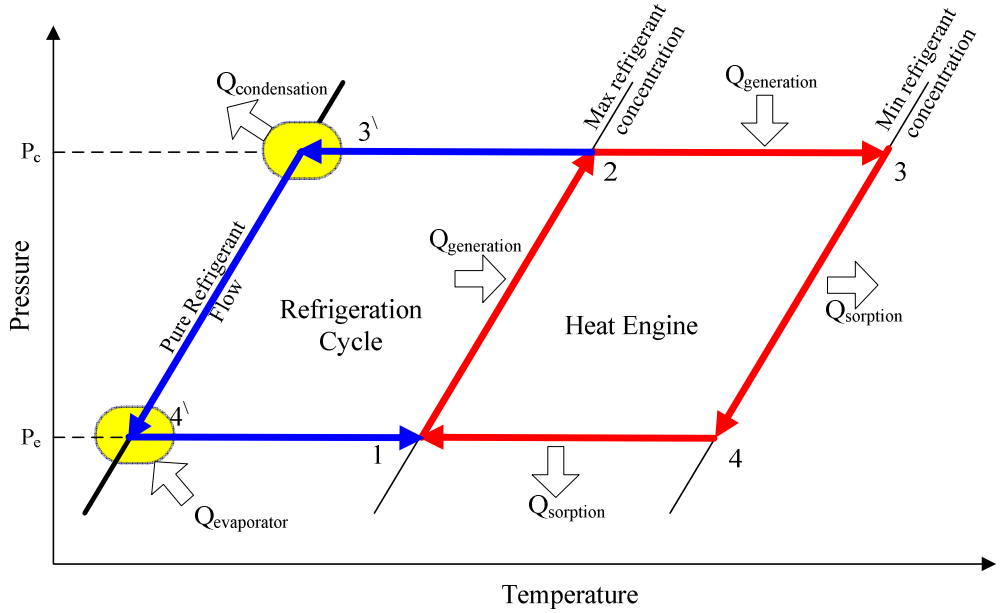

Figure 2-2, Sorption Clapeyron diagram

Table 2-1, The advantages of adsorption over absorption refrigeration systems [27, 28]

Attribute	Adsorption	Absorption
Heat source	• It is powered by sources of wide temperature range. • Temperature as low as 50˚C can be used as heat source, while heat sources with temperature close to 500˚C can be used directly without producing any kind of corrosion problem. • There is no limitation for the low temperature reservoir.	• Very sensitive against source temperature and the variation must be tightly controlled between 82˚C and 100˚C. • Heat source must be higher than 70˚C to avoid the crystallization problem, even in two-stage cycle. • Severe corrosion would start to occur for temperatures above 200˚. • Low temperature reservoir must be 18-29˚C
Operating consideration	• It is utilized by solid sorbents and hence it is suitable for conditions with serious vibration, such as in fishing boats and locomotives. • It is almost noiseless system, where there are not many moving parts. • Operation possibility over 8000hr per year.	• It is utilized by liquid sorbent and hence it is suitable for stationary units only, where unfavourable absorbent flow from the generator / absorber to the evaporator / condenser. • Daily shutdown due to the dilution of sorbent solution
Maintenance	• There are no special requirements for maintenance, where few used moving parts (vacuum pump). • Annual cleaning of condenser tubes is required. • Simple control system is required	• It needs regular monitoring and maintenance for: – Liquid analysis - pumps – Control system – Back up boiler – Air leakage – Sorbent exchange – Heat exchanger replacement due to salt corrosion.
Lifetime	• It has relatively very long lifetime and there are no special disposal requirements.	• The maximum life time is 7-9 years, due to the problem of salt corrosion.

2.3 Adsorption historical background

The adsorption phenomenon was applied at ancient times, where charcoal was the dominant adsorbent. It was used to reduce copper, zinc and tin ores for bronze manufacturing by Egyptians and Sumerians 3750BC [29]. The first quantitative observations were carried out by Scheele 1773 and Fontana 1777, where they experimentally reported some gases adsorption by charcoal and clays. Saussure 1814 reported that all gases can be taken up by porous materials (sea foam, cork, charcoal and asbestos) exothermally.

The first invention of an adsorption cooling system happened in 1848, when Faraday demonstrated an adsorption refrigeration system utilising ammonia and silver chloride as working pair. In 1929, Hulse and Miller described an adsorption system for the air conditioning of railway carriages using silica gel and sulphur dioxide as the working pair [30].

Due to the low performance of adsorption cooling systems compared to the vapour compression systems, research and development of adsorption cooling systems was slowed down. In the last three decades, the adsorption cooling systems are laboratory and commercially developed to be applied in different applications [31]. The adsorption cooling development is due to the need of replacing the conventional vapour compression systems to meet the new environmental regulations.

2.4 Environmental regulations

The environmental regulations were adopted to solve the problems of ozone depletion and global warming, which are the major problems nowadays. The thinning of ozone layer that

absorbs 98% of the sun's high frequency ultraviolet lights has been confirmed in 1980s [32]. In 1985, Vienna convention provided a framework for Montreal protocol that ratified ozone depleting substances in 1987. The original protocol has been amended several times for developed (Annex-1) and developing countries (Annex-2), between 1990 (London) - 2007 (Montreal) [33]. Conventional vapour compression refrigeration cycles are utilized ozone depleting refrigerants such as CFCs and HCFCs. The Montreal protocol ratified to stop the production of CFCs in developed countries in 1995 and planned to phase-out HCFCs completely by 2030 [34, 35], Figure 2-3.

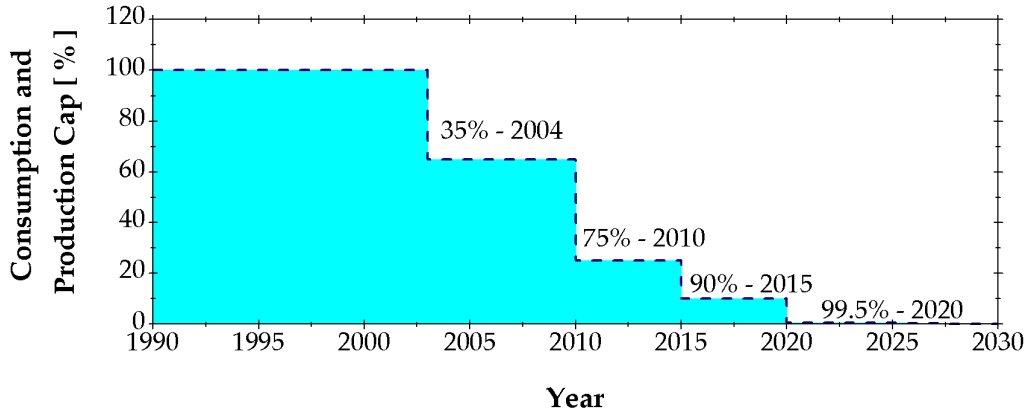

Figure 2-3, Montreal protocol HCFCs phase-out plan

The global warming is the phenomenon of increasing the Earth's average temperature due to the trapping of energy emitted from the Earth. This amount of energy is about 1/3 of the incoming solar radiation and is trapped by means of greenhouse gases (GHG). Some trapping of heat is desired, but excess trapping will affect the natural environment balance by melting polar ice caps and more evaporation of ocean water. Polar ice caps melting causes unusual floods and ocean water evaporation causes more clouds cover and hence reduces the incoming solar radiation to offset the greenhouse effect.

In 1997, the Kyoto protocol was initially adopted in Japan to stabilise greenhouse gas concentrations in the atmosphere at a level that would prevent dangerous anthropogenic interface with climate system. The protocol cue into force in 2005, and 191 states have ratified the protocol in September 2011. The protocol addressed six greenhouse gases namely; carbon dioxide (CO_2), Methane (CH_4), Nitrous oxide (N_2O), Hydrofluorocarbon (HFC), Perfluorocarbons (C_xF_y) and Sulphur hexafluoride (SF_8). It is statistically predicted that the equivalent CO_2 level will be doubled by 2050, tripled by 2100 and quadruple by 2150, even if Kyoto protocol is adopted [36].

Many vapour compression refrigeration systems utilize HFCs, but the direct effect of the released HFCs to the atmosphere is negligible. HFCs contributed about 3% during time period 2000-2100 of the total contributed by all the greenhouse gases. However, electrically driven vapour compression refrigeration systems contribute about 15% of the world man made CO_2 output, and hence contribute more significantly to carbon footprint and global warming compared with refrigerant contribution. Industrial countries that ratified Kyoto protocol have legally bound targets and timetables for mandatory cutting greenhouse gas emissions [37].

2.5 Adsorption refrigeration cycles

2.5.1 Simple two-bed adsorption refrigeration cycle

A simple two-bed adsorption refrigeration cycle of separated heat exchangers consists of four main parts namely: reactors (adsorber or desorber based on operating mode), evaporator, and condenser [38, 39]. The reactors are packed with adsorbent material which has the capability of adsorbing or desorbing the adsorbate / refrigerant during the adsorption

or desorption process. Interconnecting valves are used to control the refrigerant flow as shown in the flow diagram, Figure 2-4. Adsorption is an exothermic process, so the heat of adsorption needs to be removed by means of continuous cooling. On the other hand, during the desorption process heating is required to release the refrigerant from the adsorbent pores.

The aforementioned components are controlled to work sequentially through four modes Figure 2-2 namely; isosteric heating (preheating switching) (1-2), isobaric desorption / condensation (2-3 / 2-3`), isosteric cooling (precooling switching) (3-4) and isobaric adsorption / evaporation (4-1 / 4`-1). In the isosteric heating/cooling also named switching periods, the refrigerant amount in the reactor chambers remains constant. During the switching modes all interconnected valves are closed to keep the amount of refrigerant in the reactors constant during preheating / precooling. As a result, during the preheating mode the reactor pressure increases from the evaporation pressure to the condensation pressure and vice versa during the precooling. During the isobaric cooling, one of the reactors is connected to the evaporator to suck the refrigerant vapor from the evaporator producing the cooling effect. During the isobaric heating the other reactor is connected to the condenser to deliver the refrigerant to be condensed and then flow to the evaporator through the liquid line. Using two adsorption reactors is necessary to obtain continuous cooling by making both of them work in parallel, while one reactor is in adsorption phase, the other one will be in desorption mode. Table 2-2 and Figure 2-5 present the cyclic operating modes and valving system for a simple two-bed adsorption refrigeration cycle.

Table 2-2, Two bed cyclic operation and valving

Component / Mode	Bed-A	Bed-A	V1	V2	V3	V4
Mode-A Switching	Heating	Cooling	X	X	X	X
Mode-B Ads/Des	Heating	Cooling	O	X	O	X
Mode-C Switching	Cooling	Heating	X	X	X	X
Mode-D Ads/Des	Cooling	Heating	X	O	X	O

X = closed, O = Open

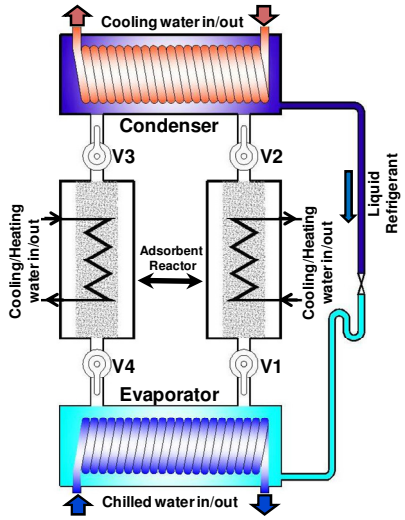

Figure 2-4, Flow diagram of simple two-bed adsorption refrigeration cycle

During the switching mode heat and/or mass recovery can be used [40-42]. During mass recovery, the adsorber and desorber are connected to speed up the pressure reduction of the hot bed and pressure increase of the cold bed and hence the mechanical equilibrium by means of pressure swing [43]. During the heat recovery period, the cooling water flows through the hot bed and then to the cold bed, which reduces the heat required for regenerating the refrigerant and hence improve the cycle performance [44, 45]. Based on the review of literature the COP of two-bed adsorption refrigeration cycle of different operating schemes is usually between 0.60-0.70.

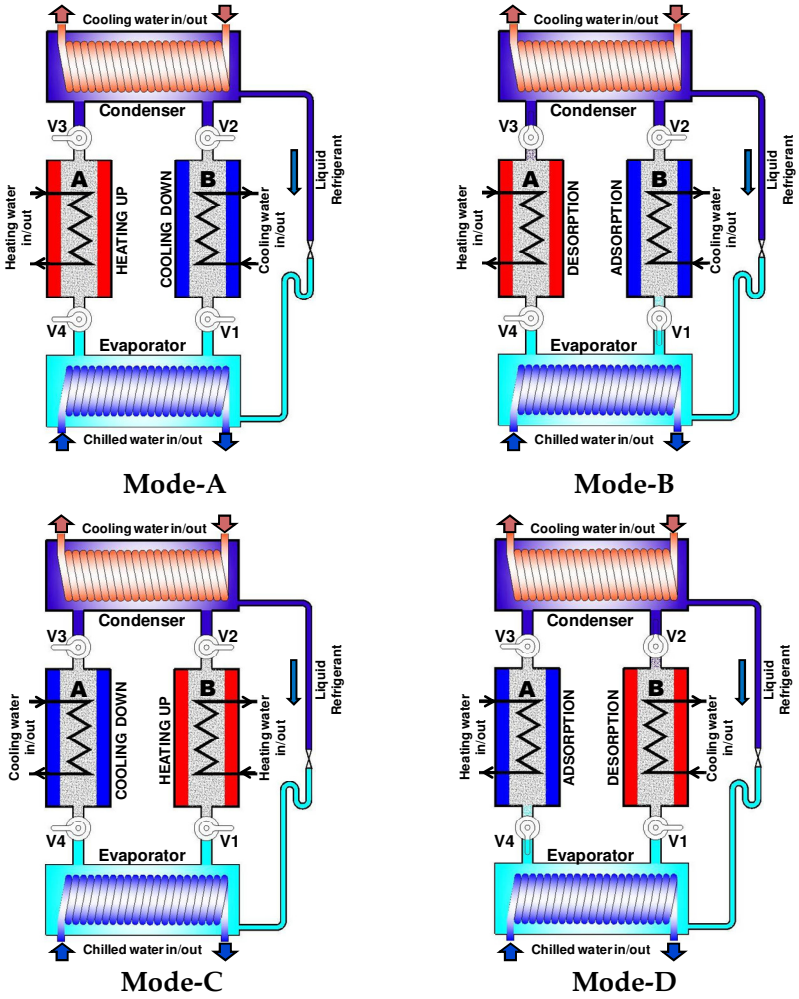

Figure 2-5, Two bed adsorption cycle operating modes

2.5.2 Integrated adsorption refrigeration cycle

The integrated adsorption refrigeration cycle consists of two units where each one consists of adsorbent bed, condenser and evaporator [46], Figure 2-6. The major difference between this cycle and the simple two-bed adsorption refrigeration cycle is the absence of switching mode, which makes it more reliable [47]. The cycle operation is based on two modes; adsorption / evaporation and desorption / condensation where each unit alternatively works in different modes. There is a group of control valves used to control the flow of secondary fluid to each unit.

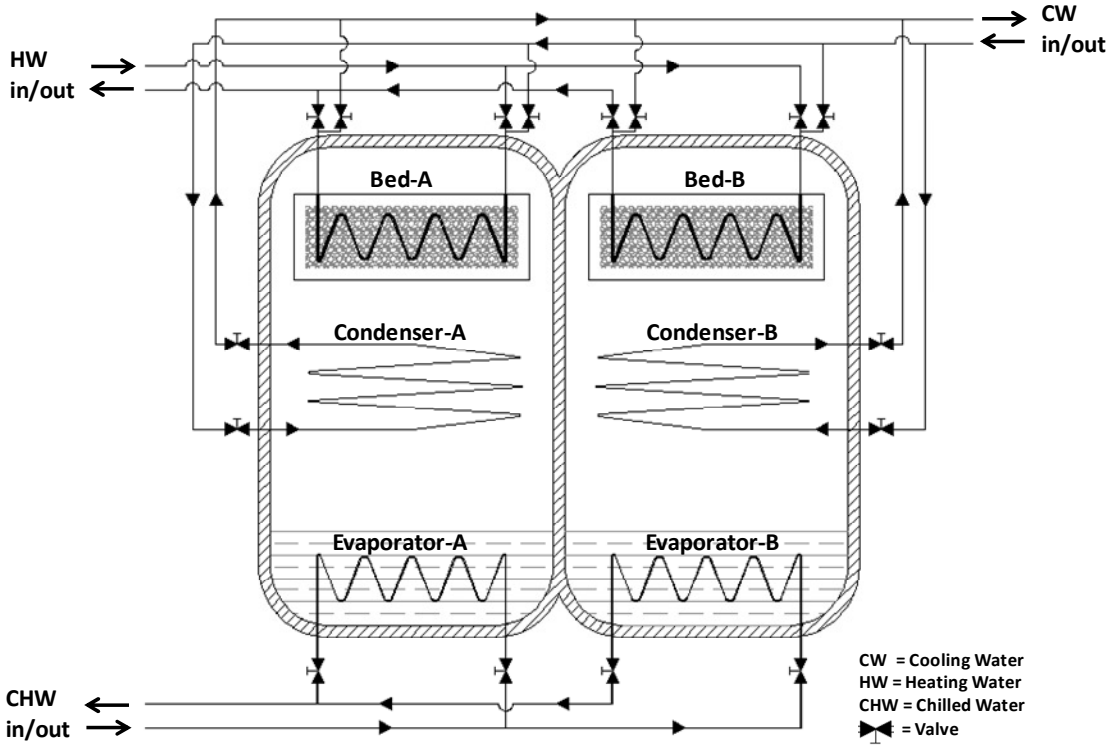

Figure 2-6, Schematic diagram of integrated adsorption refrigeration cycle

This cycle in Figure 2-7 was modified to reduce the number of heat exchangers, where each unit consists of one adsorbent bed and one coil that is working as condenser or evaporator depending on the operating mode [48]. The integrated cycle was also enhanced by combining it with a third chamber of a different refrigerant which acts as a heat pipe [49-52], as shown in Figure 2-8. The integrated adsorption cycle can also be enhanced by including heat and mass recovery methods. Based on the review of literature the reported COP of the integrated adsorption refrigeration cycle using different operating schemes is 0.15-0.49 (average 0.32) and by applying the heat pipe its value is 0.32-0.45 (average 0.39).

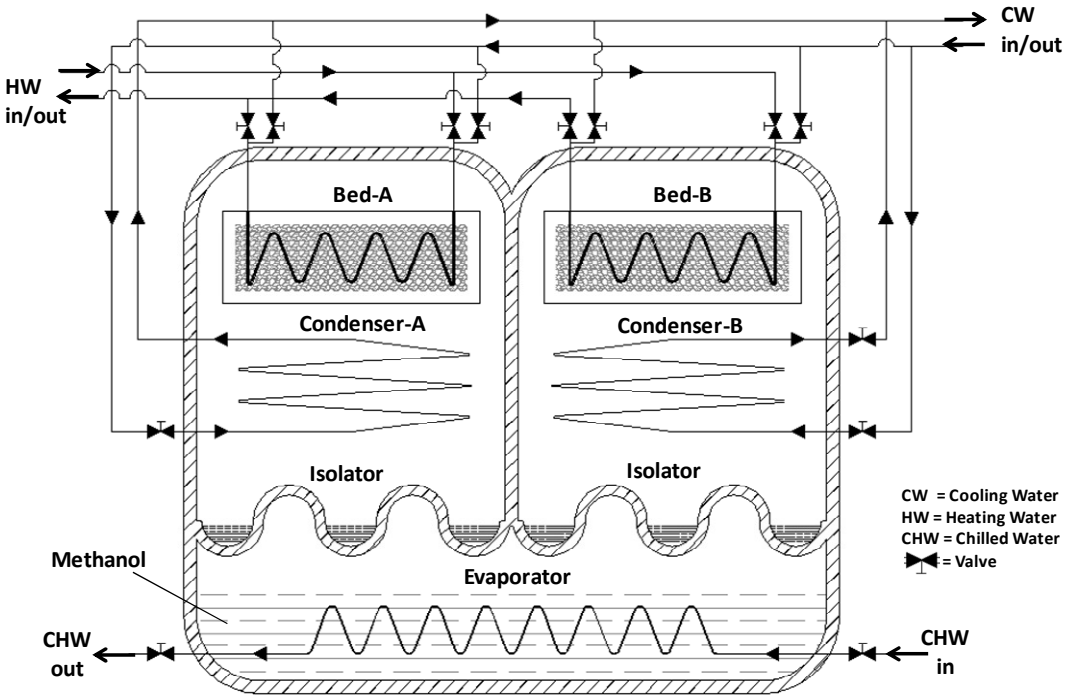

Figure 2-7, Schematic diagram for the integrated adsorption refrigeration cycle combined with heat pipe

2.5.3 Three bed adsorption heat cycle

A three-bed adsorption refrigeration cycle consists of three adsorbent beds (reactors) in addition to condenser and evaporator. The aim of using three-bed is to obtain continuous evaporation and hence continuous cooling. A three-bed adsorption cycle is controlled by four operating modes (preheating, desorption, precooling and adsorption) and 12 operating steps [53]. During the preheating and precooling mode, the interconnecting valves between the adsorbent bed and the evaporator / condenser are shut to change the reactor pressure level. During adsorption mode, a cooling water stream flows through the adsorbent bed, while the interconnecting valve between the bed and the evaporator is opened. The interconnecting valve between the bed and condenser is closed to avoid a reverse flow. During the desorption mode, the interconnecting valve between the adsorbent bed and the

condenser is opened to condense the desorbed refrigerant water then flows through the liquid line to the evaporator. Table 2-3 presents the operating modes and steps of the three-bed adsorption refrigeration cycle. Mass recovery scheme can be applied in three-bed adsorption refrigeration cycle [54]. Based on the review of literature the reported COP of the integrated adsorption refrigeration cycle using different operating schemes is 0.20-0.80.

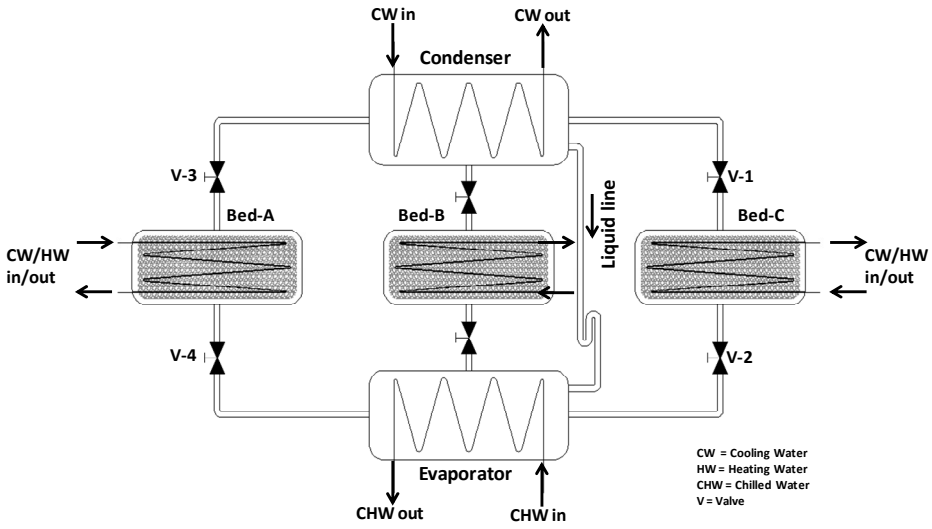

Figure 2-8, Schematic diagram for three-bed adsorption cycle

Table 2-3, Operating modes and steps of three-bed adsorption cycle

Component / Steps	Bed-A	Bed-B	Bed-C
Step-1	Desorption	Adsorption	Desorption
Step-2	Desorption	Adsorption	Precooling
Step-3	Desorption	Adsorption	Adsorption
Step-4	Desorption	Preheating	Adsorption
Step-5	Desorption	Desorption	Adsorption
Step-6	Precooling	Desorption	Adsorption
Step-7	Adsorption	Desorption	Adsorption
Step-8	Adsorption	Desorption	Preheating
Step-9	Adsorption	Desorption	Desorption
Step-10	Adsorption	Precooling	Desorption
Step-11	Adsorption	Adsorption	Desorption
Step-12	Preheating	Adsorption	Desorption

2.5.4 Three bed with dual evaporator adsorption refrigeration cycle

This adsorption refrigeration cycle was designed to achieve adsorption equilibrium uptake difference. This means more refrigerant flow rate and hence more cooling capacity [55]. This cycle consists of three adsorbent-bed reactors in addition to two evaporator heat exchangers, Figure 2-9. One of the evaporators is working at low evaporative temperature, while the other one is working at high evaporative temperature. There are five operating modes controlled by five steps and these operating modes are namely; low pressure adsorption, high pressure adsorption, desorption, preheating and precooling. Table 2-4 presents the operating modes and steps of a three-bed dual evaporator adsorption refrigeration cycle. During low pressure adsorption, the adsorbent-bed reactors are connected to the low pressure evaporator via the interconnecting valves. During high pressure adsorption, the adsorbent-bed reactor is connected to the high pressure evaporator using the interconnecting valves. During preheating and precooling, the interconnecting valves are completely closed to change the adsorbent-bed reactor pressure level. Based on the review of literature the reported COP of the integrated adsorption refrigeration cycle using different operating schemes is 0.3-0.7.

Table 2-4, Operating modes and valving system of three-bed dual evaporator adsorption refrigeration cycle

Component / Step	Bed-A	Bed-B	Bed-C
Step-1	Desorption	HP Adsorption	LP Adsorption
Step-2	Precooling	Preheating	LP Adsorption
Step-3	LP Adsorption	Desorption	HP Adsorption
Step-4	LP Adsorption	Precooling	Preheating
Step-5	HP Adsorption	LP Adsorption	Desorption
Step-6	Preheating	LP Adsorption	Precooling

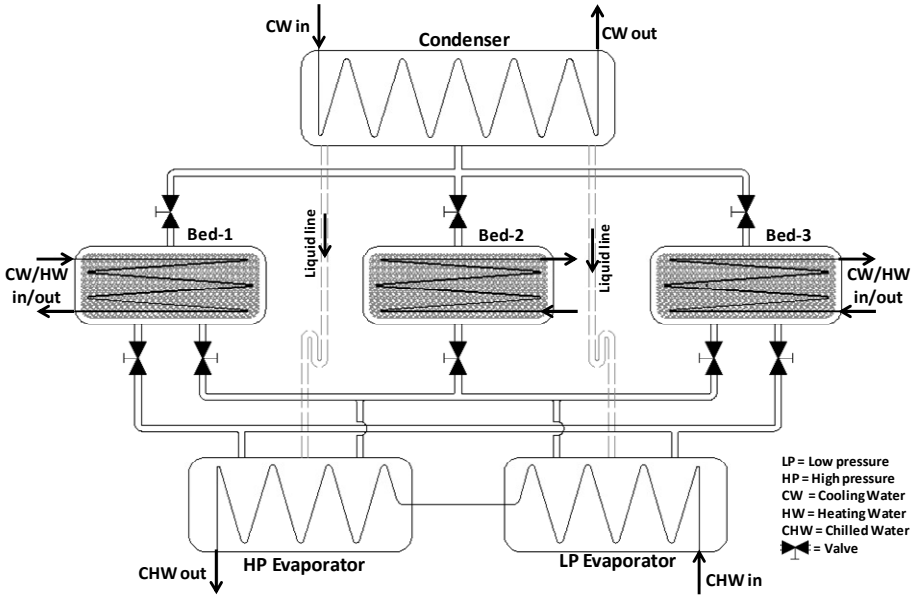

Figure 2-9, schematic diagram for three-bed dual evaporator adsorption refrigeration cycle

2.5.5 Multi-stages adsorption refrigeration cycle

A multistage adsorption refrigeration cycle is used to utilize low temperature generation temperature sources 45-60°C, a heat sink temperature of 30°C and an evaporative temperature of 7°C [56, 57]. These operating temperatures are not suitable for a simple two-bed adsorption refrigeration cycle operation [58]. In this cycle the pressure increases from evaporation pressure to condensation pressure through three progressive steps using the same adsorption / desorption temperatures. Figure 2-10 is a schematic diagram for a three-stage adsorption refrigeration cycle. In this cycle three adsorbent-bed reactors are heated in parallel with the cooling the other beds. Preheating and precooling are needed prior desorption and adsorption modes in order to change the pressure level.

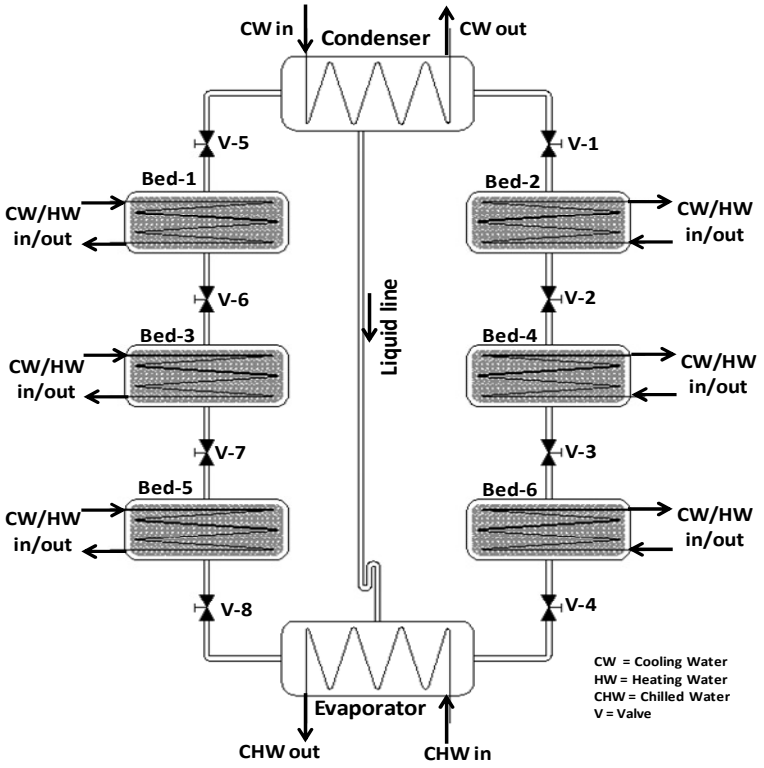

Figure 2-10, Schematic diagram of three-stage adsorption refrigeration cycle

Table 5-2 presents the operating modes of the three stage adsorption cycle. A modified three stages regenerative adsorption refrigeration cycle was investigated by Saha [26]. Based on the review of literature the reported COP of the integrated adsorption refrigeration cycle using different operating schemes is 0.08-0.25.

Table 2-5, Cyclic operation and valving of three stages adsorption refrigeration cycle

Component / Steps	Mode-A	Mode-B	Mode-C	Mode-D
Bad-1	Precooling	Adsorption	Preheating	Desorption
Bed-2	Preheating	Desorption	Precooling	Adsorption
Bed-3	Preheating	Desorption	Precooling	Adsorption
Bed-4	Precooling	Adsorption	Preheating	Desorption
Bed-5	Precooling	Adsorption	Preheating	Desorption
Bed-6	Preheating	Desorption	Precooling	Adsorption
V-1	X	O	X	X
V-2	X	X	X	O
V-3	X	O	X	X
V-4	X	X	X	O
V-5	X	X	X	O
V-6	X	O	X	X
V-7	X	X	X	O
V-8	X	O	X	X

Every cycle has some features that make it more compatible with applied resources. Table 2-5 presents the main features of the reviewed cycle and the reported COP using different operating schemes.

Table 2-6, The features of different adsorption refrigeration cycles

Cycle name	Main features
Simple two-bed cycle	• Simple and commonly commercially applied • COP=0.60-0.70
Integrated cycle	• Simple design • Compact • Reliable • COP=0.15-0.49
Three-bed cycle	• More continuity in cooling compared by two-bed • COP=0.08-0.25
Three-bed with dual evaporator	• Brings more cooling with the same operating temperature • COP=0.3-0.7
Multi-stages cycle	• Utilise low driving heat sources • COP=0.08-0.25

2.6 Adsorbents

The adsorbents are classified based on the adsorption process as: physical adsorbents, chemical adsorbents and composite adsorbents. This section presents in details the characteristics of each type of these adsorbents.

2.6.1 Physical adsorbents

Physical adsorbents are usually porous materials with different pore sizes, Figure 2-11. It adsorbs the adsorbate (refrigerant) by an intermolecular force called (Van der Waals force). The physical adsorbent can retain its original properties after removing the refrigerant by adding heat during the desorption process as explained previously. This advantage lets the physical adsorbent be commonly used in practical application. The performance of adsorption refrigeration cycle increases when the amount of cycled refrigerant increases [59]. Most of the physical adsorbents suffer from low adsorption kinetics and hence low cyclic refrigerant flow rate. The main physical adsorbent classes are mesoporous silicates, zeolites, metalaluminophosphates, porous carbons and metal organic frameworks [60].

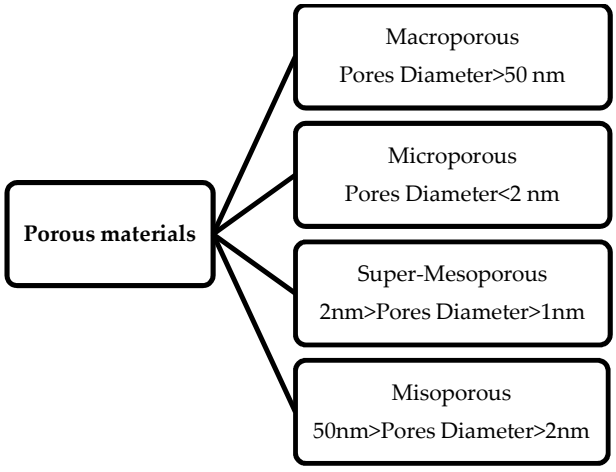

Figure 2-11, Porous materials classification

2.6.1.1 **Porous carbons**

Activated carbon (AC) is a joint name of porous carbons with high degree of porosity (500-1500 m^2/g). It is obtained by gasifying the char using an oxidizing agent and the raw material of wood, peat, coal, fossil oil, char, bone, coconut shell or nut stone. It is usually applied in gas separation and liquid purification, and the potential of using it in adsorption refrigeration systems is promising too [61, 62]. The adsorption heat of the activated carbon pairs is relatively low among the other types of physical adsorbent pairs (1800-2000 kJ/kg_{ads}). Its adsorption capacity is low (0.3-0.4 kg_{ref}/kg_{ads}) and has a weak polarity because the whole surface of activated carbon is also covered by an oxide matrix and some inorganic materials [59]. There are many types of activated carbon, where Critoph et al studied the adsorption performance of 26 types of activated carbon with ammonia [63].

Activated carbon fibre (ACF) is a fibre form of activated carbon that has many advantages over activated carbon in terms of mass and heat transfer performance. Compared to activated carbon, ACF has a larger surface area and its pores are more uniform. The disadvantages of the activated carbon fibre are anisotropic thermal conductivity and high thermal resistance between the fibres and adsorbent-bed heat exchanger surface compared to activated carbon.

2.6.1.2 **Mesoporous silicates**

The most commonly used mesoporous silicates are the synthetic amorphous silica gel which consists of rigid and continuous net of colloidal silica connected to very small grains of hydrated SiO_4. It retains chemically bonded traces of water (about 5%) and loses its adsorbitivity by overheating (above 120°C) due to loss of this bond [61]. Silica gel porosity

level is lower than activated carbon (100-1000 m^2/g), but the adsorption heat is higher (2500-2800kJ/kg) [64]. Based on pore dimension there are two types of silica gel named; regular density (silica gel RD) of 2 nm pore diameter and low density (silica gel LD) 15-20 nm pore diameter. Silica gel has large adsorption ability and can be regenerated using low temperature sources (50-100°C), despite its low porosity level.

There are two types of porous materials in the same family of silica gel named; super-microporous silica and silica aerogel [65]. Super-microporous or high density (HD) silica gel is a porous material of pore size 1-2nm [66, 67]. It steeply adsorbs water vapour at pressure ratio lower than 0.3 with negligible hysteresis, where it can be driven using lower generation temperature. Its maximum equilibrium uptake is 2.75 time of silica gel RD [68].

Silica aerogel is an exceptionally porous material with high porosity (1000 m^2/g), low density (0.003-0.35 g/cm^3) and low thermal conductivity (0.014 W/mK). It is derived from a gel in which a liquid component of the gel has been replaced with a gas. Silica aerogel is unstable for long time application due to their fragility.

2.6.1.3 **Zeolites**

Zeolites are a crystalline microporous alumina silicate minerals and well known physical adsorbents. There are more than 180 types of zeolite frameworks and most of them adsorb water vapour with different capacity [69]. Zeolites hydrophilicity is related to the silicon / aluminium ratio, where the lower this ratio is the higher hydrophilicity is the zeolite. It adsorbs most of water vapor at low partial pressure. Zeolites have heat of adsorption of 3300-4200kJ/kg, the regeneration temperature of 250-300˚C and can withstand high temperature treatment (up to 800˚C). Based on the aforementioned characteristics, zeolite is

only applicable for systems where high generation temperature sources are available, but cannot be applied in low generation temperature applications.

2.6.1.4 **Metalaluminophosphates**

Examples of metalaluminophosphates are Silica-aluminophosphates (SAPOs) and aluminophosphates (AlPOs) have a pore system with three-dimensional networks similar to zeolites. These adsorbents have good water vapour adsorption and perform better than silica gel and zeolite [70]. Many of the aluminophosphates exhibit good thermal stability against high temperature treatment as they undergo up to 400-600°C during synthesis. These attractive features invited researchers to study the ability to be applied in adsorption refrigeration application, Henninger et al [71].

2.6.1.5 **Metal organic framework**

Metal organic frameworks (MOFs) are new micro-porous materials with exceptional high porosity, uniform pore size, well-defined molecular adsorption sites and large surface area (up to 5500m^2/g) [72, 73]. MOFs have two main components: the organic linkers considered as organic secondary building unit, act as struts that bridge metal centres known as inorganic primary building units and act as joints in the resulting MOF architecture. The two main components are connected to each other by coordination bonds, together with other intermolecular interactions, form a network with defined topology [74, 75]. MOFs are less hydrophilic than silica gel or zeolite and thus can release more water vapour at the same partial pressure [76]. The capability of using MOFs in adsorption refrigeration systems will be discussed in this thesis (chapter 7), where the adsorption characteristics of MOFs are studied.

2.6.2 Chemical adsorbents

Chemical adsorbent sorbs the adsorbate (refrigerant) chemically by Valence force, where one layer of refrigerant reacts with the surface molecules of the adsorbent. Chemical adsorbent sorbs more adsorbate at higher rate compared to physical adsorbent [77]. Its stability is lower than a physical adsorbent, where chemical pair molecules never keep their original state which limits its practical applications. Chemical adsorbents suffer from swelling and agglomeration which negatively affect the heat and mass transfer performance, especially in cycles that operate under low pressure [78]. Chemical adsorbents mainly include metal chlorides, metal hydrides and metal oxides.

2.6.2.1 **Metal chlorides**

Metal chlorides that are applied for adsorption refrigeration are calcium chloride, strontium chloride, barium chloride and magnesium chloride [79]. Metal chlorides have high adsorption capacity (up to 1 kg_{ref}/kg_{ads}), but swelling and agglomeration are the main problems of metal chlorides. Calcium chloride has a good potential for use as solid chemical adsorbent for methanol and ethanol vapours, however ammonia is the usual refrigerant used with metal chlorides [61].

2.6.2.2 **Salt and metal hydrides**

Salt and metal hydrides used in adsorption refrigeration systems are lithium hydrides, calcium hydrides, covalent high polymerized hydrides and non-metal molecular hydrides. Salt and metal hydrides perform promisingly with hydrogen refrigerant. The cycle based on this pair is sensitive to the driving temperature where the COP changed from 0.2 to 0.45 with increasing the heat source temperature from 120 to 160˚C [61].

2.6.2.3 **Metal oxides**

The metal oxides are usually employed as catalyst for oxidation and deoxidation reactions. Oxygen is the suitable refrigerant when the metal oxides are used as adsorbents. Metal oxides / oxygen pair is suitable for heat pumps with temperature below 120K because of the large enthalpy of reaction between oxides and oxygen [61]. Similar to most chemical adsorbents, metal oxides suffer from the swelling and agglomeration problems.

2.6.3 Chemical / Physical adsorbent composites

Adsorption and desorption are respectively exothermic and endothermic processes and the chemi-sorption heat is higher than the physi-sorption heat. Higher adsorption rate (kinetics) means more refrigerant flow rate and hence better cooling capacity. A chemical adsorbent using salt of poor heat and mass transfer due to low thermal conductivity and with agglomeration phenomenon is not practical especially in low pressure systems [78]. The aim of using composite adsorbents is to enhance the performance of physical adsorbents (increase the adsorption capacity) and avoid the aforementioned drawbacks of the chemical adsorbents (swelling, agglomeration and poor conductivity) [61]. Examples of composite adsorbents, the combination between metal chloride and activated carbon fibres, expanded graphite, silica gel or zeolite.

2.6.3.1 **Hygroscopic salts/silica gel composites**

Adding hygroscopic salts (LiCl, LiBr, $MgCl_2$, etc) to silica gel increases its water vapour adsorbitivity and avoids the problem of poor mass transfer due to swelling and agglomeration [80-82]. The adsorption characteristics of the silica gel composite adsorbents (selective water sorbents SWS) can be modified by changing the salt type and changing the

percentage of salt in silica gel [83-86]. Higher salt amount increases the agglomeration possibility and decreases composite porosity; however it enhances the heat transfer in the bed and the adsorption capacity [87-89]. Using calcium chloride as a hygroscopic salt approximately doubles silica gel adsorption capacity and hence the adsorption refrigeration cycle [90-93].

2.6.3.2 **Chlorides / porous media composite adsorbents**

Adding chloride salts to expandable graphite, activated carbon, activated carbon fibre, zeolite and vermiculite is used to enhance these materials adsorbitivity. Chloride salts / expandable graphite composite showed enhanced heat and mass transfer performance without expansion during adsorption [94]. Impregnating activated carbon and activated carbon fibres with chloride salts enhanced the adsorption capacity (up to 95 kg_{ref}/kg_{ads}), but activated carbon performs better than activated carbon fibres in term of not separating from the salt [95]. The above mentioned composites utilized ammonia refrigerant. However, impregnation of zeolite with chloride salt showed unexpected low performance of water vapour adsorption [96].

2.7 Refrigerants

There are many refrigerants utilized in adsorption refrigeration systems, but the appropriate refrigerant need to be selected based on a number of considerations such as;

- **Latent heat of vaporization**: where the higher the refrigerant latent heats of vaporization, the better the performance of the cycle.

- **Thermal stability**: stable refrigerant thermophysical properties mean stable cycle over the operating temperature range.
- **Environmental friendly**: most of adsorption refrigeration cycles utilize environmentally friendly refrigerants with no ozone depletion and low global warming potential. Natural refrigerants such as water, ammonia are most commonly used ones.
- **Flammability**: some of the refrigerants utilized in adsorption refrigeration systems are flammable within certain concentration. The flammability issue should be taken into account especially when high generation temperature is used in the cycle.
- **Toxicity**: some of the refrigerants applied in adsorption refrigeration cycle are toxic and hence stringent safety measures should be implemented which may limit their application.
- **Explosion**: hydrogen refrigerant utilized with salts hydrides, it is an explosive one. This means more consideration and initial cost during manufacturing of such type of cycle.
- **Compatibility**: some refrigerants are corrosive and need special material of relatively high cost. Thus the machines cost increases limiting its market potential.

The optimum refrigerant is the one that satisfies the maximum number of consideration with high grade. The commonly applied refrigerants in adsorption cycles are water, ammonia, methanol and ethanol. Some other refrigerants are used in the adsorption technology, but

not commercially applied such as hydrogen, oxygen, methyl alcohol, R134a, R22, R732 and R407.

2.8 Adsorption pairs

Evaluating adsorbent or adsorbate (refrigerant) independently is not sufficient, where adsorption characteristics vary based on adsorption pairs. Table 2-7 presents the characteristics of the most commonly used adsorption pairs based on the practical cyclic operating conditions [97-104].

The best adsorption pair is the one that satisfies the important requirements which differs depending on the application. Herein, a comparison has been made for the commonly used and applied adsorption pairs based on 16 criteria, Table 2-8. For each criterion the best adsorption pair is marked by 5 and the worst is marked by 1. The same weight is used for each criterion due to their equal importance. For example, complex manufacturing techniques influence the capital cost and hence the commercialization of the system. On the other hand, the temperature and quantity of energy required for adsorption influences the energy savings and the range of industries that can benefit from such systems. Therefore they should be equally weighted.

Table 2-7, Characteristics of commonly used adsorption pairs

Refrigerant / Characteristic		AC, ACF/ Ammonia	AC, ACF/ Methanol	AC, ACF/ Ethanol	AC, ACF/ 134a	Silica gel/ water	zeolite/ water
Operating pressure		+ve	Vacuum	Vacuum	+ve	Vacuum	Vacuum
Generating temperature ˚C		80-200	80-100	80-120	80-100	50-100	250-300
Adsorption capacity kg_{ref}/kg_{ads}		0.29	0.45	0.19	0.36	0.30	0.17
Refrigerant boiling point ˚C		-34	65	79	-48	100	100
Refrigerant latent heat of vaporization kJ/kg		1368	1102	842	217	2258	2258
Adsorption heat kJ/kg		1800-2000	1800-2000	1200-1400	1830-2300	2500-2800	3200-4200
Cooling density	Cooling power	2000 W/kg	140-500 W/kg	--	--	190 W/kg	90-150 W/kg
	Cooling effect	--	--	118-159 kJ/kg	57 kJ/kg	--	--

Table 2-8, evaluation of commonly used adsorption pairs

Criteria	AC, ACF/ Ammonia	AC, ACF/ Methanol	AC, ACF/ Ethanol	AC, ACF/ R134a	Silica-gel/ Water	Zeolites/ Water
Adsorption rate	2.7	5	3.3	3.7	2.9	1
Adsorption heat	4	4	5	3.8	2.8	1
Desorption temperature	2.4	4	4	4.4	5	1
Maximum recovered temp	5	1	2.4	4.7	3.2	3.2
Vaporization Latent heat	3.3	2.7	2.2	1	5	5
Manufacturing complexes	5	2.9	1.6	4.8	1	1
Thermal stability	5	1	5	5	5	5
ODP	5	5	5	5	5	5
GWP	5	5	5	1	5	5
Non-toxicity	1	4	4	5	5	5
Non-flammability	1	1	1	5	5	5
Non-explosive	2.2	1	1	1.9	5	5
Refrigerant compatibility	1	4	4	5	4	4
Refrigerant solidification	4.1	5	2.6	4.8	1	1
Average COP and SCE	1	3.9	4.4	1.2	5	5
Cost	3	3	3	3	5	4
Sum	50.7	52.5	53.5	59.3	62.7	56.2

2.9 Adsorbent bed designs and improvement techniques

The adsorbent bed replaces the mechanically driven compressor in conventional vapour compression refrigeration system (refrigeration cycle heart). Improving the adsorbent bed design positively affect the cycle overall performance. It increases the power density of the adsorption cycle to compete with the conventional vapour compression cycle. Both of heat and mass transfer are the key parameters that affect the performance of adsorbent bed

reactors. Mass transfer process influences both of adsorption capacity and adsorption rate (kinetics), that influence the refrigerant flow rate of a given cycle time and hence the cooling capacity. However, the heat transfer from / to the adsorbent is an important process for extracting / delivering both of adsorption / desorption heat, that directly influence the adsorption kinetics [105]. The adsorption kinetics significantly affect the adsorption / desorption cycle time, where a short cycle time is more preferable to obtain continuous cooling. The following section presents the parameters that affect the heat and mass transfer of the adsorbent bed.

2.9.1 The parameters that affect the adsorbent bed performance

2.9.1.1 **Adsorbent porosity**

The adsorbent porosity measures the free spaces (voids) inside the adsorbent granule and is given as the ratio between the voids volume over the total volume, Figure 2-12. The heat transfer and the refrigerant concentration are influenced with adsorbent porosity. As the adsorbent porosity increases the adsorption capacity increases and with time the adsorbent becomes saturated, hence the adsorption rate decreases with time. The cycle time should be within the time period of high adsorption kinetics, otherwise the cycle performance deteriorates. Inversely, the adsorbent thermal conductivity decreases as adsorbent porosity increases and hence the adsorption kinetics (adsorption rate) also decrease [106].

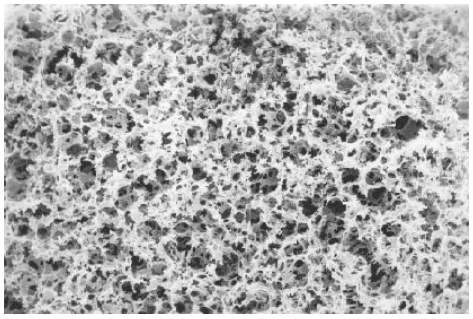

Figure 2-12, SEM for porous material shows the high porosity degree

2.9.1.2 **Pore size**

The pore size is linked to adsorbent porosity, where as the pores size reduces the adsorbent porosity increases and as a result the adsorption specific surface area of the granule increases. On the other hand, the smaller the pore diameter, the higher is the adsorption isosteric energy and subsequently the regeneration temperature increases [68]. One of selecting criteria of the suitable working pair is the compatibility between the pore size and refrigerant molecules average diameter. If the pore size is too small to accommodate the refrigerant, the adsorption kinetics will be significantly reduced.

2.9.1.3 **Granular size**

The granules size affect both of heat and mass transfer of the adsorbent bed [107]. Decreasing the adsorbent granular size reduces the contact thermal resistance between the granules and heat exchanger surface. The heat transfer continuity through the adsorbent bed of small granules size is higher than that of large granules, due to the reduction of voids between granules [105].

There are two types of mass transfer resistances in adsorbent bed the first is the mass transfer within the adsorbent granules (intra-particle) and the second is the mass transfer through the

voids between the granules (inter-particles). The intra-particle mass transfer performance of small granules is higher than that of large granules. This is because the total surface area of the bulk granules is higher for the smaller size. The adsorbent bed of large granules size (larger voids) has higher permeability level and hence better inter-particle heat transfer performance, which is more critical in cycles for low evaporative pressure (water, methanol and ethanol refrigerants) [108].

2.9.1.4 **Adsorbent / Metal mass ratio**

As the adsorbent mass increases the amount of refrigerant uptake increases, but the thermal resistance increases where porous materials have low thermal conductivity. Sometimes adsorbent bed heat exchanger design tends to have high metal mass relative to adsorbent to enhance the specific cooling power. This dramatically reduces the adsorption refrigeration cycle COP, where more heat absorbed by metal compared to that absorbed by adsorbent during regeneration period [109, 110]. An optimum mass ratio needs to be determined in order to obtain the optimum specific cooling power with maximum COP.

2.9.2 Heat transfer in the adsorbent bed

In adsorbent beds the adsorption and regeneration heat are handled by means of secondary fluid, usually water. During the heat transfer from / to the secondary fluid there are four heat transfer resistances developing the temperature gradient shown in Figure 2-13. These resistances could vary depending on the heat exchanger design, but generally named;

- Metal / secondary fluid convective heat transfer resistance - R1.
- Conductive heat transfer resistance through the wall of heat exchanger - R2.
- Metal / adsorbent interface contact heat transfer resistance - R3.

- Conductive heat transfer resistance through the adsorbent material - R4.

The convective heat transfer resistance between the secondary fluid and the heat exchanger wall is inversely proportional to the fluid velocity. The conductive heat transfer resistance is directly proportional to the thickness of the heat transfer medium and inversely proportional to the wall thermal conductivity. The conductive heat transfer resistance is very small through the heat exchanger wall but relatively high through the adsorbent medium and have a strong effect on the heat transfer performance of the adsorption cycle [111]. Metal / adsorbent interface contact heat transfer resistance usually dominates the heat transfer process and strongly depends on the nature of the physical contact between the adsorbent and the heat exchanger metal.

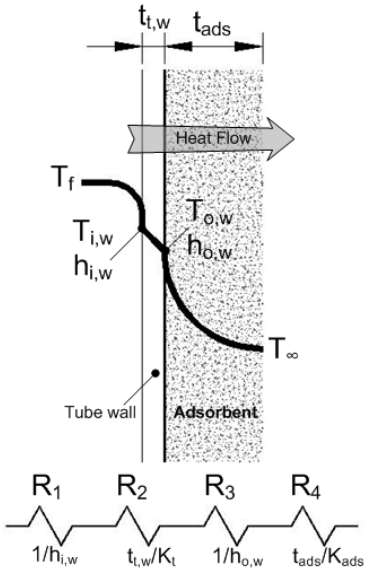

Figure 2-13, Schematic diagram of the heat transfer resistances in the adsorbent bed

2.9.3 Granular packed adsorbent bed

In most commercially available adsorption systems, the adsorbent granules are packed in circular finned or rectangular finned tube bundles. In those designs, adsorbent granules are packed between the fins to fill in the gaps. A stainless steel mesh is used to wrap the adsorbent bed to prevent granules falling as shown in Figure 2-14. A granular packed adsorbent bed has the drawbacks of poor heat transfer performance due to; high contact thermal resistance between adsorbent granules and heat exchanger metal surface [112], discontinuity of heat transfer through granules due to the voids in-between the granules [113] and poor thermal conductivity of the commonly used physical adsorbents.

A granular packed adsorbent bed has the advantage of high mass transfer performance due to the high permeability level [108]. To enhance the thermal performance of adsorbent bed reactors, the heat exchanger design need to be optimized, but that is not sufficient to obtain better thermal performance [114]. Therefore many methods were investigated to enhance the heat transfer performance of adsorbent material such as mixing adsorbent granules with metal additives to improve their thermal conductivity, coating the bed heat exchanger metal with all the adsorbent to eliminate the contact thermal resistance, covering adsorbent granules by polyaniline net, adsorbent deposition over metallic foam and using consolidated bed techniques (compressed granules and clay, using expandable graphite, moulding granules and binder addition and adsorbent granules and metal foam). The following section broadly presents these enhancement techniques.

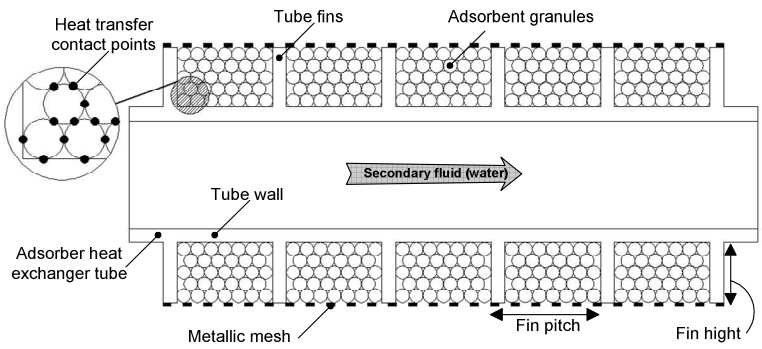

Figure 2-14, Schematic diagram for the granular packed adsorbent bed

2.9.3.1 **Covering the adsorbent particles by polyaniline net**

Covering the adsorbent granules by electrically conductive polyaniline net increases its thermal conductivity and hence the overall thermal performance of the adsorbent bed. A thin conducting net on the surface of adsorbent particles is grown by a chemical oxidative in situ polymerization of aniline onto the surface of adsorbent granules. This technique was applied using zeolite granules where the overall thermal conductivity of the adsorbent bed increased by 4.6 times compared to granular packed adsorbent bed [115]. However, adsorbent bed mass transfer performance was reduced, due to the blockage of the pores by the polyaniline net thus reduces the adsorbent bed uptake by 10%.

2.9.3.2 **Adding metallic particles to adsorbent granules**

Adding metal particles to the adsorbent bed granules increases its overall thermal conductivity and hence the heat transfer performance. This technique was experimentally applied by adding aluminium, graphite and copper particles to zeolite granules using 16 - 84 wt% [115]. This has increased the thermal conductivity of the adsorbent bed by 2.2 times. This technique is easy to apply, but it has been reported that it does not significantly improve the adsorbent bed performance [109]. However the effect of this technique on the overall

adsorption systems performance has not been investigated to prove this conclusion, so that it will be investigated in this thesis.

Covering the adsorbent granules by polyaniline net or mixing the adsorbent granules by metal particles increases the overall thermal conductivity of the adsorbent bed, but does not affect the adsorbent / heat exchanger metal contact thermal resistance. The contact thermal resistance is relatively the highest among the resistances described in section 2.10.2 and significantly affects the adsorbent bed heat transfer performance. The following enhancement techniques aim at minimizing the contact thermal resistance to improve the heat transfer performance.

2.9.4 Coating the heat exchanger by the adsorbent material

Generally, thermal contact resistance between adsorbent granules and heat exchanger metal surface contributes with averagely 25% of the overall heat transfer resistance. This contact heat transfer resistance can be eliminated using adsorbent coating technique. Firstly the heat exchanger surface is cleaned using organic agent while the adsorbent granules are mixed with suitable binder to make slurry. The mixture is then pasted over the heat exchanger surface and then thermally treated to be dried and stabilized.

The adsorbent coating technique has been investigated and its performance has been reported. The adsorbent / metal thermal contact resistance was eliminated (almost zero) and the thermal conductivity of the adsorbent bed increased averagely by 3.5 times and enhanced the overall heat transfer coefficient by 50 times. This heat transfer enhancement increased the adsorption kinetics and hence the cycle specific cooling power by more than 4 times and the cycle time was halved [116-118].

The adsorbent coated layer is within a few millimetres and does not exceed one centimetre to avoid reducing the permeability, Figure 2-15. This result in higher metal / adsorbent mass ratio compared with granular packed adsorbent beds. That increases the adsorbent bed dimensions to accommodate the same amount of adsorbent and reduces the cycle coefficient of performance due to the increase of metal heat capacity. Chang et al [119] reported the preferable thin coated layer of large particle size to compromise the contradictory effect of heat and mass transfer of the coated bed.

Figure 2-15, Zeolite coated tube

2.9.5 Consolidated adsorbent bed

Consolidated adsorbent bed reactors using (compressed granules and clay, using expandable graphite, moulding granules and binder addition and metal foam impregnated with adsorbent granules) have the advantage of high heat transfer performance. Compressed granules and clay adsorbent bed which is moulded in hollow column shape has been investigated by [115]. The bed effective thermal conductivity is 30% higher than that of the granular packed bed. The micro-porosity between particles did not contribute to the adsorption process, but the overall porosity was enough for adsorbate molecules movement.

A consolidated adsorbent bed using expandable graphite and silica gel as adsorbent has been investigated by [113]. The adsorbent bed was made through four sequential steps as; (1) heating up expandable graphite to 600°C for10 min (2) add silica gel powder to expanded graphite and water slurry of appropriate ratio (3) the mixture is moulded and dried at 80°C for one hour (4) completely remove the water in vacuum at 145°C for 2 hours. The graphite fraction and moulding pressure control the composite block thermal conductivity and permeability, where the permeability increased by increasing the graphite fraction and the decrease of the moulding pressure. The bed thermal conductivity was increased to 88 times that of granular packed bed and its cooling power was doubled [120]. Fragmentation in the consolidated block was observed during strength test.

Moulding granules with binder using activated carbon adsorbent was investigated by [121-123]. That adsorbent bed was produced based on the steps of; (1) mixing the adsorbent granules with pitch binder and water (2) compression moulding the mixture (3) heating up the adsorbent block to 120°C for three hours. The overall heat transfer coefficient of the produced consolidated adsorbent bed is about 4.5 times of the granular packed bed. The adsorption heat pump that utilized this consolidated bed has specific cooling power and COP of 1.1 and 0.9 times thus of granular packed bed respectively. The observed problems were bed permeability and cracking, but the later problem can be avoided by dividing the adsorbent block into smaller segments.

Zeolite / aluminium foam consolidated adsorbent bed performance and its influence on the adsorption cycle overall performance have been investigated and reported [124]. The thermal conductivity of the consolidated zeolite / aluminium foam adsorbent bed is about 32 times

that of the granular packed bed and the specific cooling power of the heat pump utilizing that consolidated bed was doubled. Seven steps have been used to make the zeolite / aluminium foam consolidated bed as:

- Zeolite particles are put into a mould and tightly compressed.
- Sodium chloride particles are added and shaken to be distributed into the space between the zeolite particles.
- The whole mould was put into a furnace and preheated to 400-600°C.
- Pure aluminium was melted in a furnace and superheated to 700-800°C, and then the molten aluminium is poured into the preheated mould.
- Under the gravity action of the aluminium and the piston the molten aluminium flowed through the zeolite and salt bed.
- The mould is cooled and the cast is removed from the mould to be washed by water to dissolve the salt particles.
- The consolidated bed heated to 400°C for more than 4 hours to be dried.

2.9.6 Adsorbent deposition over metallic foam

The adsorbent bed heat transfer performance using adsorbent deposition over metallic foam technique was investigated, using zeolite and copper metal foam [108, 125]. Using this technique, adsorbent / metal contact heat transfer coefficient was found to be 75 and 1.9 times to that of granular packed and consolidated adsorbent bed respectively. The thermal conductivity of the coated metal foam adsorbent bed was 300 and 90 times that of granular packed and consolidated adsorbent bed. Results showed that adsorption cooling cycles using coated foam bed specific cooling power of 12 and 2 times that when granular packed and

consolidated bed were used. However, the cycle COP was reduced to 0.6 and 0.7 that when granular packed and consolidated bed reactors were used. The adsorbent deposition over metallic foam can be produced using two mainly steps as:

- Coating the commercial copper tubes by copper foam using three basic components.
  - Epoxy risen
  - Foaming agent
  - Metal powder
- Zeolite deposition using the colloidal seeds solutions passing through four steps
  - Seeding
  - Hydrothermal synthesis
  - Washing
  - Drying

The aforementioned adsorbent bed designs improved the heat transfer performance of the adsorbent bed and hence the adsorption kinetics. The coated bed technique improves contact heat transfer between metal and adsorbent. The consolidated bed technique dramatically improves bed thermal conductivity and reduces the overall bed size. Mixing the adsorbent bed granules with metal additives is a simple practical technique that improves the bed thermal conductivity, but increases the metal mass.

All of these techniques reduce the adsorbent bed permeability which is the mostly important parameter in the adsorption process [112]. This thesis will investigate the feasibility of combining two enhancement techniques namely the addition of metal particles and the

coating of the bed metal with a thin layer of adsorbent material. This eliminates contact thermal resistance and increases thermal conductivity simultaneously without reducing the adsorbent material permeability.

2.10 Summary

Based on the above mentioned comprehensive literature survey, the following points are concluded.

- The global demand for commercial refrigeration systems is dramatically increasing, however most of the applied conventional refrigeration systems are environmentally harmful and do not meet the current environmental constrains. These contradictory requirements direct the engineering research towards new environmentally friendly solutions in terms of the utilised material and energy demand.
- Sorption refrigeration systems are good alternative for conventional systems, and adsorption systems are more preferable than absorption ones. In terms of energy demand, they are driven effectively using low grade energy, solar energy and waste heat. In terms of used material, they utilise environmentally friendly and non corrosive materials.
- There are many adsorption refrigeration cycles of different arrangements, where each one has its advantages and disadvantages. However, the two bed adsorption refrigeration cycles are the most commercially applied due to their durability and simplicity.
- The working materials (adsorbents / refrigerants) are one of the key factors of the adsorption refrigeration systems. Silica gel / water pair showed the best performance

and one of the commonly applied pairs for water chilling, which makes it the baseline for the development process.

- The parameters that affect the adsorption refrigeration systems performance are the foundation to understand the adsorbent bed (thermal driven compressor) enhancement techniques. These enhancement techniques are shown in Figure 2-16.

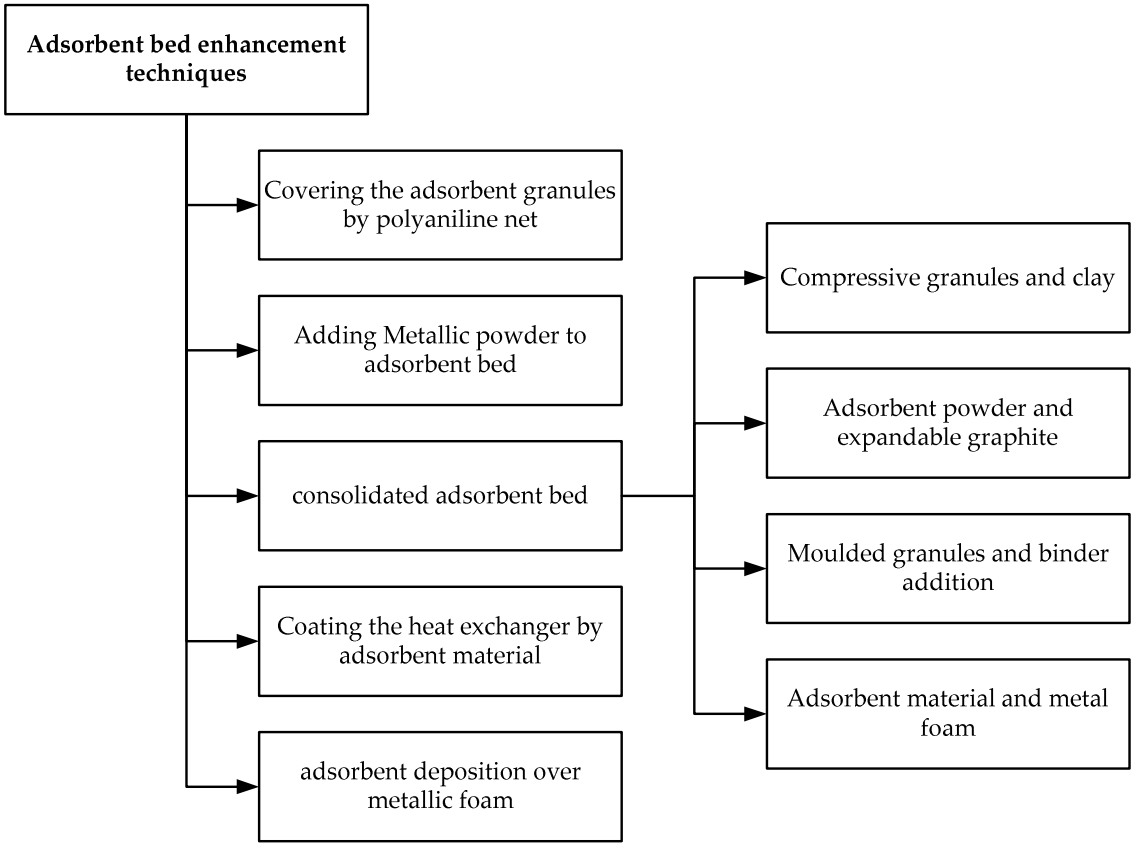

Figure 2-16, Adsorbent bed enhancement techniques

CHAPTER 3: MODELLING AND OPTIMISATION

3.1 Introduction

Modelling is a primary tool for design and optimisation of geometric specification and operating conditions of adsorption refrigeration systems [126, 127]. There are many modelling techniques which were applied to simulate the adsorption refrigeration systems such as lumped-parameter simulation technique [128, 129], lumped analytical simulation technique [130-136], dynamic simulation technique [137-141] and distributed-parameter simulation technique [39]. Object oriented simulation tool such as MODELICA was also used [142] to simulate the adsorption refrigeration units. All these simulation techniques present the overall heat transfer coefficient for adsorbent beds, evaporator and condenser as constant values. This approach limits the prediction capability of the effect of any physical change on the adsorption chiller performance, especially the adsorbent bed. This chapter presents the development of a novel empirical lumped analytical simulation model for a commercial 450kW two-bed silica gel / water adsorption water chiller. This machine is produced by the industrial partner 'Weatherite Manufacturing LTD'. The chiller utilises heat and mass recovery schemes.

3.2 The adsorption chiller

Figure 3-1 and 3-2 present schematic diagram and pictorial view of the simulated two-bed adsorption chiller. Each adsorbent bed is connected to the evaporator or condenser by flap valves operated by the effect of pressure difference between heat exchangers during adsorption or desorption respectively. On the other hand, the flow of cooling and heating

water to the adsorbent bed, flow of the chilled water through the evaporator and flow of cooling water to the condenser are controlled by 12 pneumatic valves, Table 3-1.

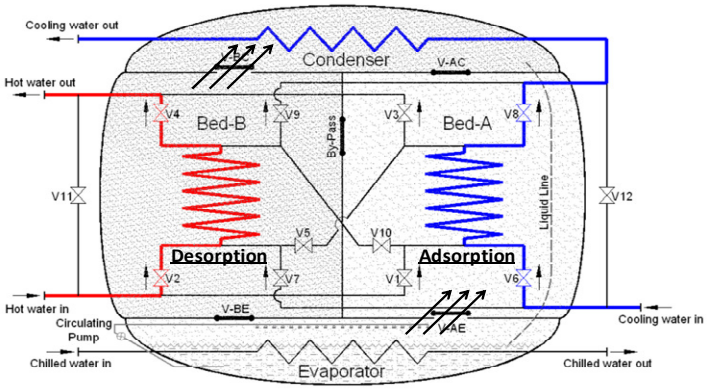

Figure 3-1, Schematic diagram for the simulated adsorption chiller

(a)

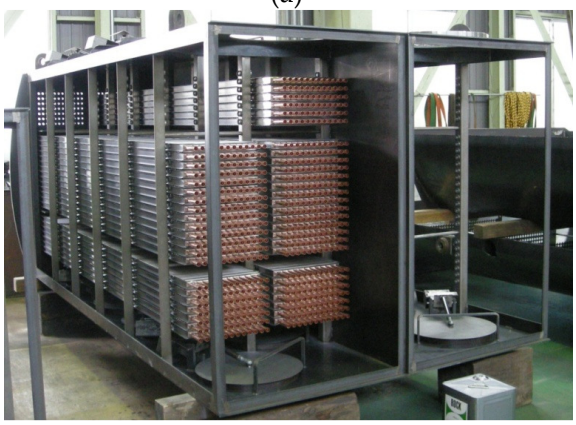

(b)

Figure 3-2, Descriptive presentation for the produced adsorption chiller

To operate the simulated chiller, each cycle consists of three operating modes namely; adsorption / desorption, mass recovery and heat recovery modes. In the adsorption / desorption mode the adsorbent bed-A is heated up by means of heating water stream, while bed-B is cooled down by means of cooling water stream (usually from cooling tower). The adsorbent bed-A is connected to the condenser, while bed-B is connected to the evaporator to generate the cooling effect by means of evaporation. The cooling water exits from the adsorbent bed flow through the condenser tubes to condense the desorbed water vapour. The second mode is the mass recovery mode, where the bypass valve between the adsorbent beds is opened to allow the water vapour flows from hot bed-B to cold bed-A by means of pressure swing. The mass recovery time should be extended until the mechanical equilibrium between the adsorbent bed reactors, where the excess time is not recommended. In the heat recovery mode, the cooling water flows through the hot bed then to the cold bed. The following cycle consists of the same operating modes, but by switching between bed-A and bed-B.

Figure 3-3a, 3-3b and 3-3c present the chiller flow diagram at adsorption / desorption, mass recovery and heat recovery modes respectively during the first cycle and Figure 3-3d, 3-3e and 3-3f present the chiller flow diagram at adsorption / desorption, mass recovery and heat recovery modes respectively during the second cycle.

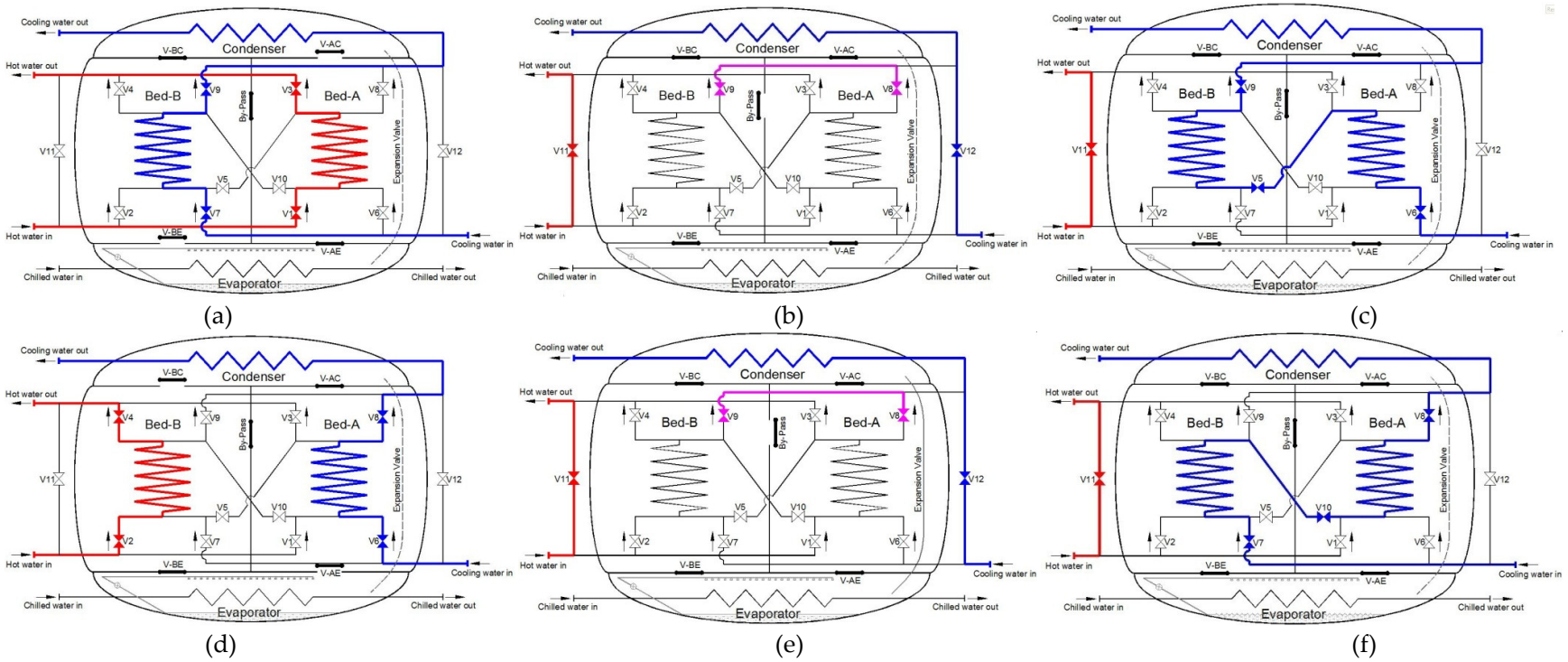

Figure 3-3, Chiller flow diagram at different operating mode

Table 3-1, Chiller cyclic operation and valving

Mode	B-A	B-B	V-AE	V-AC	V-BE	V-BC	BP	V1	V2	V3	V4	V5	V6	V7	V8	V9	V10	V11	V12
A-Ads/Des	HW	CW	X	O	O	X	X	O	X	O	X	X	X	O	X	O	X	X	X
B-Mass Recovery	NF	NF	X	X	X	X	O	X	X	X	X	X	X	X	O	O	X	O	O
C-Heat Recovery	CW	CW	X	O	O	X	X	X	X	X	X	O	O	X	X	O	X	O	X
D- Ads/Des	CW	HW	O	X	X	O	X	X	O	X	O	X	O	X	O	X	X	X	X
E-Mass Recovery	NF	NF	X	X	X	X	O	X	X	X	X	X	X	X	O	O	X	O	O
F-Heat Recovery	CW	CW	X	X	X	X	X	X	X	X	X	X	X	O	O	X	O	O	X

3.2.1 Chiller physical characteristics

Physically, the adsorbent bed heat exchanger is constructed from plain copper tubes with aluminium rectangular fins and silica gel granules are packed to fill the gaps between fins, Figure 3-4 and 3-5. An adsorbent bed module is assembled from a number of finned tubes and has specific dimensions as shown in Table 3-2. Each module is wrapped by metallic mesh to prevent the falling of silica gel granules but allows water vapour to penetrate. The evaporator and condenser are shell and tube heat exchangers where the refrigerant flows on the shell side and the secondary fluid (water) flows inside the tubes. The condenser heat exchanger is constructed from plain copper tubes while the evaporator is constructed from externally enhanced high efficiency finned copper tubes (GEWA-B)®. Figure 3-6 shows the evaporator and condenser heat exchangers. The evaporator was spray-assisted so as to enhance its boiling heat transfer performance [143].

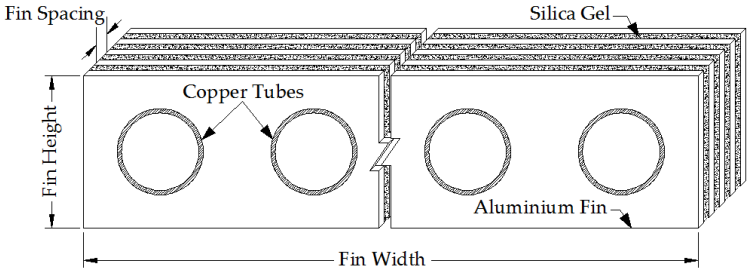

Figure 3-4, Schematic diagram for rectangular finned tube adsorbent bed

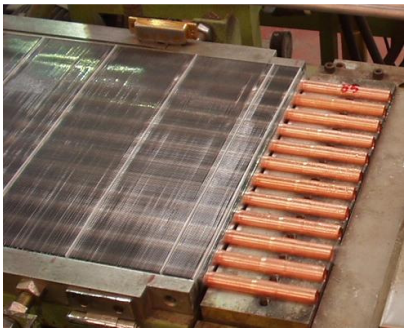

Figure 3-5, Descriptive presentation for rectangular finned tube adsorbent bed

Table 3-2, Simulated chiller physical data

Adsorbent bed reactor	
Adsorbent material	Fuji Davison RD Silica gel
Adsorbent mass	895 kg per bed
Average granules diameter	0.16 mm
Tube type	Bare copper tube
Tube outside diameter	5/8''
Tube wall thickness	0.8 mm
Tube length	3400 mm
Tube number	672 tube per bed (divided into 56 module and each module contains 12 tube)
Fins type	Rectangular aluminium fins
Fin length	340 mm
Fins height	28 mm
Fins thickness	0.95 mm
Fin pitch	1.5 mm
Fins number in one module	3400 ÷ (fin pitch = 1.5)
Total fins number in one bed	(3400 ÷ 1.5) X 56
Condenser	
Tube type	Bare copper tube
Outside diameter	¾''
Tube wall thickness	0.8 mm
Tube number	457
Tube length	2654
Evaporator	
Tube type	Externally enhanced copper tube
Nominal tube diameter	¾''
Root diameter	17.75mm
Fin diameter	18.85mm
Fin thickness	0.2mm
Fin pitch	0.45mm
Fin height	0.55mm
Inside diameter	16.33mm
Total tube number	224
Tube length	3894

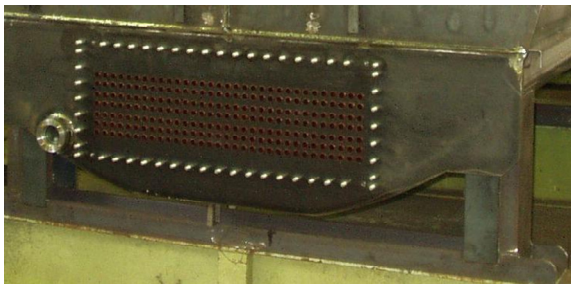

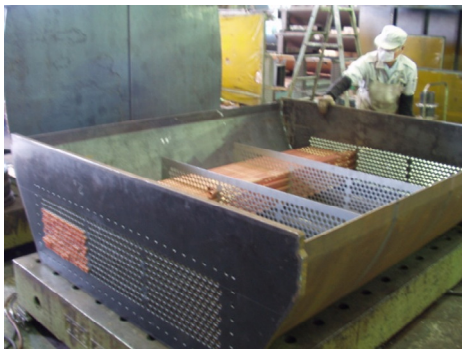

(a) (b)

Figure 3-6, Descriptive presentation for (a) Evaporator tube sheet (b) Condenser assembly

3.3 Chiller modelling

3.3.1 Silica gel / water adsorption isotherms

Adsorption isotherms present the amount of refrigerant that is contained in the adsorbent pores at the equilibrium conditions. Many correlations have been used to describe the adsorption isotherms for different types of adsorbent materials. The simulated adsorption chiller is packed with RD silica gel produced by Fuji. Wang [144] and Chua [145] represented the adsorption equilibrium uptake based on Tóth equation 3-1 as:

$$w^* = \frac{K_o \exp\left[\frac{\Delta H_{ads}}{\bar{R}T}\right] P}{\left\{1+\left[\left(\frac{K_o}{q_m}\right)\exp\left(\frac{\Delta H_{ads}}{\bar{R}T_{bed}}\right)P\right]^{C_t}\right\}^{\left(\frac{1}{C_t}\right)}} \qquad 3\text{-}1$$

Where, w^* is the uptake value at equilibrium conditions, ΔH_{ads} is the isosteric enthalpy of adsorption, q_m is the monolayer (adsorption) capacity, K_o is a pre-exponential constant and C_t is the Tóth constant. Wang [129] presented the equilibrium adsorption uptake for RD silica gel using Henry's law, equation 3-2.

$$w^* = K_o \exp\left[18 \frac{\Delta H_{ads}}{\bar{R} T}\right] P \qquad 3\text{-}2$$

The constant 18 is an empirical constant based on the experimental data and there is deference between the pre-expositional constants in both of Henry's model and Toth's model. One of the most common and realistic models that are used for determining RD-silica gel / water adsorption isotherms is Freundlich model. Freundlich model links refrigerant conditions in the adsorbent bed and the corresponding interconnected heat exchanger (condenser and evaporator) depending on the operation mode (desorption / condensation or adsorption / evaporation), equation 3-3.

$$w^* = w^\infty \left[\frac{P_{sat}(T_{ref})}{P_{sat}(T_{ads})}\right]^{1/k} \qquad 3\text{-}3$$

Where, $P_{sat}(T_{ads})$ is the saturation pressure corresponding to the bed temperature and $P_{sat}(T_{ref})$ is the saturation pressure corresponding to the interconnected heat exchanger (condenser or evaporator) in case of (desorption or adsorption) respectively. w^∞ is the maximum uptake value and k is a constant. Chihara and Suzuki (1983) evaluated experimentally the values for w^∞ and k for the silica gel/water pair as 0.346 kg_{ref}/kg_{ads} and 1.6, respectively. Saha (1995) presented a modified form for the Freundlich model to give more precise fitting of the experimental data for silica gel / water pair [131], equations 3-4 to 3-6. The numerical values of A_0-A_3 and B_0-B_3 are presented in Table 3-3. The modified Freundlich model was used to determine RD-Silica gel / water adsorption isotherms as it takes into account the effect of partial pressure between the adsorbent bed and the interconnected heat exchanger.

$$w^* = A(T_{ads})\left[\frac{P_{sat}(T_{ref})}{P_{sat}(T_{ads})}\right]^{B(T_{ads})} \quad 3\text{-}4$$

$$A(T_{ads}) = A_0 + A_1 T_{ads} + A_2 T_{ads}^2 + A_3 T_{ads}^3 \quad 3\text{-}5$$

$$B(T_{ads}) = B_0 + B_1 T_{ads} + B_2 T_{ads}^2 + B_3 T_{ads}^3 \quad 3\text{-}6$$

Table 3-3, Modified Freundlich equation constants

Constant	Value	Unit	Constant	Value	Unit
A_o	-6.5314	Kg/kg K	B_o	-15.587	K
A_1	0.72452E-1	Kg/kg K	B_1	0.15915	K^{-1}
A_2	-0.23951E-3	Kg/kg K^2	B_2	-0.50612E-3	K^{-2}
A_3	0.25493E-6	Kg/kg K^3	B_3	0.53290E-6	K^{-3}

3.3.2 Adsorption kinetics

The adsorption kinetics is strongly influenced by heat and mass transfer performance of the adsorbent bed. The better the heat transfer performance, the higher the adsorption rate for the same adsorbent material. In the simulated adsorption chiller, silica gel is packed in-between the adsorbent bed fins forming a thin layer around the heat exchanger outer surface; as a result water vapour can reach all silica gel at the same time. Therefore neglecting inter-particle mass transfer and modelling the adsorption / desorption rate by surface diffusion using linear driving force kinetic (LDF) can be used [98], equation 3-7. The overall mass transfer coefficient $k_s a_v$ of the adsorbent / refrigerant pair can be calculated by equation 3-8. The values of adsorbent particle radius (R_P), activation energy (Ea) and the pre-exponential constant (D_{so}) are furnished in Table 3-4.

$$\frac{dw}{dt} = k_s a_v (w^* - w) \quad 3\text{-}7$$

$$k_s a_v = \frac{15 D_{so}}{R_p^2} \exp\left(\frac{-Ea}{\overline{R}T}\right) \qquad 3\text{-}8$$

Table 3-4, Simulated silica gel characteristics

Parameter	Value	Unit
D_{so}	2.54×10^{-4}	m^2/s
E_a	4.2×10^{4}	J/mol
R_p	0.16×10^{-3}	m
ΔH_{ads}	2.939×10^{6}	J/kg

3.3.3 Adsorbent bed model

The compressor is the heart of refrigeration cycle that is pumping the refrigerant from the low-pressure / low-temperature side (evaporator) to high-pressure / high-temperature side (condenser). The adsorption refrigeration cycle is a heat powered cycle, where the adsorbent bed is the thermally driven compressor. The adsorption compressor operates in two modes adsorption and desorption when it is interconnected to the evaporator and condenser respectively. To switch between adsorption and desorption modes, an intermediate period is required to heat up the cold bed and cool down the hot bed and reverse their operating modes. In the simulated chiller the switching period is two sequential processes. The first is the mass recovery process where the refrigerant vapour in the high-pressure / high-temperature bed reactor moves towards the low-pressure / low-temperature bed reactor until mechanical equilibrium. The second is the heat recovery process, where the cooling water flows through the hot bed and the heating water flows through the low temperature bed.

Using lumped simulation model, the adsorbent, adsorbate and heat exchanger metal in the reactor container are assumed to be momentarily at the same temperature. The simulated chiller is assumed to be perfectly insulated where there is no heat or mass transfer to the surroundings. Applying the aforementioned assumptions, the energy balance for the adsorbent bed can be estimated by equation 3-9.

$$\begin{aligned}&\left(\zeta M_{w,ads}\, Cp_{w}(T_{bed}) + M_{ads}\, w_{bed}\, Cp_{ref}(T_{bed}) + M_{ads}\, Cp_{ads} + M_{Hex,bed}\, Cp_{Hex,bed}\right)\frac{dT_{bed}}{dt} = \\ &(\varphi \bullet \partial) M_{ads}\frac{dw_{bed}}{dt}\left[\gamma\left\{h_g(T_{Hex}) - h_g(P_{Hex},T_{bed})\right\} + (1-\gamma)\left\{h_g(P_{Hex},T_{Hex}) - h_g(P_{bed},T_{bed})\right\}\right] \\ &+ \varphi M_{ads}\frac{dw_{bed}}{dt}\Delta H_{ads} + (1-\zeta)\sum_{n=1}^{n=N_{bed}} dUA_{bed,k} \times LMTD_{bed}\end{aligned} \quad 3\text{-}9$$

Where, flag ϕ is equal to 0, 0 and 1 during mass recovery, heat recovery and adsorption / desorption operation process respectively. Flag ∂ is equal to 0 and 1 during desorption / condensation and adsorption / evaporation respectively. Flag γ is equal to 1 or 0 in case of connecting the bed reactor to evaporator or to the other bed reactor respectively. Flag ζ is equal to 0, 1 and 0 during adsorption / desorption, mass recovery or heat recovery mode respectively.

The terms on the left hand side of equation 3-9, are the rate of heat required to heat or cool the stagnant water inside the adsorbent bed tubes, rate of heat required to heat or cool the adsorbed refrigerant inside silica gel pores, the rate of heat required to heat or cool silica gel granules and the rate of heat required to heat or cool the heat exchanger metal mass including fins and tubes respectively.

The terms on the right hand side of equation 3-9, presents the rate of heat received during adsorption / evaporation or mass recovery process by the refrigerant vapour moved from

high pressure high temperature bed, the rate of heat generated or extracted during the adsorption and desorption processes respectively and the rate of heat added or removed from secondary fluid during adsorption or desorption processes respectively. The overall heat transfer coefficient was analyzed incrementally where each element consists of rectangular finned tube surrounded by silica gel on both sides and cooling or heating water flowing inside the tube as shown in Figure 3-7(a). Each rectangular fin was modified to be circular fin with the same fin total surface area as shown in Figure 3-7(b) [146].

Based on this configuration shown in Figure 3-7(c), there are six resistances to heat transfer namely; (1) radial convective thermal resistance from the secondary fluid stream to the internal tube wall R1, (2) conduction thermal resistance through tube wall R2, (3) two contact thermal resistances between silica gel granules and tube outside surface and fins surface R3 and R4 and (4) two conduction thermal resistances through silica gel granules in radial and axial direction R5 and R6. The thermal resistances electrical analogy is presented in Figure 3-7(d). The overall incremental heat transfer conductance dUA_{bed} was then written as;

$$dUA_{bed} = \frac{1}{R_{w,bed} + R_{t,bed} + R_{o,bed}} \qquad 3\text{-}10$$

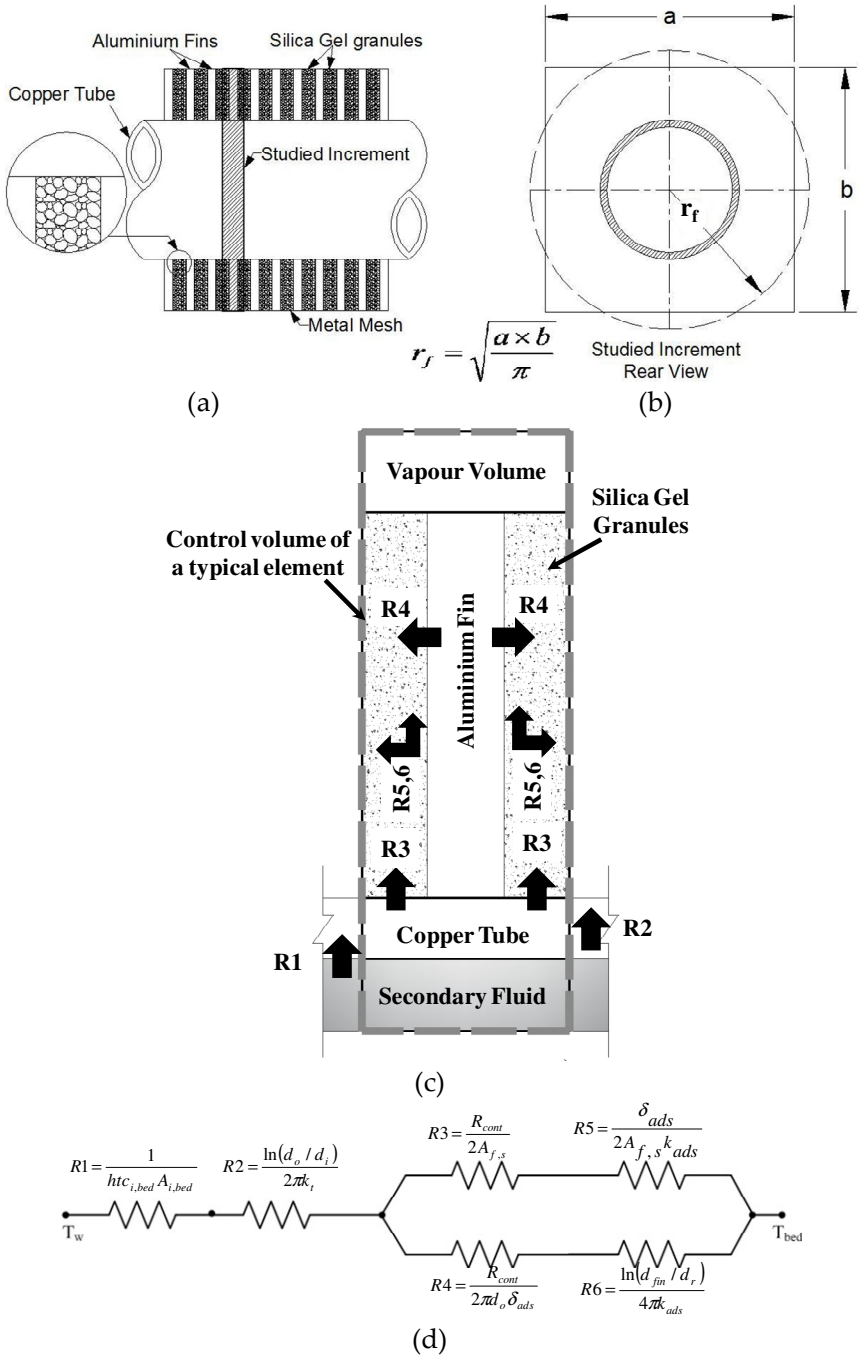

Figure 3-7, Incremental thermal analysis schematic diagram

Contact thermal resistance between two different materials depends on contact area, voids area, filling material and thermal conductivity for both materials [147], where equation 3-11 describes this function. Calculating the thermal contact resistance for silica gel-Aluminium

fins and silica gel-copper tube requires an accurate measurement contact and void areas. However, the experimental measurement for the overall value of the thermal contact resistance is more preferable, but there is a lack for the published experimental results that determines silica gel-aluminium and silica gel-copper thermal contact resistances.

Zhu experimentally determined the contact thermal resistance between zeolite granules and heat exchanger metal (copper) surface [148], see Figure 3-8. Where equations 3-113-12 - 3-14 are the polynomial regression with R^2 value of 0.99 for Zhu experimental results of different zeolite granules sizes 50, 100 and 200 mesh scale corresponding to 0.297, 0.149 and 0.074 mm granules diameter respectively.

$$\frac{1}{R_{contact}} = \frac{1}{L_g}\left(\frac{A_c}{A}\frac{2K_AK_B}{K_A+K_B} + \frac{A_v}{A}K_f\right) \qquad 3\text{-}11$$

$$R_{contact,\#50} = 0.0013T_{bed}^2 - 0.1773T_{bed} + 8.6221 \qquad 3\text{-}12$$

$$R_{contact,\#100} = 0.0012T_{bed}^2 - 0.1624T_{bed} + 7.6785 \qquad 3\text{-}13$$

$$R_{contact,\#200} = 0.0008T_{bed}^2 - 0.1214T_{bed} + 6.422 \qquad 3\text{-}14$$

$$R_{contact\#n} = R_{contact\#n\,1} + \left(R_{contact\#n\,2} - R_{contact\#n\,1}\right)\frac{(d-d_1)}{(d_2-d_1)} \qquad 3\text{-}15$$

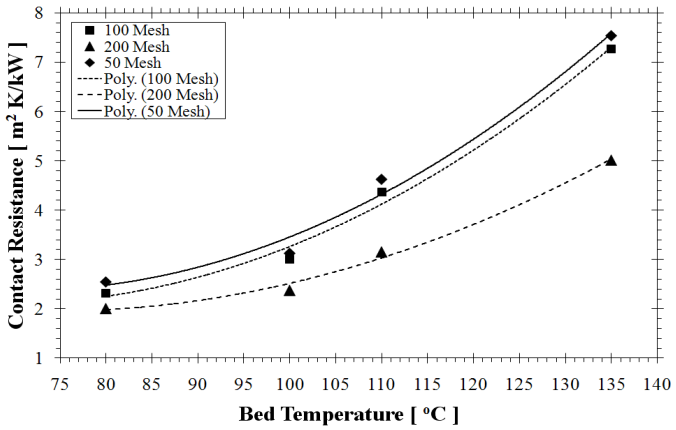

Figure 3-8, Zeolite granules contact thermal resistance, Zhu [148]

Using equation 3-11, the thermal contact resistances have been determined for zeolite-copper, silica gel-copper and silica gel aluminium with different void and contact area ratios (see Table 3-5). It has been observed that the absolute percent deviation between zeolite-copper and silica gel-copper, aluminium thermal contact resistances are between 0.29% and 1.52%, where the average value of the absolute percent deviation for the all calculated values is 0.78%. Based on the acceptable range of the deviation between the calculated contact thermal resistances, equations 3-12 - 3-14 are used to determine silica gel-copper and silica gel-aluminium thermal contact resistances. The contact resistance for the granules sizes between (0.297 and 0.149 mm diameter) and (0.149 and 0.074 mm diameter) are calculated using the interpolation technique, equation.

Table 3-5, Thermal contact resistance calculations

Zeolite-copper thermal contact resistance calculation					
K_{cu}	**$K_{zeolite}$**	**Ac/A**	**Av/A**	**Rc**	
400	0.097	0.3	0.7	0.0475	
400	0.097	0.4	0.6	0.0553	
400	0.097	0.5	0.5	0.0662	
400	0.097	0.6	0.4	0.0825	
400	0.097	0.7	0.3	0.1095	
Silica gel-copper thermal contact resistance calculation					
K_{cu}	**$K_{silica\ gel}$**	**Ac/A**	**Av/A**	**Rc**	**%age dev**
400	0.198	0.3	0.7	0.0474	0.29
400	0.198	0.4	0.6	0.0551	0.44
400	0.198	0.5	0.5	0.0658	0.66
400	0.198	0.6	0.4	0.0817	0.99
400	0.198	0.7	0.3	0.1078	1.52
Silica gel-aluminium thermal contact resistance calculation					
K_{Al}	**$K_{silica\ gel}$**	**Ac/A**	**Av/A**	**Rc**	**%age dev**
237	0.198	0.3	0.7	0.0474	0.29
237	0.198	0.4	0.6	0.0551	0.44
237	0.198	0.5	0.5	0.0658	0.66
237	0.198	0.6	0.4	0.0817	0.99
237	0.198	0.7	0.3	0.1078	1.52

3.3.4 Evaporator model

In the simulated chiller a flooded type evaporator is utilized where the refrigerant (water) in the shell side covers the tube bundle and the secondary fluid (chilled water) flows through the tubes. During adsorption / evaporation mode, the low pressure / temperature adsorbent bed is connected to the evaporator to evaporate part of the refrigerant that covers the tube bundle, where the cooling effect is generated by means of latent heat of evaporation of the adsorbed refrigerant. The more refrigerant adsorbed, the greater the cooling effect is obtained. In such type of evaporator, the vapour refrigerant exits at saturation condition and the rate form of the energy balance can be expressed by equation 3-16. The evaporator was spray-assisted so as to enhance wetting of the heat exchanger surface thus resulting in a more effective heat transfer [143].

$$\left[Cp_{ref,f}\left(T_{evap}\right)M_{ref,evap} + Cp_{Hex,evap}M_{Hex,evap}\right]\frac{dT_{evap}}{dt} = \frac{d}{dt}E_{pump} \\ \varphi\left[h_{ref,evap,in} - h_{ref,evap,out}\right]M_{ads}\frac{dw_{bed}}{dt} + UA_{evap} \times LMTD_{evap} \qquad 3\text{-}16$$

The terms on the left hand side of equation 3-16, presents the rate of heat transfer to the refrigerant maintained in the evaporator and the rate of heat transfer to the evaporator metal mass. The terms on the right hand side are the rate of heat removed from the refrigerant that is pumped continuously to the evaporator by the spray assistance system during all operating modes, the rate of heat transfer due to the refrigerant flow through the evaporator by the adsorption effect and the rate of heat removed from the chilled water respectively. The overall conductance of the evaporator (UA_{evap}) depends on water to internal tube wall

convective thermal resistance, tube wall conductive resistance and refrigerant to outer tube wall convective boiling resistance, equation 3-17.

$$UA_{evap} = \frac{1}{R_{w,evap} + R_{t,evap} + R_{ref,evap}} \qquad 3\text{-}17$$

Refrigerant evaporation in flooded type evaporators is classified as pool boiling where the refrigerant covers most of heat exchanger tubes. There are four types of pool boiling regimes named; free convective, nucleate, transition and film pool boiling. Different boiling regimes may be delineated according to the temperature difference between the refrigerant temperature and the tube wall outer surface temperature [149, 150]. Water boiling in the simulated evaporator can be classified as a nucleate pool boiling, where the temperature difference between the tube wall and the refrigerant pool usually lower than 30°C. Water refrigerant nucleate pool boiling convective heat transfer coefficient can be estimated using equations 3-18 and 3-19.

$$htc_{ref,evap} = \frac{\mu_{ref,l} h_{ref,fg}}{\Delta T_{evap}} \left[\frac{g\left(\rho_{ref,l} - \rho_{ref,v}\right)}{\sigma} \right]^{\frac{1}{2}} \cdot \left(\frac{Ja_{ref,evap}}{C_{s,f}\ \mathrm{Pr}_{ref,l}^{1}} \right)^{3} \qquad 3\text{-}18$$

$$Ja_{ref,evap} = \frac{Cp_{ref,l} \Delta T_{evap}}{h_{ref,fg}} \qquad 3\text{-}19$$

The total average refrigerant to tube outer wall heat transfer resistance can then be calculated using equation 3-20.

$$R_{ref,evap} = \frac{1}{htc_{ref,evap} \cdot \pi \cdot d_{evap,o} \cdot L_{evap} \cdot N_{evap,t}} \qquad 3\text{-}20$$

The evaporator refrigerant mass balance taking into account the condition of no flow of water vapour from the evaporator during mass and heat recovery (Q_{evap}=0) can be estimated by equation 3-21. Where ϕ is a flag equal to 0, 0 and 1 during mass recovery, heat recovery and adsorption / desorption operating process respectively.

$$\frac{dM_{ref,f,evap}}{dt} = -\varphi \cdot M_{ads}\left(\frac{dw_{des}}{dt} + \frac{dw_{ads}}{dt}\right) \qquad 3\text{-}21$$

3.3.5 Condenser model

The condenser condenses the desorbed water vapour that is generated from high temperature / pressure adsorbent bed reactor during desorption / condensation mode. The condensate water is delivered to the evaporator via liquid line. The energy balance for the condenser can be described by equation 3-22.

$$\begin{aligned}&\left[Cp_{ref,l}(T_{cond})M_{ref,cond} + Cp_{Hex,cond}M_{Hex,cond}\right]\frac{dT_{cond}}{dt} = UA_{cond} \times LMTD_{cond} + \\ &\varphi\left[\left(h_{ref,cond,l} - h_{ref,cond,g}\right) + Cp_{ref}\left(T_{cond} - T_{bed}\right)\right]M_{ads}\frac{dw_{bed}}{dt}\end{aligned} \qquad 3\text{-}22$$

The terms on the left hand side present the rate of heat transfer from the condensate layer over condenser tubes and the rate of heat transfer from the condenser metal mass. The terms on the right hand side include the rate of heat transfer due to the refrigerant flow to the condenser and the rate of heat removed during the condensation process by cooling water. Condenser overall conductance (UA_{cond}) is a function of cooling water to wall convective resistance, tubes wall conductive resistance and condensation over outside tube wall convective resistance, equation 3-23.

$$UA_{cond} = \frac{1}{R_{w,cond} + R_{t,cond} + R_{ref,cond}} \quad 3\text{-}23$$

Refrigerant-tube outer surface convective heat transfer coefficient can be determined by the average laminar film condensation over a vertical tier of horizontal tubes [149]. The average heat transfer coefficient for laminar falling film condensation over tube bank can be described by equation 3-24, and refrigerant-tube wall convective heat transfer resistance is then determined using equation 3-25.

$$htc_{ref,cond} = 0.729\left[\frac{g\rho_{ref,l}\cdot\left(\rho_{ref,l}-\rho_{ref,v}\right)\cdot k_{ref,l}^{3}\cdot h'_{ref,fg}}{N_{cond}\cdot\mu_{ref,l}\cdot\left(T_{ref,sat}-T_{t,s}\right)\cdot d_{cond,o}}\right]^{1/4} \quad 3\text{-}24$$

$$R_{ref,cond} = \frac{1}{htc_{ref,cond}\cdot\pi\cdot d_{cond,o}\cdot L_{cond}\cdot N_{cond,t}} \quad 3\text{-}25$$

3.3.6 In tube flow heat transfer

The previous section discussed the calculation of adsorption rate and the heat transfer behaviour on the refrigerant side in adsorbent-beds reactor, condenser and evaporator heat exchangers. The secondary fluid in all previously mentioned heat exchangers is water that flows inside tube. This section presents in-tube flow and the calculation of water-to-tube wall convective thermal resistance. The convective heat transfer coefficient between water and internal tube wall is a function of Nusselt number, secondary fluid thermal conductivity and hydraulic diameter, equation 3-26.

$$htc_{w} = \frac{Nu_{w}K_{w}}{d_{t,i}} \quad 3\text{-}26$$

Single-phase in-tube flow Nusselt number in case of laminar flow (Re<2300) and based on instantaneously constant heat flux concept is a constant number, equation 3-27. In turbulent flow, the Nusselt number can be calculated using various correlations, but the simple the correlation the less in accuracy. The more recent Gnielinski modified correlation 3-28, can be used to calculate in-tube Nusselt number with error as small as 10% [149]. This correlation is valid over a wide range of Reynolds number and Prandtl number of ($3000 < Re < 5 \times 10^6$) and ($0.5 < Pr < 2000$).

$$Nu_w = 4.36 \quad \text{For (Re<2300)} \tag{3-27}$$

$$Nu_w = \frac{\left(\frac{f_w}{8}\right)\left(\mathrm{Re}_w - 1000\right)\mathrm{Pr}_w}{1 + 12.7\left(\frac{f_w}{8}\right)^{1/2}\left(\mathrm{Pr}_w^{2/3} - 1\right)} \quad \text{(Re>3000)} \tag{3-28}$$

It is observed that the Gnielinski modified correlation takes into account the change of the heat transfer coefficient due to the tube roughness that enhances the heat transfer rate which appears in the friction factor term. In case of laminar flow (Re<2300), the friction factor is inversely proportional to the Reynolds, equation 3-29. In case of in-tube turbulent flow (Re>3000), the friction factor is dependent on Reynolds number and tube roughness. Haaland presented the friction factor in an explicit form [151]. Water-tube wall convective heat transfer resistance and the conductive heat transfer resistance in radial direction through the tube wall can be calculated using equation 3-31 and 3-32 respectively.

$$f_{w,cond} = \frac{64}{\mathrm{Re}_{w,cond}} \quad \text{For (Re<2300)} \tag{3-29}$$

$$\frac{1}{\sqrt{f_w}} \approx -1.8\log\left[\frac{6.9}{\mathrm{Re}_w}+\left(\frac{\varepsilon/d_{cond,i}}{3.6}\right)^{1.11}\right] \text{ For (Re>3000)} \quad 3\text{-}30$$

$$R_w = \frac{1}{htc_w \cdot \pi \cdot d_{t,i} \cdot L_{hex} \cdot N_t} \quad 3\text{-}31$$

$$R_{t,hex} = \frac{\ln\left(\frac{d_{t,o}}{d_{t,i}}\right)}{2\pi \cdot K_t \cdot d_o \cdot L_{hex} \cdot N_t} \quad 3\text{-}32$$

where L_{hex} and N_t are the length and the number of the tubes used in the condenser respectively. f_w and ε are the friction factor and the tube internal wall roughness respectively.

3.3.7 Performance indicators

To evaluate the adsorbent bed reactors thermal performance two performance indicators were used; namely heat capacity ratio HCR and number of transfer unit NTU. HCR is the ratio between the thermal capacities of silica gel to the adsorbent bed metal, equation 3-33. Higher HCR means higher amount of heat received by silica gel compared to that received by the metal which directly enhances the chiller COP. NTU is a dimensionless parameter whose magnitude influences adsorbent bed heat transfer performance, equation 3-34. It is noteworthy to mention that enhancement of HCR and NTU improve adsorbent bed overall performance.

$$HCR = \frac{M_{sg}C_{sg}}{M_{met}C_{met}} \quad 3\text{-}33$$

$$NTU = \frac{UA_{bed}}{\dot{m}_w C_w} \quad 3\text{-}34$$

To evaluate adsorption chiller overall performance four indicators are used; namely cooling capacity (Q_{evap}) equation 3-35, specific cooling power (SCP) equation 3-36, heating load (Q_{heat}) equation 3-37 and coefficient of performance (COP) equation 3-38. The Carnot coefficient of performance (COP_{Carnot}) equation 3-39 and chiller efficiency (η) equation 3-40 were also determined to evaluate the chiller performance compared to ideal reversed Carnot cycle.

$$Q_{evap} = \int_0^{t_{cycle}} \dot{m}_{chw} C_w \left(T_{chw,in} - T_{chw,out}\right) dt \Big/ t_{cycle} \qquad 3\text{-}35$$

$$SCP = \frac{Q_{evap}}{M_{ads}} \qquad 3\text{-}36$$

$$Q_{heat} = \int_0^{t_{cycle}} \dot{m}_{hw} C_w \left(T_{hw,in} - T_{hw,out}\right) dt \Big/ t_{cycle} \qquad 3\text{-}37$$

$$COP = \frac{Q_{evap}}{Q_{heat}} \qquad 3\text{-}38$$

$$COP_{Carnot} = \left[\frac{\left(\overline{T}_{ads} - \overline{T}_{des}\right)}{\overline{T}_{des}}\right] \times \left[\frac{\overline{T}_{evap}}{\left(\overline{T}_{ads} - \overline{T}_{evap}\right)}\right] \qquad 3\text{-}39$$

$$\eta_{chiller} = \frac{COP}{COP_{Carnot}} \qquad 3\text{-}40$$

3.4 Optimisation technique

Most of the currently published work that investigated the effect of operating conditions on adsorption chiller performance are based on parametric runs of chosen parameters, therefore the need for using an optimisation technique to obtain the optimum parameters is essential [134]. The basic optimization problem is that of minimizing or maximizing an objective function subjected to constraints imposed on the variables of that function. The objective

function and constraints can be linear or nonlinear. The constraints could be bound constraints, equality, inequality constraints, or integer constraints. Mainly there are two types of optimisation techniques namely; local and global optimisation. The global optimization is an enhanced version of local optimisation to find the absolutely best set of admissible conditions that minimize or maximize the objective function. The global optimization algorithm converges to a local optimal, regardless of the selected starting point [152].

Evolutionary algorithms (EAs) are population-based global optimization algorithms that use biology-inspired mechanisms like mutation, crossover, natural selection, and survival rules in order to refine a set of solution candidates iteratively. The advantage of evolutionary algorithms is their "black box" character that makes only few assumptions about the underlying objective functions. Furthermore, the definition of objective functions usually requires lesser insight to the structure of the problem space than the manual construction of an admissible heuristic. EAs therefore perform consistently well in many different problem categories. All evolutionary algorithms proceed in principle according to the scheme shown in Figure 3-9.

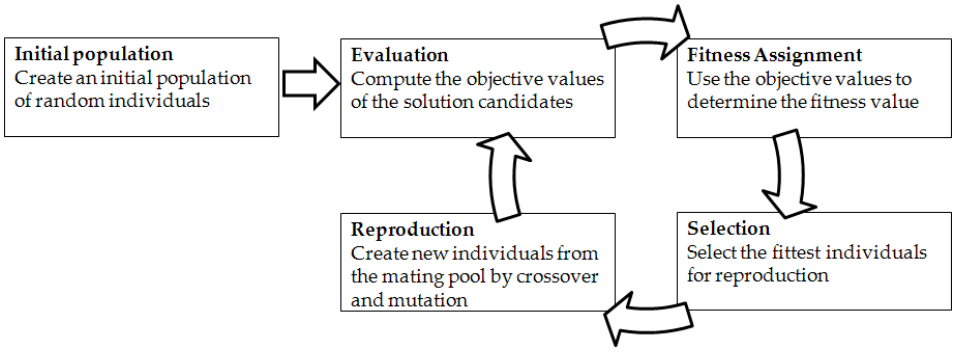

Figure 3-9, basic scheme of evolutionary algorithms [153]

Genetic algorithm (GA) is a subclass of evolutionary algorithms and one of the robust population-based global optimisation tools. GA has the advantage of the ability to solve a variety of problems of discontinuous, non differentiable, stochastic, or highly nonlinear objective functions. GA dates back to the mid-1950s, where the biologist Barricelli and the computer scientist Fraser began to apply computer-aided simulations in order to gain more insight into genetic processes and the natural evolution and selection. GA has been being developed continually and today there are many applications in science, economy, and research and development that can be tackled with genetic algorithms.

GA algorithm starts the first iteration with initial random population for each parameter to get a set of individuals ($N_{population} \times N_{parameter}$). This population is used for calculating the corresponding objective function values. A new generation is then developed to be used as a new population in next iteration using a selection function based on three rules named; elite selection, crossover and mutation. The individuals that achieved the best objective function values in the current generation and granted to survive to the next generation are elite individuals. Crossover enables the algorithm to extract the best individuals and recombine them into potential superior individuals using a specified crossover fraction. The mutation rule replaces the remaining population with randomly selected new ones. The transition between two generations is schematically illustrated in Figure 3-10. Crossover fraction of 1 does not enhance the solution where the new generation is just a new combination of the initial population. However, crossover fraction of zero gets the new generation based on mutation only which diverge the solution.

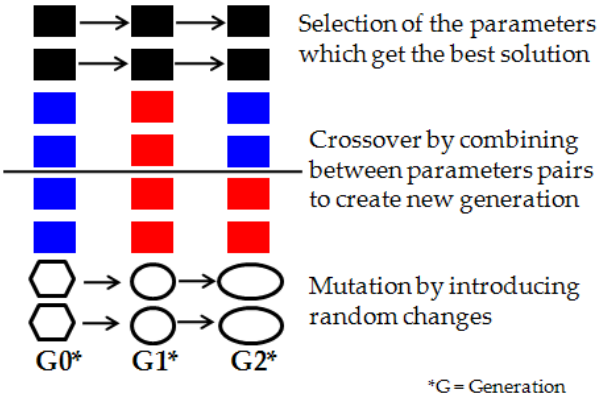

Figure 3-10, schematic illustration for generation development for GA solver

In this investigation, GA is applied to determine global optimum parameter within a specific range that could include the optimum combination that maximizes the objective function. The number of population for each individual parameter is selected to be 20 while the number of elite count is 2, the crossover fraction is 0.8 and the rest of individuals are managed by mutation rule. These were recommended by Mathwork GA Manual® [153]. After certain number of iterations the GA solver stopped, where no more improvement in the solution in terms of objective function value, average diversity and best, worst and mean score. The GA optimisation tool will be used in determining the optimum cycle timing in order to obtain the best performance in term of cooling capacity and / or coefficient of performance.

3.5 Summary

The modelling is a primary tool for evaluating the performance of adsorption cooling systems. This chapter presented the development of a novel empirical lumped analytical simulation model. The case study was a commercialised 450kW silica gel / water adsorption

chiller utilised by mass and heat recovery modes. Figure 3-11 presents the modelling concept graphical presentation and how the heat exchanger models interact. The importance of applying the genetic algorithm global optimisation tool has been presented in this chapter.

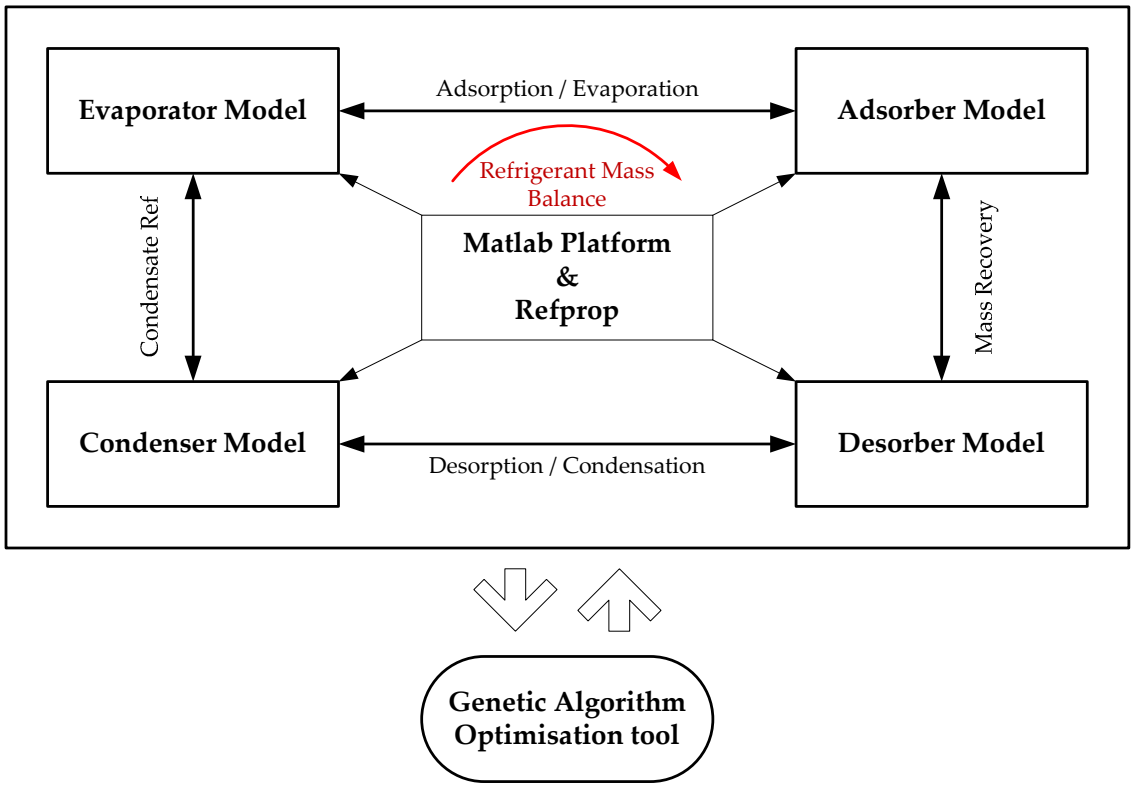

Figure 3-11, Simulation modelling concept graphical presentation

CHAPTER 4: SCALED DOWN-ADSORBENT BED TEST FACILITY

4.1 Introduction

Experimentally investigating the effect of operating condition on the mass and heat transfer performance of the applied adsorbent bed is important. This chapter presents the design, construction and commissioning of a test facility that experimentally evaluates the heat and mass transfer performance of a scaled down adsorbent bed, which is typically applied in the simulated chiller. This test rig is flexible in replacing the current applied modules with other ones of different designs.

4.2 Test facility description

The test rig design is based on the volumetric method of determining adsorbent characteristics. Instead of studying the sample performance, a real scaled down adsorbent-bed module is applied. Figure 4-1 and 4-2 are schematic diagram and pictorial presentation of the test rig. The main component of the test facility is the adsorbent bed reactor which is 8″ flanged tube that is fitted with two scaled down adsorbent bed modules, Figure 4-3. The adsorbent bed modules are a rectangular finned tube heat exchanger and silica gel granules are packed to fill the inter fin gaps. The modules are covered by stainless steel mesh to prevent granules falling. These modules are arranged in two passes and fitted in the front plate by means of 15mm compression fittings, Figure 4-4.

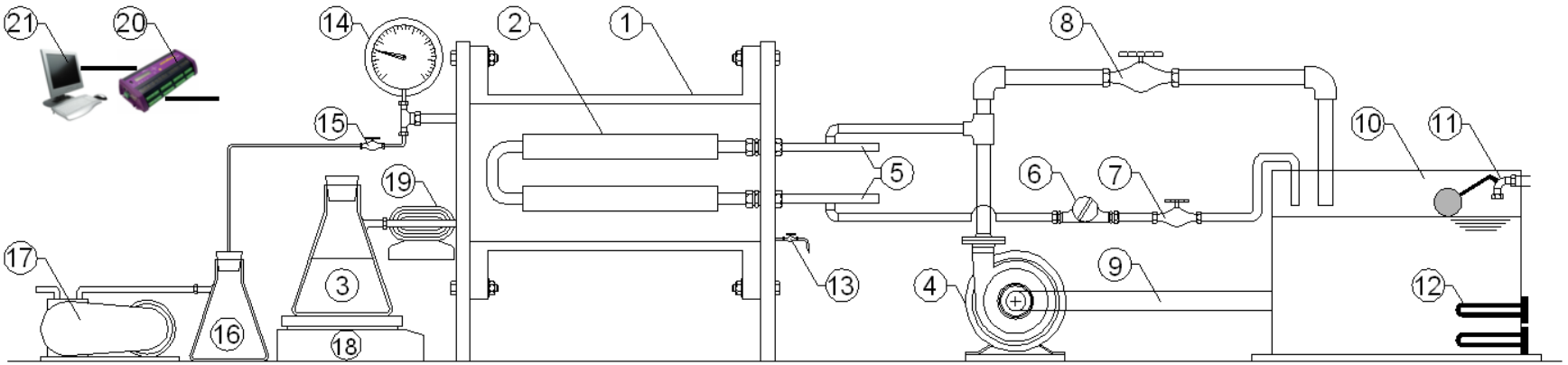

1	Adsorbent bed reactor shell	**12**	2 × 3kW heaters
2	Adsorbent bed modules	**13**	Drainage line
3	Refrigerant flask	**14**	Vacuum gage
4	Cooling / heating water pump	**15**	Vacuum line control valve
5	Supply and return water headers	**16**	Separation flask
6	Flow meter	**17**	Vacuum pump
7	Cooling / heating water flow control valve	**18**	Heating plate
8	Bypass flow control valve	**19**	Air heater
9	Cooling / heating water supply line	**20**	Data logger
10	Cooling / heating water tank	**21**	Computer
11	Main water supply		

Figure 4-1, Test rig schematic diagram

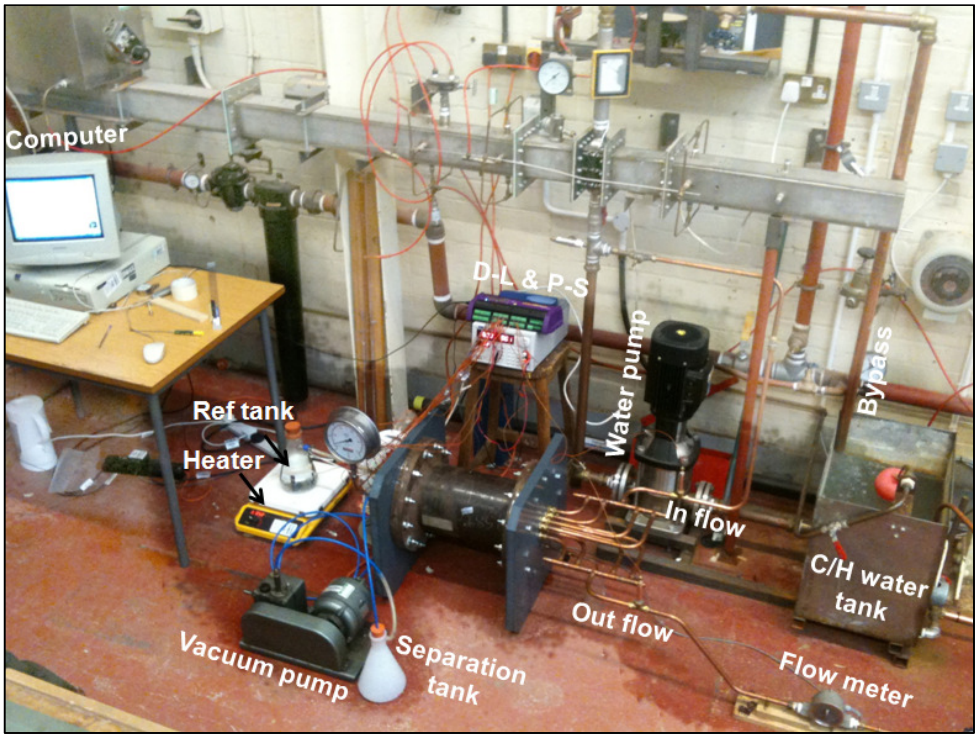

Figure 4-2, pictorial view of the test rig

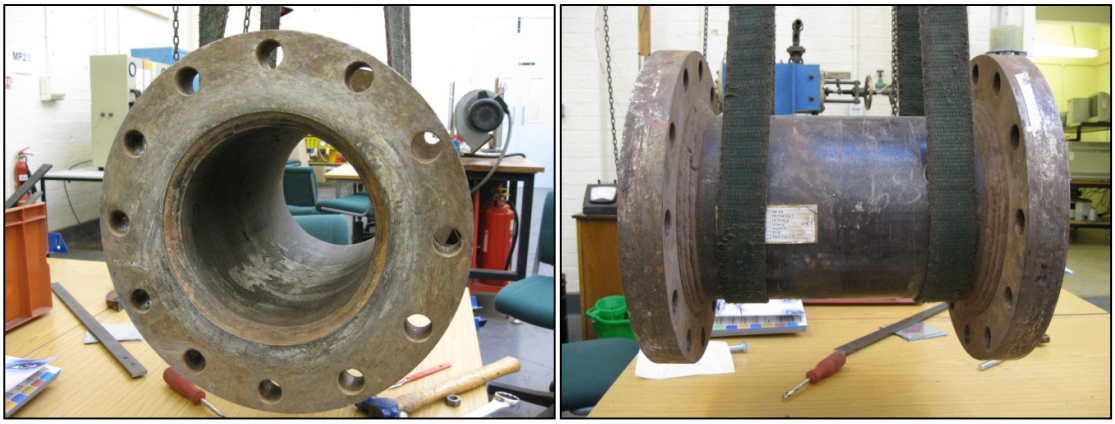

Figure 4-3, Adsorbent bed reactor shell

The inlet and outlet headers are used to distribute and collect the inlet and outlet water flow respectively, Figure 4-5. Inlet and outlet points were selected to maintain uniform distribution through the tubes of adsorbent bed modules. Group of accessible holes were

applied in the rear plate to enable temperature and pressure measurements by means of thermocouples and vacuum gauge.

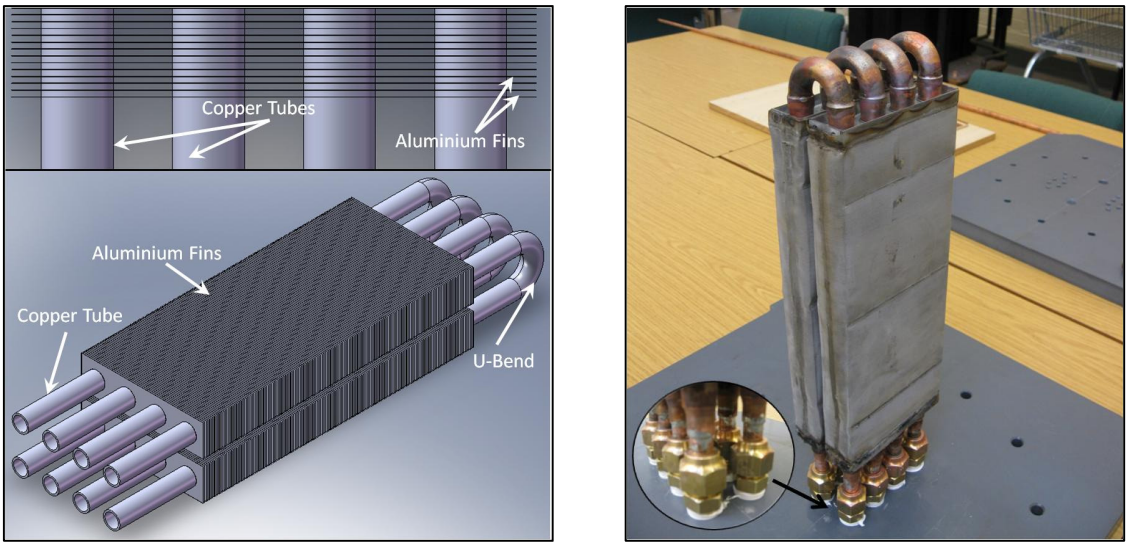

Figure 4-4, Adsorbent bed modules

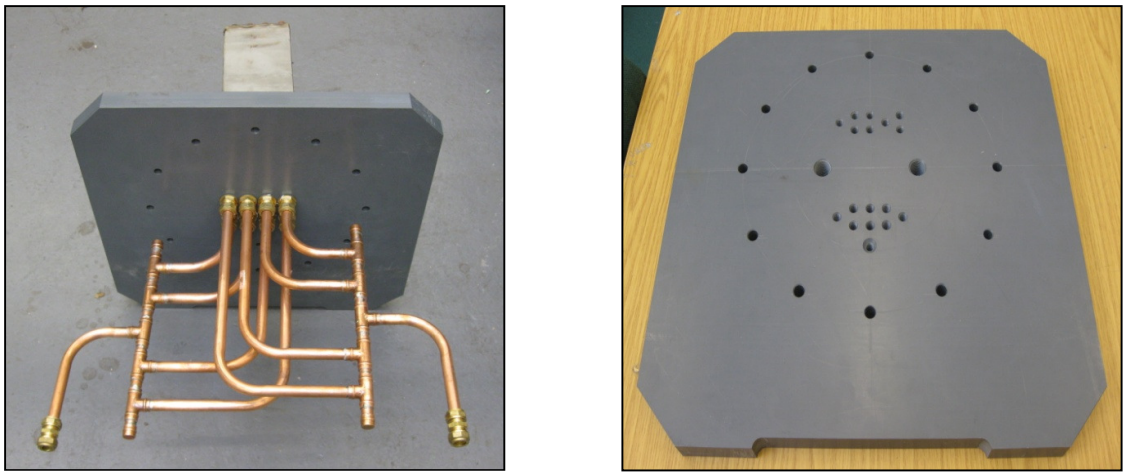

Figure 4-5, Front and rear plates assembly

The refrigerant tank is a conical glass flask that is selected to withstand full vacuum operation. The refrigerant flask is used for measuring the change in refrigerant amount during the adsorption process; therefore it was calibrated before use by means of a

calibrating tank. Water vapour is a condensable gas and the tube connections between the refrigerant flask and adsorbent bed reactor is heated by hot air stream to maintain the connection line temperature 10 degrees above the generated vapour temperature in the tank and hence prevent condensation to occur. The refrigerant flask temperature increased up to 40˚C using a preset heating plate.

Secondary fluid (Cooling / heating water) is pumped using Grundfos® in-line centrifugal pump of maximum flow rate (240 l/min / 40kPa-NPSH). Secondary fluid flow rate is controlled by means of flow control valve that is fitted in the flow outlet line. A bypass line is required to avoid the pump cavitations problem in case of low flow rates. The flow rate in the bypass line is controlled by means of bypass control valve. The secondary fluid is initially maintained in 350×450×450 mm (length × width × height) tank and is filled from the main by a float control valve to avoid overflow. The secondary fluid is heated up by means of 2×3kW domestic heaters that can raise the water temperature up to 65˚C. Adsorbent bed reactor was assisted by a drainage line that is used for condensate drainage. This line is fitted with a shut off valve, to isolate the system during the experiment.

The test rig is kept at full vacuum during the adsorption process, based on the industrial recommendation. A vacuum pump (SPEEDDIVAC ES 35 – Edwards high vacuum limited) is used to generate the required vacuum level. The connection between the vacuum pump and the reactor is controlled by a shut off valve and assisted by a separation tank. This tank has the function of capturing the water vapour that gets out from the reactor during vacuum pump operation. The separation tank is cooled down by immersing it in ice to capture the

water vapour by condensation. The flow rate and temperature signals measurements are logged by dataTaker-DT85, data logger.

4.3 Instrumentation

The test rig is assisted by a computerised measuring system by which the temperatures and flow rates can be monitored and recorded on the computer. However, the pressure is measured manually. Descriptions of the various measuring devices are given in this section.

4.3.1 Temperature measurement

Thermocouples were installed at different points in the test facility to measure the secondary fluid at inlet and outlet, adsorbent bed module, shell space and shell surface temperatures. All applied thermocouples are copper-constantan T-type of compact transition joint probes [TJC100-CPSS, Omega UK], as shown in Figure 4-6. These were made of stainless steel sheath that resists aqueous environments.

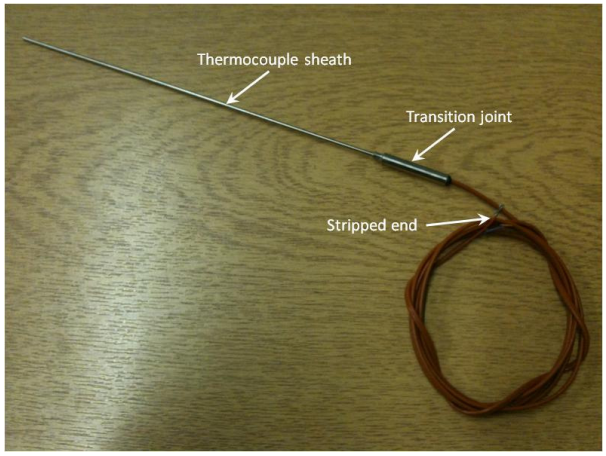

Figure 4-6, Applied TJC100-CPSS thermocouple

All thermocouples except the ones that measure inlet, outlet and shell outside surface temperature are inserted individually using compression fittings as shown in Figure 4-7. Inlet and outlet water flow temperatures were measured using thermocouples of 1.5 and 50 mm sheath diameter and length respectively. Figure 4-8 presents the assembly of in tube flow temperature measurement.

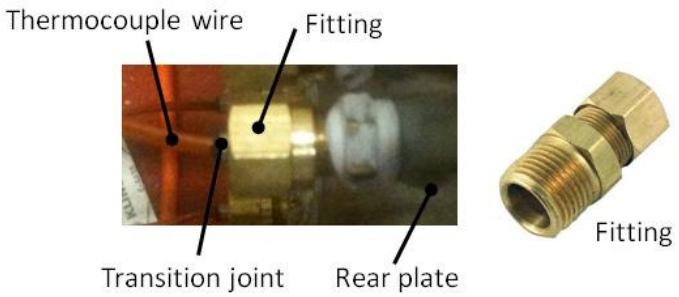

Figure 4-7, Thermocouple fixing fittings

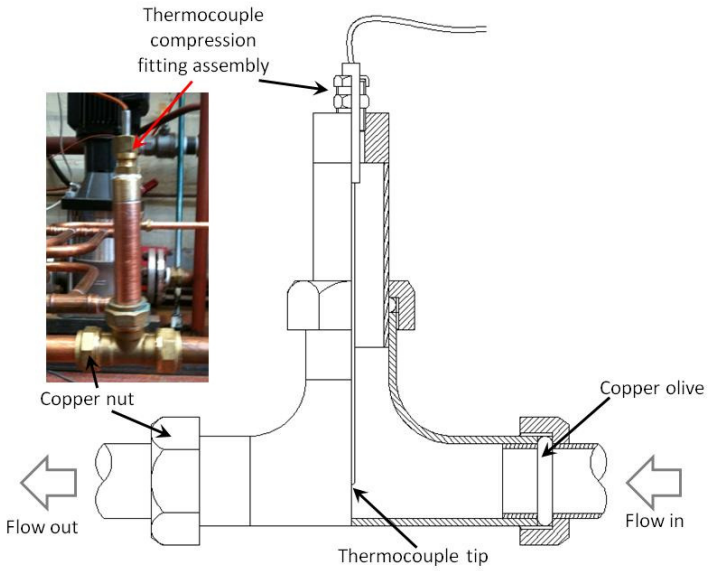

Figure 4-8, In tube flow temperature measurement assembly

Each adsorbent-bed module average temperature has been measured by means of four thermocouples of 0.5 mm diameter, fixed symmetrically at different positions. Two of these thermocouples measure the surface temperature and the other two were immersed to measure silica gel granules temperature, Figure 4-9. The thermocouples were fixed using aluminium tape to ensure firm contact with the surface. To avoid excessive thermocouple lengths, the thermocouples close to rear plate are selected to be with 150 mm probe length and the other ones are with 300 mm probes length. The secondary fluid temperature at exit from the first adsorbent bed module and, entry to the second one is measured using thermocouples of 150 mm length and 0.5 mm diameter.

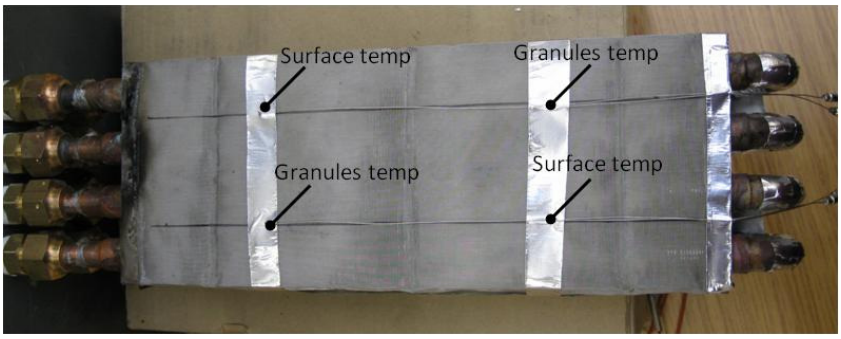

Figure 4-9, Adsorbent bed module temperature measurement

The adsorbent bed reactor internal space temperature is used for determining the saturation pressure ratio of the vapour inside the granule pores and that of the vapour maintained in the reactor space. This average space temperature is measured by means of three thermocouples with 100mm length and 1.5 mm diameter. These thermocouples are fixed in the rear plate and self suspended.

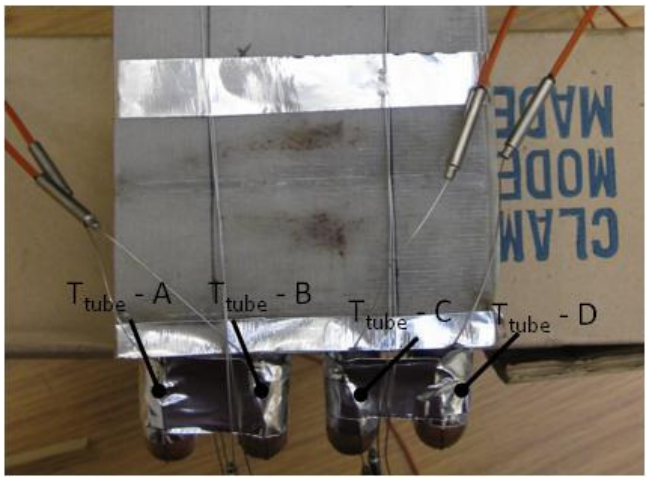

Figure 4-10, Adsorbent be module tube temperatures

Reactor shell surface acts as a condenser where its temperature is usually lower than the modules temperature averagely by 35K (based on the experimental results). The condensate is drained out of the reactor by the drainage line. The shell outside surface temperature is measured by a thermocouple with 0.5 mm diameter.

Temperatures voltage signal are logged to dataTaker-DT85, where each three thermocouples are plugged in one channel including a common terminal as shown in Figure 4-11. Before the installation, the thermocouples were calibrated using a water bath with temperature control and Resistance Thermometer Detector (RTD) thermocouples Figure 4-12. The calculated uncertainty of the temperature measurements is ±0.3.

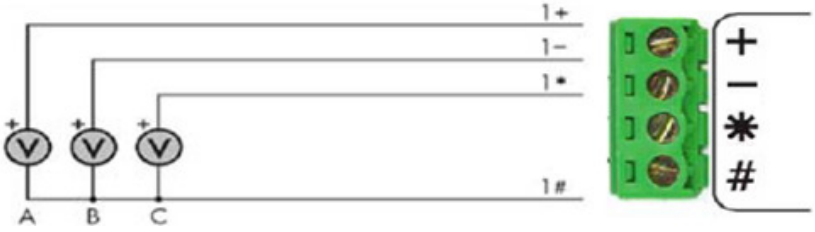

Figure 4-11, Shared terminal voltage input

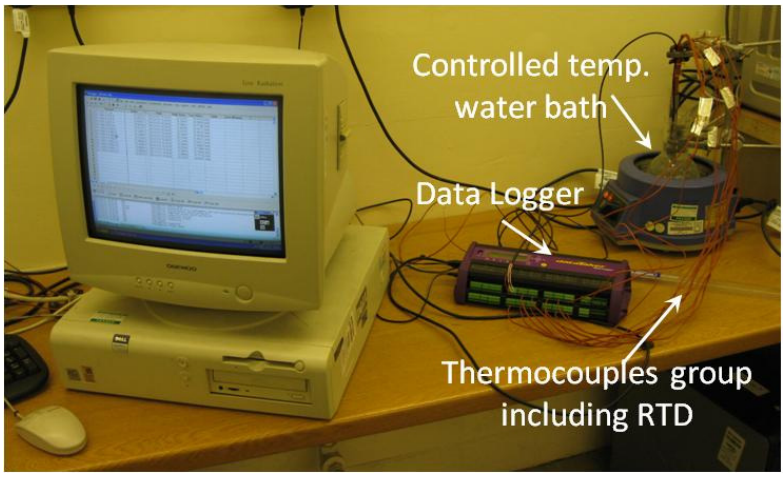

Figure 4-12, Thermocouples calibration

4.3.2 Flow rate measurement

Secondary fluid flow rates are measured using turbine flow sensor that generally has relative high level of accuracy, repeatability and resolution. The selected flow meter is FP-200 Omega-UK with 2-68 kg/min flow rate range, Figure 4-14. The turbine flow sensor integrates a tangential turbine with analogue to digital conversion circuit that is hermetically encapsulated within the body of the senor. The electronic circuit is two-wire loop-powered design that transmits 4-20 mA signals, which is proportional to the flow rate. The circuit energized by 12-35 V-DC power source. Figure 4-15 presents sensor, power supply and data logger circuit wiring. The flow meter was calibrated against a rotameter of metallic tube, where the average standard deviation of the output current was found to be I-0.1 mA. The commonly used calibration method (bucket and stop watch) was not used because of the large flow rate. The relation between flow rate and output current is shown in Figure 4-13 and equation 4-1 is a linear fitting with R^2 of 0.998.

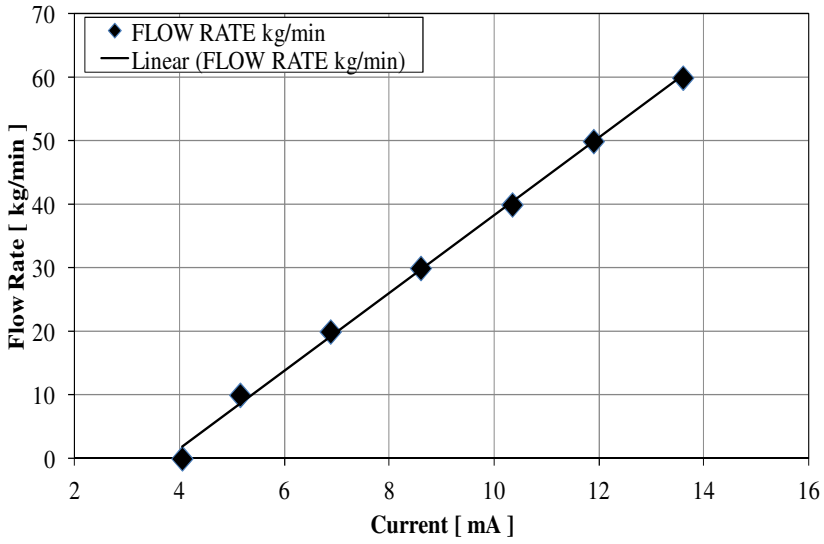

Figure 4-13, Flow meter calibration chart

$$\dot{m} = 6.128 \times I - 22.957 \qquad 4\text{-}1$$

Where $\dot{m}$ and I are water mass flow rate in (kg/min) and output current in (mA) respectively. Equation 4-1 is valid for the flow meter in range 0-60 kg/min and in the experiments the flow range used is 15-30 kg/min.

Figure 4-14, FP-200 flow meter

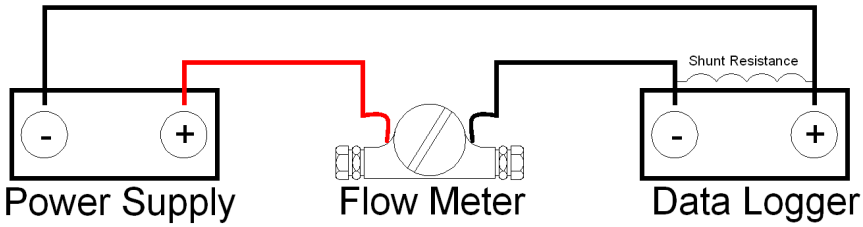

Figure 4-15, Flow meter wiring diagram

4.3.3 Vacuum pressure measurement

A factory-calibrated Bourdon vacuum pressure gage was installed to measure the vacuum level of the test rig. The vacuum measurements included adsorbent bed reactor during regeneration period and reactor / refrigerant flask during adsorption mode.

4.4 Test rig commissioning

After the installation of the adsorbent bed reactor and integrating it with the test plant, including cooling / heating water tank and refrigerant flask, the system was ready for commissioning and initial testing for the various aspects of the investigation. Firstly, the system was pressurized up to 1bar$_g$ to inspect the leakage locations using liquid soap. After ensuring that the test rig is capable of holding vacuum, the refrigerant flask was filled with 900 mL of deionised water. The leakage in the secondary flow side was also inspected before and after component assembly. During testing the following consideration where taken into account.

4.5 Testing procedure

The following steps describe the testing procedure in details.

1- The adsorbent bed reactor is fully vacuumed and the refrigerant flask is isolated. After obtaining full vacuum condition, the vacuum pump was switched off and isolated.

2- The secondary fluid (water) tank is filled and water started to be heated up. The secondary fluid flow control valve is closed.

3- When the water temperature becomes over 60°C, the water pump is turned on and the flow control valve is closed while the bypass valve is open. The water temperature decreased where the pump, tubes and valves temperature lower than hot water temperature.

4- When the water tank temperature is raised again over 60°C the flow control valve is opened to start adsorbent bed regeneration. The water flow rate is regulated using the flow control valve and the bypass valve simultaneously.

5- The reactor is kept heated for one hour, then the reactor pressure increased gradually by opening the drain line to facilitate condensing the refrigerant vapour to be collected via the drainage line.

6- The previous step is repeated four times to insure the dryness of the adsorbent bed reactor.

7- The water control valve is closed then the pump is turned off and subsequently the water tank is drained and then filled with cold water from the mains.

8- The water pump is turned on, while the bypass valve is fully open. During very short time the flow is stabilised and the flow control valve is opened gradually to allow the water flow through the adsorbent bed. The required flow rate is controlled by the flow control valve and bypass valve.

9- The adsorbent bed is pre-cooled for five minutes and subsequently the refrigerant flask is connected to the adsorbent bed to start the adsorption process. During this process the connection line including the connection valve temperatures are maintained at about 10 degrees above the refrigerant temperature to avoid water vapour condensation. During the pre-cooling and adsorption process the vacuum pump is turned on.

10- After the adsorption period for the predefined sorption time, the refrigerant flask is isolated, flow control valve is fully closed, vacuum pump is stopped and secondary flow pump is turned off.

11- The data logged is unloaded, the refrigerant level in the flask is recorded and the condensed water vapour in the separation tank is measured for analysis.

4.6 Repeatability test

Initially, the test facility was examined through a repeatability test to determine the consistency of the measuring devices. Table 4-1 presents the results of three independent tests including the average value of the measured parameters and the standard deviation. It can be seen that the three tests measurements with maximum standard deviation 1.71, which indicates the consistency of the measuring devices.

Table 4-1, Preliminary test results

Regeneration period [4hrs]							
Test	**Flow rate (l/m)**	**Bed temp (°C)**	**Bed space temp (°C)**	**i/p temp (°C)**	**o/p temp (°C)**	**Ref temp (°C)**	**Flask level (ml)**
1	29.71	61.29	34.56	63.01	62.81	40.10	900
2	26.70	61.28	35.20	62.93	62.81	40.27	900
3	27.56	61.37	36.29	63.00	62.80	40.55	900
Average	27.99	61.31	35.35	62.98	62.81	40.31	900
Std dev	1.55	0.05	0.88	0.01	0.04	0.23	0.00
Pre-cooling period [5min]							
Test	Flow rate (l/m)	Bed temp (°C)	Bed space temp (°C)	i/p temp (°C)	o/p temp (°C)	Ref temp (°C)	Flask level (ml)
1	30.91	29.04	18.04	26.54	27.13	40.81	900
2	29.50	29.09	13.62	26.07	26.31	40.33	900
3	29.46	29.65	14.04	27.24	27.63	40.69	900
Average	29.96	29.26	15.23	26.62	27.02	40.61	900
Std dev	0.83	0.34	2.44	0.67	0.59	0.25	0.00
Adsorption period [15min]							
Test	Flow rate (l/m)	Bed temp (°C)	Bed space temp (°C)	i/p temp (°C)	o/p temp (°C)	Ref temp (°C)	Flask level (ml)
1	30.99	23.96	17.88	21.84	22.19	25.67	850
2	28.59	23.32	15.08	20.83	21.04	25.59	850
3	30.53	24.21	14.45	21.92	22.26	25.53	851
Average	30.37	23.83	15.81	21.53	21.83	25.60	850.33
Std dev	1.71	0.46	1.83	0.68	0.61	0.07	0.58

CHAPTER 5: OPERATING CONDITIONS EFFECT ON CHILLER PERFORMANCE

5.1 Introduction

Chapter 3 presented the construction of a global simulation model for two bed silica gel/water adsorption chiller. Chapter 4 presented the construction of the test rig that is used for evaluating the effect of operating conditions on a scaled down rectangular finned tube adsorbent bed performance. The operating conditions affect adsorption chiller performance and it hence could be optimised to obtain better performance [154]. Operating temperatures of cooling, heating and chilled water influence the chiller performance and it could be used as a load control tool in part load operation [155-157]. The flow rate of cooling, heating and chilled water is also one of the operating parameters that influence the chiller performance [131, 134]. The time required for different operating modes (adsorption / desorption, mass recovery and heat recovery) also influences the chiller performance [158-163]. Therefore the effect of operating conditions on the performance of simulated chiller is important to determine the conditions that can increase the output of the chiller.

The effect of operating conditions on the chiller performance will be experimentally and theoretically investigated in this chapter. A population based global optimization technique, namely genetic algorithm (GA) will be used as a tool to determine the optimum operating conditions corresponding to the best cooling capacity. Prior to investigating the effect of operating conditions on the performance of the simulated adsorption chiller, the simulation

model was validated. The chiller performance at the design operating conditions will be used as the baseline for comparison and these listed in Table 5-1.

Table 5-1, Chiller reference operating conditions at design operation

Operation condition	Value
Chilled water inlet temperature	11°C
Cooling water inlet temperature	29.5°C
Heating water inlet temperature	88.5°C
Chilled water flow rate	1180 LPM
Cooling water flow rate	4000 LPM
Heating water flow rate	1100 LPM
Adsorption desorption time	430 seconds
Mass recovery time	30 seconds
Heat recovery time	20 seconds

5.2 Validation of the simulation model

Figure 5-1 compares the predicted chilled, cooling and heating water outlet temperatures and their actual analogous values which were supplied by the manufacturer based on the same average inlet conditions. Table 5-2 presents the average percent deviation (APD) and absolute average percent deviation (ABS-PD) for cooling, heating and chilled water outlet temperatures for the test results shown in Figure 5-1. The deviation between the predicted COP, heating load and cooling capacity are also presented. It is known that the predicted values of thermal simulation models can be accepted if the absolute average percent deviation is below 30%, [164]. Table 5-2 and Figure 5-1 indicate clearly the good agreement between the model and experimental results.

$$\mathrm{APD} = \frac{1}{N_{data}} \sum_{0}^{N_{data}} \frac{\text{Predicted value - experiment value}}{\text{experiment value}} \cdot 100 \qquad 5\text{-}1$$

$$ABS - PD = \frac{1}{N_{data}} \sum_{0}^{N_{data}} \frac{\left|Predicted\ \ value\ \ -\ \ experiment\ \ value\right|}{experiment\ \ value} \cdot 100 \qquad 5\text{-}2$$

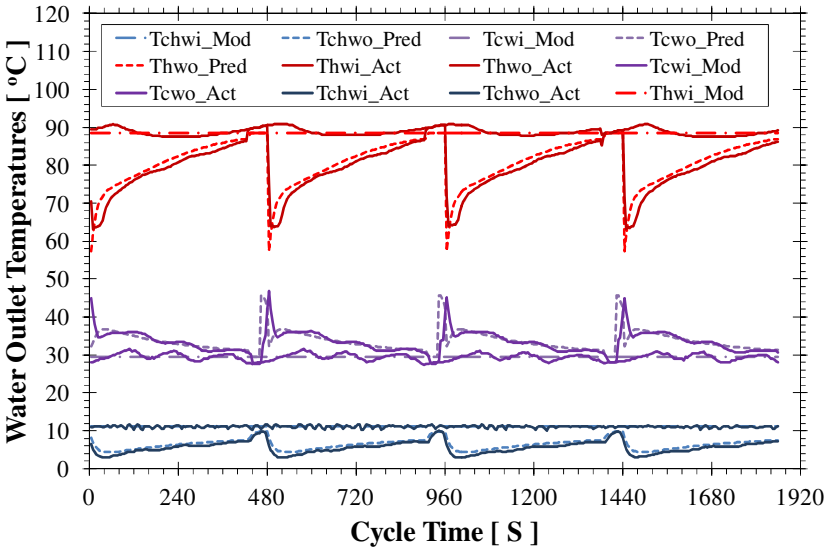

Figure 5-1, Comparison between predicted data and actual data

Table 5-2, Simulation model deviation analysis
($\dot{m}_{hw}$ =1100 LPM, $\dot{m}_{cw}$ =4000 LPM, $\dot{m}_{chw}$ =1180 LPM)

Term	APD	ABS-PD	Term	APD	ABS-PD
$T_{hw,o}$	-1.6%	2.4%	Q_{evap}	12.9%	12.9%
$T_{cw,o}$	-1.1%	3.4%	Q_{heat}	10.9%	10.9%
$T_{chw,o}$	-16.5%	16.5%	COP	2.8%	2.7%

Table 5-3 presents the absolute average percent deviation for average cooling, heating and chilled water outlet temperature in addition to cooling capacity, heating power and COP for different experimental runs. It can be seen that the maximum absolute percent deviation calculated based on steady state cycle is 17.8%.

Table 5-3, Simulation model deviation analysis at one steady state cycle

Term	RUN-1		RUN-2		RUN-3		RUN-4		unit
$\dot{m}_{hw}$	1100		1100		1100		2200		LPM
$\dot{m}_{cw}$	4000		4000		4000		4000		LPM
$\dot{m}_{chw}$	1180		1180		1180		1320		LPM
$T_{hw,i,av}$	88.6		89.0		88.8		88.2		°C
$T_{cw,i,av}$	29.5		29.4		29.4		29.2		°C
$T_{chw,i,av}$	11.1		11.1		11.1		11.1		°C
Deviation analysis (actual o/p temperature & ABS-PD)									
$T_{hw,o}$	79.7	1.6	80.1	1.5	79.9	1.6	83.3	0.9	°C & %
$T_{cw,o}$	33.4	0.9	33.4	0.8	33.3	1.0	33.6	0.0	°C & %
$T_{chw,o}$	5.8	12.3	5.7	13.1	5.7	13.3	5.8	15.7	°C & %
Q_{heat}	650	10.3	654	9.9	652	9.9	704	10.6	°C & %
Q_{cool}	439	13.1	446	13.6	444	13.5	487	17.8	°C & %
COP	0.68	3.7	0.68	3.9	0.68	3.8	0.69	7.8	°C & %

5.3 Operating temperatures

Cooling / Heating water inlet temperature influences adsorption chiller performance. Lowering cooling water inlet temperature not only increases cooling capacity, but also enhances adsorption chiller COP, due to the significant increase in adsorption rate. Increasing heating water temperature also enhances chiller cooling capacity due to enhancing desorption rate that generate the adsorbed refrigerant prior to the adsorption / evaporation mode. However, it negatively influences the chiller COP depending on the cooling water inlet temperature. As a result, the generation temperature lift defined as the difference between heating water inlet temperature and cooling water inlet temperature [129] was calculated and used in the investigation. It is noteworthy to mention that the chilled water inlet temperature depends mainly on the application and hence it was kept constant at its design value.

Figure 5-2 presents the change in chiller cooling capacity versus generation temperature lift at various cooling water inlet temperatures. Other operating conditions (cycle time and secondary fluid flow rate) remain constant at their design values. As the generation temperature lift increases the chiller cooling capacity increases for all cooling water inlet temperatures. On Figure 5-2, the experimental results at the operating conditions as shown in table 5-3 are presented with good agreement with the model.

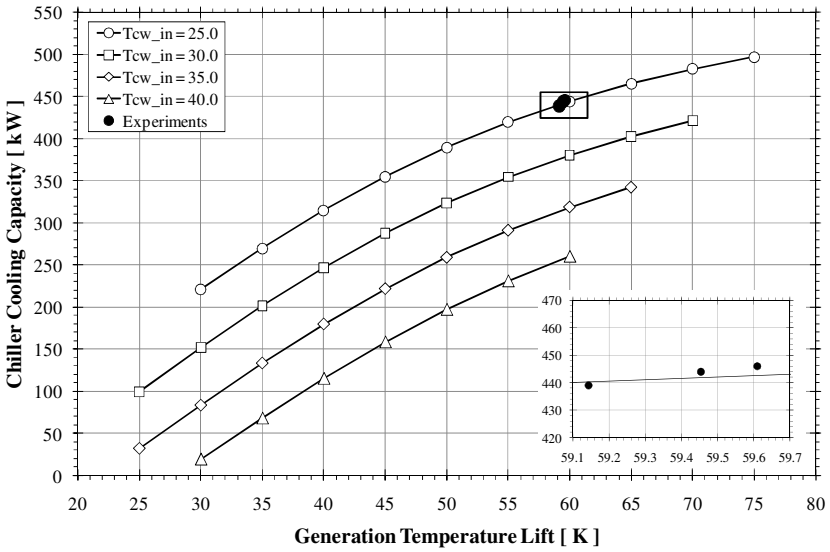

Figure 5-2, Generation temperature lift influence on chiller performance

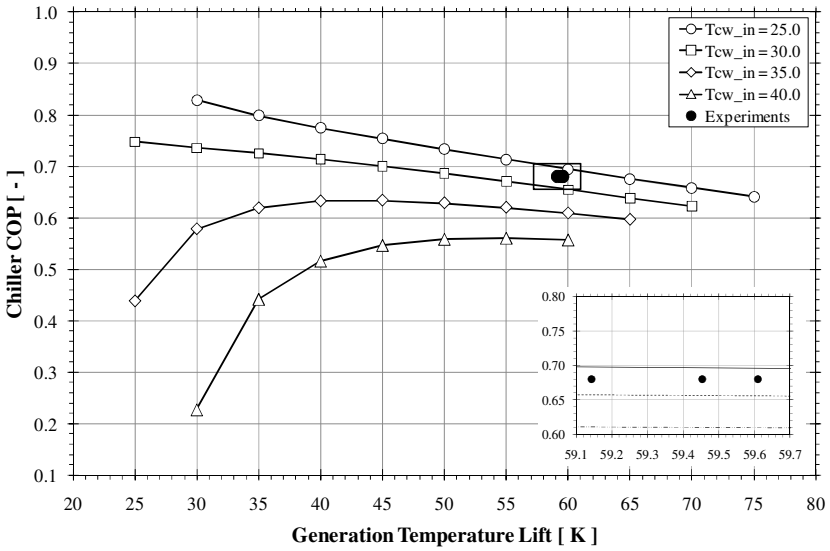

Figure 5-3, The influence of generation temperature lift on chiller COP.

Figure 5 3 and 5-4 present the variation in the chiller COP and its efficiency versus generation temperature lift. Here it is noteworthy that the efficiency is defined as the rate of the chiller actual COP to the COP of ideal reversed Carnot cycle equations 3 38 and 3 39. It is observed that at low cooling water temperature, the chiller COP and efficiency decreased with increasing the generation temperature lift within the tested range. However, at higher cooling water temperature (Tcw>30°C), the chiller' COP initially increased to a certain point and then remained relatively constant with the increase in the generation temperature lift. On the other hand, the chiller efficiency after reaching the maximum point decreased with increasing the generation temperature lift. The decrease in chiller COP and efficiency at low generation temperature lift and high cooling water temperature is due to the insufficient refrigerant circulation required to generate the cooling power. On the other hand, the decrease in chiller COP and efficiency at high temperature lift is due to the increase in heat losses [130].

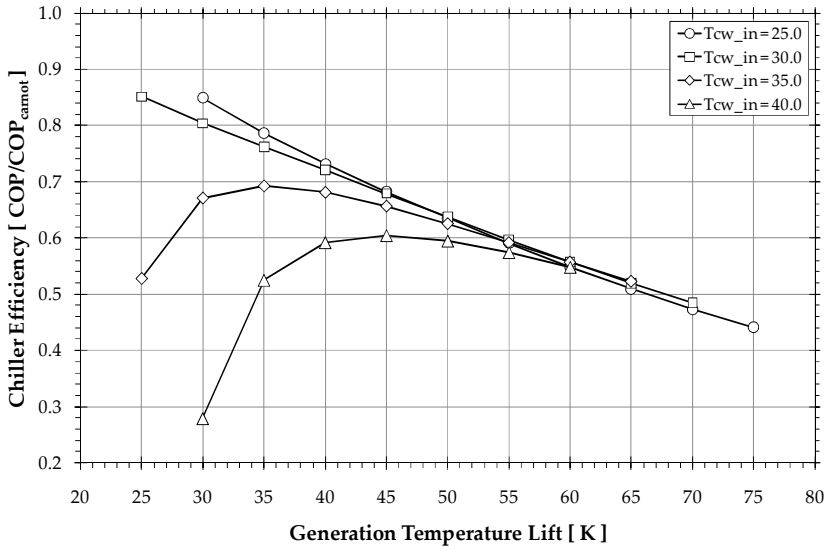

Figure 5-4, the influence of generation temperature lift on chiller efficiency

The variation of chiller COP and efficiency with the generation temperature lift can be used as a load control tool. For example, at cooling water temperature of 35°C, the chiller cooling capacity increased almost linearly (from 180 to 342kW) with increasing the generation temperature lift (from 40 to 65K). The reduction in chiller COP (from 0.63 to 0.60) and efficiency (from 0.68 to 0.52) are relatively small.

5.4 Cycle timing

During the physical adsorption process, the solid adsorbent adsorbs the refrigerant from the evaporator container to develop a cooling effect by means of refrigerant evaporation. The adsorption process is an exothermic and the heat generated is removed to sustain the adsorption process and maintain the cooling effect. However for specific adsorption time, the rate of adsorption decreases with increasing the amount of refrigerant adsorbed until the bed becomes saturated with refrigerant. Hence the cooling effect reduces with increasing the adsorption time. The adsorbent bed is regenerated by heating and the desorbed refrigerant is condensed and passed back to the evaporator to repeat the aforementioned process. As the adsorption time increases, the heating load decreases and hot water outlet temperature approaches the inlet temperature. This will increase the COP but decrease the cooling capacity.

Continuous cooling is achieved by using two beds, where one bed is connected to the evaporator in adsorption mode and the other bed to the condenser in desorption mode. Before reversing adsorption and desorption modes sufficient time period is required to preheat / pre-cool the adsorption / desorption beds to avoid premature connection between the hot bed and evaporator which results in momentary desorption of adsorbed refrigerant

and undesirable reduction in instantaneous cooling capacity. It is noteworthy that during switching period there is no interconnection between adsorbent beds and evaporator / condenser where no cooling effect can be achieved. As a result, appropriate switching time can improve the cooling capacity and COP of the adsorption chiller. The following section experimentally investigate the effect of adsorption time period on the adsorbent bed performance followed by theoretical investigation for the effect of operating conditions on the simulated adsorption chiller performance.

5.4.1 Experimental investigation of the adsorption time period

This section experimentally investigates the effect of adsorption time period on the performance of the scaled down adsorbent bed fitted in the test facility described in chapter 4. The adsorption time is the most important operation period. The investigated parameters are the amount of adsorbed refrigerant, the change of liquid refrigerant temperature during adsorption process and the heat removed from the liquid refrigerant. Figure 5-5 presents the amount of adsorbed refrigerant at various adsorption time period. The amount of refrigerant, the refrigerant temperature at the beginning of adsorption process and the regeneration temperature are fixed at 900gm, 40°C and 65°C respectively. Eight independent runs have been achieved and it is observed that the amount of adsorbed water vapour significantly increases during the first 600 seconds and then minimally increases to reach the saturation conditions.

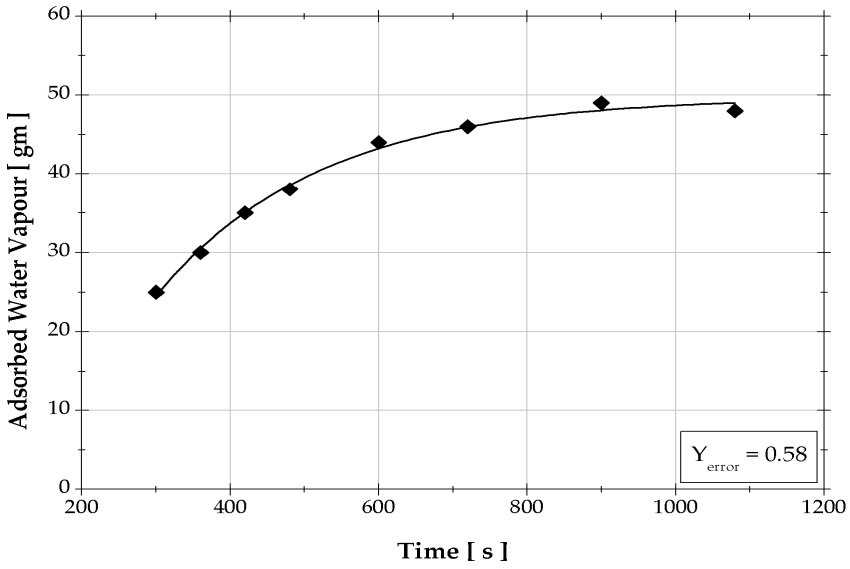

Figure 5-5, Adsorption amount versus adsorption time

Figure 5-6 presents the temperature of liquid refrigerant during adsorption period. Figure 5-7 presents the heat removed from the liquid refrigerant versus adsorption time, where the experimental data were exponentially fitted. It can be observed that the liquid refrigerant temperature decreases gradually during the first 600 seconds. This corresponds to gradual increase of the heat removed during this time period 0-60.7 kJ. Subsequently, the change in the liquid refrigerant temperature and the heat removed is negligible. This is due to the reduction in the refrigerant evaporation by means of adsorption.

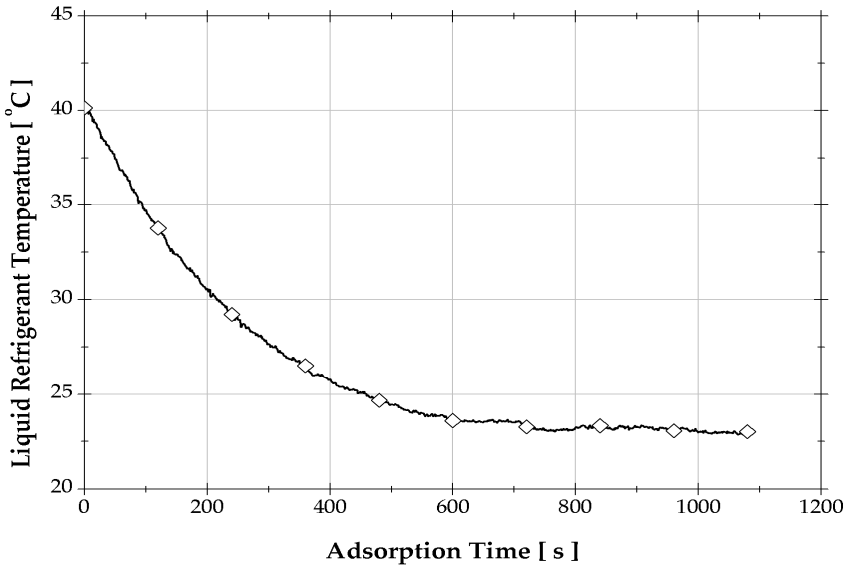

Figure 5-6, Refrigerant temperature during adsorption period

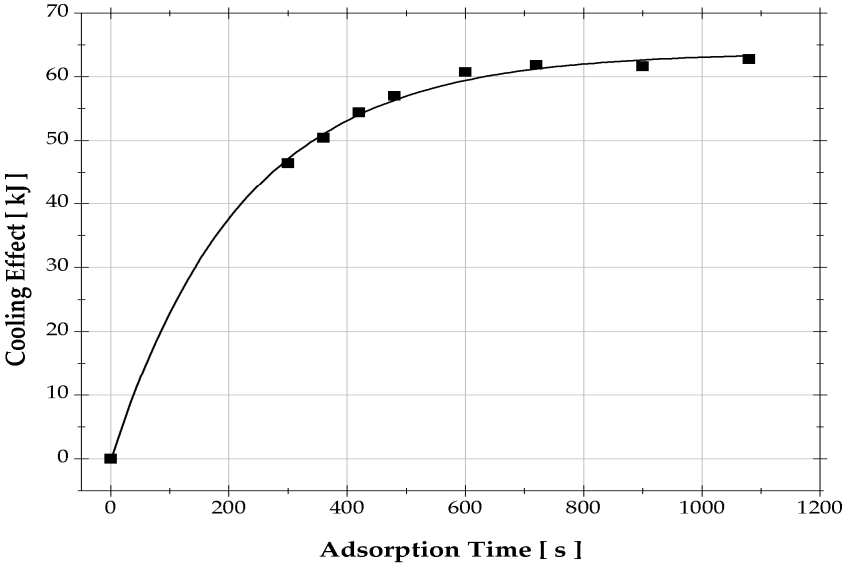

Figure 5-7, Heat removed (cooling effect) from the liquid refrigerant

5.4.2 Theoretical investigation of the cycle timing

In the simulated adsorption chiller, the switching period is divided into mass and heat recovery periods. Figure 5-8, 5-9 and 5-10 present the effect of changing adsorption / desorption and mass recovery time periods simultaneously on chiller performance for

different heat recovery times. The operating temperatures and flow rates are kept constant at design values, shown in Table 5-1. Figure 5-8 shows that as adsorption / desorption time period increases, chiller cooling capacity gradually increases, reaches a maximum at certain time (250 – 450 seconds) and then decreases gradually. Within the investigated range, it was observed that the maximum cooling capacity using 20s, 60s and 100s as heat recovery times are 6.1% and 0.4% higher and 5.7% lower than the cooling capacity obtained at the design operating times given in Table 5-1. The observed cooling capacity trends are similar to that of the experimental results of adsorbed water vapour and heat versus adsorption time Figure 5-6 and 5-7.

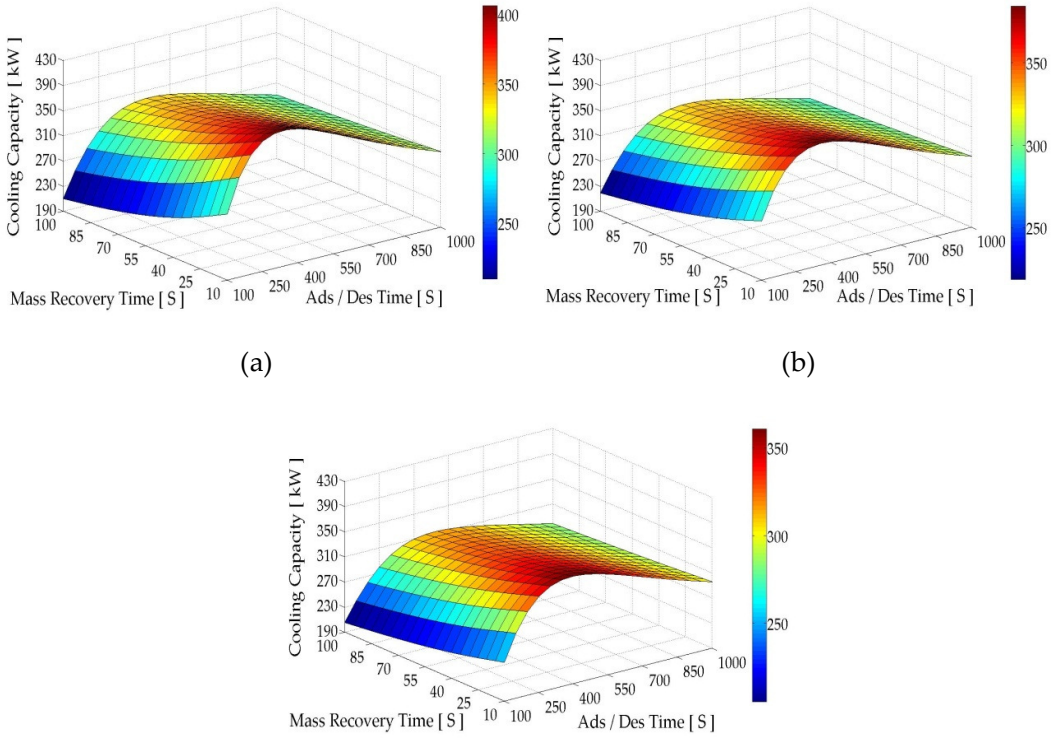

Figure 5-8, the effect of Ads/Des and mass recovery time period on chiller cooling capacity (a) $t_{heat\ recovery}$=20s (b) $t_{heat\ recovery}$=60s (c) $t_{heat\ recovery}$=100s

Figure 5-10 shows that the COP of the simulated chiller increases gradually by increasing both of adsorption / desorption and mass recovery time, as the heating capacity consumed by the chiller is decreasing. Within the investigation range, the maximum COP can be obtained at maximum adsorption / desorption and mass recovery time, which correspond to the minimum heating capacity and maximum adsorbed refrigerant amount. The maximum value of chiller COP within the investigated range changes by changing heat recovery time according to Figure 5-11. Based on the aforementioned results, the optimum cycle time (adsorption / desorption, heat recovery and mass recovery) need to be determined using global optimisation technique such as genetic algorithm.

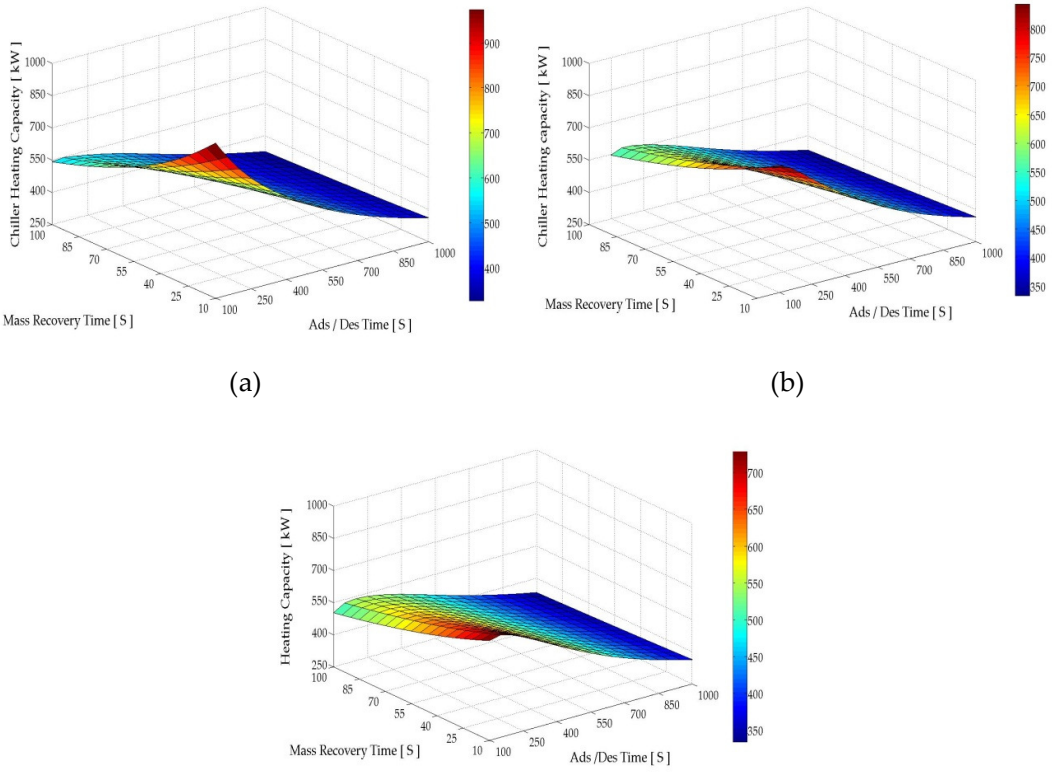

Figure 5-9, The effect of Ads/Des and mass recovery time period on chiller heating capacity (a) $t_{heat\ recovery}$=20s (b) $t_{heat\ recovery}$=60s (c) $t_{heat\ recovery}$=100s

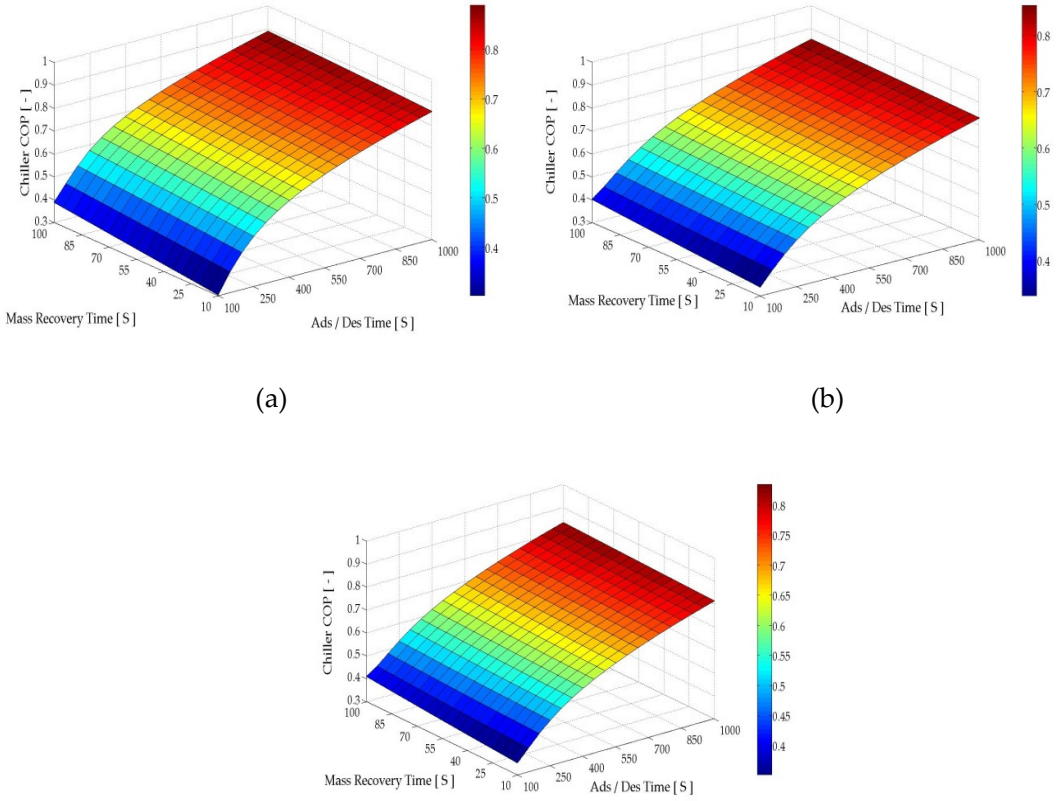

Figure 5-10, The effect of Ads/Des and mass recovery time period on chiller COP(a) $t_{heat\ recovery}$=20s (b) $t_{heat\ recovery}$=60s (c) $t_{heat\ recovery}$=100s

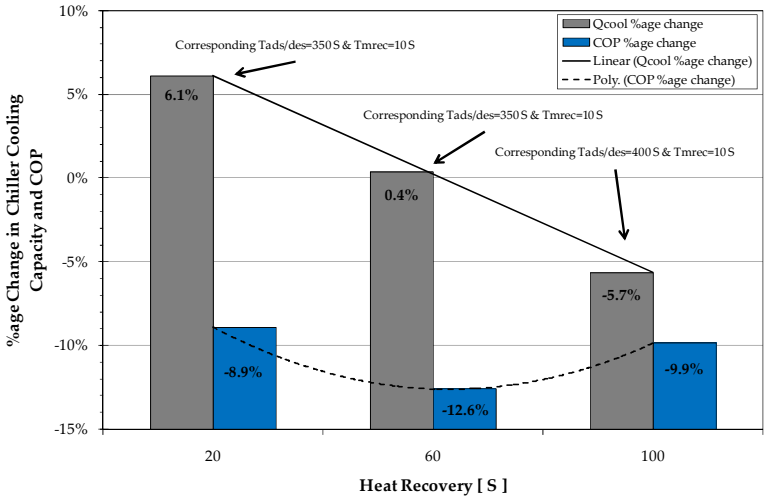

Figure 5-11, Chiller performance at maximum cooling capacity point

5.4.3 Cycle time optimisation

Within time range of 250-450 seconds for adsorption / desorption time period and 10-50 seconds for mass and heat recovery time periods a point of maximum cooling capacity have been recognized. The corresponding value of COP could be lower than design value as shown in Figure 5-11. Within this time region a GA global optimization is applied using chiller cooling capacity and COP as objective functions, one at a time using two independent runs. The number of population for each individual parameter (adsorption / desorption, mass recovery and heat recovery time) is selected to be 20 while the number of elite count is 2, the crossover fraction is 0.8 and the rest of individuals are managed by mutation rule as described in chapter 3. These were recommended by Mathwork GA Manual® [153].

After 30 and 16 iterations, the GA solver terminated while determining the maximum chiller cooling capacity and COP respectively, where no more improvement in the solution in terms of objective function value, average diversity and best, worst and mean score shown in Figure 5-12 and 5-13. The determined optimum adsorption / desorption, mass recovery and heat recovery time period values corresponding to maximum cooling capacity are 345, 12 and 14 seconds respectively (OPTIM-A). However, the optimum adsorption / desorption, mass recovery and heat recovery time values corresponding to maximum chiller COP are 443, 49 and 24 seconds respectively (OPTIM -B). Chiller cooling capacity at OPTIM-A increased by 8.3%, but its COP reduced by 9% compared to their analogues reference values. Chiller COP at OPTIM-B increased by 1.5%, but its cooling capacity dropped by 4.2% compared to their analogues reference values as shown in table 5-4. Based on these results it could be concluded that there are two optional operation cycle timing, OPTIM-A where it

can be used in case of maximum load demand or OPTIM-B which can be used in case of maximum COP demand. Reducing the chiller COP by 9% to increase the cooling capacity by 8.3%, where most of the adsorption chillers are driven by waste heat sources.

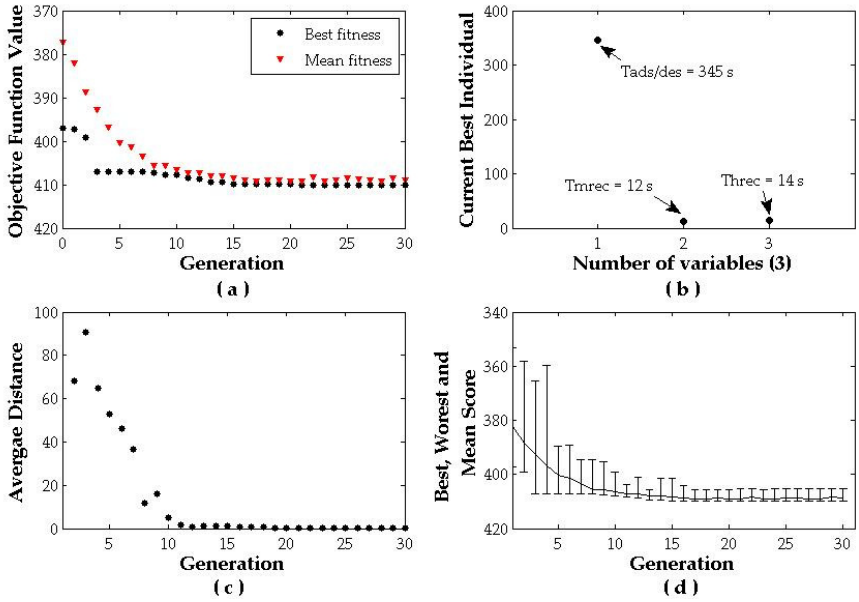

Figure 5-12, Optimisation toolbox results for determining OPTIM-A

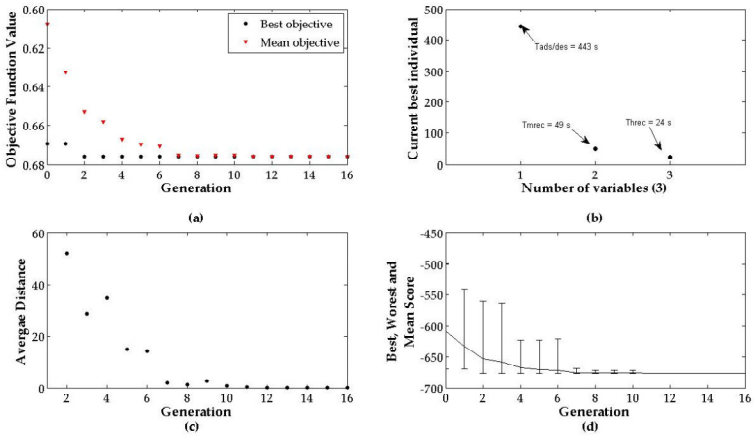

Figure 5-13, Optimisation toolbox results for determining OPTIM-B

Table 5-4, Chiller performance at different operation conditions

Operation conditions	Cooling capacity [kW]	COP [-]
Design operating	382.32	0.66
OPTIM-A	410	0.60
OPTIM-B	366.29	0.67

5.5 Secondary fluid flow rate

Cooling / heating water flow rate significantly influences chiller performance while chilled water flow is determined by the application. As cooling / heating water flow rate increases the heat transfer to the adsorbent bed increases, and then the rate of adsorption / desorption increases. This results in increasing the refrigerant circulating flow rate through the adsorption chiller and then the cooling capacity. Moreover, the condensation rate increases due to the increase in the rate of cooling, because the condensation cooling stream is linked to bed cooling stream during the adsorption mode.

5.5.1 Experimental investigation of cooling water flow rate

During the switching time period the adsorbent bed temperature and hence the saturation pressure of the refrigerant vapour are switched to avoid premature connection between the hot bed and evaporator. This section experimentally investigates the effect of changing cooling water flow rate on the adsorbent bed performance in terms of adsorbent bed module/space temperature during switching time and the amount of adsorbed refrigerant during adsorption period. During the experiments the amount of refrigerant, the refrigerant temperature at the beginning of adsorption process and the regeneration temperature are fixed at 900gm, 40°C and 65°C respectively.

Figure 5-14 presents the change of the adsorbent bed modules temperature during pre-cooling using two different flow rates. It is observed that during the first 50 seconds the adsorbent bed temperature decreases steeply and the determined temperature drop is 21.8 and 26.4 degrees using cooling water flow rate of 0.27 and 0.48 l/s respectively. During the next 550 seconds the adsorbent bed temperature minimally decreases and the recorded temperature drop is 11 and 8 degrees using cooling water flow rate of 0.27 and 0.48 l/s. During pre-cooling period the adsorbent bed temperature utilizing 0.48 l/s cooling flow rate is averagely 4 degrees lower than that utilizing 0.28 l/s.

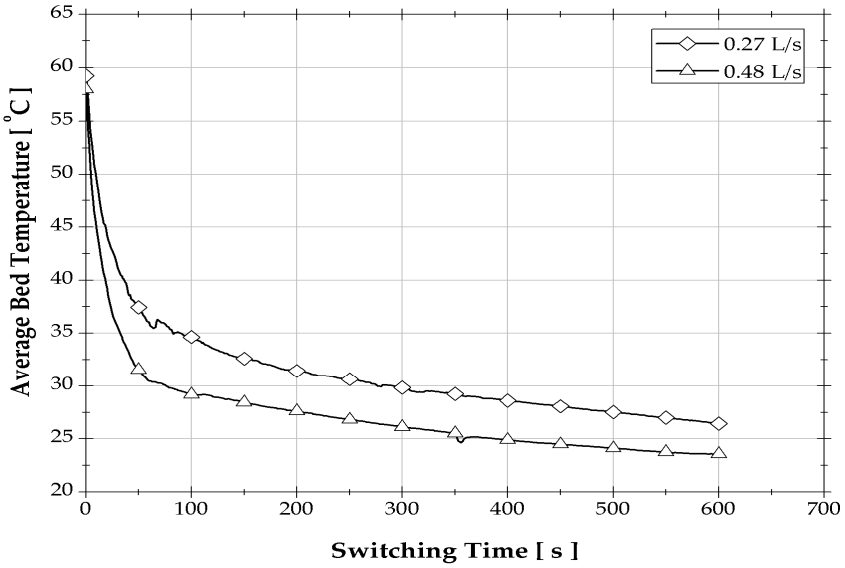

Figure 5-14, Average adsorbent bed temperature versus switching time at different flow rate

Figure 5-15 presents the change of adsorbent bed reactor shell space temperature during switching period by applying cooling water flow rates of 0.27 l/s and 0.48 l/s. It is observed that the space temperature drops steeply then remains almost constant. At flow rate of 0.27 l/s, the shell space temperature decreases from 35°C to 20°C (temperature difference of 15K)

during the first 90 seconds. At flow rate of o.48 l/s, the shell space temperature dropped from 35°C to 20°C within the first 20 seconds. The average reactor space temperature in case of applying 0.48 l/s is lower than that of applying 0.27 l/s by 5 degrees. By applying a higher flow rate the switching time period is shorter and lower temperature of the adsorbent bed, including adsorbent bed modules and reactor space.

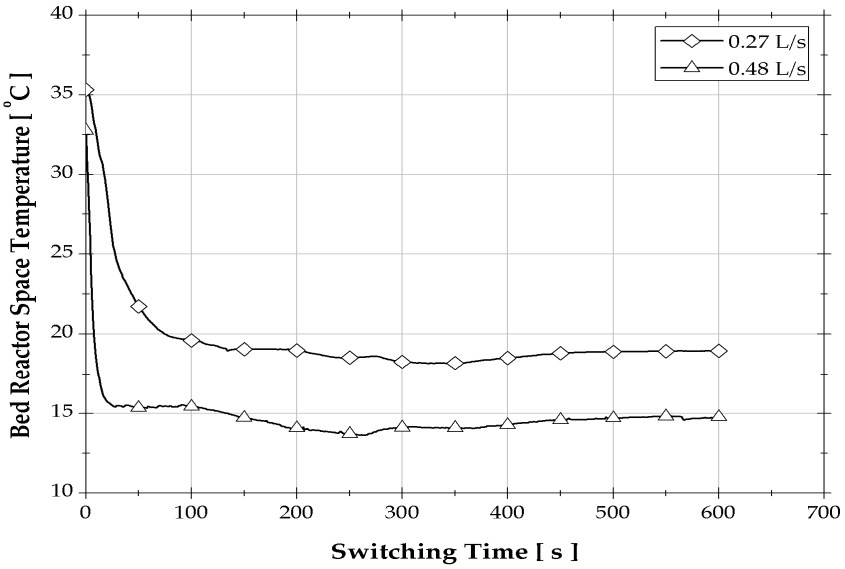

Figure 5-15, Average adsorbent bed reactor space temperature versus switching time at different flow rate

Figure 5-16 presents the amount of adsorbed refrigerant at different adsorption time (300, 360, 420 and 480 min) using two flow rates 0.27 and 0.48 l/s. It can be seen that for all applied adsorption time, the adsorbed refrigerant in case of applying 0.48 l/s is averagely higher than that when applying 0.27 l/s by 5 mg of water, where;

- The adsorbent bed temperature (including adsorbent bed modules and the bed reactor space) at the end of switching period is lower in case of higher flow rate.

- The rate of heat removed from the adsorbent bed in case of higher flow rate is larger and hence more adsorption heat removed which enhances the adsorption capability of the same bed.

In general, applying higher secondary flow rates enhances the adsorption performance of the adsorbent bed; however it will increase the pumping power. This will be further explained by studying the cyclic operation of the simulated adsorption chiller theoretically.

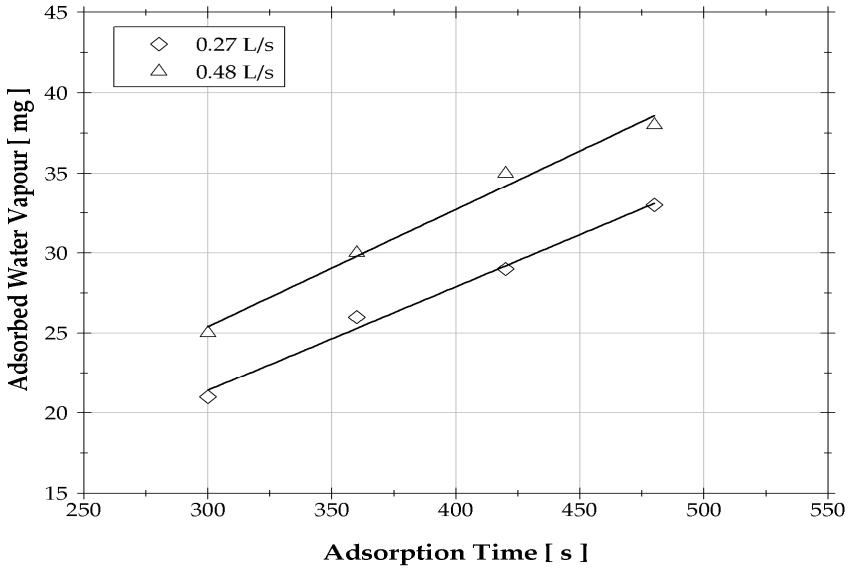

Figure 5-16, The amount of adsorbed refrigerant during adsorption time at different flow rate

5.5.2 Theoretical investigation of the cycle time

Figure 5-17, 5-18 and 5-19 present the effect of cooling and heating water flow rate on chiller performance while other operating conditions remain at design values including chilled water flow rate, Table 5-1. Figure 5-17 shows the effect of cooling water on chiller cooling capacity. As cooling water flow rate increases the chiller cooling capacity increases steeply

and then minimally. The rate of increase in cooling capacity decreases with increasing the cooling water flow rate.

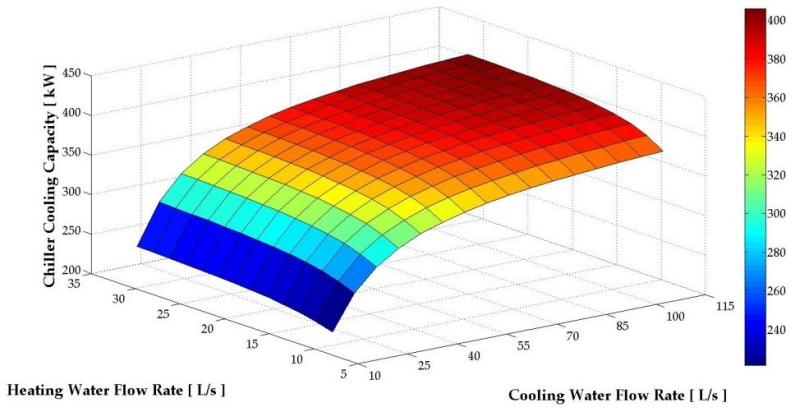

Figure 5-17, The effect of cooling and heating water flow on chiller cooling capacity

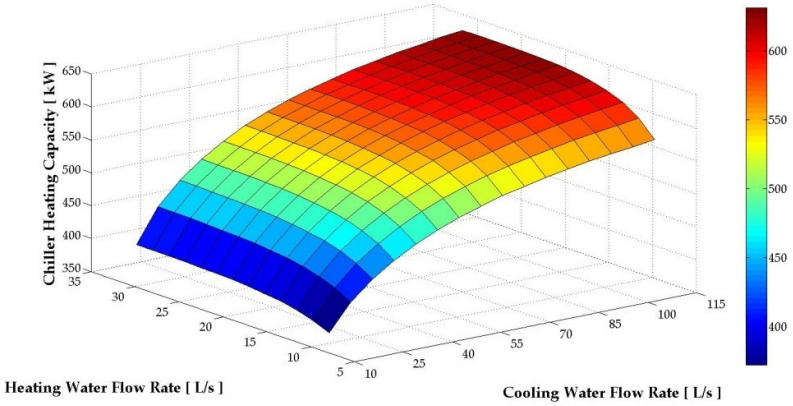

Figure 5-18, The effect of cooling and heating water flow on chiller heating capacity

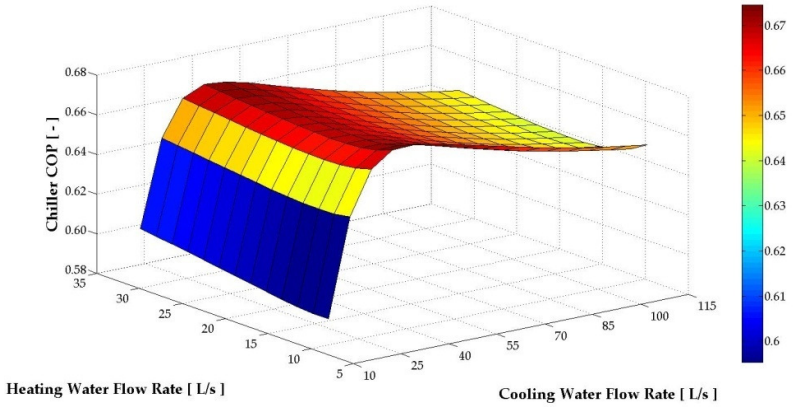

Figure 5-19, The effect of cooling and heating water flow on chiller COP

This is because the change in adsorption rate decreases as adsorbent bed becomes saturated in shorter time. This trend is the same for different heating water flow rate but with different value. As heating water flow rate increases the cooling capacity increases gradually and then remains constant due to the increase in the desorbed refrigerant.

Figure 5-18 shows that as the cooling water flow rate increases the corresponding heating capacity gradually increases to desorb the larger amount of refrigerant adsorbed due to the favourable lower adsorbent bed temperature. As heating water flow rate increases, the chiller heating capacity increases gradually and subsequently remains constant. By applying maximum cooling / heating water flow rates (150% its design value) the chiller cooling capacity increased by 25.2%.

Figure 5 19 shows the effect of cooling water and heating water flow rate on chiller COP. As the cooling water flow rate increases, chiller COP increases steeply reaches a peak at 40 l/s cooling water flow rate and subsequently reduces minimally. Also as the heating water flow rate increases, the chiller COP gradually increases. The maximum COP of 0.67 is corresponding to 8.5 and 40 l/s of heating and cooling water flow rate respectively. On the other hand, the pumping power for cooling and heating water increases gradually by increasing the flow rate as shown in Figure 5-20.

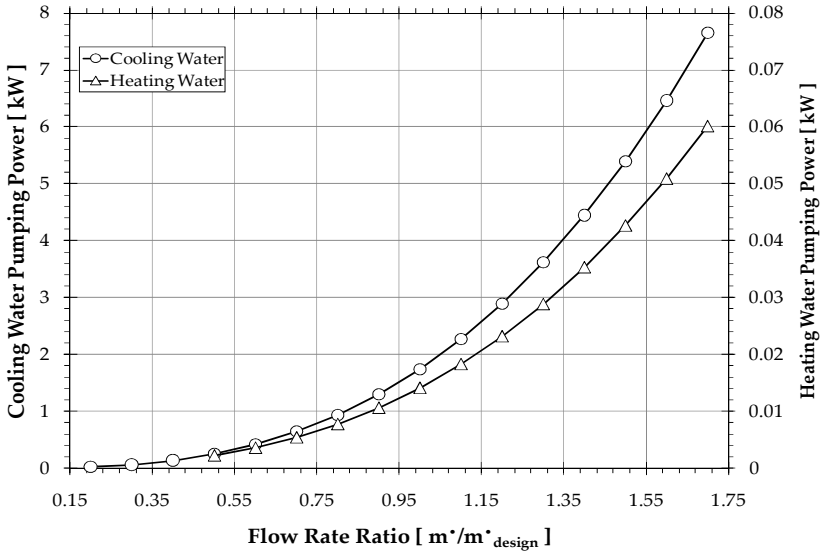

Figure 5-20, Cooling and Heating water pumping power at different flow rates

5.6 Summary

The validity of the simulation model has been investigated and a good agreement between the predicted and the experimental data has been shown. The effect of operating conditions (cycle time, operating temperature and secondary fluid flow rate) has been investigated. It has been concluded that the chiller cooling capacity increases as the generation temperature lift increases with minimal change in the chiller COP.

The effect of cycle timing has been investigated experimentally and theoretically. Generally, it is observed that as the cycle time increases the system performance is gradually enhanced and subsequently minimally reduced. Applying genetic algorithm optimisation and using the cooling capacity as an objective function, it is concluded that the chiller cooling capacity can be increased by 9%, while the COP reduced from 0.66 to 0.60.

Based on the experimental and theoretical investigation it is observed that increasing the secondary fluid flow rate enhances the overall chiller performance. However, it increases the pumping power consumption. It is conclude that generation temperature lift is preferable for the load control instead of changing the secondary fluid flow rate.

CHAPTER 6: PHYSICAL PARAMETERS EFFECT ON CHILLER PERFORMANCE AND ENHANCING TECHNIQUES

6.1 Introduction

Many commercially available adsorption cooling systems use granular packed adsorbent bed design, including the simulated chiller presented in chapter 2. Such type of adsorbent bed has the advantage of high mass transfer performance due to the high permeability level [108], but it has the drawbacks of poor heat transfer performance where; high contact thermal resistance between adsorbent granules and heat exchanger metal surface [112], discontinuity of heat transfer through granules due to the voids in-between the granules [113] and poor thermal conductivity of the commonly used physical adsorbents. Therefore many methods were investigated to enhance the heat transfer performance of adsorbent material such as mixing adsorbent granules with metal additives to improve their thermal conductivity [115], coating the bed heat exchanger metal with the adsorbent to eliminate the contact thermal resistance [112], covering adsorbent granules by polyaniline net [115], adsorbent deposition over metallic foam [108] and using consolidated bed techniques [62] (compressed granules and clay [115], using expandable graphite [120], moulding granules and binder addition [122] and adsorbent granules and metal foam [124]). Most of these methods improve the heat transfer performance of adsorbent material but reduce its mass transfer performance [125]. Detailed review for these enhancement techniques and their influence on the overall chiller performance has been presented in chapter 2.

These techniques have been proposed and / or applied, but the feasibility of applying them in the simulated chiller design has not been studied. This chapter evaluates some of the methodologies used to enhance the heat transfer performance of the adsorbent in terms of improving the bed thermal performance and the overall cooling capacity of the adsorption system.

6.2 Heat transfer resistances and bed performance

Enhancing the adsorption kinetics is necessary in order to improve the adsorption chiller performance. Using the same adsorbent / adsorbate pair, enhancing adsorption kinetics can be achieved by enhancing both heat and mass transfer performance. The parameters that affect the heat and mass transfer through the adsorbent bed ranked based on their importance are the adsorbent bed permeability, thermal contact resistance between adsorbent granules and heat exchanger metal surface and adsorbent layer thermal conductivity [112]. In packed finned-tube adsorbent bed design increasing the overall heat transfer coefficient U and heat transfer area A increase the overall heat transfer conductance UA and hence the adsorption kinetics [165, 166]. During the heat transfer from / to the secondary fluid to/from adsorbent bed surface in desorption / adsorption mode, there are six heat transfer resistances namely; (1) radial convective thermal resistance from the secondary fluid stream to the internal tube wall R1, (2) radial conduction thermal resistance through tube wall R2, (3) two contact thermal resistances between silica gel granules and tube outside surface and fins surface R3 and R4 in both radial and axial directions respectively and (4) two conduction thermal resistances through silica gel granules in radial and axial direction R5 and R6 as shown schematically in Figure 6-1.

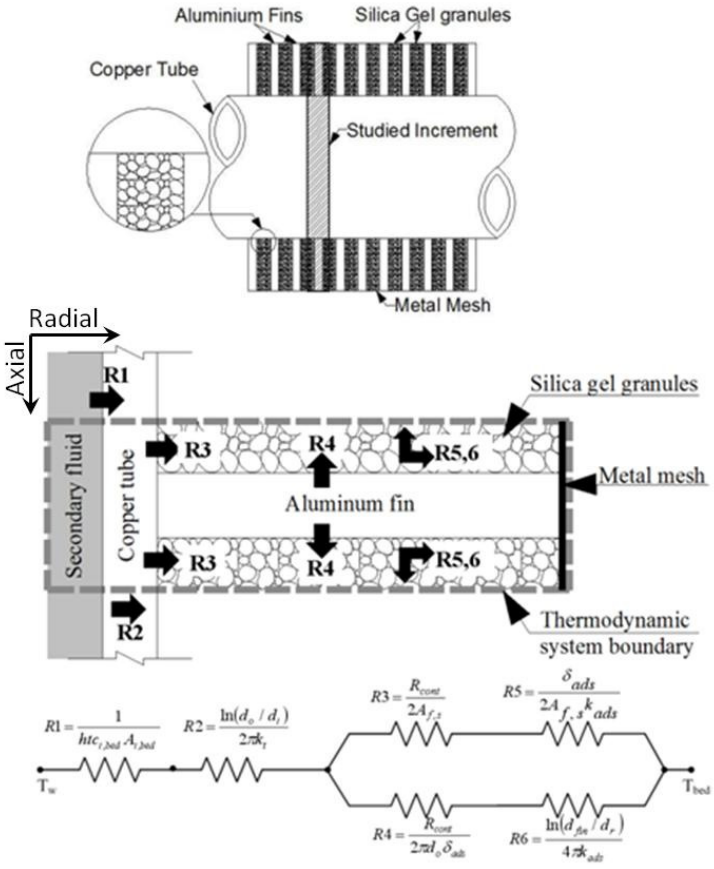

Figure 6-1, Heat transfer resistance schematic diagram

6.3 Adsorbent bed fin spacing parametric study

The simulation model is used to investigate the effect of fin configuration (fin width, height and spacing) on the adsorbent bed thermal performance, where the tube diameter is kept constant. Figure 6-2 presents different configurations for the adsorbent bed heat exchanger named loose arrangement and tight arrangement. In both cases the silica gel mass are kept constant and the minimum fin and tube spacing were selected to accommodate the same granules. Figure 6-3 presents the effect of changing fin spacing and fin width simultaneously on the fin height required to accommodate the same amount of silica gel. Figure 6-4 and 6-5

show the effect of varying the fin width and spacing ratios on the adsorbent bed heat transfer performance in terms of heat capacity ratio (HCR) and number of transfer unit (NTU). The fin spacing ratio (FSR) is the value of fin spacing relative to its design value. The fin width ratio is the fin width value relative to its design value. It is observed that changing fin width does not affect the bed HCR or NTU in case of heating and cooling.

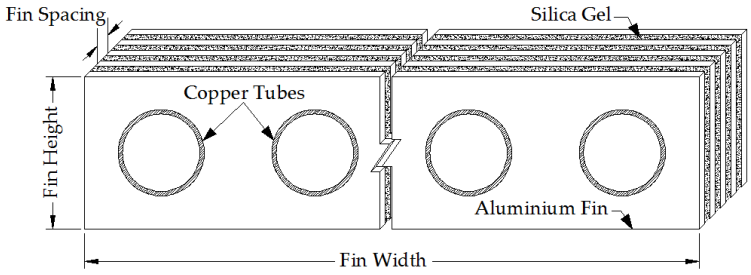

(a)

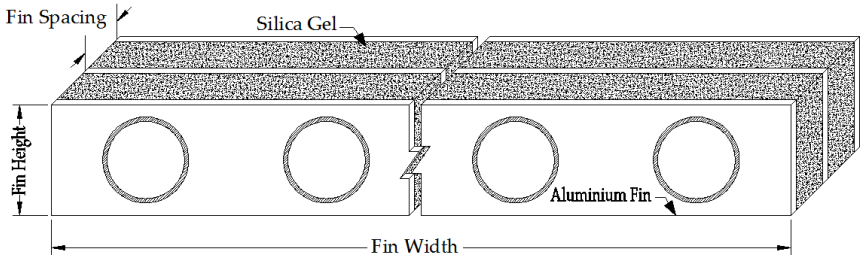

(b)

Figure 6-2, Finned tube adsorbent bed configuration (a) tight arrangement (b) loose arrangement

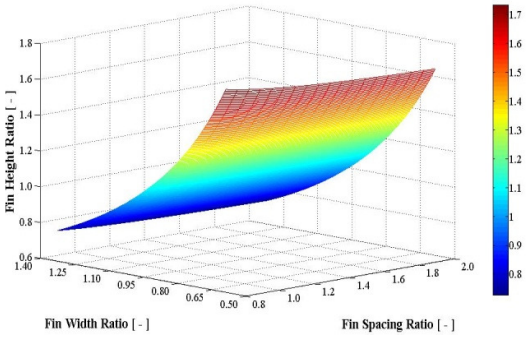

Figure 6-3, Fin height versus fin configuration

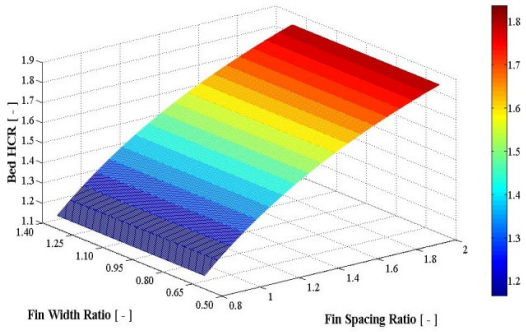

Figure 6-4, HCR versus fin configuration

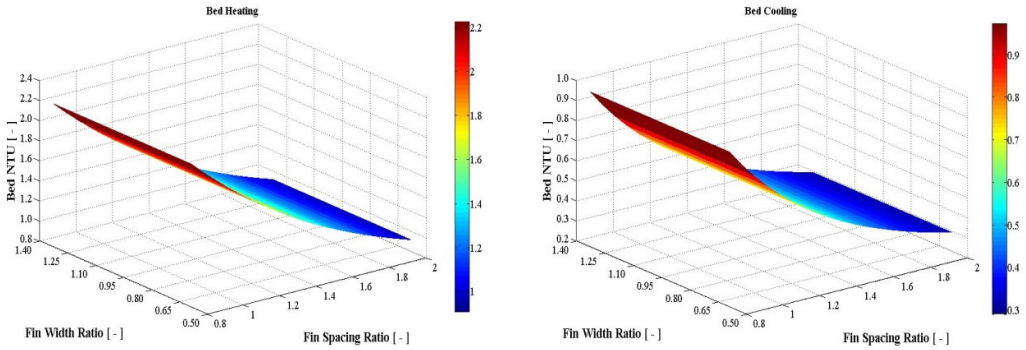

(a) (b)

Figure 6-5, Bed NTU versus fin configuration (a) bed heating (b) bed cooling

6.4 Effect of fin spacing with fixed silica gel mass

In this section, the effect of fin spacing was investigated while keeping the fin height and mass of silica gel constant. The fin height was kept constant to maintain the same level of bed permeability. To maintain the mass of silica gel constant, the fin width was altered to balance the change in fin spacing. Decreasing fin spacing results in increasing the number of fins which will increase bed NTU defined by equation 3-34 but reduces its HCR defined by equation 3-33 due to increasing the surface area and the mass of metal in the bed

respectively. Increasing the adsorbent bed heat transfer performance by means of fin spacing reduction enhances the adsorption kinetics and hence chiller cooling capacity as shown in Figure 6-6. In contrast, the reduction in the bed HCR increases chiller heating capacity to heat up the increased metal mass, these trends confirmed by [109, 137]. However, the rate of cooling capacity increase is lower than the rate of heating capacity increase which causes the chiller COP to decrease by reducing fin spacing in used fin spacing range. To sum up, changing fin spacing from design value (FSR=1) to minimum permissible value (FSR=0.8) increases chiller cooling capacity by 3%, but decreases chiller COP by 2.3% due to the increase of heating capacity by 5.4%.

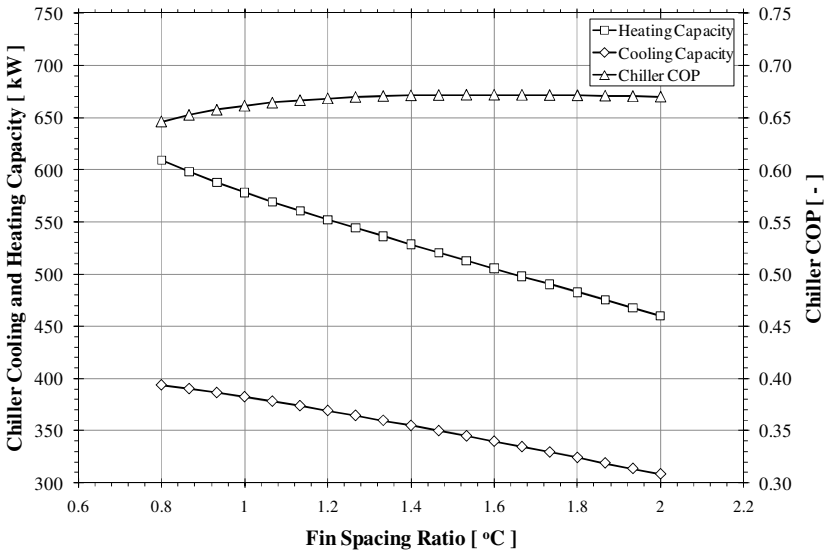

Figure 6-6, The effect of fin spacing on chiller performance

6.5 Effect of fin spacing with fixed bed dimension

Changing the fin spacing while keeping silica gel mass constant by changing fin dimension as discussed in section 6.4 may not be practical, but it helps understanding the change in

chiller performance by changing fin configuration. This section investigates the effect of changing fin spacing on chiller performance while the overall adsorbent bed dimensions are kept constant. Changing fin spacing while keeping fin dimensions (width / height) constant affects the heat transfer area, packed silica gel mass and metal mass of the adsorbent bed. Figure 6-7 presents the effect of fin spacing ratio on both of adsorbent bed number of transfer units (NTU) and heat capacity ratio (HCR). It is observed that the adsorbent bed HCR decreased by 14.7% with reducing the fin spacing ratio from 2 to the minimum permissible spacing of 0.8 due to increasing the metal mass of the higher fin number. On the other hand, the NTU increased by 135.3% and 215% during heating and cooling respectively by reducing fin spacing ratio from 2 to 0.8. The NTU level of heating is higher than NTU level of cooling due to the difference in secondary fluid flow rate values. In the simulated adsorption chiller, the cooling and heating water flow rates are 66.6 l/s and 18.3 l/s respectively, where cooling water flow rate is more than three folds that of heating water.

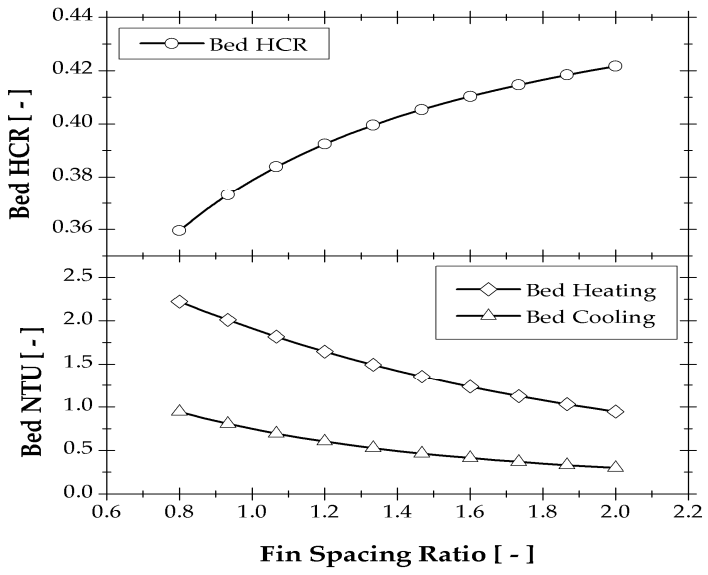

Figure 6-7, Adsorbent bed performance versus fin spacing with fixed fin dimension

Figure 6-8 shows that reducing the fin spacing ratio from 2 to 0.8 increased the chiller cooling capacity by 28.1% due to the heat transfer performance improvement, but the heating capacity increased by 16.4% mainly to heat up the excess amount of metal [109, 137]. The rate of increasing the cooling capacity is higher than the rate of increase of heating capacity and hence the chiller COP increased by 10% as shown in Figure 6-8.

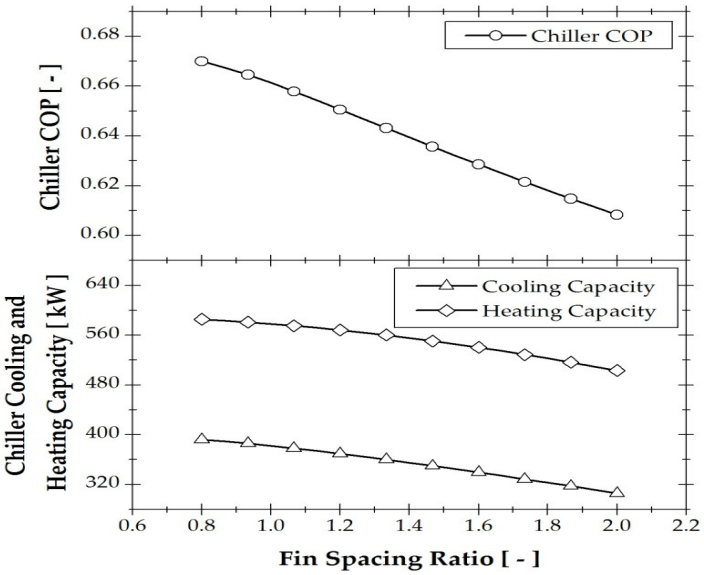

Figure 6-8, Effects of physical parameters on chiller performance.

6.6 The effect of thermal contact resistance

Based on the simulation model, the thermal contact resistance between the silica gel granules and the heat exchanger metal surface (tubes and fins) presents 25% of the overall heat transfer resistance. Adsorbent bed coating techniques were used to eliminate the thermal contact resistance of various adsorbents and bed designs [167-169]. The disadvantage of these techniques was (section 2.9.3) the dramatic reduction in adsorbent bed permeability which counteracts any improvement due to reducing the contact thermal resistance. Also,

the coated adsorbent layer is usually within few millimeters which increased the bed heat exchanger metal mass and reduced the HCR. Using bed coating technique, it was also recommended to use granules of relatively larger size [119]. However the larger the granules size, the worse the adsorption kinetics, where the adsorption rate is inversely proportional to the squared average granules radius. Therefore, this section investigates the effect of gluing the first layer of the silica gel granules and packing the rest at various fins spacing ratio (FSR).

Figures 6-9 and 6-10 show the effect of eliminating the contact thermal resistances (R3 and R4 equal zero) on the adsorbent bed and overall chiller performance at various fins spacing ratio (FSR). These show that eliminating the contact resistance increased the adsorbent bed heat exchanger NTU and the chiller cooling capacity and COP without changing the bed (HCR). There is no change in HCR where the same mass of metal and silica gel were used. At fin spacing ratio of 2, the NTU increased by 25.3% and 31.0% for heating and cooling respectively while the chiller cooling capacity, heating capacity and COP increased by 12.1%, 7.5% and 4.2% respectively. On the other hand, at fin spacing of 0.8, the NTU increased by 24.2% and 47.1% for heating and cooling respectively and the chiller cooling capacity, heating capacity and COP increased by 5.0%, 0.97% and 4.0%. Thus the chiller cooling capacity, heating capacity and COP averagely increased by 8.9%, 4.1% and 4.6% respectively. This improvement is due to the elimination of thermal contact resistance, that improves the heat transfer performance and hence the adsorption kinetics.

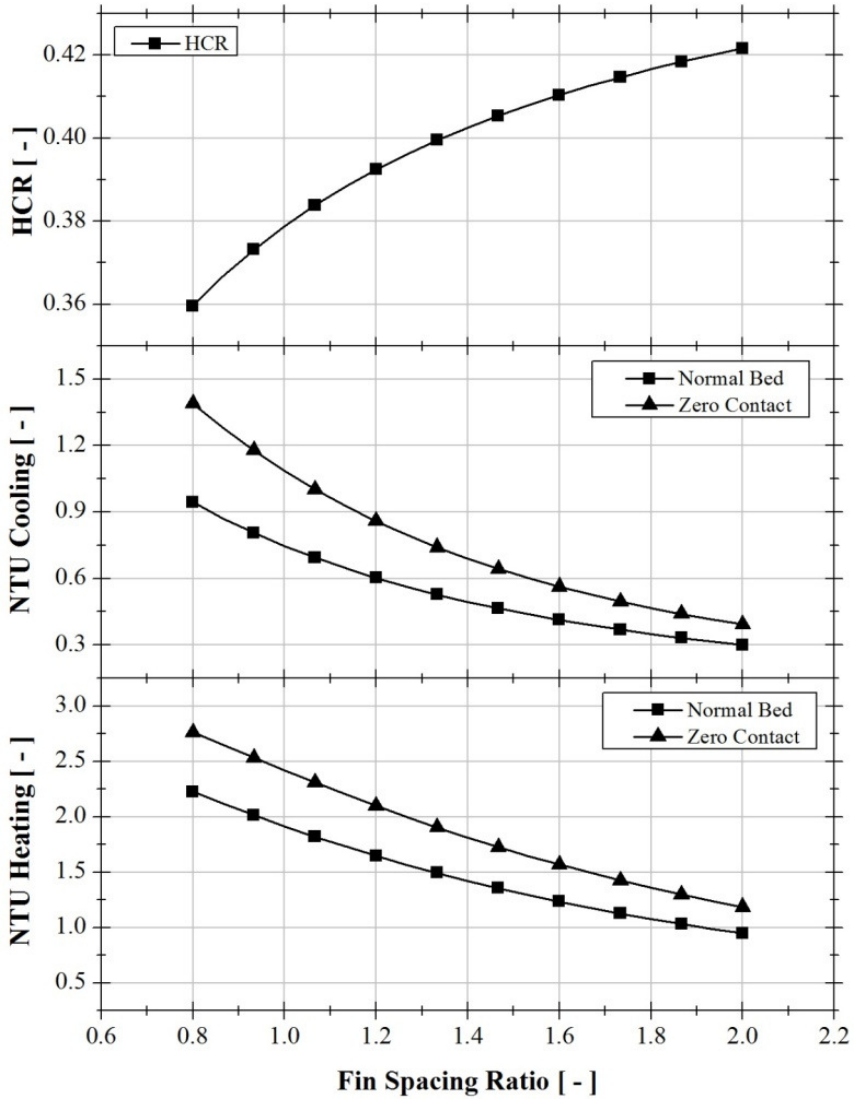

Figure 6-9, Eliminating contact resistance effect on adsorbent bed thermal performance at various Fin spacing.

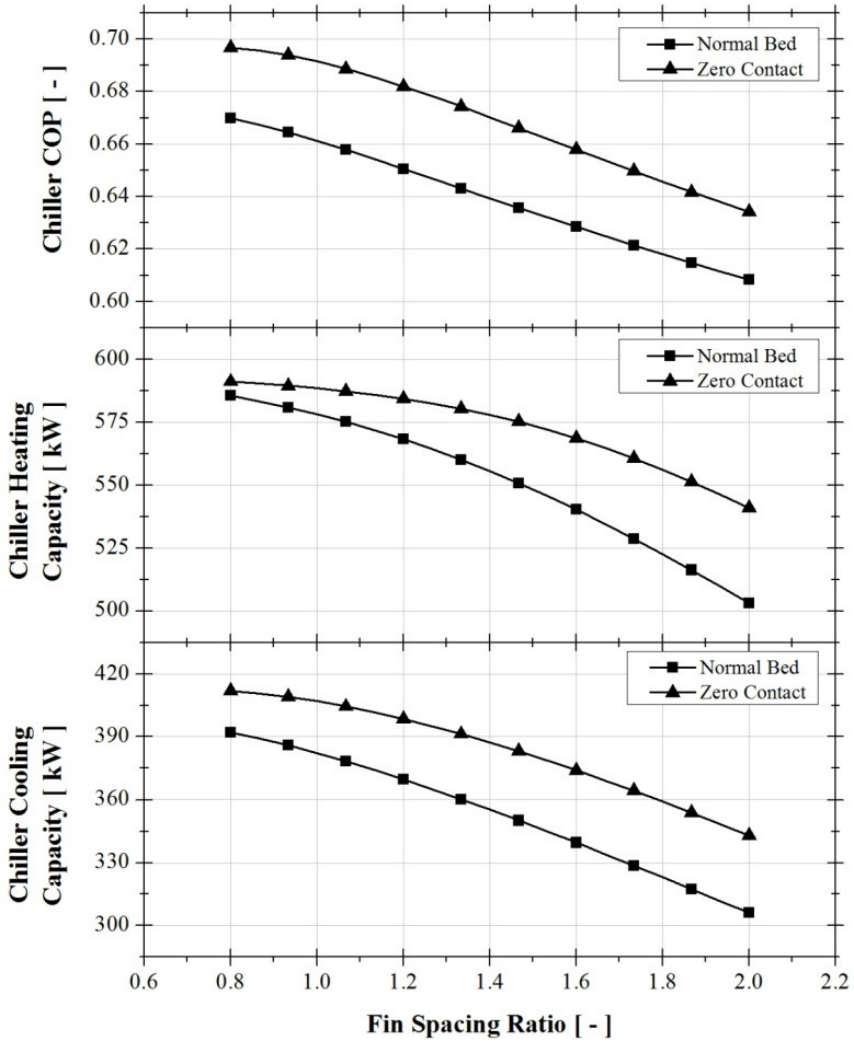

Figure 6-10, Eliminating contact resistance effect on chiller overall performance at various

6.7 Using metal additives

Researchers have shown that adding metal particles to adsorbent materials enhances their thermal conductivity, but little has been shown regarding the effect of the metal additives on the overall system performance [115]. This section investigates the effect of different metal additives on the overall performance of the simulated silica gel / water adsorption chiller.

Demir et al [170] has experimentally investigated the effect of different metal additives (aluminium, copper, brass and stainless steel) on the thermal conductivity of unconsolidated packed silica gel bed using different silica gel / metal weight ratios (5, 10 and 15wt%). They used silica gel granules with 3-5 mm diameter and thermal conductivity of 0.106 $Wm^{-1}K^{-1}$, while the radius of the frontal area of the metal particles was 1-2.8 mm. The volume based two phase effective thermal conductivity (K) method was used to develop a prediction technique for the thermal conductivity of silica gel / metal particles mixture as given in equation 6-1.

$$K = \left[k_1 V_1 \left(dT/dx\right)_1 + k_2 V_2 \left(dT/dx\right)_2\right] / \left[V_1 \left(dT/dx\right)_1 + V_2 \left(dT/dx\right)_2\right] \qquad 6\text{-}1$$

Where k_1 and V_1 are the thermal conductivity and volume fraction of metal respectively and k_2 and V_2 are thermal conductivity and volume fraction of silica gel respectively. The overall average temperature gradient $(dT/dx)_1$ and $(dT/dx)_2$ of the two phases were determined as:

$$\left(dT/dx\right)_1 / \left(dT/dx\right)_2 = nk_1 / \left[k_2 + (n-1)k_1\right] \qquad 6\text{-}2$$

Factor (n) depends mainly on the metal additive shape [171]. Using factor n of 1.031, 1.047, 1.11 and 2.331 for aluminium, copper, brass and stainless steel metal additives respectively and various metal/silica gel mass ratio (5, 10 and 15wt%), the effective thermal conductivity of silica gel / metal mixture was predicted with deviation of less than ±15%. Figure 6-11 compares the predicted thermal conductivity and the experimental values reported by Demir et al [170].

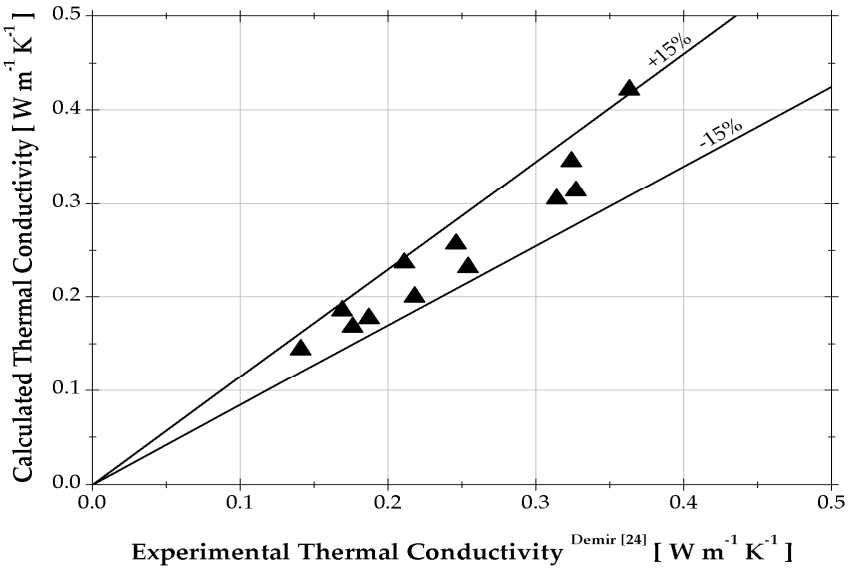

Figure 6-11, Comparison between experimental and calculated thermal conductivity.

Table 6-1, The predicted metal/silica gel type-RD effective thermal conductivity.

Met/Sg mixture	K_{met} (W m^{-1} K^{-1})	K_{eff} (W m^{-1} K^{-1})	Thermal conductivity improvement (%)
Silica gel	--	0.198	--
Sg+5% Al	237	0.340	72
Sg+10% Al	237	0.498	152
Sg+15% Al	237	0.675	241
Sg+5% Cu	401	0.305	54
Sg+10% Cu	401	0.424	114
Sg+15% Cu	401	0.557	181
Sg+5% Brass	150	0.291	47
Sg+10% Brass	150	0.394	99
Sg+15% Brass	150	0.509	157
Sg+5% St-St	14.9	0.254	28
Sg+10% St-St	14.9	0.316	60
Sg+15% St-St	14.9	0.385	94

The above described validated prediction method has been used to calculate the effective thermal conductivity of the metal / silica gel mixtures of silica gel type RD2060 with thermal conductivity and average granules diameter of 0.198 W m^{-1} K^{-1} and 0.16mm respectively [143] used in the current investigation. Table 6-1 shows the effective thermal conductivity of silica

gel RD2060 and aluminium, copper, brass and stainless steel with weight ratios of 5, 10, and 15%. It also includes percentage improvement in thermal conductivity of the mixtures, where aluminium produces the highest values.

The predicted effective thermal conductivities of metal / silica gel RD2060 were incorporated in the overall chiller model. Figure 6-12 presents the effects of aluminium, copper, brass and stainless steel metal additives of 15wt% on the adsorbent bed thermal performance at various fin spacing ratios. It is observed that the adsorbent bed NTU during heating averagely increased by 39.5, 34.7, 32.2 and 23.8% and during cooling by 58.2, 50.2, 46.3 and 33.3% using aluminium, copper, brass and stainless steel respectively. This increase in the NTU is due to the thermal conductivity improvement due to the addition of metal particles. The observed enhancement was found to be proportional to the thermal conductivity of the metal additives, where the higher improvement was observed using aluminium additive followed by copper, brass and stainless steel. On the other hand, the heat capacity ratio (HCR) of the adsorbent bed averagely decreased by 5.1, 2.2, 2.2 and 2.7% using aluminium, copper, brass and stainless steel additives respectively. This decrease in heat capacity ratio (HCR) is due to the reduction of silica gel mass which was replaced with metal additives of different specific heats. The change in HCR is proportional to the metal additives specific heat, where the higher HCR value corresponds to the lower heat capacity for brass followed by copper, stainless steel and aluminium.

Table 6-2, Metal additives specific heat values

Metal additive	Specific heat (kJ/kg K)
Aluminium	0.896
Copper	0.385
Brass	0.380
Steel	0.460

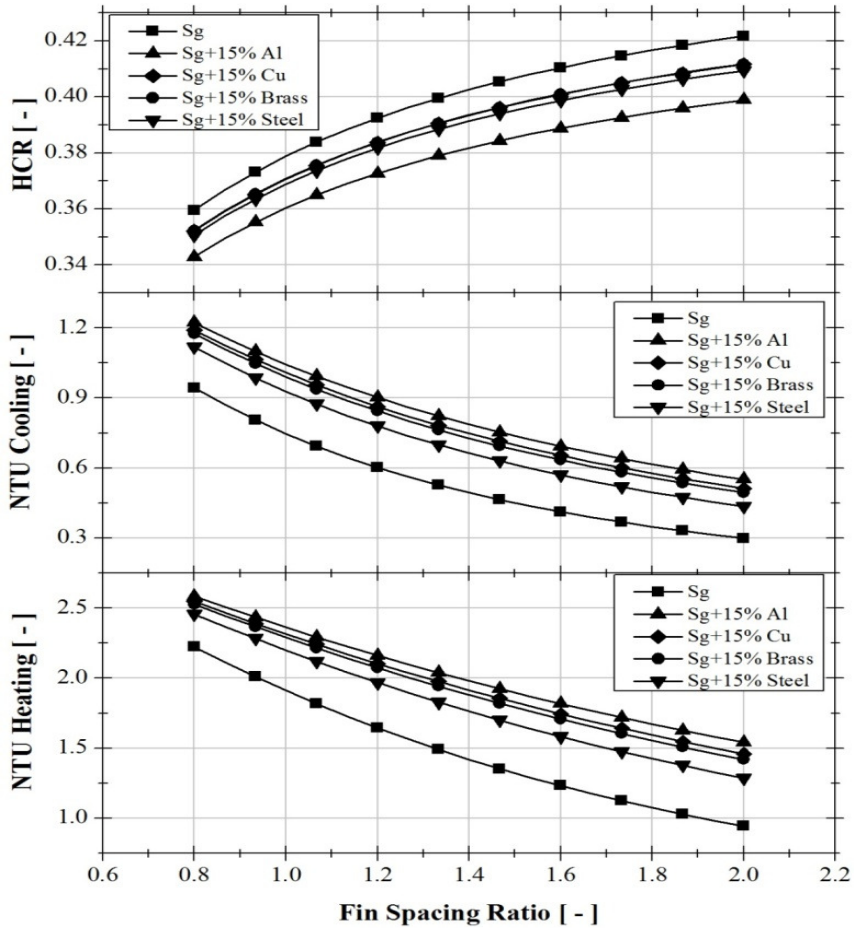

Figure 6-12, The effect of metal additives on the thermal performance of the adsorbent bed.

Figure 6-13 shows the effect of the same metal additives on the chiller cooling capacity, heating capacity and COP. Results showed that the addition of metal particles at 15% wt enhanced the chiller cooling capacity and coefficient of performance at varying degree depending on the fin spacing ratio and the metal type. At FSR of 2, the cooling capacity and

COP increased by 12.5% and 2.4% for aluminium, 11.2% and 2.9% for copper, 10.4% and 2.4% for brass and 7.3% and 0.7% for stainless steel. This is due to adsorbent bed thermal conductivity improvement that improves the thermal performance and hence the adsorption kinetics. At FSR of 0.8, the cooling capacity and COP decreased by 3.8% and 1.8% for aluminium, 4.0% and 1.1% for copper, 4.1% and 1.2% for brass and 4.4% and 1.8% for stainless steel. This is because of the reduction in silica gel mass that produce insufficient cooling in addition to the excess amount of metal by means of fins and metal additives.

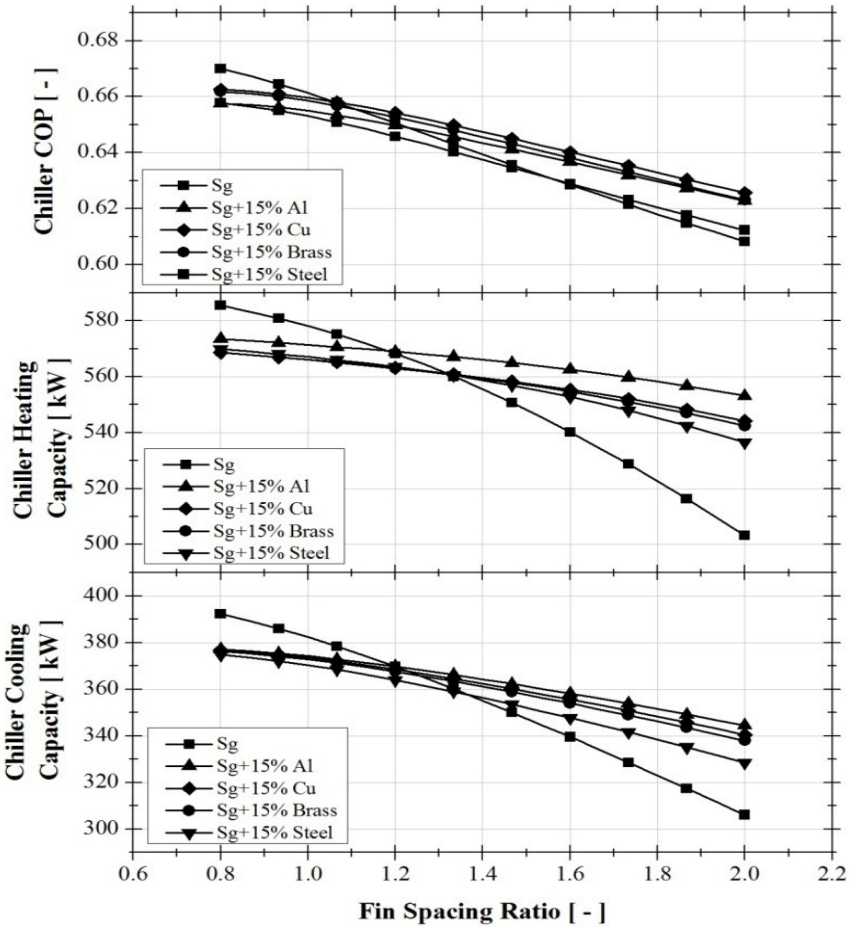

Figure 6-13, The effect of metal additive on chiller overall performance.

6.8 Effect of zero contact resistance and metal additives

Figure 6-14 and 6-15 show the combined effect of gluing the first layer of silica gel / metal particles on the adsorbent-bed reactor and chiller performance respectively in comparison with regular mixture packing. Results show that using both enhancement techniques (gluing the first adsorbent / metal mixture layer) increased the adsorbent bed NTU during heating averagely by 89.5, 81.2, 77.0 and 63.2% and during cooling by 173.6, 151.8, 141.5 and 110.0% using aluminium, copper, brass and stainless steel respectively, because of the reduction in thermal resistances resulting from imported thermal conductivity and eliminating of contact thermal resistance. The heat capacity ratios (HCRs) for different mixtures remain constants where there is no change in metal or silica gel mass by gluing the fist layer as shown in Figure 6-14-C. Figure 6-15 shows that the chiller cooling capacity and COP averagely increased by 11.0, 10.4, 10 and 8.5 and 7.1, 7.4, 7 and 5.5 using aluminium, copper, brass and stainless steel respectively, because of thermal performance improvement.

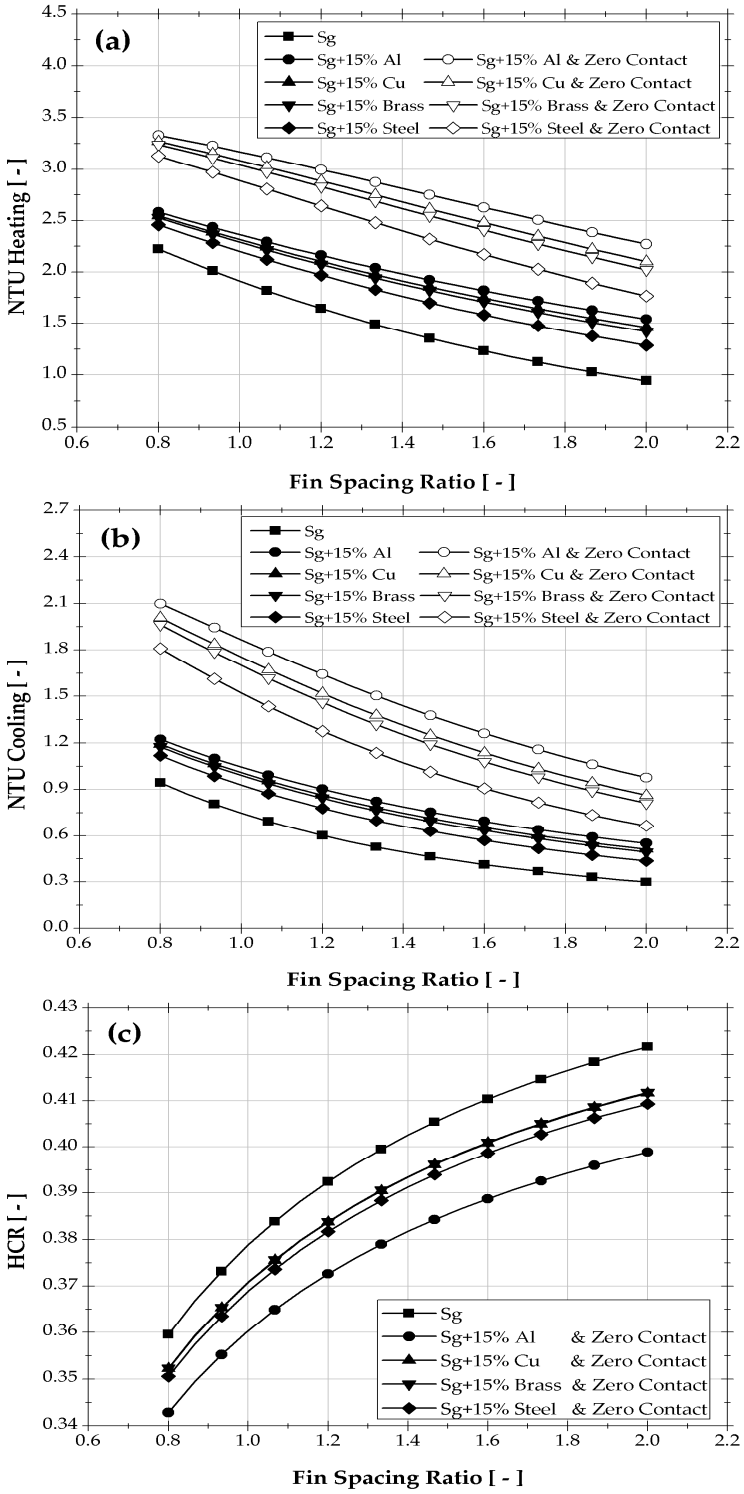

Figure 6-14, The effect of metal additives and thermal contact resistance on adsorbent bed's thermal performance

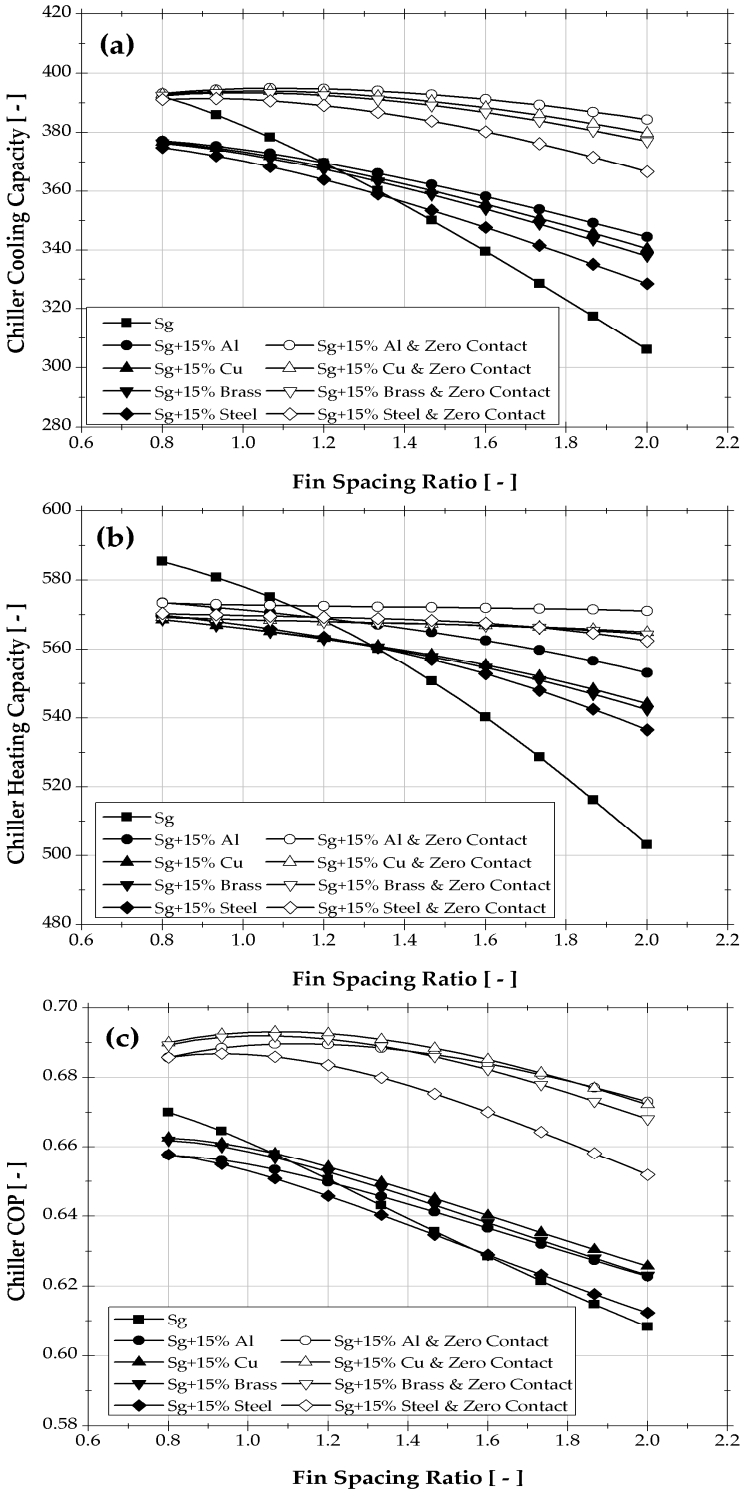

Figure 6-15, The effect of metal additive and thermal contact resistance on chiller overall performance

6.9 Summary

This chapter presented the effect of changing adsorbent bed physical parameters on chiller performance. The effect of changing fin spacing on the adsorbent bed performance has been investigated. It is concluded that reducing fin spacing increases the total heat transfer area and hence improves the adsorbent bed heat transfer performance. That increases the chiller cooling capacity and negligibly reduces its COP.

The adsorbent coating is one of the proposed solutions to eliminate the contact thermal resistance, but it dramatically reduces the adsorber bed permeability. It is proposed to glue the first adsorbent granules layer and pack the rest of silica granules to eliminate the contact thermal resistance and maintain the same level of permeability. An improvement of the overall chiller performance has been observed without decreasing its COP, due to no change in adsorbent bed metal mass.

Adding metal particles to the adsorbent granules averagely enhances the heat transfer performance of the adsorbent bed. The combined effect of adding metal additives and gluing the first adsorbent layer has been investigated. It averagely enhanced the adsorbent bed heat transfer performance.

CHAPTER 7: CHARACTRISATION OF METAL ORGANIC FRAMEWORKS / WATER ADSORPTION PAIR

7.1 Introduction

In adsorption applications, the choice of adsorption working pair is determined by the amount of heat that can be extracted from the evaporator per adsorption cycle. The heat extracted from the evaporator is proportional to the amount of vapour adsorbed and the latent heat of evaporation of the selected refrigerant. Therefore the adsorbent uptake difference over a given cycle and latent heat of evaporation are the most effective parameters that influence the cycle cooling capacity and COP [70]. As a refrigerant, water has the advantages of high latent heat of evaporation, non-toxic and environmentally friendly refrigerant [172]. Silica gel has been used as water adsorbent in many commercially available adsorption systems due to its low generation temperature and good adsorption uptake. However, the main problem of silica gel as adsorbent is that most of water adsorption occurs at high partial pressure. The partial pressure is the ratio between the supplied vapour pressure and the saturation vapour pressure corresponding to the operating temperature. For cooling applications, this means that the amount of water vapour adsorbed / desorbed in a cycle is only a small part of the total adsorption capacity of the silica gel RD [76].

Metal organic frameworks (MOFs) are new micro-porous materials with exceptional high porosity, uniform pore size, well-defined molecular adsorption sites and large surface area (up to 5500m^2/g). MOFs consists of two main components: the organic linkers considered as organic secondary building unit, act as struts that bridge metal centres known as inorganic

primary building units and act as joints in the resulting MOF architecture. The two main components are connected to each other by coordination bonds, together with other intermolecular interactions, to form a network with defined topology [74, 75]. Although MOFs have been originally designed and investigated for gaseous fuel storage such as hydrogen and methane [173, 174], their use in water adsorption cooling is promising [175, 176]. Also, MOFs are less hydrophilic than silica gel RD or zeolite thus it can release more water vapour at the same partial pressure [76].

There are limited data on MOFs water adsorption; therefore this chapter experimentally investigates the water adsorption characteristics of seven different MOFs namely; HKUST-1 (copper based), MIL-100 (iron based), MIL-53 (chromium based), MIL-53 (iron based), Birm-1, Birm-1-K and Birm-1-Li. HKUST-1 and MIL-100 are manufactured by BASF, USA and commercially marketed by Sigma Aldrich UK as Basolite C300® and Basolite F300® respectively. MIL-53 (chromium based) and MIL-53 (iron based) were designed and made in Warwick University [177]. Three dimensional porous material designated Birm-1, Birm-1-K and Birm-1-Li were designed and made in University of Birmingham UK [178].

7.2 Experimental Work

There are two methods for measuring adsorption characteristics namely; volumetric method and gravimetric method [144, 145]. In this investigation a dynamic vapour sorption (DVS) gravimetric analyser has been used to study the water adsorption characteristics (adsorption isotherms, kinetics and isosters) of the selected MOFs, Figure 7-1. The DVS analyser has the advantages of directly measuring the adsorbent mass and preventing adsorbate vapour

condensation on the moving balance parts. The adsorbent mass is measured using ultra-sensitive recording microbalance (Cahn D200) which has high long-term stability in microgram level as it adsorbs controlled concentrations of water or organic vapours. Dry Nitrogen is used to purge the balance head and reaction chamber prior to sample loading. The purge flow is automatically controlled to prevent vapour condensation in the balance head and hence accurate uptake measurement is achieved. Mass flow controller is used to control the vapour pressure with a mixture of dry and saturated vapour gas. The test conditions were verified using optical vapour pressure sensor and RTD temperature probe very close to sample pan. The DVS analyser is controlled by a PC microcomputer, which is interfaced with the microbalance. The accuracy of the DVS analyser microbalance is verified by using 100 mg standard calibration mass, where the expected accuracy of the tested sample is ±0.05 mg.

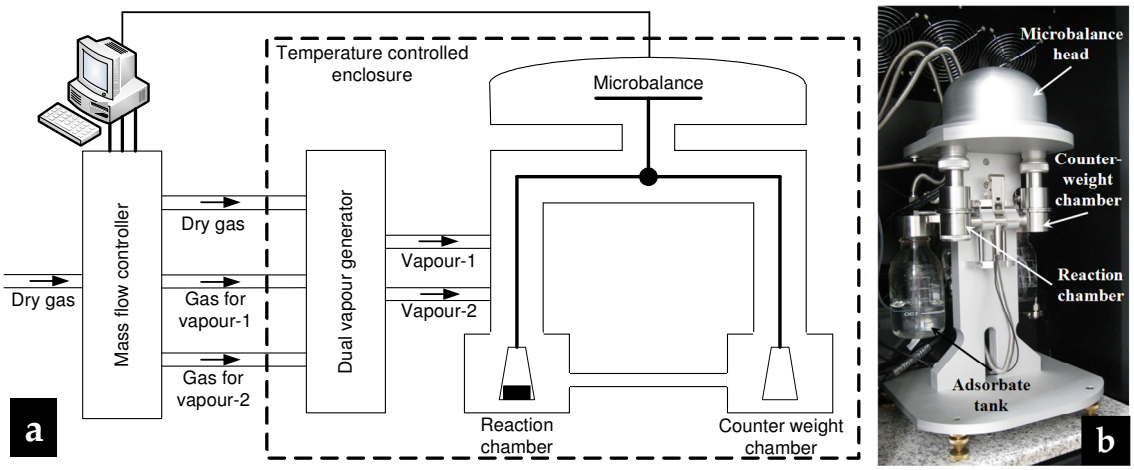

Figure 7-1, Schematic and pictorial diagram for the used DVS analyser

The adsorption characteristics that affect the chiller performance are adsorption isotherms, isosteric heat of adsorption and adsorption kinetics. Samples of 10 mg each has been placed in the reaction chamber and were dried at fixed temperature of 55 °C until the condition of no change of mass, then allowed to undergo through adsorption / desorption tests at various partial pressures. The drying temperature was selected to be 5 degrees below the DVS analyser maximum operating temperature of 60 °C. The sample mass is recorded every 4 seconds at different vapour pressure values to determine the adsorption kinetics, Figure 7-2. The sample isotherm is measured at each value of vapour pressure at the point of no change in adsorbent mass by measuring the adsorbent uptake.

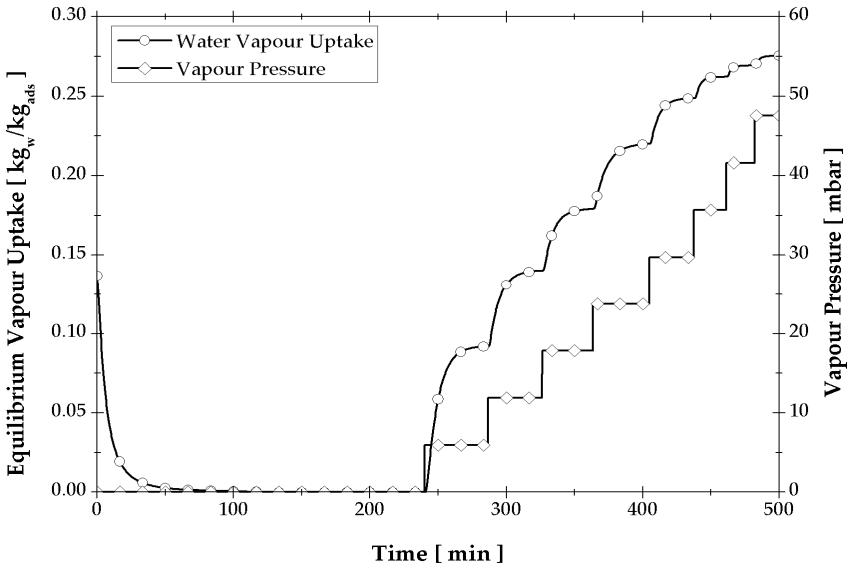

Figure 7-2, Temporal evaluation of the vapour pressure over sample and water vapour uptake (T=36°C).

7.3 MOFs performance comparison

In order to identify best performing MOF materials in terms of maximum water uptake, the above described testing procedure was initially used to test seven MOF samples to be

compared with silica gel RD sample at constant temperature of 36 °C. Figure 7-3 compares the maximum water vapour equilibrium uptake of the tested MOFs and silica gel RD. From this figure, it is clear that HKUST-1 significantly outperform silica gel RD by up to 97.7% increase in the maximum water vapour uptake. MIL-100 has shown modest improvement on the silica gel RD with up to 28.2% increase. Other MOFs were inferior to the silica gel RD. Therefore, samples of HKUST-1 and MIL-100 were tested to characterise their adsorption isotherms, cyclic and kinetic performance. This was carried out at temperatures ranging from 20 ^{0}C to 52 ^{0}C at increment of 8 degrees and vapour pressure ranging from 200 Pa to 10000 Pa and the results were compared to those of the reference material silica gel RD. Figure 7-4 presents SEM images and Table 1 presents the granular size, BET surface area and bulk density for these materials.

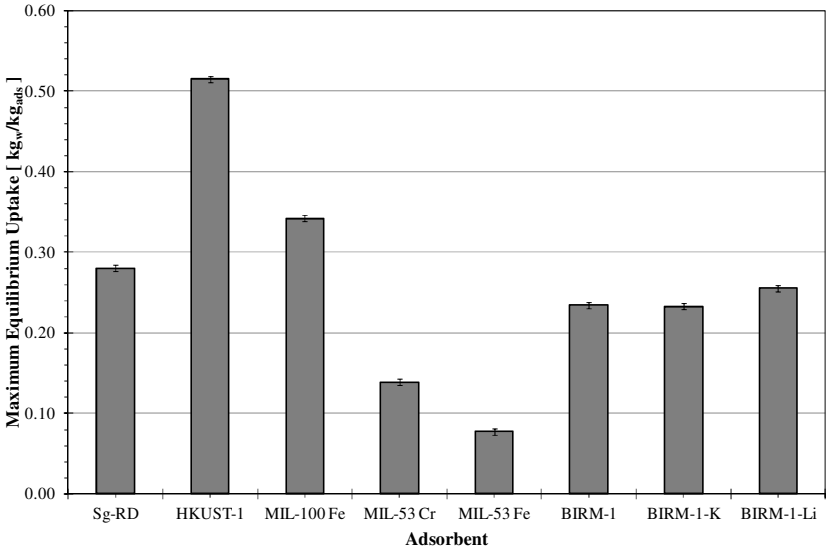

Figure 7-3, Preliminary comparison for tested samples

Table 7-1, Physical properties of tested materials

Property	HKUST-1	MIL-100	Silica gel RD 2060
Granules size	16 μm	5 μm	0.18-1 mm
BET surface area	1500-2100 m^2/g	1300-1600 m^2/g	840 m^2/g
Bulk density	0.35 g/cm^3	0.16-0.35 g/cm^3	1 g/cm^3

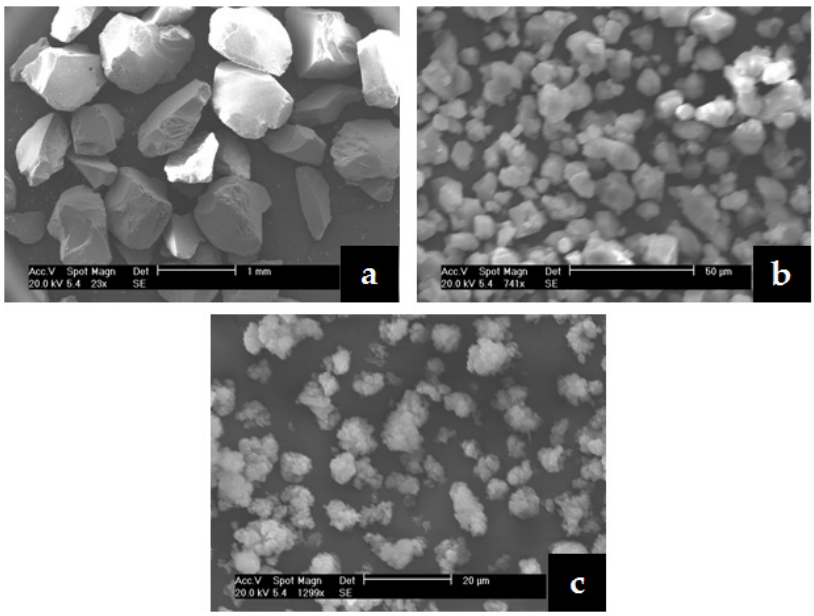

Figure 7-4, SEM images for (a) RD-2060 silica gel (b) HKUST-1 (c) MIL-100

7.4 Silica gel RD-2060 performance

The adsorption characteristics of silica gel RD in terms of adsorption isotherms and isosteric heat of adsorption is investigated to be used as a reference material and to validate the test procedure. Figure 7-5 shows the experimental results for adsorption isotherms of silica gel RD at temperatures 20, 28, 36, 44 and 52 °C compared to the prediction of the modified Freundlich equations 7-1 - 7-3. The deviation between the experimental and predicted results within ±16% and is shown Figure 7-5.

$$w^* = A(T_{ads})\left[P_{sat}(T_{ref})/P_{sat}(T_{ads})\right]^{B(T_{ads})} \quad 7\text{-}1$$

$$A(T_{ads}) = A_0 + A_1 T_{ads} + A_2 T_{ads}^2 + A_3 T_{ads}^3 \quad 7\text{-}2$$

$$B(T_{ads}) = B_0 + B_1 T_{ads} + B_2 T_{ads}^2 + B_3 T_{ads}^3 \quad 7\text{-}3$$

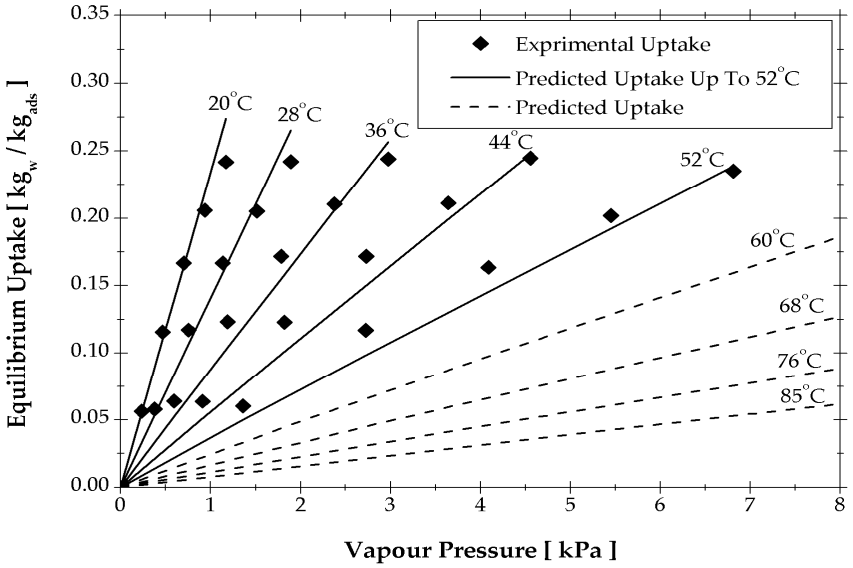

Figure 7-5, Comparison between experimental and modified Freundlich isotherms

Isosteric analysis is one of the key characteristics of adsorbents that need to be studied [179]. Based on the experimentally measured isotherms, a family of adsorption isosters is calculated and presented as straight lines in an $\ln(P_v)$ versus $1/T_{ads}$ as shown in Figure 7-6. The slope of the presented isosters allows obtaining the isosteric heat of adsorption [90] using equation 7-4. The average calculated isosteric heat of adsorption of silica gel RD was found to be 2.43×10^6 J/kg, with deviation from published data ranging from 3.2% to 13.2% as shown in Table 7-2.

$$Ln(P_v) = cons\tan t - \Delta H_s/\overline{R}T \quad 7\text{-}4$$

Table 7-2, Isosteric heat of adsorption.

Author	ΔH_s (J/kg)	Deviation
Wang [129] and Chua [145]	2.51×10^6	3.2%
Zimmermann [144]	2.69×10^6	9.7%
Akahira [132] and Uyun [136]	2.80×10^6	13.2%

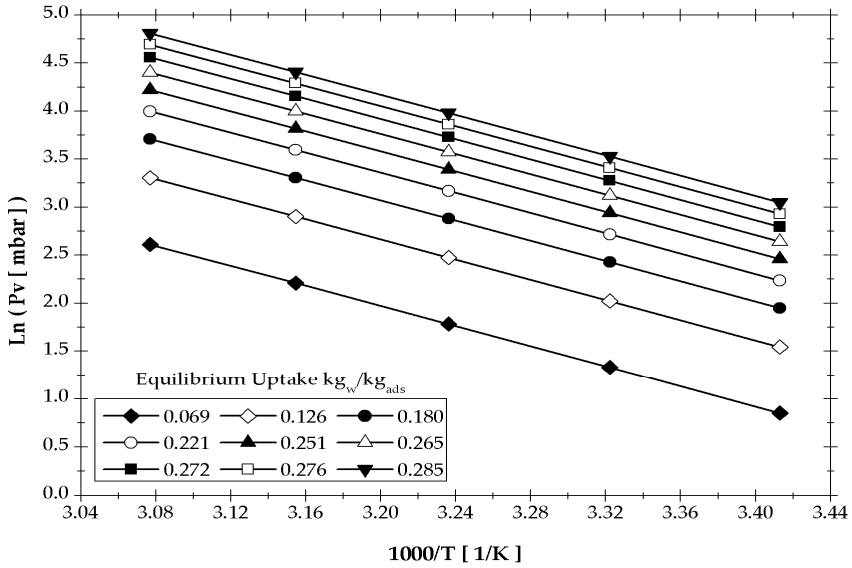

Figure 7-6, Isosters of water/silica gel RD-2030

Adsorption rate can be measured using the gravimetric method for different adsorbent / adsorbate pairs [180-182]. In the adsorption process, the intraparticle mass transfer resistance dominates interparticle resistance [183]. The key parameter of intraparticle mass transfer is the diffusion time constant which is directly proportional to the surface diffusion, but inversely proportional to the adsorbent granules size. The rate of intraparticle mass transfer for different adsorbent / adsorbate pairs is normally measured using the gravimetric analyser and modelled with linear driving force model (LDF) [26, 98, 138, 180-182, 184], (equations 7-5 - 7-6). Figure 7-7 shows that the maximum deviation between the experimental results and those predicted by the LDF model are within ±20%.

$$w = w^* - \exp\left[-k_s a_v \cdot t + \ln(w^* - w_t)\right] \quad 7\text{-}5$$

$$k_s a_v = \left(15 D_{so}/R_p^2\right) \exp\left(-E_a/\bar{R}T\right) \quad 7\text{-}6$$

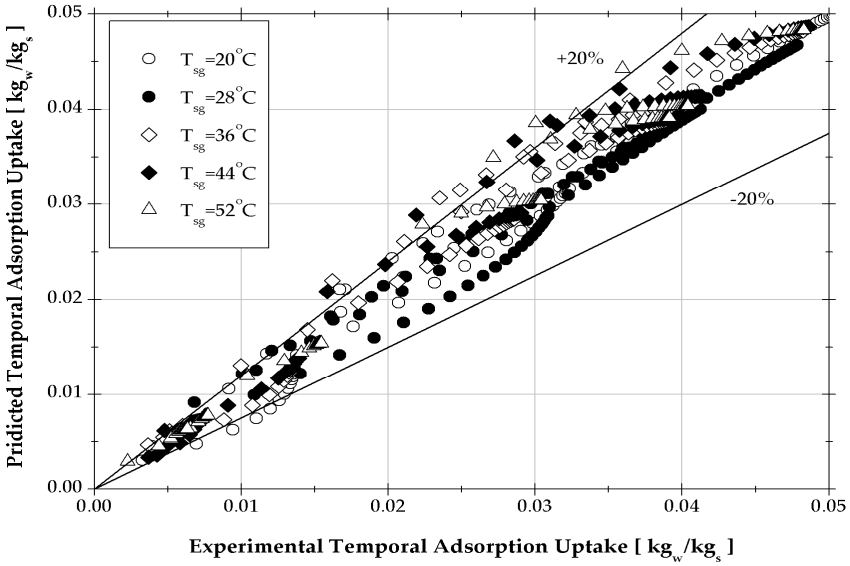

Figure 7-7, Comparison between the temporal experimental and predicted water vapour uptake

7.5 HKUST-1 and MIL-100 Water Adsorption Performance

This section presents the characterisation of HKUST-1 and MIL-100 for water adsorption compared to silica gel RD in terms of the adsorption isotherms, adsorption kinetics and adsorption cycle analysis. The characterisation is based on the experimental measurements for temperatures below 52 °C and prediction technique based on published models for temperatures above 52 °C.

7.5.1 Adsorption Isotherms

Figure 7-8 presents the experimental adsorption and desorption isotherms for silica gel RD, HKUST-1 and MIL-100 for the temperatures 20 °C and 52 °C. It is shown that silica gel RD,

HKUST-1 and MIL-100 isotherms behave as type-I, type-II and type-V adsorbents respectively, Brunauer [185]. For all tested vapour pressures, HKUST-1 adsorbs more water vapour than silica gel RD and MIL-100 where the average maximum water vapour uptake value is 0.55kg_w/kg_{ads} which is 95.7% higher than that of the tested silica gel RD. Figure 7-8 also shows that the MIL-100 has low water adsorption at low vapour pressure and higher values at high vapour pressures. The average maximum equilibrium uptake value of MIL-100 is 0.35kg_w/kg_{ads} which is 26.8% higher than that of silica gel RD. Based on these results, the maximum equilibrium uptake is highest for HKUST-1 followed by MIL-100 and silica gel RD. It is observed that HKUST-1 exhibit larger degree of hysteresis compared to silica gel RD and MIL-100. This is an indication of instability of this material, which will be investigated in details.

Regarding MIL-100 isotherms, the measured values differ from those reported by Küsgens et al. [74], Jeremias et al [186] and Akiyama et al [187] both in terms of the maximum uptake value and the trend. Küsgens et al [74] investigated MIL100(Fe) ($Fe_3^{III}\,O(H_2O)_2F.[H_3(CO_2)_3]_2.nH_2O\ \ with\ n = 14.5$) synthesised based on procedure developed by Horcajada et al [188] using a solution of Fe powder, 1,3,5-benzene tricarboxylic acid (H_3BTC), hydrofluoric acid, nitric acid and de-ionised water. The adsorption isotherms at temperatures of 298 K (25^{o}C) and 323K (50^{o}C) as reported by Küsgens et al [74] showed sharp increase in the water uptake. At 298K, the sharp increase occurred at partial pressure of 0.2-0.3 while at 323K, it occurred at 0.3-0.4 partial pressure. Jeremias et al [186] also investigated MIL-100 based on the same synthesis procedure reported by Horcajada et al [188] with a general structure of MIL-100 having the empirical formula 3D-

{$M_3O(X)(H_2O)_2[btc]_2.nH_2O$} where in their case M is Fe (Iron), X is F (Fluorine) and btc is benzene-1,3,5-tricarboxylate, trimesate. The water adsorption of the synthesised material was investigated at two temperatures namely 298 K (25°C) and 313 K (40°C). The sharp increase in water adsorption at partial pressure of 0.25 to 0.4 was also observed with maximum water uptake of 0.7g_{ref}/g_{ads}. Akiyama et al [187] synthesised three new MIL-100 type based on the empirical structure of 3D-{$M_3O(X)(H_2O)2[btc]_2.nH_2O$} but with M to be Cr (Chromium), X to be F (Fluorine) or Cl (Chlorine) or SO_4 (Sulphur Tetra oxide) and btc is benzene-1,3,5-tricarboxylate, trimesate). They investigated the water adsorptive of the developed materials at 298K (25°C) and observed the sharp increase in water uptake at partial pressure of 0.2 to 0.3 with maximum uptake of 0.7 g/g. The MIL-100 used in this investigation is the commercially available material from Sigma Aldrich Fe-btc with btc being 1, 3, 5-benzene tricarboxyalte and chemical formula $C_9H_3FeO_6$. This differs from that of Akiyama et al [187] where Chromium is used instead of Iron and Fluoride acid is used in the synthesis. It also differs from those synthesised by Küsgens et al [74] and Jeremias et al [186] where F (Fluorine) is apparent in the chemical formula. This difference in chemical formula / synthesis process may explain the difference in water uptake performance. Nevertheless the low water uptake at low partial pressure and the step increase in the water uptake of partial pressure higher than 0.2 (vapour pressure of 0.5 kPa) (T_{ads}=20°C) and vapour pressure of 3kPa (Tads=52C) are consistent with those shown in Figure 7-8.

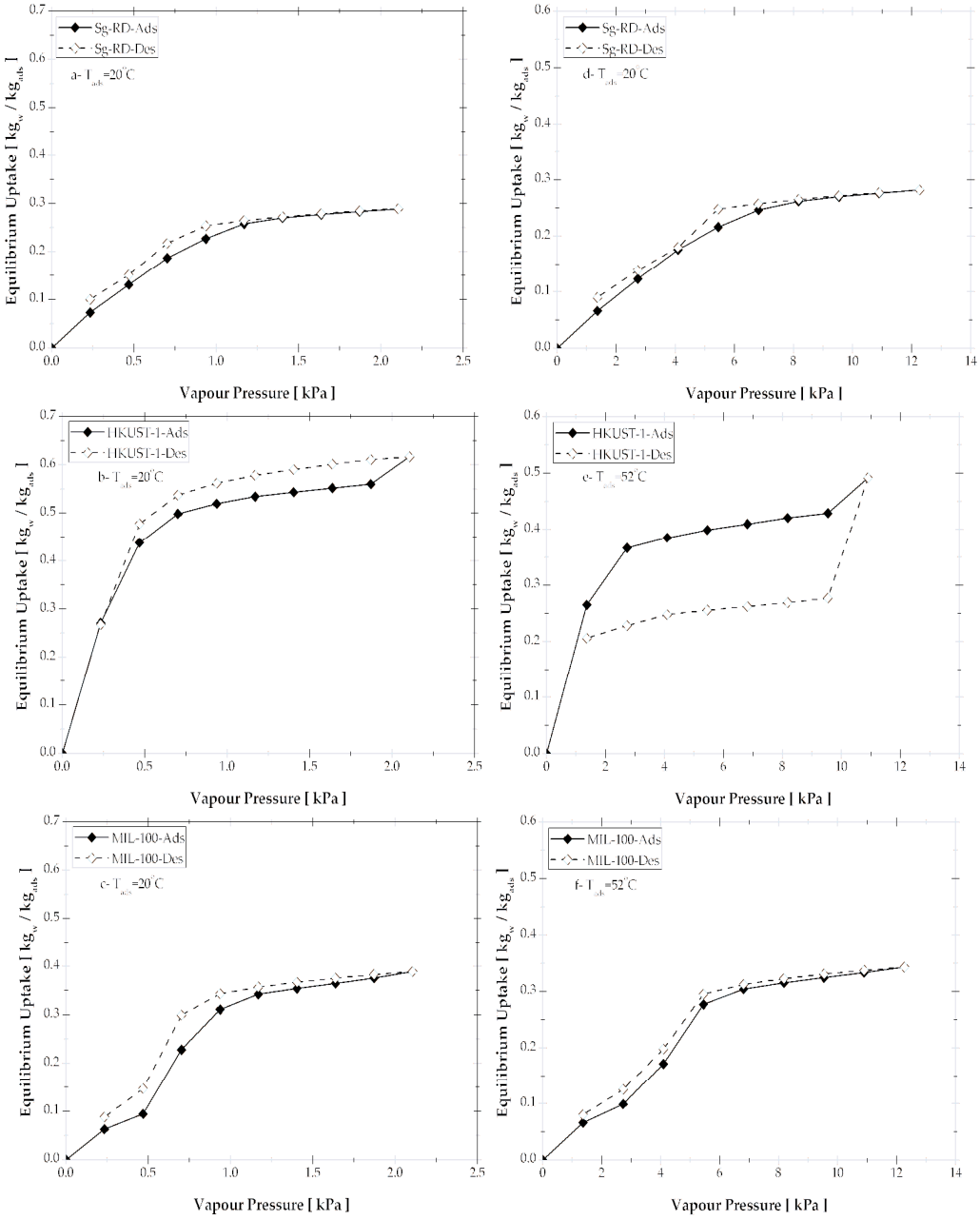

Figure 7-8, Adsorption and desorption isotherms comparison for different adsorbents

7.5.2 Adsorption Kinetics

The adsorption kinetics is an essential factor that need to be considered during comparison between different adsorption pairs [182]. It determines the rate at which the adsorbent

material adsorbs / desorbs the refrigerant. Figure 7-9 presents the adsorption kinetics of the tested adsorbents at different temperatures and vapour pressures. It is clear that HKUST-1 shows the maximum adsorption rate followed by silica gel RD and MIL-100 except in the first few seconds. The fast adsorption rate of HKUST-1 / water pair implies that short adsorption / desorption cycle time can be used in the development of waste heat driven adsorption cooling systems [189].

The linear driving force (LDF) kinetics model is used to model the adsorption kinetics for HKUST-1 and MIL-100 using equation 7-5. The mass transfer coefficient is calculated using equation 7-7, where the equation parameters are furnished in Table 7-3. The deviation between the predicted uptake values and its experimental values using LDF model are presented in Figure 7-10 – 7-11.

$$k_s a_v = \left(F \cdot D_{so}/R_p^2\right) \exp\left(-E_a/\overline{R}T\right) \qquad 7\text{-}7$$

Table 7-3, Liner driving force equation parameters

Parameter	Value	Unit
HKUST-1		
$F \cdot D_{so}$	4.08×10^{-3}	m^2/s
E_a	1.99×10^{4}	J/mol
R_p	8×10^{-6}	m
MIL-100		
$F \cdot D_{so}$	2.63×10^{-3}	m^2/s
E_a	2.70×10^{4}	J/mol
R_p	2.5×10^{-6}	m

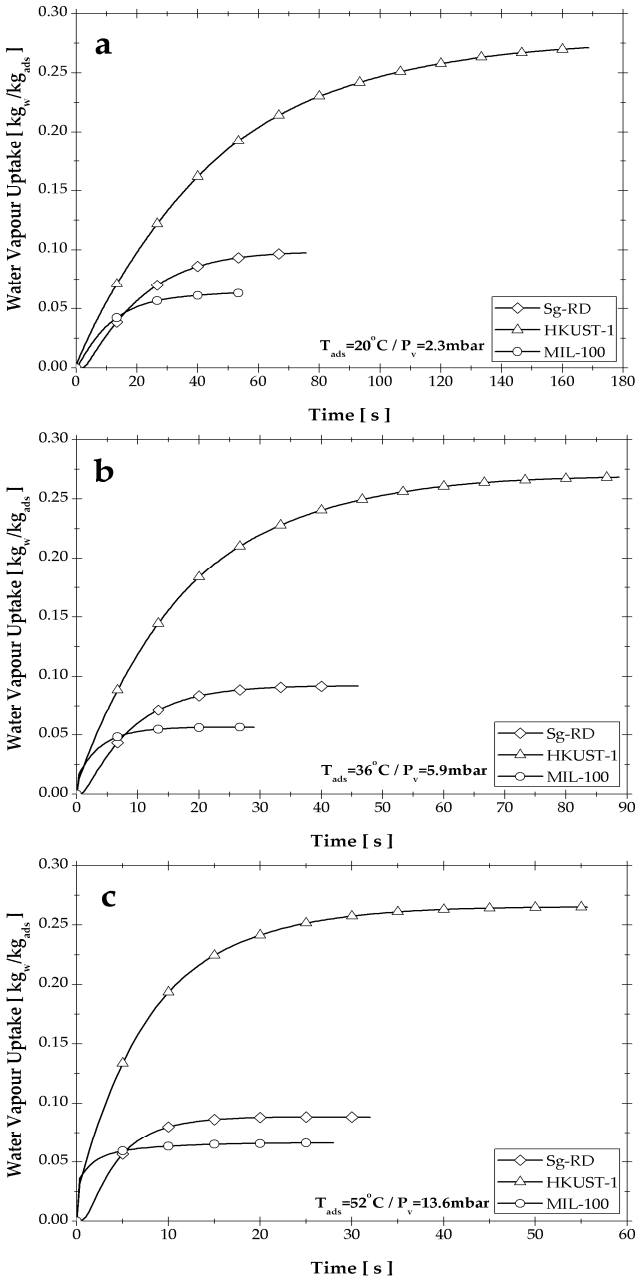

Figure 7-9, Adsorption kinetics comparison for different adsorbents

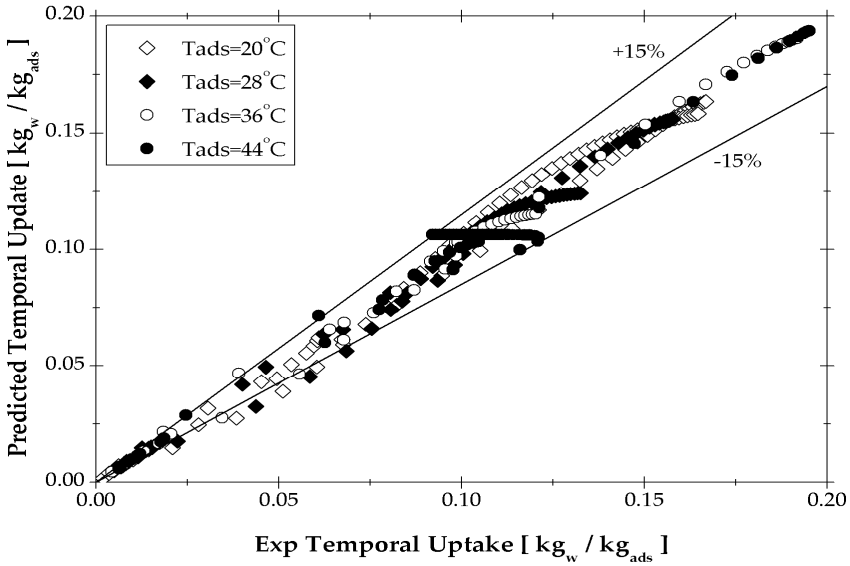

Figure 7-10, Deviation analysis for applying LDF model for HKUST-1

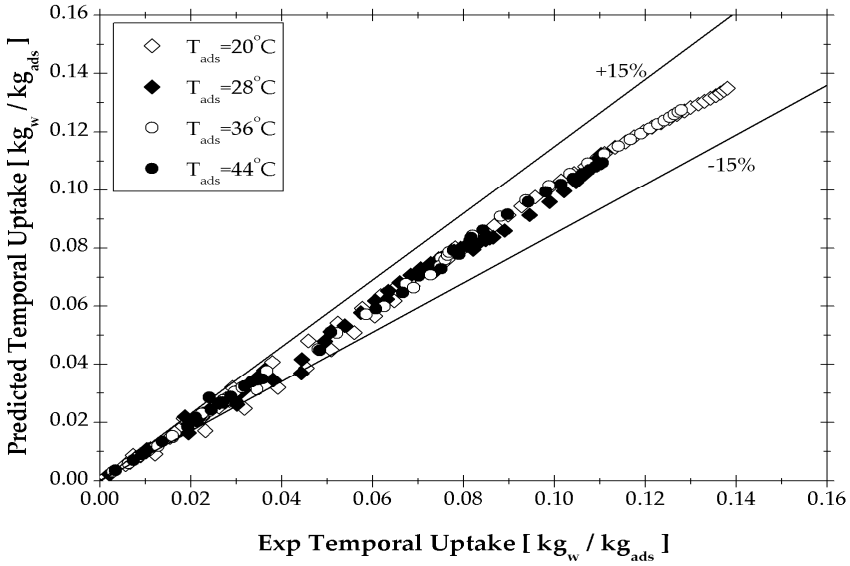

Figure 7-11, Deviation analysis for applying LDF model forMIL-100

7.5.3 Adsorption Cycle Analysis

Many adsorption isotherms models have been reported in the literature including Dubinin-Astakhov (D-A), Sips, Tóth, Freundlich, Langmuir and Temkin and Hill-de Boer [190-193]. The selection of a suitable model to fit the experimental data depends on the adsorption

isotherm profile. With the limitation of the DVS analyser used where the maximum operating temperature is 60 °C, the adsorption isotherms for MIL-100 and HKUST-1 at temperatures above 52 °C were determined using Sips and Langmuir models [38, 194].

Figure 7-12 shows the experimental data for HKUST-1 fitted using Langmuir's equation with 95% confidence and prediction levels. The calculated values of coefficients W^{∞} and b are 0.64 and 8.33 respectively with R^2 value of 0.98, equation 7-8. Figure 7-13 shows the experimental data for MIL-100 fitted using Sip's equation with 95% confidence and prediction levels. The calculated values of coefficients W^{∞}, b and n are 0.38, 2.75 and 3.63 respectively with R^2 value of 0.98, equation 7-9. W^{∞} presents the maximum adsorption capacity in kg_w/kg_{ads} and the deviation between the experimental and predicted values are 3.2% and 2.7% for HKUST-1 and MIL-100 respectively. It is noteworthy to mention that S shape profile of the Sip's model fits the experimental data of the MIL-100. Therefore, equations 7-8 and 7-9 were used to predict the adsorption isotherms of HKUST-1 and MIL-100 at temperatures above $52\ ^0C$.

$$w^* = W^{\infty}\left[b \cdot \left(P_{sat,T_{ref}} / P_{sat,T_{ads}}\right) / \left(1 + b \cdot \left(P_{sat,T_{ref}} / P_{sat,T_{ads}}\right)\right)\right] \qquad 7\text{-}8$$

$$w^* = W^{\infty}\left[\left(b \cdot P_{sat,T_{ref}} / P_{sat,T_{ads}}\right)^n / \left(1 + \left(b \cdot P_{sat,T_{ref}} / P_{sat,T_{ads}}\right)^n\right)\right] \qquad 7\text{-}9$$

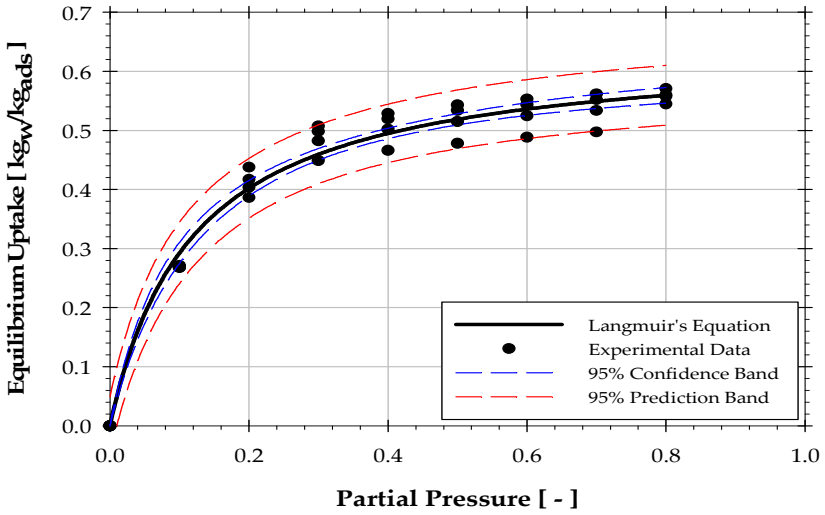

Figure 7-12, HKUST-1 experimental isotherms fitting using Langmuir's equation

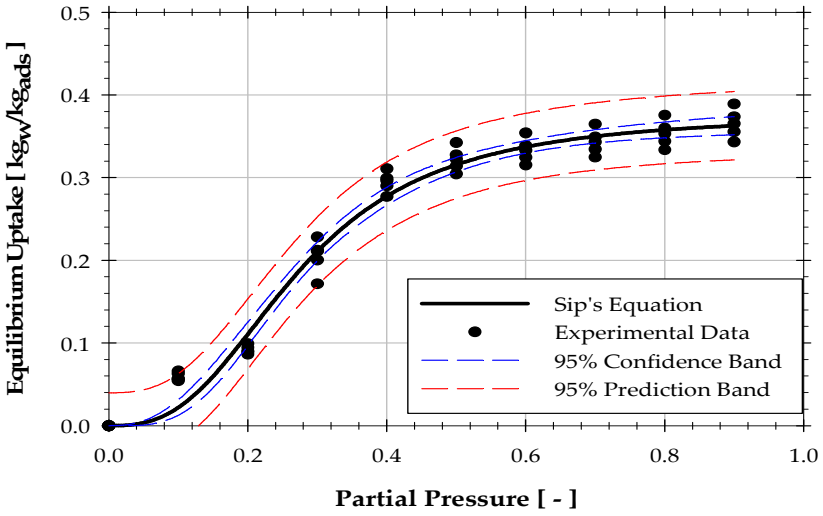

Figure 7-13, MIL-100 experimental isotherms fitting using Sip's equation

The thermodynamic relation between pressures, adsorption temperatures and water vapour concentration is presented by the P-T-W (pressure-temperature-concentration) diagram where the concentration is defined as the mass of water vapour per unit mass of dry adsorbent. Using the above procedure, Figure 7-14 presents the P-T-W diagram for HKUST-

1, MIL-100 and silica gel RD with the ideal adsorption cooling cycle superimposed. For all the materials tested, the ideal adsorption cooling cycle consists of adsorption and condensation at 32 °C, desorption at 85 °C and evaporation at 5 °C as typically used in chilled water systems. Results show that the values of the water vapour concentration at the end of desorption – adsorption are 0.22- 0.42 kg_w/kg_{ads}, 0.05-0.10 kg_w/kg_{ads} and 0.06-0.13 kg_w/kg_{ads} for HKUST-1, MIL-100 and silica gel RD respectively. It is clear that HKUST-1 has the highest values of water vapour concentration at the end of desorption – adsorption processes indicating higher rates of refrigerant circulation which leads to higher cooling capacities.

Figure 7-15 shows the adsorption cooling cycle for HKUST-1 and MIL-100 (1-2-3-4-1) compared to that of silica gel RD (1s-2s-3s-4s-1s). From Figure 7-15-a, the values of the water uptake difference (W3-W1) for HKUST-1 material is 0.20 kg_w/kg_{ads} and that of silica gel RD (W3s-W1s) is 0.07 kg_w/kg_{ads} which yields 185.7% enhancement in the water uptake difference. Following the same analysis for the MIL-100, Figure 7-15-b shows that the water uptake difference is significantly lower than that of silica gel RD by up to 28%. This makes this tested type of MIL-100 not suitable for chilled water systems where evaporating temperature of 5^oC is needed. However, at vapour pressure higher than 1.2kPa (corresponding to evaporation temperature of $10^{\circ}C$), the water uptake of MIL-100 becomes higher than that of silica gel and hence can produce higher refrigerant circulation rate as shown in Figure 7-15-c. Therefore it is useful here to highlight that its cycle analysis using evaporating temperature of $12^{\circ}C$ demonstrate the potential of MIL-100 to be used as an upper cycle for cascade cooling applications.

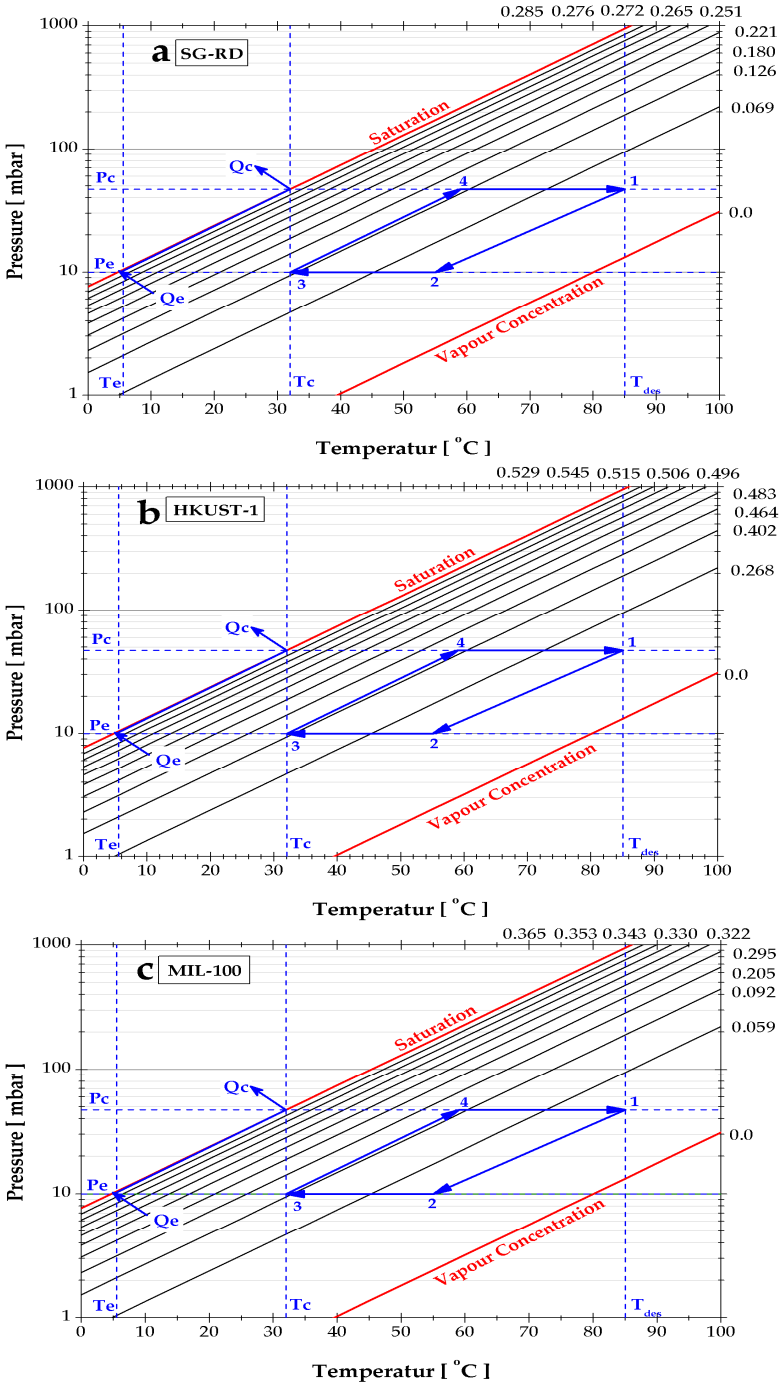

Figure 7-14, PTW diagram for different adsorption pair with ideal cycle superimposed

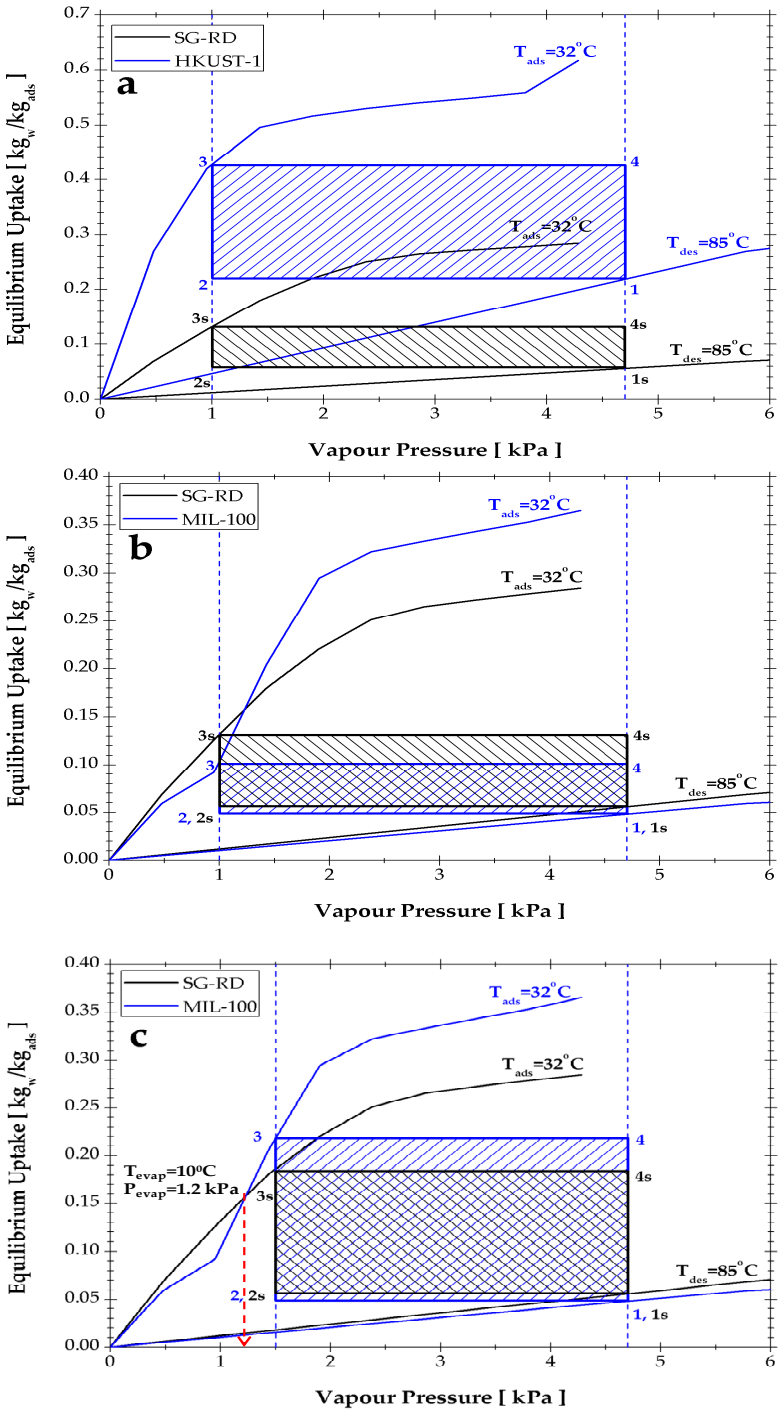

Figure 7-15, Isotherms comparison with ideal cycle superimposed

7.5.4 Stability of HKUST-1

In an adsorption cooling system, the adsorbent material undergoes large number of adsorption / desorption cycles which necessitates that the adsorbents have stable adsorptive performance with time. Figure 7-16 shows the adsorption isotherms of HKUST-1 at four consecutive cycles with every isotherm obtained from a cycle of drying, adsorption and desorption at 36 °C. The figure shows a marked loss of performance in terms of the water uptake at each repeated cycle, which highlights the thermal instability of HKUST-1 MOF towards water vapour.

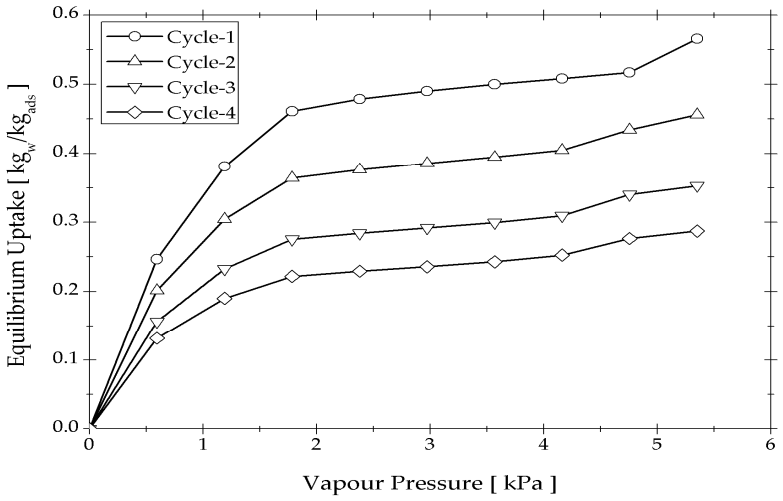

Figure 7-16, Isotherms degradation for HKUST-1

7.6 Summary

This chapter investigated a new adsorbent material named MOF, where there is limited research regarding water adsorption. The testing methodology has been verified by comparing the experimental results of silica gel RD with published model and good agreement has been concluded. The tests conducted for different MOFs of different structures named HKUST-1, MIL-100, MIL-53-Cr, MIL-53-Fe, Birm-1, Birm-1-K and Birm-1-Li. Results showed that HKUST-1 has significant improvement of up to 95.7%; MIL-100 has modest improvement with up to 26.8% while others were inferior to the silica gel.

Based on the cycle analysis, the HKUST-1 / water pair has the best adsorption characteristics with 185.7% increase in the water vapour uptake difference compared to silica gel at evaporating temperature of 5°C. This favourable trend is persistent throughout the tested temperature range. As for the MIL-100, it has shown an inferior performance compared to that of silica gel with 28% reduction in the water vapour uptake difference in the cycle with evaporating temperature of 5°C. This trend is reversed for evaporating temperatures above 12°C at the same adsorption, condensation and desorption temperatures. The significance of this finding implies that the MIL-100 can be used in cascade cooling applications where the evaporation temperature can be higher than 12°C. The previous work showed the potential of MOFs towards water vapour adsorption, however there is no clear evaluation for using these materials in adsorption cooling systems.

CHAPTER 8: CONCLUSIONS AND FUTURE WORK

8.1 Introduction

Adsorption cooling systems have received significant interest during the last few decades in order to satisfy the market demand of cooling systems and cope with the current environmental issues. This thesis investigates experimentally and theoretically the performance of silica gel / water adsorption cooling systems. It also evaluates the effect of various geometric and physical parameters on the cooling load and the coefficient of performance of the adsorption cooling systems. The effects of enhancing the adsorber bed through adding metal particles and eliminating contact resistance between the adsorbent bed granules and heat exchanger surfaces was investigated. Finally, the potential of new class of porous materials called MOFs to replace the currently applied silica gel as a water adsorbent was investigated.

8.2 Conclusions

This PhD project was set out to bridge the gap between the theoretical ideas of enhancing adsorption cooling systems and their practicality. To achieve that, a novel lumped analytical simulation model for a commercialised silica gel / water adsorption chiller and an experimental test rig have been constructed to be used as performance evaluation tools. Three main objectives have been achieved; (1) the investigation of different operating conditions effect on the adsorbent-bed and chiller performance, theoretically and experimentally, (2) theoretical investigation of the effect of physical parameters on chiller performance in addition to propose different enhancement techniques and (3) experimental

characterisation of a new species of adsorbents that could replace the currently used silica gel. The following points conclude the project contributions.

- The presented lumped analytical simulation model predicted the performance of commercial 450kW adsorption water chiller with good accuracy ±15%. The model is a global model that has the ability to investigate the effect of various physical parameters on the performance of the adsorption chiller.
- Chiller operating conditions such as operating temperature, cycle time and secondary fluid flow rate directly influence chiller performance. Operating temperature can be used as a load control tool to mange chiller operation in case of part load with limited efficiency loss. It has been shown that at a particular cooling water temperature, increasing the generation temperature lift increases the cooling capacity with insignificant reduction in the chiller COP and efficiency. Cycle time can be used to improve chiller performance to get more cooling and GA was used to determine the global optimum cycle time corresponding to the maximum cooling capacity, where chiller cooling capacity can be increased by 8.3%. Cooling, heating and chilled water flow rate affect the chiller performance where more cooling flow rate increases the rate of adsorbent bed temperature drop and hence more adsorbed water vapour, which have been experimentally investigated.
- By changing the fin spacing, the adsorbent bed heat transfer area changes which influences its heat transfer performance. The chiller cooling capacity increases by 3% by reducing the fin spacing from its design value to the minimum permissible value. Eliminating the contact resistance by gluing the first layer of adsorbent granules and

packing the remaining ones averagely improves chillers cooling capacity and COP by 8.9% and 4.6% respectively. Using different metal additives (Aluminium, Copper, Brass and Stainless steel) with different weight ratios of 5%, 10% and 15% improves the heat transfer performance of adsorbent bed, up to 58.2% increase in the adsorbent-bed NTU during cooling with Aluminium additives which leads to 12.5% enhancement in the chiller cooling capacity at maximum fin spacing. However, at lower fin spacing (FSR<1.2), a negative enhancement was experienced which can be attributed to the increase in the ratio of metal to silica gel mass. Results for the combined techniques showed that the enhancement in the cooling capacity increases with the increase in the fin spacing to be up to 25% at maximum fin spacing. A similar trend has been noticed for the COP which can be enhanced by a maximum of 10%.

- MOFs adsorbents named; HKUST-1, MIL-100, MIL-53-Cr, MIL-53-Fe, Birm-1, Birm-1-K and Birm-1-Li were tested using DVS analyser for water adsorption performance. Compared to silica gel, results regarding water vapour uptake showed that HKUST-1 has significant improvement of up to 95.7%; MIL-100 has modest improvement with up to 26.8% while others were inferior to the silica gel. Regarding the cycle analysis the HKUST-1 / water pair has the best adsorption characteristics with 185.7% increase in the water vapour uptake difference compared to silica gel at evaporating temperature of 5˚C. This favourable trend is consistent throughout the tested temperature range. As for the MIL-100, it has shown an inferior performance compared to that of silica gel with 28% reduction in the water vapour uptake difference in the cycle with evaporating temperature of 5˚C. It is important here to

point out that this trend is reversed for evaporating temperatures above 12 ^{0}C at the same adsorption, condensation and desorption temperatures. The significance of this finding implies that the MIL-100 can be used in cascade cooling applications where the evaporation temperature can be higher than 12 ^{0}C.

8.3 Future work

This thesis presented research efforts towards the enhancement of silica gel / water adsorption cooling systems and it can be considered as a strong foundation for further work. The following is a list of the suggested future work;

- The thesis presented the characterisation of a new species of adsorbents named metal organic frameworks (MOFs) that presented an extraordinary behaviour against water vapour adsorption. HKUST-1 was shown to significantly outperform silica gel RD with 95% increase in the water uptake and 185.7% in cycle analysis using the same operating conditions as those typically used in silica gel / water adsorption chillers. However, this adsorbent performed negatively in term of stability against water vapour. Based on surface chemistry published work there is potential for synthesis of this MOF to be more stable against water vapour adsorption and high temperature treatment. Therefore, future research in collaborative with MOF synthesis specialist is needed. After the characterisation step of new adsorbents, the adsorption behaviour needs to be correlated and implemented in the developed simulation model to investigate the feasibility of replacing the currently applied silica gel with such new adsorbents.

- The thesis presented the construction of a test rig that is flexible in changing a scaled down adsorbent bed modules. There are many techniques that can improve the heat and mass transfer performance of the adsorbent bed, including new designs of the adsorbent bed heat exchanger. Some of these techniques have been theoretically investigated. A number of adsorber bed designs were developed in the last decade that benefits the heat and mass transfer performance. The performance of these new designs can be modelled using the empirical lumped analytical model that has been developed in this work and tested in the experimental facility.
- Metal organic frameworks were originally investigated for gaseous fuel storage such as hydrogen and methane. The use of this MOF material with environment friendly refrigerant such as ethanol is also recommended for investigation.

APPENDIX A

A.1 Home screen flow chart of the model

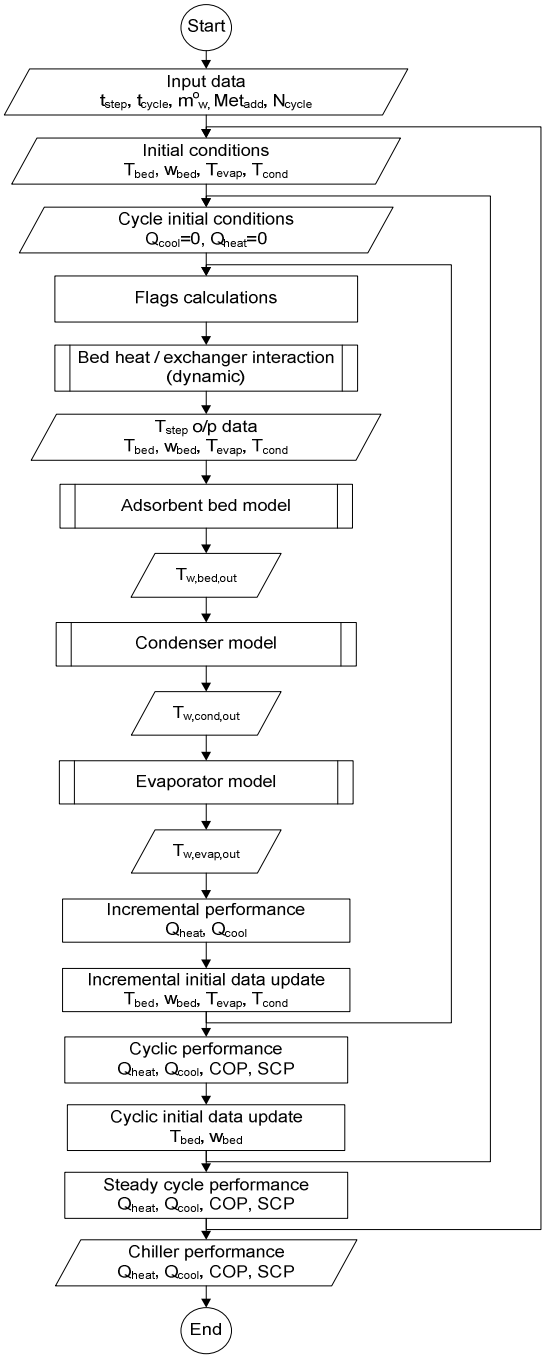

A.2 Home screen MATLAB code

```
%This is the home screen of evaluating the performance of the adsorption
%chiller ADCM1-180
%=========================================================================
clear all; close all; clc;
% Input data
fin_pitch_bed_mm=1.1;       % Minimum fin spacing
Metal='Al'; Pge=15;         % Type of metal additives and the percentage
for i=1:19
fin_pitch_bed_mm=fin_pitch_bed_mm+0.1;
fin_pitch_bed=fin_pitch_bed_mm/1000;
N_cyc=8; Dtime=5;
t_normal=430; t_regen=30; t_htrec=20;
t_cycle=(t_normal+t_regen+t_htrec);
[MC_bed, MC_SBed, MC_Ad, M_bed_ads]=MCs(fin_pitch_bed, Metal, Pge);
M_ref_tot=185; M_ref_L_cond_MAX=50;
THW_in=(88.6+273); TCW_in=(29.5+273); TCHW_in=(11.1+273);
m_dot_HW=18.3; m_dot_CW=66.6; m_dot_CHW=19.7;
%=========================================================================
% Initial conditions
Time_i=0;
t=Time_i;
T_bed_i=27+273;
T_bed2_i=27+273;
T_evap_i=27+273;
T_cond_i=27+273;
W_bed2_i=0.05;
W_bed_i=0.05;
M_ref_L_cond=50*0.9;
M_ref_L_evap_i=M_ref_tot;
%=========================================================================
step=Dtime; S=0;
%-------------------------------------------------------------------------
for M=1:N_cyc
    Q_in=0;
    Q_evap=0;
    t_round=0;
%-------------------------------------------------------------------------
for L=1:step:t_cycle
    S=S+1
    t=t+step
    Time(S)=t;
%-------------------------------------------------------------------------
 t_round=t_round+step
if (t_round<=t_normal)
    FLAG1=1; FLAG3=1; FLAG4=0; FLAG5=1;
elseif ((t_round>t_normal)&(t_round<=(t_normal+t_regen)))
    FLAG1=1; FLAG3=0; FLAG4=1; FLAG5=0;
elseif ((t_round>(t_normal+t_regen))&(t_round<=(t_normal+t_regen+t_htrec)))
    FLAG1=0; FLAG3=1; FLAG4=0; FLAG5=0;
end;
%=========================================================================
Timerange2=[Time_i t];
Initialbed2=[W_bed2_i T_bed2_i T_cond_i W_bed_i T_bed_i T_evap_i
M_ref_L_evap_i];
%=========================================================================
option2=odeset('RelTol',1E-4,'AbsTol',1E-4);
```

```
Y=ode45(@ddydwdt,Timerange2,Initialbed2,option2,M_ref_L_cond,m_dot_HW,m_dot
_CW,m_dot_CHW,THW_in,TCW_in,TCHW_in,FLAG1,FLAG3,Dtime,FLAG4,FLAG5,fin_pitch
_bed_mm,Metal,Pge);
%-----------------Hot Bed Parameters-------------------------------------
Y2_t=deval(Y,t);
W_bed2(S)=Y2_t(1);
T_bed2(S)=Y2_t(2);
T_cond(S)=Y2_t(3);
%-----------------Cold Bed Parameters------------------------------------
W_bed(S)=Y2_t(4);
T_bed(S)=Y2_t(5);
T_evap(S)=Y2_t(6);
%-----------------Evaporator Parameters----------------------------------
M_ref_L_evap(S)=Y2_t(7);
%============================================================================
TB=T_bed(S); TB2=T_bed2(S); TE=T_evap(S); TC=T_cond(S);
%----------------------------------------------------------------------------
if ((FLAG1==1)&&(FLAG3==1))
    T_w_bed_in2=THW_in; m_dot_water_bed2=m_dot_HW;

T_w_bed_out2=BedTwo(TB2,T_w_bed_in2,m_dot_water_bed2,fin_pitch_bed,Metal,Pg
e);
    T_w_bed_in=TCW_in; m_dot_water_bed=m_dot_CW;

T_w_bed_out=BedTwo(TB,T_w_bed_in,m_dot_water_bed,fin_pitch_bed,Metal,Pge);
elseif ((FLAG1==0)&&(FLAG3==1))
    T_w_bed_in2=TCW_in; m_dot_water_bed2=m_dot_CW;

T_w_bed_out2=BedTwo(TB2,T_w_bed_in2,m_dot_water_bed2,fin_pitch_bed,Metal,Pg
e);
    T_w_bed_in=T_w_bed_out2; m_dot_water_bed=m_dot_CW;

T_w_bed_out=BedTwo(TB,T_w_bed_in,m_dot_water_bed,fin_pitch_bed,Metal,Pge);
end
%-----------------Cooling Water Stream Temp------------------------------
if ((FLAG1==1)&&(FLAG3==1))
    T_w_cond_in=T_w_bed_out; m_dot_water_cond=m_dot_CW;
elseif ((FLAG1==1)&&(FLAG3==0))
    T_w_cond_in=TCW_in; m_dot_water_cond=m_dot_CW;
elseif ((FLAG1==0)&&(FLAG3==1))
    T_w_cond_in=T_w_bed_out; m_dot_water_cond=m_dot_CW;
end
TCW_inn(S)=TCW_in;
TCW_out(S)=CondTwo(TC,T_w_cond_in,m_dot_water_cond,Dtime);
%-----------------Hot Water Steam Temp-----------------------------------
if ((FLAG1==1)&&(FLAG3==1))
    THW_out(S)=T_w_bed_out2; THW_inn(S)=THW_in;
elseif ((FLAG1==1)&&(FLAG3==0))
    THW_out(S)=THW_in; THW_inn(S)=THW_in;
elseif ((FLAG1==0)&&(FLAG3==1))
    THW_out(S)=THW_in; THW_inn(S)=THW_in;
end
%-----------------Chilled Water Stream Temp------------------------------
T_w_evap_in=TCHW_in; m_dot_water_evap=m_dot_CHW;
TCHW_inn(S)=TCHW_in; TCHW_out(S)=EvapTwo(TE,T_w_evap_in,m_dot_water_evap);
Chilled_out=TCHW_out(S)-273;
%============================================================================
% Adsorption / Desorption Switching
```

```
if
((M==1)||(M==3)||(M==5)||(M==7)||(M==9)||(M==11)||(M==13)||(M==15)||(M==17)
||(M==19))
T_des(S)=T_bed2(S); W_des(S)=W_bed2(S); T_ads(S)=T_bed(S);
W_ads(S)=W_bed(S);
elseif
((M==2)||(M==4)||(M==6)||(M==8)||(M==10)||(M==12)||(M==14)||(M==16)||(M==18
)||(M==20))
T_des(S)=T_bed(S); W_des(S)=W_bed(S); T_ads(S)=T_bed2(S);
W_ads(S)=W_bed2(S);
end;
%=========================================================================
m_water_ads(S)=W_bed(S)*M_bed_ads;
m_water_des(S)=W_bed2(S)*M_bed_ads;
m_water_tot(S)=m_water_ads(S)+m_water_des(S);
%=========================================================================
% Instant Performance Indicators
dq_in=(m_dot_HW*4.18*Dtime/t_cycle)*(THW_inn(S)-THW_out(S));
Q_in=Q_in+dq_in;
dq_evap=(m_dot_water_evap*4.18*Dtime/t_cycle)*(TCHW_inn(S)-TCHW_out(S));
Q_evap=Q_evap+dq_evap;
%-----------------------------Data Plot-----------------------------------
subplot(3,2,1); PLT1=plot(Time,THW_inn,'k--',Time,TCW_inn,'k--
',Time,TCHW_inn,...
    'k--',Time,T_des,'b-',Time,T_ads,'c-',Time,T_evap,'m-',Time,T_cond,'r-
');
set(PLT1,'linewidth',2); set(gca,'fontsize',10); xlabel('Time [Sec]',
'fontsize',...
    12); ylabel('Temperature [C]','fontsize',12); title('Heat Exchangers
Temperature Profile','fontsize',14);

subplot(3,2,2); PLT2=plot(Time,THW_inn,'r-',Time,THW_out,'m-
',Time,TCW_inn,...
    'k-',Time,TCW_out,'g-',Time,TCHW_inn,'b-',Time,TCHW_out,'c-');
set(PLT2,'linewidth',2); set(gca,'fontsize',10); xlabel('Time [Sec]',
'fontsize',...
    12); ylabel('Temperatures [C]','fontsize',12); title('Heat Exchangers
Outlet Temperature','fontsize',14);

subplot(3,2,3); PLT3=plot(Time,M_ref_L_evap,'k-');
set(PLT3,'linewidth',2); set(gca,'fontsize',10); xlabel('Time [Sec]',
'fontsize',...
    12); ylabel('Evaporator Refrigerant [kg]','fontsize',12);
title('Evaporator Refrigerant mass','fontsize',14);

subplot(3,2,4); PLT3=plot(Time,m_water_tot,'k-');
set(PLT3,'linewidth',2); set(gca,'fontsize',10); xlabel('Time [Sec]',
'fontsize',...
    12); ylabel('Ads & Des Refrigerant [kg]','fontsize',12); title('Ads &
Des Refrigerant mass','fontsize',14);

subplot(3,2,5); PLT3=plot(Time,m_water_ads,'k-');
set(PLT3,'linewidth',2); set(gca,'fontsize',10); xlabel('Time [Sec]',
'fontsize',...
    12); ylabel('Adsorber Refrigerant [kg]','fontsize',12); title('Adsorber
Refrigerant mass','fontsize',14);

subplot(3,2,6); PLT3=plot(Time,m_water_des,'k-');
```

```
set(PLT3,'linewidth',2); set(gca,'fontsize',10); xlabel('Time [Sec]',
'fontsize',...
    12); ylabel('Desorber Refrigerant [kg]','fontsize',12); title('Desorber
Refrigerant mass','fontsize',14);
drawnow;
%=========================================================================
Time_i=t;
W_bed2_i=Y2_t(1);
T_bed2_i=Y2_t(2);
T_cond_i=Y2_t(3);
%-------------------------------------------------------------------------
W_bed_i=Y2_t(4);
T_bed_i=Y2_t(5);
T_evap_i=Y2_t(6);
%-------------------------------------------------------------------------
M_ref_L_evap_i=Y2_t(7);
end
% Cyclic Performance Indicators
Q_Cooling(M)=Q_evap;
Q_Heating(M)=Q_in;
COP(M)=Q_evap/Q_in;
SCP(M)=Q_evap/(M_bed_ads);
%-------------------------------------------------------------------------
W_bed2_i=Y2_t(4);
T_bed2_i=Y2_t(5);
%-------------------------------------------------------------------------
W_bed_i=Y2_t(1);
T_bed_i=Y2_t(2);
End
%-------------------------------------------------------------------------
% Complete Run Performance Indicators
[MC_bedi(i),MC_SBedi(i),MC_Adi(i),M_bed_adsi(i)]=
MCs(fin_pitch_bed,Metal,Pge);
MCSM(i)=MC_SBedi(i)/(MC_bedi(i)+MC_Adi(i));
P(i)=fin_pitch_bed_mm;
Q_Coolingi(i)=Q_Cooling(N_cyc);
Q_Heatingi(i)=Q_Heating(N_cyc);
COPi(i)=COP(N_cyc);
SCPi(i)=SCP(N_cyc);
end
```

A.3 Bed / Heat exchanger interaction flow chart

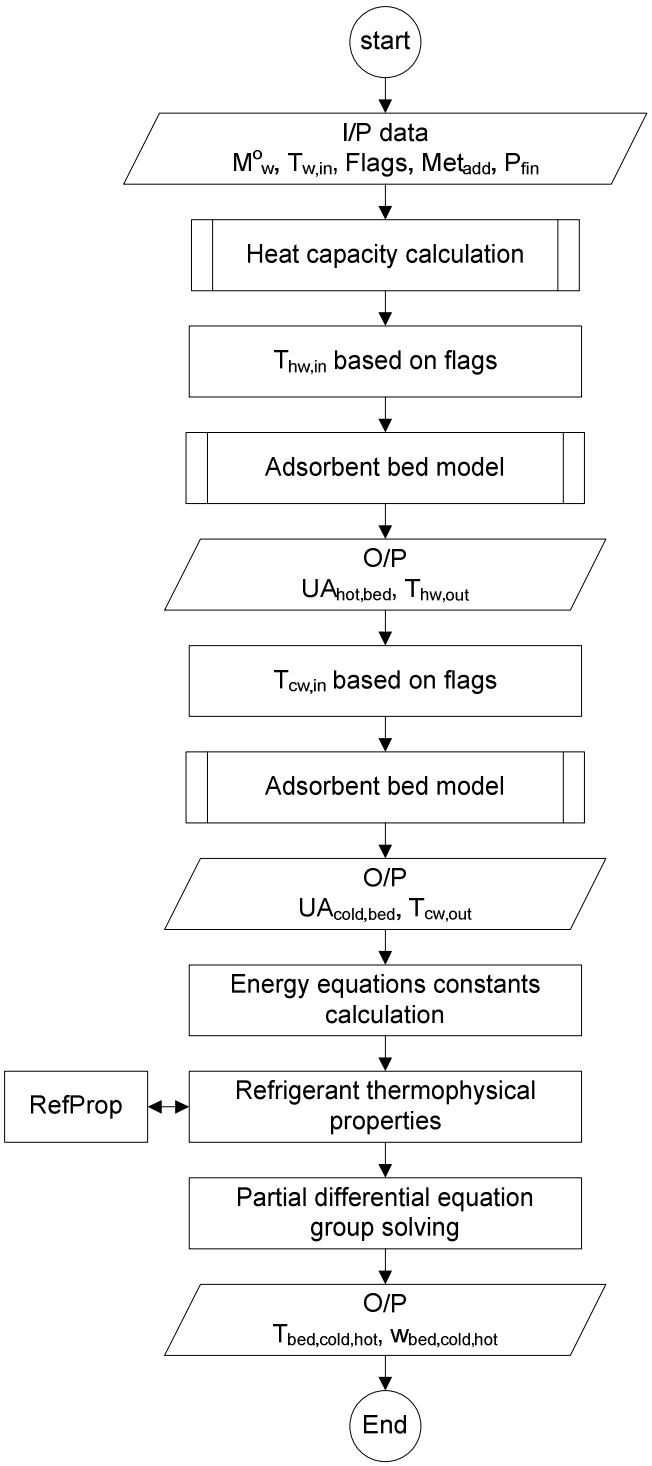

A.4 Bed / Heat exchanger interaction code

```
function dy=ddydwdt(t,y,M_ref_L_cond,m_dot_HW,m_dot_CW,m_dot_CHW,THW_in,...

TCW_in,TCHW_in,FLAG1,FLAG3,Dtime,FLAG4,FLAG5,fin_pitch_bed_mm,Metal,Pge)
%=========================================================================
% This sub-program for solving energy balance equations for different heat
% exchangers (adsorbent bed, evaporator and condenser)
%Initial vector
dy=zeros(7,1);
T_bed2=y(2); T_cond=y(3); T_bed=y(5); T_evap=y(6); M_ref_L_evap=y(7);
%=========================================================================
FLAG2=1; Cv=1.9; fin_pitch_bed=fin_pitch_bed_mm/1000;
[MC_bed, MC_SBed, MC_Ad, M_bed_ads]=MCs(fin_pitch_bed, Metal, Pge);
MCp_bed_met=MC_Ad+MC_bed+(616.816*3.83-616.816);
MCp_bed_ads=MC_SBed; MCp_bed_w=407.8*4.18;
MCp_cond_met=191.3277*1.25; MCp_evap_met=185.3718;
D_so=2.54E-4; Rp=0.15E-3; Ea=4.2E4; R=8.3145; H_ads=2.51E3;
%=========================================================================
          %Desorber temperature constant
%=========================================================================
if ((FLAG1==1)&(FLAG3==1))
    T_w_bed_in2=THW_in; m_dot_water_bed2=m_dot_HW;
elseif ((FLAG1==1)&(FLAG3==0))
    T_w_bed_in2=THW_in; m_dot_water_bed2=m_dot_HW;
elseif ((FLAG1==0)&(FLAG3==1))
    T_w_bed_in2=TCW_in; m_dot_water_bed2=m_dot_CW;
end
%-------------------------------------------------------------------------
    %Bed heating water stream
[T_w_bed_out2, UA_bed2]=
BedTwo(T_bed2,T_w_bed_in2,m_dot_water_bed2,fin_pitch_bed,Metal,Pge)
%-------------------------------------------------------------------------
P_sat_ref_cond=refpropm('P','T',T_cond,'Q',0,'water');      %P_sat_ref
P_sat_bed2=refpropm('P','T',T_bed2,'Q',0,'water');          %P_sat_ads
%-------------------------------------------------------------------------
if ((FLAG1==1)&(FLAG3==0))
    w_star_bed2=Uptake_sat(T_bed,T_bed2);
    W_bed_const1=15*D_so/Rp^2;
elseif ((FLAG1==0)&(FLAG3==1))
    w_star_bed2=Uptake_sat(T_bed2,T_bed2);
    W_bed_const1=0;
else
    w_star_bed2=Uptake_sat(T_cond,T_bed2);
    W_bed_const1=15*D_so/Rp^2;
end
%-------------------------------------------------------------------------
Cp_w_T_bed2=refpropm('C','T',T_bed2,'Q',1,'water')*1E-3;    %Cp_w_T_bed
%-------------------------------------------------------------------------
T_bed_const1=FLAG1*M_bed_ads*H_ads*(15*D_so/Rp^2);
T_bed_const2=(1-FLAG4)*m_dot_water_bed2*4.18*(T_w_bed_in2-T_w_bed_out2);
T_bed_const3=MCp_bed_ads+MCp_bed_met+(FLAG4*MCp_bed_w);
T_bed_const4=M_bed_ads*Cp_w_T_bed2;
%=========================================================================
         %Adsorber temperature constant
%=========================================================================
if ((FLAG1==1)&(FLAG3==1))
    T_w_bed_in=TCW_in; m_dot_water_bed=m_dot_CW;
```

```
elseif ((FLAG1==1)&(FLAG3==0))
    T_w_bed_in=TCW_in; m_dot_water_bed=m_dot_CW;
elseif ((FLAG1==0)&(FLAG3==1))
    T_w_bed_in=T_w_bed_out2; m_dot_water_bed=m_dot_CW;
end
%-------------------------------------------------------------------------
    %Bed cooling water stream
[T_w_bed_out,
UA_bed]=BedTwo(T_bed,T_w_bed_in,m_dot_water_bed,fin_pitch_bed,Metal,Pge)
%-------------------------------------------------------------------------
P_sat_ref_evap=refpropm('P','T',T_evap,'Q',0,'water');
P_sat_bed=refpropm('P','T',T_bed,'Q',0,'water');
%-------------------------------------------------------------------------
h_ref_g_T_hex=refpropm('H','T',T_evap,'Q',1,'water')*1E-3;
h_ref_P_hex_T_bed=refpropm('H','T',T_bed,'P',P_sat_bed,'water')*1E-3;
Cp_w_T_bed=refpropm('C','T',T_bed,'Q',1,'water')*1E-3;
%-------------------------------------------------------------------------
if ((FLAG1==1)&(FLAG3==0))
    w_star_bed=Uptake_sat(T_evap,T_bed);
    W_bed_const2=0;
elseif ((FLAG1==0)&(FLAG3==1))
    w_star_bed=Uptake_sat(T_bed,T_bed);
    W_bed_const2=0;
else
    w_star_bed=Uptake_sat(T_evap,T_bed);
    W_bed_const2=15*D_so/Rp^2;
end
%-------------------------------------------------------------------------
T_bed_const5=FLAG1*M_bed_ads*H_ads*(15*D_so/Rp^2);
T_bed_const6=FLAG1*M_bed_ads*((FLAG3*(h_ref_g_T_hex-h_ref_P_hex_T_bed))...
    +((1-FLAG3)*Cv*(T_bed2-T_bed)))*(15*D_so/Rp^2);
T_bed_const7=(1-FLAG4)*m_dot_water_bed*4.18*(T_w_bed_in-T_w_bed_out);
T_bed_const8=MCp_bed_ads+MCp_bed_met+(FLAG4*MCp_bed_w);
T_bed_const9=M_bed_ads*Cp_w_T_bed;
%=========================================================================
        %Condenser constants
%=========================================================================
if ((FLAG1==1)&(FLAG3==1))
    T_w_cond_in=T_w_bed_out; m_dot_water_cond=m_dot_CW;
elseif ((FLAG1==1)&(FLAG3==0))
    T_w_cond_in=TCW_in; m_dot_water_cond=m_dot_CW;
elseif ((FLAG1==0)&(FLAG3==1))
    T_w_cond_in=T_w_bed_out; m_dot_water_cond=m_dot_CW;
end
%-------------------------------------------------------------------------
   %Condenser water outlet temperature
[T_w_cond_out]=CondTwo(T_cond,T_w_cond_in,m_dot_water_cond,Dtime);
%-------------------------------------------------------------------------
h_ref_cond_out=refpropm('H','T',T_cond,'Q',0,'water')*1E-3;
h_ref_bed2_out=refpropm('H','T',T_bed2,'P',P_sat_bed2,'water')*1E-3;
Cp_ref_L_cond=refpropm('C','T',T_cond,'Q',0,'water')*1E-3;
h_ref_cond_in=refpropm('H','T',T_cond,'Q',1,'water')*1E-3;
C_ref_bed2_out=refpropm('C','T',T_bed2,'Q',1,'water')*1E-3;
%-------------------------------------------------------------------------
T_cond_const1=-FLAG5*M_bed_ads*(h_ref_cond_in-
h_ref_cond_out)*(15*D_so/Rp^2);
T_cond_const2=m_dot_water_cond*4.18*(T_w_cond_in-T_w_cond_out);
T_cond_const3=(M_ref_L_cond*Cp_ref_L_cond)+MCp_cond_met;
```

```
T_cond_const4=-FLAG5*M_bed_ads*C_ref_bed2_out*(T_bed2-
T_cond)*(15*D_so/Rp^2);
%=========================================================================
        %Evaporator constants
%=========================================================================
T_w_evap_in=TCHW_in;
m_dot_water_evap=m_dot_CHW;
%-------------------------------------------------------------------------
     %Evaporator cooling water stream
[T_w_evap_out]=EvapTwo(T_evap,T_w_evap_in,m_dot_water_evap);
%-------------------------------------------------------------------------
h_ref_evap_in=refpropm('H','T',T_evap,'Q',0,'water')*1E-3;
h_ref_evap_out=refpropm('H','T',T_evap,'Q',1,'water')*1E-3;
Cp_ref_L_evap=refpropm('C','T',T_evap,'Q',0,'water')*1E-3;
%-------------------------------------------------------------------------
T_evap_const1=FLAG5*M_bed_ads*(h_ref_evap_in-
h_ref_evap_out)*(15*D_so/Rp^2);
T_evap_const2=m_dot_water_evap*4.18*(T_w_evap_in-T_w_evap_out);
T_evap_const3=(M_ref_L_evap*Cp_ref_L_evap)+MCp_evap_met;
%=========================================================================
dy(1)=W_bed_const1*(w_star_bed2-y(1))*exp(-Ea/(R*y(2)));
dy(2)=(T_bed_const1*exp(-Ea/(R*y(2)))*(w_star_bed2-
y(1))+T_bed_const2)/(T_bed_const3+(y(1)*T_bed_const4));
dy(3)=((T_cond_const1+T_cond_const4)*exp(-Ea/(R*y(2)))*(w_star_bed2-
y(1))+T_cond_const2)/T_cond_const3;
%=========================================================================
dy(4)=(FLAG3*W_bed_const2*exp(-Ea/(R*y(5)))*(w_star_bed-y(4)))-((1-
FLAG3)*W_bed_const1*(w_star_bed2-y(1))*exp(-Ea/(R*y(2))));
dy(5)=((T_bed_const5+T_bed_const6)*exp(-Ea/(R*y(5)))*(w_star_bed-
y(4))+T_bed_const7)/(T_bed_const8+(T_bed_const9*y(4)));
dy(6)=(T_evap_const1*exp(-Ea/(R*y(5)))*(w_star_bed-
y(4))+T_evap_const2+(0.04*(h_ref_evap_in-h_ref_evap_out)))/T_evap_const3;
%=========================================================================
dy(7)=-M_bed_ads*FLAG5*((W_bed_const1*(w_star_bed2-y(1))*exp(-
Ea/(R*y(2))))+(W_bed_const2*exp(-Ea/(R*y(5)))*(w_star_bed-y(4))));
```

A.5 Adsorbent bed model flow chart

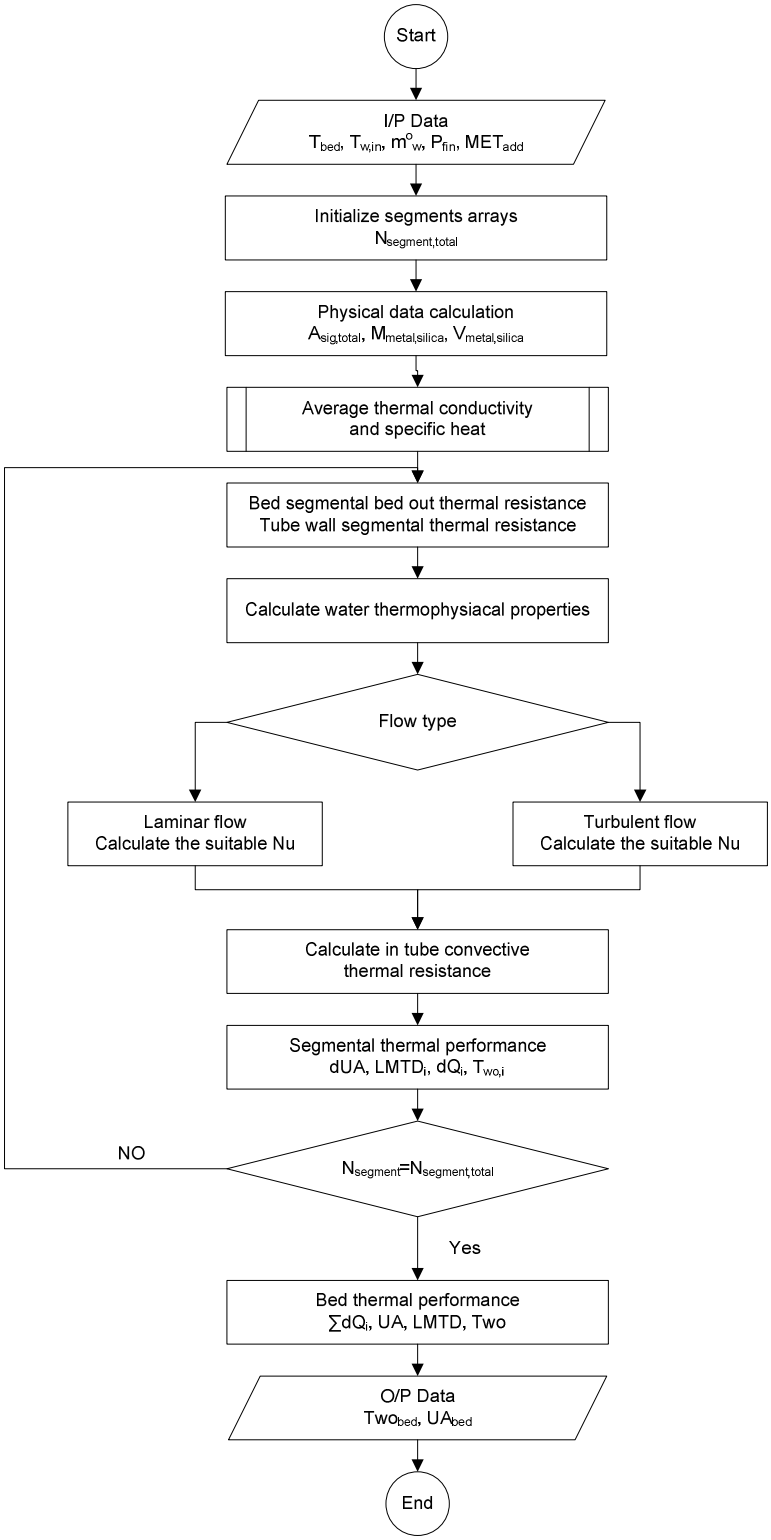

A.6 Adsorbent bed model code

```
function [T_w_bed_out,UA]=
BedTwo(T_bed,T_w_bed_in,m_dot_water_bed,fin_pitch_bed,Metal,Pge)
Ref='water'; SecFld='water';
%=========================================================================
% Input geometrical characteristics
L_fin_bed=340E-3; H_fin_bed=0.0285;              %fin_pitch_bed=1.5E-3;
Dp=0.31; L_module=3400E-3; N_t_module=12; N_pass_bed=2;
N_module=7*2*4; D_bed_o=(5/8)*0.0254; t_bed=0.8E-3; D_bed_i=D_bed_o-
(2*t_bed);
W_fin_bed=0.105E-3; epslon_bed=0.0015E-3;
N_fin_module=round(L_module/fin_pitch_bed);
%=========================================================================
% Array booking
N_inc=N_fin_module*2;
site=zeros(1,N_inc);Segma_R=zeros(1,N_inc);UA_bed=zeros(1,N_inc);T_w_out=ze
ros(1,N_inc);
DT_b=zeros(1,N_inc);DT_s=zeros(1,N_inc);LMTD=zeros(1,N_inc);dq=zeros(1,N_in
c);
T_w_in=zeros(1,N_inc);T_w_out=zeros(1,N_inc);htc_w_bedi=zeros(1,N_inc);
%=========================================================================
% Geometrical calculation
a=L_fin_bed/N_t_module; b=H_fin_bed; r_fin_bed=sqrt(a*b/pi);
D_fin_bed=r_fin_bed*2;
fin_space_bed=fin_pitch_bed-W_fin_bed; A_w_bed=pi*D_bed_i^2/4;
N_t_bed=N_module*N_t_module; N_t_bed_pass=N_t_bed/N_pass_bed;
T_bed_C=T_bed-273; R_cont_TSG=Rc(T_bed_C,Dp); R_cont_FSG=Rc(T_bed_C,Dp);
%=========================================================================
% Area calculation
L_FT=W_fin_bed*N_fin_module; L_UFT=L_module-L_FT; A_UFT=pi*D_bed_o*L_UFT;
A_UFTM=A_UFT*N_t_module;
A_FS=(L_fin_bed*H_fin_bed)-(0.25*pi*D_bed_o^2*N_t_module);
A_FTP=(2*L_fin_bed*W_fin_bed)+(2*H_fin_bed*W_fin_bed);
A_F=A_FS+A_FTP; A_FM=A_F*N_fin_module;
A_M=A_FM+A_UFTM; A_bed=A_M*N_module;
%=========================================================================
% Mass calculation
Roh_F=3661.85; C_F=0.896; Roh_T=8954; C_T=0.3831; Roh_S=690.987; C_S=0.921;
%Roh_S=708.299;
M_TM=0.25*pi*(D_bed_o^2-D_bed_i^2)*L_module*N_t_module*Roh_T;
M_FM=A_FS*W_fin_bed*Roh_F*N_fin_module;
MC_M=M_TM*C_T+M_FM*C_F;
%=========================================================================
V_TM=0.25*pi*L_module*N_t_module*D_bed_o^2;
V_FM=A_FS*W_fin_bed*N_fin_module;
V_M=L_module*L_fin_bed*H_fin_bed;
V_SM=V_M-V_FM-V_TM; M_SM=V_SM*Roh_S; M_SBed=(M_SM*N_module);
%=========================================================================
[K_SG, C_Ad]=KC_mix(Metal, Pge);
M_bed_ads=M_SBed*(1-Pge/100); MC_SBed=M_SBed*C_S;
MC_Ad=(M_SBed*Pge/100)*C_Ad; MC_bed=MC_M*N_module;
%=========================================================================
% Outside surface heat transfer resistance
A_s_fin_bed=(a*b)-(pi*D_bed_o^2/4);
d_SG=fin_space_bed/2;
RA1=R_cont_FSG/(2*A_s_fin_bed);% Axial contact thermal resistance (Per
increament)
```

```
RA2=d_SG/(2*A_s_fin_bed*K_SG);% Axial thermal resistance (Per increament)
RA=RA1+RA2; % Total axial thermal resistance (Per increament)
RB1=R_cont_TSG/(2*pi*D_bed_o*d_SG); % Radial Contact thermal resistance
(Per increment)
RB2=(log(D_fin_bed/D_bed_o))/(4*pi*K_SG*d_SG); % Radial thermal resistance
(Per increament)
RB=RB1+RB2; % Total radial thermal resistance (Per increment)
R_bed=RA*RB/(RA+RB); % Bed side thermal resistance for one increment
%=========================================================================
% Tube wall heat heat transfer resistance
K_t_bed=310*1E-3; %kW/m.K
R_t_bed=(log(D_bed_o/D_bed_i))/(2*pi*K_t_bed*fin_pitch_bed);
%=========================================================================
% Start of calculation loop
T_w_in(1)=T_w_bed_in;
for i=1:N_inc
site(i)=i;
%=========================================================================
% Water side heat transfer resistance
% Thermo-physical properties
T_w_bed=T_w_in(i);
P_atm=refpropm('P','T',373.15,'Q',0,SecFld);
Roh_w_bed=refpropm('D','T',T_w_bed,'P',P_atm,SecFld); %Kg/m3
Meu_w_bed=refpropm('V','T',T_w_bed,'P',P_atm,SecFld); %Pa s
Cp_w_bed=refpropm('C','T',T_w_bed,'P',P_atm,SecFld)*1E-3; %kJ/kg.K
K_w_bed=refpropm('L','T',T_w_bed,'P',P_atm,SecFld)*1E-3; %kW/m.K
Pr_w_bed=Cp_w_bed*Meu_w_bed/K_w_bed;
% Calculations
VeL_t_bed=m_dot_water_bed/(Roh_w_bed*A_w_bed*N_t_bed_pass);
Re_w_bed=Roh_w_bed*VeL_t_bed*D_bed_i/Meu_w_bed;
if (Re_w_bed<3000)
    f_bed_i=64/Re_w_bed;
    Nus_w_bed=4.36;
elseif (Re_w_bed>=3000)
    f_bed_i=(-1.8*log10((6.9/Re_w_bed)+(epslon_bed/(3.7*D_bed_i))^1.11))^-
2;
    Num5=(Pr_w_bed*f_bed_i/8)*(Re_w_bed-1000);
    Den5=1+(12.7*((f_bed_i/8)^0.5)*((Pr_w_bed^(2/3))-1));
    Nus_w_bed=Num5/Den5;
end
htc_w_bed=Nus_w_bed*K_w_bed/D_bed_i;
R_w_bed=1/(htc_w_bed*pi*D_bed_i*fin_pitch_bed);
%=========================================================================
% Thermal balance and outlet temperature calculation
Segma_R(i)=(R_w_bed+R_t_bed+R_bed);
UA_bed(i)=1/Segma_R(i);
T_w_out(i)=T_bed+(T_w_in(i)-T_bed)*(exp(-
UA_bed(i)/(m_dot_water_bed*4.18/N_t_bed_pass)));
if (T_w_bed_in>T_bed)
    DT_b(i)=T_w_in(i)-T_bed; DT_s(i)=T_w_out(i)-T_bed;
else
    DT_b(i)=T_bed-T_w_in(i); DT_s(i)=T_bed-T_w_out(i);
end
LMTD(i)=(DT_b(i)-DT_s(i))/(log(DT_b(i)/DT_s(i)));
dq(i)=UA_bed(i)*LMTD(i)*(12*7*4);
%=========================================================================
htc_w_bedi(i)=htc_w_bed;
%=========================================================================
if (i==N_inc)
```

```
    break
else
    T_w_in(i+1)=T_w_out(i);
end
end
T_w_bed_out=T_w_out(N_inc);
%=========================================================================
% Chick the tolerance in calculations
Q_bed1=sum(dq);
Q_bed2=m_dot_water_bed*4.18*(abs(T_w_bed_in-T_w_bed_out));
Tolerance=abs(Q_bed1-Q_bed2);
%=========================================================================
if (T_w_bed_in>T_bed)
    DT_b_bed=T_w_bed_in-T_bed; DT_s_bed=T_w_bed_out-T_bed;
else
    DT_b_bed=T_bed-T_w_bed_in; DT_s_bed=T_bed-T_w_bed_out;
end
LMTD_bed=(DT_b_bed-DT_s_bed)/(log(DT_b_bed/DT_s_bed));
UA=Q_bed1/(LMTD_bed);
U_bed=Q_bed1/(A_bed*LMTD_bed);
```

A.7 Condenser model flow chart

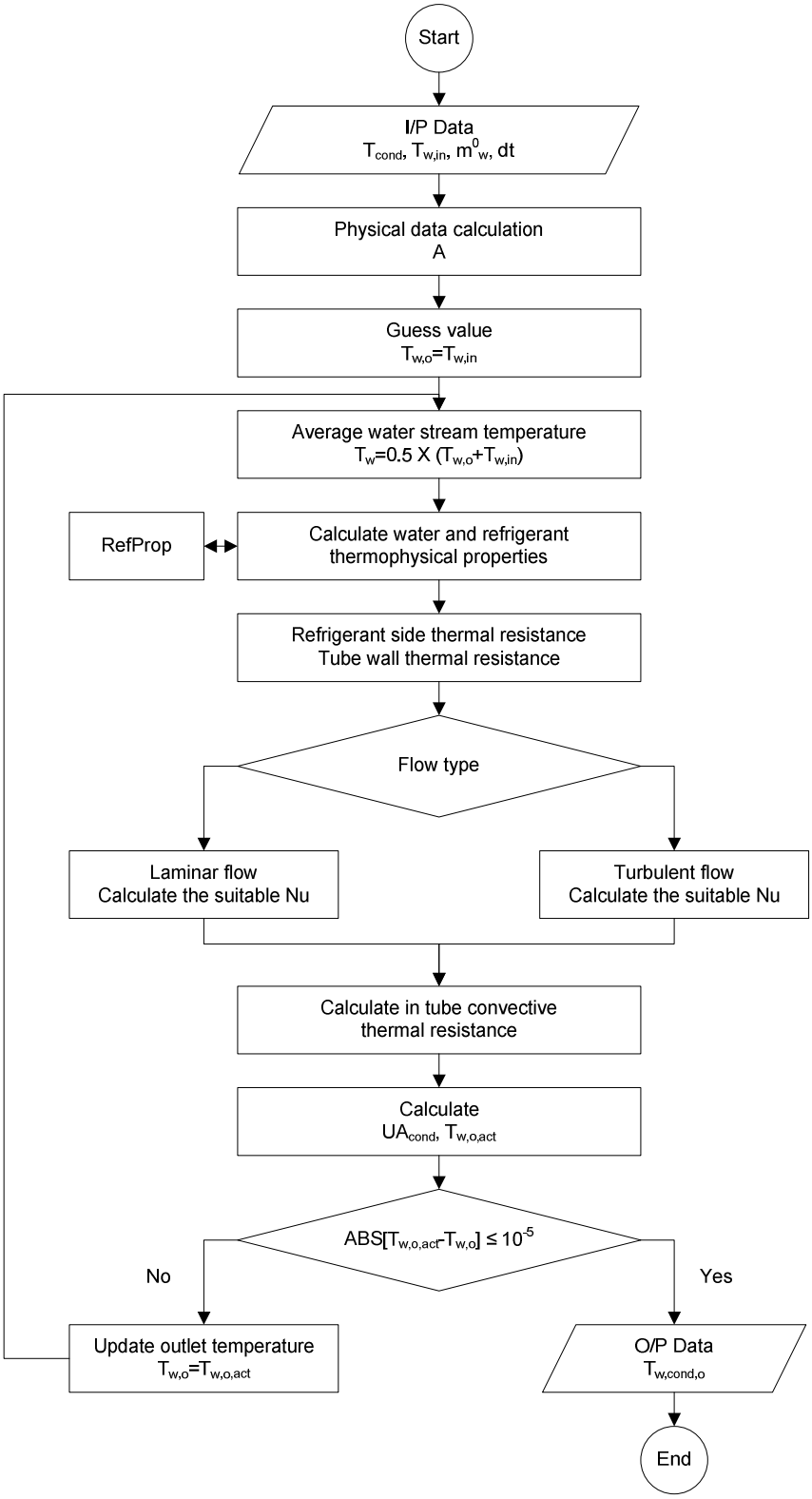

A.8 Condenser model code

```
function [T_w_cond_out]=CondTwo(T_cond,T_w_cond_in,m_dot_w_cond,Dtime)
Ref='water'; SecFld='water';
% Input geometrical characteristics
D_cond_o=0.75*0.0254;
t_cond_f=0.8E-3;
D_cond_i=D_cond_o-(2*t_cond_f);
N_t_cond=457;
L_t_cond=2654E-3;
N_pass_cond=3;
N_row_cond=11;
epslon_cond=0.0015E-3;
% Geometrical characteristics calculations
A_cond=pi*D_cond_o*L_t_cond*N_t_cond;
%=========================================================================
ItrC=0;
T_w_cond_out=T_w_cond_in;
for n=1:10
ItrC=ItrC+1;
% A- refrigerant side convective resistance
% A-1 Thermo-physical properties
T_ref_cond_sat=T_cond;
T_w_cond=(T_w_cond_in+T_w_cond_out)/2;
T_ref_cond_surf=T_w_cond;
T_ref_cond_v=(T_ref_cond_surf+T_ref_cond_sat)/2;
Roh_ref_cond_L=refpropm('D','T',T_ref_cond_sat,'Q',0,Ref); %kg/m3
Roh_ref_cond_v=refpropm('D','T',T_ref_cond_v,'Q',1,Ref); %kg/m3
K_ref_cond_L=refpropm('L','T',T_ref_cond_sat,'Q',0,Ref)*1E-3; %kW/m K
h_ref_cond_L=refpropm('H','T',T_ref_cond_sat,'Q',0,Ref)*1E-3; %kJ/kg
h_ref_cond_v=refpropm('H','T',T_ref_cond_v,'Q',1,Ref)*1E-3; %kJ/kg
h_ref_cond_fg=abs(h_ref_cond_v-h_ref_cond_L);
Cp_ref_cond_v=refpropm('C','T',T_ref_cond_v,'Q',1,Ref)*1E-3; %kJ/kg K
Meu_ref_cond_L=refpropm('V','T',T_ref_cond_sat,'Q',0,Ref); %Pa s
% A-2 Calculations
gr=9.81; C1_ref_cond=0.729;
DeltaT_surf_sat=abs(T_ref_cond_sat-T_ref_cond_surf);
h_ref_cond_fg_bar=h_ref_cond_fg+0.68*Cp_ref_cond_v*abs(T_ref_cond_surf-
T_ref_cond_sat);
Num3=gr*Roh_ref_cond_L*(Roh_ref_cond_L-
Roh_ref_cond_v)*K_ref_cond_L^3*h_ref_cond_fg_bar;
Den3=N_row_cond*Meu_ref_cond_L*DeltaT_surf_sat*D_cond_o;
htc_ref_cond=C1_ref_cond*((Num3/Den3)^(1/4));
R_ref_cond=1/(htc_ref_cond*A_cond);
%-------------------------------------------------------------------------
% A-3 Mass balance
m_dot_ref_cond=htc_ref_cond*pi*D_cond_o*DeltaT_surf_sat/h_ref_cond_fg_bar;
m_dot_ref_cond_tot=m_dot_ref_cond*L_t_cond*N_t_cond;
m_ref_cond_tot_out=m_dot_ref_cond_tot*Dtime;
%=========================================================================
% B- Water side convective resistance
% B-1 Thermo-physical properties
P_atm=refpropm('P','T',373.15,'Q',0,'water');
Roh_w_cond=refpropm('D','T',T_w_cond,'P',P_atm,SecFld);     %Kg/m3
Meu_w_cond=refpropm('V','T',T_w_cond,'P',P_atm,SecFld);     %Pa s
Cp_w_cond=refpropm('C','T',T_w_cond,'P',P_atm,SecFld)*1E-3; %kJ/kg.K
K_w_cond=refpropm('L','T',T_w_cond,'P',P_atm,SecFld)*1E-3;  %kW/m.K
Pr_w_cond=Cp_w_cond*Meu_w_cond/K_w_cond;
```

```
% B-2 Calculations
A_w_cond=pi*D_cond_i^2/4;
N_t_cond_pass=N_t_cond/N_pass_cond;
VeL_t_cond=m_dot_w_cond/(Roh_w_cond*A_w_cond*N_t_cond_pass);
Re_w_cond=Roh_w_cond*VeL_t_cond*D_cond_i/Meu_w_cond;
if (Re_w_cond<3000)
    f_cond_i=64/Re_w_cond
    Nus_w_cond=4.36
elseif (Re_w_cond>=3000)
    f_cond_i=(-
1.8*log10((6.9/Re_w_cond)+(epslon_cond/(3.7*D_cond_i))^1.11))^-2;
    Num4=(Pr_w_cond*f_cond_i/8)*(Re_w_cond-1000);
    Den4=1+(12.7*((f_cond_i/8)^0.5)*((Pr_w_cond^(2/3))-1));
    Nus_w_cond=Num4/Den4;
end
htc_w_cond=Nus_w_cond*K_w_cond/D_cond_i;
R_w_cond=1/(htc_w_cond*pi*D_cond_i*L_t_cond*N_t_cond);
%=========================================================================
% C- Tube wall conductance resistance
K_t_cond=310*1E-3; %kW/m.K
R_t_cond=(log(D_cond_o/D_cond_i))/(2*pi*K_t_cond*L_t_cond*N_t_cond);
%=========================================================================
% D- Overall thermal conductance
UA_cond=1/(R_w_cond+R_t_cond+R_ref_cond);
Twco=T_cond-((T_cond-T_w_cond_in)*exp(-UA_cond/(m_dot_w_cond*Cp_w_cond)));
Tol_cond_w_out=abs(Twco-T_w_cond_out);
if (Tol_cond_w_out<=1E-5)
    break
else
    T_w_cond_out=Twco;
end
end
```

A.9 Evaporator flow chart

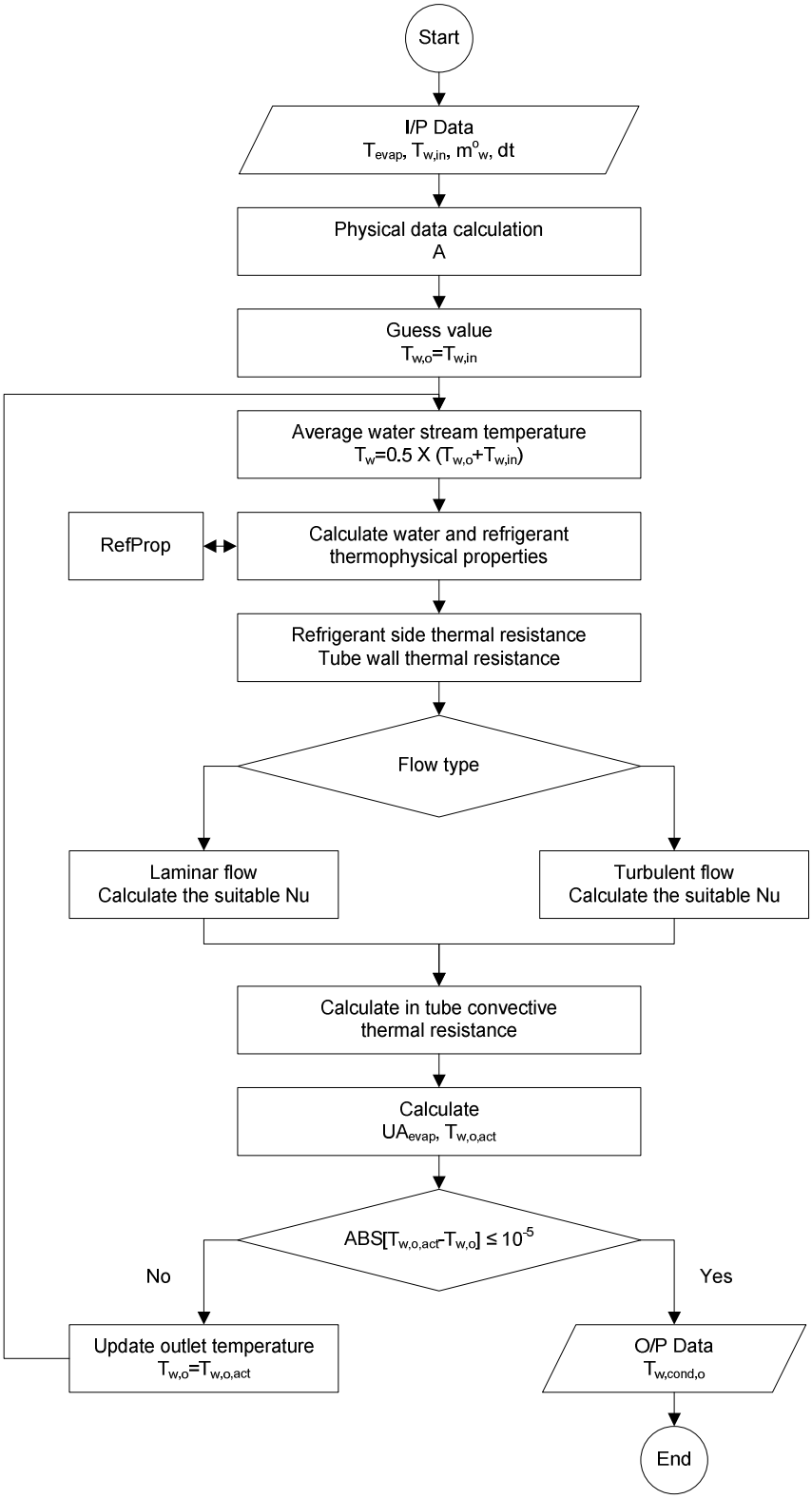

Evaporator model code

```
function [T_w_evap_out]=EvapTwo(T_evap,T_w_evap_in,m_dot_w_evap)
Ref='water'; SecFld='water';
% Input geometrical characteristics
D_evap_i=16.33E-3;
D_evap_f=18.85E-3;
D_evap_r=17.75E-3;
t_evap_f=0.20E-3;
Pt_evap=0.45E-3;
L_t_evap=3894e-3;
N_t_evap=224;
N_pass_evap=3;
Eta_evap_f=0.98;
epslon_evap=0.0015E-3;
%=========================================================================
% Geometrical characteristics calculations
r1_evap=D_evap_r/2;
r2_evap=D_evap_f/2;
r2_c_evap=r2_evap+(t_evap_f/2);
A_f_evap=2*pi*(r2_c_evap^2-r1_evap^2);
A_uf_evap=pi*D_evap_r*(Pt_evap-t_evap_f);
A_fs_evap=2*(pi/4)*(D_evap_f^2-D_evap_r^2);
A_ft_evap=pi*D_evap_f*t_evap_f;
A_evap_seg=A_f_evap+A_uf_evap;
Term1_evap=1.3*Eta_evap_f;
Term2_evap=A_fs_evap/(A_evap_seg*(0.25*pi*(D_evap_f^2-
D_evap_r^2)/D_evap_f)^0.25);
Term3_evap=A_ft_evap/(A_evap_seg*D_evap_f^0.25);
Term4_evap=A_uf_evap/(A_evap_seg*D_evap_r^0.25);
D_evap=(Term1_evap*(Term2_evap+Term3_evap+Term4_evap))^-4;
N_evap_seg=L_t_evap/Pt_evap;
A_evap=A_evap_seg*N_evap_seg*N_t_evap;
%=========================================================================
itrE=0;
T_w_evap_out=T_w_evap_in;
for n=1:10
    itrE=itrE+1;
% A- Refrigerant side convective Resistance
% A-1 Thermo-physical properties calculations
T_w_evap=(T_w_evap_out+T_w_evap_in)/2;
T_ref_evap_surf=T_w_evap;
T_ref_evap_sat=T_evap;
T_ref_evap_v=(T_ref_evap_surf+T_ref_evap_sat)/2;
Roh_ref_evap_L=refpropm('D','T',T_ref_evap_sat,'Q',0,Ref); %Kg/m3
Roh_ref_evap_v=refpropm('D','T',T_ref_evap_v,'Q',1,Ref); %Kg/m3
h_ref_evap_L=refpropm('H','T',T_ref_evap_sat,'Q',0,Ref)*1E-3; %kJ/kg
h_ref_evap_v=refpropm('H','T',T_ref_evap_v,'Q',1,Ref)*1E-3; %kJ/kg
h_ref_evap_fg=abs(h_ref_evap_v-h_ref_evap_L); %kJ/kg
Cp_ref_evap_v=refpropm('C','T',T_ref_evap_v,'Q',1,Ref)*1E-3; %kJ/kg.K
Cp_ref_evap_L=refpropm('C','T',T_ref_evap_sat,'Q',0,Ref)*1E-3; %kJ/kg.K
Meu_ref_evap_v=refpropm('V','T',T_ref_evap_v,'Q',1,Ref); %Pa.s
Meu_ref_evap_L=refpropm('V','T',T_ref_evap_sat,'Q',0,Ref); %Pa.s
Neu_ref_evap_v=Meu_ref_evap_v/Roh_ref_evap_v;
K_ref_evap_v=refpropm('L','T',T_ref_evap_v,'Q',1,Ref)*1E-3; %kW/m.K
K_ref_evap_L=refpropm('L','T',T_ref_evap_sat,'Q',0,Ref)*1E-3; %kW/m.K
%-------------------------------------------------------------------------
% A-2-1 Calculations 'Film Boiling'
```

```
gr=9.81; C1_ref_evap=0.62;
DeltaT_surf_sat=abs(T_ref_evap_surf-T_ref_evap_sat);
h_ref_evap_fg_bar=h_ref_evap_fg+0.8*Cp_ref_evap_v*(T_ref_evap_surf-
T_ref_evap_sat);
Num1=gr*(Roh_ref_evap_L-Roh_ref_evap_v)*h_ref_evap_fg_bar*D_evap^3;
Den1=Neu_ref_evap_v*K_ref_evap_v*DeltaT_surf_sat;
Nus_ref_evap=C1_ref_evap*((Num1/Den1)^0.25);
htc_ref_evap1=Nus_ref_evap*K_ref_evap_v/D_evap;
%-------------------------------------------------------------------------
% A-2-2 Calculations 'Nuclate Boiling'
C_s_f_evap=0.0068; n=1;
Ja_ref_evap=Cp_ref_evap_L*DeltaT_surf_sat/h_ref_evap_fg;
Pr_ref_evap_L=Cp_ref_evap_L*Meu_ref_evap_L/Meu_ref_evap_L;
TERM_A=Meu_ref_evap_L*h_ref_evap_fg/DeltaT_surf_sat;
TERM_B=gr*(Roh_ref_evap_L-Roh_ref_evap_v)/72.81E-3;
TERM_C=Ja_ref_evap/(C_s_f_evap*Pr_ref_evap_L^n);
htc_ref_evap=TERM_A*(TERM_B^0.5)*(TERM_C^3);
R_ref_evap=1/(htc_ref_evap*A_evap);
%=========================================================================
% B- Water side convective resistance
% B-1 Thermo-physical properties
P_atm=refpropm('P','T',373.15,'Q',0,'water');
Roh_w_evap=refpropm('D','T',T_w_evap,'P',P_atm,SecFld); %Kg/m3
Meu_w_evap=refpropm('V','T',T_w_evap,'P',P_atm,SecFld); %Pa s
Cp_w_evap=refpropm('C','T',T_w_evap,'P',P_atm,SecFld)*1E-3; %kJ/kg.K
K_w_evap=refpropm('L','T',T_w_evap,'P',P_atm,SecFld)*1E-3; %kW/m.K
Pr_w_evap=Cp_w_evap*Meu_w_evap/K_w_evap;
% B-2 Calculations
A_w_evap=pi*D_evap_i^2/4;
N_t_evap_pass=N_t_evap/N_pass_evap;
VeL_t_evap=m_dot_w_evap/(Roh_w_evap*A_w_evap*N_t_evap_pass);
Re_w_evap=Roh_w_evap*VeL_t_evap*D_evap_i/Meu_w_evap;
if (Re_w_evap<3000)
    f_evap_i=64/Re_w_evap;
    Nus_w_evap=4.36;
elseif (Re_w_evap>=3000)
    f_evap_i=(-
1.8*log10((6.9/Re_w_evap)+(epslon_evap/(3.7*D_evap_i))^1.11))^-2;
    %f_evap_i=((0.790*log(Re_w_evap))-1.64)^-2
    Num2=(Pr_w_evap*f_evap_i/8)*(Re_w_evap-1000);
    Den2=1+(12.7*((f_evap_i/8)^0.5)*((Pr_w_evap^(2/3))-1));
    Nus_w_evap=Num2/Den2;
end
htc_w_evap=Nus_w_evap*K_w_evap/D_evap_i;
R_w_evap=1/(htc_w_evap*pi*D_evap_i*L_t_evap*N_t_evap);
%=========================================================================
% C- Tube wall conductance resistance
K_t_evap=310*1E-3; %kW/m.K
D_evap_1=A_evap_seg/(pi*Pt_evap);
R_t_evap=(log(D_evap_1/D_evap_i))/(2*pi*K_t_evap*L_t_evap*N_t_evap);
%=========================================================================
% D- Overall thermal conductance
UA_evap=1/(R_w_evap+R_t_evap+R_ref_evap);
Tweo=T_evap+(T_w_evap_in-T_evap)*exp(-UA_evap/(m_dot_w_evap*Cp_w_evap));
Tol_evap_w_out=abs(Tweo-T_w_evap_out);
if (Tol_evap_w_out<=1E-5)
    break
else
    T_w_evap_out=Tweo;
```

```
end
end
T_w_evap_out=Tweo;
```

A.10 Mixture specific heat and thermal conductivity

```
function [K_SG, C_Ad]=KC_mix(Metal, Pge)
switch (Metal)
   case 'Al'
               C_Ad=0.896; %kJ/kg.K
       switch Pge
           case 0
               K_SG=0.198E-3; %kW/m.K
           case 5
               K_SG=0.218E-3; %kW/m.K
           case 10
               K_SG=0.314E-3; %kW/m.K
           case 15
               K_SG=0.363E-3; %kW/m.K
       end

   case 'Cu'
               C_Ad=0.385; %kJ/kg.K
       switch Pge
           case 0
               K_SG=0.198E-3; %kW/m.K
           case 5
               K_SG=0.187E-3; %kW/m.K
           case 10
               K_SG=0.246E-3; %kW/m.K
           case 15
               K_SG=0.324E-3; %kW/m.K
       end

   case 'Brass'
               C_Ad=0.380; %kJ/kg.K
       switch Pge
           case 0
               K_SG=0.198E-3; %kW/m.K
           case 5
               K_SG=0.176E-3; %kW/m.K
           case 10
               K_SG=0.211E-3; %kW/m.K
           case 15
               K_SG=0.327E-3; %kW/m.K
       end

    case 'Steel'
                C_Ad=0.460; %kJ/kg.K
        switch Pge
            case 0
                K_SG=0.198E-3; %kW/m.K
            case 5
                K_SG=0.141E-3; %kW/m.K
            case 10
                K_SG=0.169E-3; %kW/m.K
            case 15
                K_SG=0.254E-3; %kW/m.K
        end
    case 'None'
                C_Ad=0.0; %kJ/kg.K
```

```
                K_SG=0.198E-3; %kW/m.K
end
```

A.11 Specific heat separate calculations

```
function [MC_bed, MC_SBed, MC_Ad, M_bed_ads]=MCs(fin_pitch_bed, Metal, Pge)
%=========================================================================
% Input geometrical characteristics
L_fin_bed=340E-3; H_fin_bed=0.0285; W_fin_bed=0.105E-3;
%fin_pitch_bed=1.5E-3;
L_module=3400E-3; N_t_module=12;
N_fin_module=round(L_module/fin_pitch_bed);
N_module=7*2*4; D_bed_o=(5/8)*0.0254; t_bed=0.8E-3; D_bed_i=D_bed_o-
(2*t_bed);
%=========================================================================
% Area calculation
L_FT=W_fin_bed*N_fin_module; L_UFT=L_module-L_FT; A_UFT=pi*D_bed_o*L_UFT;
A_UFTM=A_UFT*N_t_module;
A_FS=(L_fin_bed*H_fin_bed)-(0.25*pi*D_bed_o^2*N_t_module);
A_FTP=(2*L_fin_bed*W_fin_bed)+(2*H_fin_bed*W_fin_bed);
A_F=A_FS+A_FTP; A_FM=A_F*N_fin_module;
A_M=A_FM+A_UFTM; A_bed=A_M*N_module;
%=========================================================================
% Metal mass calculation
Roh_F=3661.85; C_F=0.896; Roh_T=8954; C_T=0.3831; Roh_S=690.987; C_S=0.921;
%Roh_S=708.299;
M_TM=0.25*pi*(D_bed_o^2-D_bed_i^2)*L_module*N_t_module*Roh_T;
M_FM=A_FS*W_fin_bed*Roh_F*N_fin_module;
MC_M=M_TM*C_T+M_FM*C_F;
%=========================================================================
% Silica mass calculation
V_TM=0.25*pi*L_module*N_t_module*D_bed_o^2;
V_FM=A_FS*W_fin_bed*N_fin_module;
V_M=L_module*L_fin_bed*H_fin_bed;
V_SM=V_M-V_FM-V_TM; M_SM=V_SM*Roh_S; M_SBed=(M_SM*N_module);
%=========================================================================
[K_SG, C_Ad]=KC_mix(Metal, Pge);
M_bed_ads=M_SBed*(1-Pge/100); MC_SBed=M_SBed*C_S;
MC_Ad=(M_SBed*Pge/100)*C_Ad; MC_bed=MC_M*N_module;
```

A.12 Contact thermal resistance calculations

```
function [Rc_bed]=Rc(T_bed_C,Dp)
if (Dp>0.297)
    Dp1=0.297; Dp2=0.149;
    R1=(0.0013*T_bed_C^2)-(0.1773*T_bed_C)+8.6221; %(0.297)
    R2=(0.0012*T_bed_C^2)-(0.1624*T_bed_C)+7.6785; %(0.149)
    Rc_bed=R1+((R1-R2)*(Dp-Dp1)/(Dp1-Dp2));
elseif (Dp<=0.297)&(Dp>=0.149)
    Dp1=0.297; Dp2=0.149;
    R1=(0.0013*T_bed_C^2)-(0.1773*T_bed_C)+8.6221; %(0.297)
    R2=(0.0012*T_bed_C^2)-(0.1624*T_bed_C)+7.6785; %(0.149)
    Rc_bed=R1-((R1-R2)*(Dp1-Dp)/(Dp1-Dp2));
elseif (Dp<0.149)&(Dp>=0.074)
    Dp1=0.149; Dp2=0.074;
    R1=(0.0012*T_bed_C^2)-(0.1624*T_bed_C)+7.6785; %(0.149)
    R2=(0.0008*T_bed_C^2)-(0.1214*T_bed_C)+6.422; %(0.074)
    Rc_bed=R1-((R1-R2)*((Dp1-Dp)/(Dp1-Dp2)));
elseif (Dp<0.074)
    Dp1=0.149; Dp2=0.074;
    R1=(0.0012*T_bed_C^2)-(0.1624*T_bed_C)+7.6785; %(0.149)
    R2=(0.0008*T_bed_C^2)-(0.1214*T_bed_C)+6.422; %(0.074)
    Rc_bed=R2-((R1-R2)*(Dp2-Dp)/(Dp1-Dp2));
end
```

REFERENCES

1. *Industry market research for business, strategists, decision makers*, 2010, The Freedonia Group.
2. Hassan, H.Z., A.A. Mohamad, and R. Bennacer, *Simulation of an adsorption solar cooling system.* Energy, 2011. **36**(1): p. 530-537.
3. Verde, M., et al., *Modelling of an adsorption system driven by engine waste heat for truck cabin A/C. Performance estimation for a standard driving cycle.* Applied Thermal Engineering, 2010. **30**(13): p. 1511-1522.
4. Qureshi, B.A. and S.M. Zubair, *Performance degradation of a vapor compression refrigeration system under fouled conditions.* International Journal of Refrigeration, 2011. **34**(4): p. 1016-1027.
5. Navarro-EsbrÃ-, J., et al., *A low data requirement model of a variable-speed vapour compression refrigeration system based on neural networks.* International Journal of Refrigeration, 2007. **30**(8): p. 1452-1459.
6. Pons, M., et al., *Thermodynamic based comparison of sorption systems for cooling and heat pumping: Comparaison des performances thermodynamique des systÃ¨mes de pompes Ã chaleur Ã sorption dans des applications de refroidissement et de chauffage.* International Journal of Refrigeration, 1999. **22**(1): p. 5-17.
7. Xu, L., et al., *Experimental study on the performance of double-effect and double-way thermochemical sorption refrigeration cycle.* Applied Thermal Engineering, 2011. **31**(17â€“18): p. 3658-3663.
8. Li, S. and J.Y. Wu, *Theoretical research of a silica gel-water adsorption chiller in a micro combined cooling, heating and power (CCHP) system.* Applied Energy, 2009. **86**(6): p. 958-967.
9. Tora, E.A. and M.M. El-Halwagi, *Integrated conceptual design of solar-assisted trigeneration systems.* Computers & Chemical Engineering, 2011. **35**(9): p. 1807-1814.
10. Huangfu, Y., et al., *Experimental investigation of adsorption chiller for Micro-scale BCHP system application.* Energy and Buildings, 2007. **39**(2): p. 120-127.
11. Wang, R.Z. and R.G. Oliveira, *Adsorption refrigerationâ€"An efficient way to make good use of waste heat and solar energy.* Progress in Energy and Combustion Science, 2006. **32**(4): p. 424-458.
12. Luo, H., R. Wang, and Y. Dai, *The effects of operation parameter on the performance of a solar-powered adsorption chiller.* Applied Energy, 2010. **87**(10): p. 3018-3022.
13. Chen, C.J., et al., *Study on a compact silica gel-water adsorption chiller without vacuum valves: Design and experimental study.* Applied Energy, 2010. **87**(8): p. 2673-2681.
14. Sarabia Escriva, E.J., E.V. Lamas Sivila, and V.M. Soto Frances, *Air conditioning production by a single effect absorption cooling machine directly coupled to a solar collector field. Application to Spanish climates.* Solar Energy, 2011. **85**(9): p. 2108-2121.
15. Lemmini, F. and A. Errougani, *Experimentation of a solar adsorption refrigerator in Morocco.* Renewable Energy, 2007. **32**(15): p. 2629-2641.
16. Luo, H.L., et al., *An efficient solar-powered adsorption chiller and its application in low-temperature grain storage.* Solar Energy, 2007. **81**(5): p. 607-613.

17. Saha, B.B., A. Akisawa, and T. Kashiwagi, *Solar/waste heat driven two-stage adsorption chiller: the prototype.* Renewable Energy, 2001. **23**(1): p. 93-101.
18. Wang, R.Z., et al., *Solar sorption cooling systems for residential applications: Options and guidelines.* International Journal of Refrigeration, 2009. **32**(4): p. 638-660.
19. Li, T.X., et al., *Performance analysis of a multi-mode thermochemical sorption refrigeration system for solar-powered cooling.* International Journal of Refrigeration, 2012. **35**(3): p. 532-542.
20. Luo, H.L., et al., *Experimental investigation of a solar adsorption chiller used for grain depot cooling.* Applied Thermal Engineering, 2006. **26**(11â€“12): p. 1218-1225.
21. Núñez, T., W. Mittelbach, and H.-M. Henning, *Development of an adsorption chiller and heat pump for domestic heating and air-conditioning applications.* Applied Thermal Engineering, 2007. **27**(13): p. 2205-2212.
22. Riffel, D.B., et al., *Transient modeling of an adsorber using finned-tube heat exchanger.* International Journal of Heat and Mass Transfer, 2010. **53**(7-8): p. 1473-1482.
23. Garousi Farshi, L., S.M. Seyed Mahmoudi, and M.A. Rosen, *Analysis of crystallization risk in double effect absorption refrigeration systems.* Applied Thermal Engineering, 2011. **31**(10): p. 1712-1717.
24. Wang, L.W., R.Z. Wang, and R.G. Olivera, *A review on adsorption working pairs for refrigeration.* Renewable & Sustainable Energy Review, 2009. **13**: p. 518 - 534.
25. Demir, H., M. Mobedi, and S. Ulku, *Effect of Factors on Variations of Desorption Pressure of Adsorption Heat Pump*, in *Heat Powered Cycle Conference 2009*2009: Berline.
26. Saha, B.B., S. Koyama, and T. Kashiwagi, *waste heat driven dual-mode, multi-stage, multi-bed regenerative adsorption system.* International Journal of Refrigeration, 2003. **26**: p. 749-757.
27. Chua, H.T., et al., *Multi-bed regenerative adsorption chillerÂ â€" improving the utilization of waste heat and reducing the chilled water outlet temperature fluctuation.* International Journal of Refrigeration, 2001. **24**(2): p. 124-136.
28. zycon. *http://zycon.hubpages.com/hub/Adsorption-vs-Absorption-Chillers-Applications-Use-Overview*. HubPages 2012.
29. Dabrowski, A., *Adsorption -- from theory to practice.* Advances in Colloid and Interface Science, 2001. **93**(1-3): p. 135-224.
30. Critoph, R.E., *Evaluation of alternative refrigerant-adsorbent pairs for refrigeration cycles.* Applied Thermal Engineering, 1996. **16**: p. 891-900.
31. Gordon, J.M., et al., *The electro-adsorption chiller: a miniaturized cooling cycle with applications to micro-electronics.* International Journal of Refrigeration, 2002. **25**(8): p. 1025-1033.
32. Guid, M.A., *Refrigerants*, 2002, McQuay international. p. 1-66.
33. United-Nations-Environment-Programme, *The Montreal Protocol on Substances that Deplete the Ozone Layer*. 8 ed2009: Duncan Brack. 565.
34. Grof, T., *Greening of Industry under the Montreal Protocol*, 2009, United nations industrial development organization: Manila. p. 1-20.
35. ENVIRONMENTAL-INVESTIGATION-AGENCY *The montreal protocol in 2011* 2011.
36. *2009 Greenhouse Gas Inventory Based on Data from 2000 through 2006*, in *The University of Texas at Austin*2009.

37. Hasse, V., L. Ederberg, and D. Colbourne, *Natural Refrigerants*2008, Eschborn: German Technical Cooperation.
38. Hamamoto, Y., et al., *Study on adsorption refrigeration cycle utilizing activated carbon fibers. Part 2. Cycle performance evaluation.* International Journal of Refrigeration, 2006. **29**(2): p. 315-327.
39. Wang, X. and H.T. Chua, *A comparative evaluation of two different heat-recovery schemes as applied to a two-bed adsorption chiller.* International Journal of Heat and Mass Transfer, 2007. **50**(3-4): p. 433-443.
40. Taylan, O., D.K. Baker, and B. KaftanoÄŸlu, *COP trends for ideal thermal wave adsorption cooling cycles with enhancements.* International Journal of Refrigeration, 2010. **35**(3): p. 562-570.
41. Lu, Z.S., L.W. Wang, and R.Z. Wang, *Experimental analysis of an adsorption refrigerator with mass and heat-pipe heat recovery process.* Energy Conversion and Management, 2012. **53**(1): p. 291-297.
42. Wang, R.Z., *Performance improvement of adsorption cooling by heat and mass recovery operation.* International Journal of Refrigeration, 2001. **24**(7): p. 602-611.
43. Ng, K.C., et al., *Experimental study on performance improvement of a four-bed adsorption chiller by using heat and mass recovery.* International Journal of Heat and Mass Transfer, 2006. **49**(19â€“20): p. 3343-3348.
44. Wang, X., H.T. Chua, and K.C. Ng, *Experimental investigation of silica gelâ€“water adsorption chillers with and without a passive heat recovery scheme.* International Journal of Refrigeration, 2005. **28**(5): p. 756-765.
45. Baker, D.K., *Thermodynamic limits to thermal regeneration in adsorption cooling cycles.* International Journal of Refrigeration, 2008. **31**(1): p. 55-64.
46. Liu, Y.L., R.Z. Wang, and Z.Z. Xia, *Experimental performance of a silica gel-water adsorption chiller.* Applied Thermal Engineering, 2005. **25**(2-3): p. 359-375.
47. Chen, C.J., et al., *Study on a silica gel - water adsorption chiller integrated with a closed wet cooling tower.* International Journal of Thermal Sciences, 2010. **49**(3): p. 611-620.
48. Chang, W.S., C.C. Wang, and C.C. Shieh, *Design and performance of a solar-powered heating and cooling system using silica gel/water adsorption chiller.* Applied Thermal Engineering, 2009. **29**(10): p. 2100-2105.
49. Di, J., et al., *Theoretical and experimental study on characteristics of a novel silica gel-water chiller under the conditions of variable heat source temperature.* International Journal of Refrigeration, 2007. **30**(3): p. 515-526.
50. Wu, J.Y. and S. Li, *Study on cyclic characteristics of silica gel-water adsorption cooling system driven by variable heat source.* Energy, 2009. **34**(11): p. 1955-1962.
51. Wang, D.C., et al., *Study of a novel silica gelâ€“water adsorption chiller. Part I. Design and performance prediction.* International Journal of Refrigeration, 2005. **28**(7): p. 1073-1083.
52. Xia, Z., D. Wang, and J. Zhang, *Experimental study on improved two-bed silica gel-water adsorption chiller.* Energy Conversion and Management, 2008. **49**: p. 1469-1479.
53. Saha, B.B., et al., *Performance evaluation of a low-temperature waste heat driven multi-bed adsorption chiller.* International Journal of Multiphase Flow, 2003. **29**(8): p. 1249-1263.
54. Khan, M.Z.I., et al., *Study on solar/waste heat driven multi-bed adsorption chiller with mass recovery.* Renewable Energy, 2007. **32**(3): p. 365-381.

55. Miyazaki, T., A. Akisawa, and B.B. Saha, *The performance analysis of a novel dual evaporator type three-bed adsorption chiller.* International Journal of Refrigeration, 2010. **33**(2): p. 276-285.
56. Saha, B.B., et al., *Study on a dual-mode, multi-stage, multi-bed regenerative adsorption chiller.* Renewable Energy, 2006. **31**(13): p. 2076-2090.
57. Hamamoto, Y., et al., *Performance evaluation of a two-stage adsorption refrigeration cycle with different mass ratio.* International Journal of Refrigeration, 2005. **28**(3): p. 344-352.
58. Khan, M.Z.I., et al., *Performance evaluation of multi-stage, multi-bed adsorption chiller employing re-heat scheme.* Renewable Energy, 2008. **33**: p. 88-98.
59. Maggio, G., et al., *Simulation of a solid sorption ice-maker based on the novel composite sorbent "lithium chloride in silica gel pores".* Applied Thermal Engineering, 2009. **29**: p. 1714-1720.
60. Yuriy I, A., *Challenging offers of material science for adsorption heat transformation: A review.* Applied Thermal Engineering, 2011(0).
61. Srivastava, N.C. and I.W. Eames, *A review of adsorbents and adsorbates in soild-vapor adsorption heat pump system.* Applied Thermal Engineering, 1998. **18**: p. 707-714.
62. Wang, L.W., et al., *Development of thermal conductive consolidated activated carbon for adsorption refrigeration.* Carbon, 2012. **50**(3): p. 977-986.
63. Tamainot-Telto, Z., et al., *Carbon-ammonia pairs for adsorption refrigeration application: ice making, air conditioning and heat pump.* International Journal of Refrigeration, 2009. **In press**: p. 1-18.
64. Loh, W.S., et al., *Adsorption cooling cycles for alternative adsorbent/adsorbate pairs working at partial vacuum and pressurized conditions.* Applied Thermal Engineering, 2009. **29**: p. 793-798.
65. Yamada, Y. and K. Yano, *Synthesis of monodispersed super-microporous/mesoporous silica spheres with diameters in the low submicron range.* Microporous and Mesoporous Materials, 2006. **93**(1-3): p. 190-198.
66. Guo, X., et al., *Synthesis of a novel super-microporous layered material and its catalytic application in the vapor-phase Beckmann rearrangement of cyclohexanone oxime.* Microporous and Mesoporous Materials, 2005. **80**(1-3): p. 269-274.
67. Lin, Y.-S., H.-P. Lin, and C.-Y. Mou, *A simple synthesis of well-ordered super-microporous aluminosilicate.* Microporous and Mesoporous Materials, 2004. **76**(1-3): p. 203-208.
68. Yano, K. and Y. Fukushima, *Synthesis of Hexagonally Ordered Super-Microporous Silicas, Using Conventional Alkyltrimethlammonium Bromide, as Adsorbents for Water Adsorption Heat-Pump System.* The Chemical Socity of Japan, 2003. **76**: p. 2103-2109.
69. McCusker, L. http://www.iza-online.org/. 2011.
70. Henninger, S.K., F.P. Schmidt, and H.M. Henning, *Water adsorption characteristics of novel materials for heat transformation applications.* Applied Thermal Engineering, 2010. **30**(13): p. 1692-1702.
71. Henninger, S.K., et al., *Cycle stability of sorption materials and composites for the use in heat pumps and cooling machines.* Renewable Energy, 2011. **36**(11): p. 3043-3049.
72. Saha, D. and S. Deng, *Ammonia adsorption and its effects on framework stability of MOF-5 and MOF-177.* Journal of Colloid and Interface Science, 2010. **348**(2): p. 615-620.
73. Saha, D. and S. Deng, *Hydrogen Adsorption on Metal-Organic Framework MOF-177.* Tsinghua Science & Technology, 2010. **15**(4): p. 363-376.

74. Küsgens, P., et al., *Characterization of metal-organic frameworks by water adsorption.* Microporous and Mesoporous Materials, 2009. **120**(3): p. 325-330.
75. Qiu, S. and G. Zhu, *Molecular engineering for synthesizing novel structures of metal-organic frameworks with multifunctional properties.* Coordination Chemistry Reviews, 2009. **253**(23-24): p. 2891-2911.
76. Henninger, S.K., H.A. Habib, and C. Janiak, *MOFs as Adsorbents for Low Temperature Heating and Cooling Applications.* Journal of the American Chemical Society, 2009: p. 2776-2777.
77. Li, S.L., et al., *Study on adsorption perfromance of composite adsorbent of $CaCl_2$ and expanded graphite with ammonia as adsorbate.* Energy Conversion and Management, 2009. **50**: p. 1011-1017.
78. Li, T.X., et al., *A combined double-way chemisorption refrigeration cycle based on adsorption and resorption processes.* International Journal of Refrigeration, 2009. **32**: p. 47-57.
79. Zhong, Y., et al., *Isothermal sorption characteristics of the BaCl2-NH3 pair in a vermiculite host matrix.* Applied Thermal Engineering, 2007. **27**(14-15): p. 2455-2462.
80. Aristov, Y.I., et al., *A family of new working materials for solid sorption air conditioning systems.* Applied Thermal Engineering, 2002. **22**: p. 191-204.
81. Dawoud, B. and Y. Aristove, *Experimental study of the kinetic of water vapor sorption on selective water sorbents, silica gel and alumina under typical operation conditions of sorption heat pumps.* Heat and mass transfer, 2003. **46**: p. 273-281.
82. Freni, A., et al., *Testing of a compact adsorbent bed based on the selective water sorbent 'Silica modefied by calcium nitrate'*, in *Heat Powered Cycles*2009: Techniche Universtat Berlin.
83. San, J.-Y. and H.-C. Hsu, *Performance of a multi-bed adsorption heat pump using SWS-1L composit adsorbent and water as working pair.* Applied Thermal Engineering, 2009. **29**: p. 1606-1613.
84. Freni, A., et al., *Experimental testing of a lab-scale adsorption chiller using a novel selective water sorbent â€œsilica modified by calcium nitrateâ€ .* International Journal of Refrigeration, 2012. **35**(3): p. 518-524.
85. Daou, K., et al., *Theoritical comparison of the refrigerating performance of a CaCl2 impregnated composite adsorbent to those of the host silica gel.* international Journal of Thermal Sciences, 2008. **47**: p. 68-75.
86. Hai-Jun, C., et al., *Attapulgite based LiCl composite adsorbents for cooling and air conditioning application.* Applied Thermal Engineering, 2008. **28**: p. 2187-2193.
87. Restuccia, G., et al., *Selective water sorbent for solid sorption chiller: experimental results and modelling.* International Journal of Refrigeration, 2004. **27**: p. 284-293.
88. Freni, A., et al., *Experimental testing of a lab-scale adsorption chiller using a novel selective water sorbent â€œsilica modified by calcium nitrateâ€ .* International Journal of Refrigeration, 2010. **35**(3): p. 518-524.
89. Freni, A., et al., *An advanced solid sorption chiller using SWS-1L.* Applied Thermal Engineering, 2007. **27**: p. 2200-2204.
90. Tokarev, M., et al., *New composite sorbent CaCl2 in mesopores for sorption cooling/heating.* International Journal of Thermal Sciences, 2002. **41**(5): p. 470-474.

91. Daou, K., R.Z. Wang, and Z.Z. Xia, *Development of a new synthesized adsorption for refrigeration and air conditioning applications.* Applied Thermal Engineering, 2006. **26**: p. 56-65.
92. Zuh, D., H. Wu, and S. Wang, *Expermental study on composite silica gel supported CaCl2 sorbent for low grade heat storage.* International Journal of Thermal Sciences, 2006. **45**: p. 804-813.
93. Daou, K., et al., *Experimental comparison of the sorption and refrigerating performances of CaCl2 impregnated composite adsorbent and those of the host silica gel.* international Journal of Refrigeration, 2007. **30**: p. 68-75.
94. Deshmukh, V.N. and S.V. Joshi, *Review: Use of composite adsorption in adsorption refrigeration.* INTERNATIONAL JOURNAL OF INNOVATIVE TECHNOLOGY & CREATIVE ENGINEERING, 2012. **2**: p. 11-16.
95. GHORISHI, S.B., et al., *Development of a Cl-Impregnated activated carbon for entrained-flow capture of elemental mercury.* Environ. Sci. Technol., 2002. **36**: p. 4454-4459.
96. Cortes, F.B., et al., *Water sorption on silica- and zeolite-supported hygroscopic salts for cooling system applications.* Energy Conversion and Management, 2012. **53**(1): p. 219-223.
97. Saha, B.B., et al., *Adsorption characteristics and heat of adsorption measurements of R-134a on activated carbon.* International Journal of Refrigeration. **In Press, Accepted Manuscript**.
98. Chua, H.T., et al., *Modeling the performance of two bed, silica gel-water adsorption chiller.* International Journal of Refrigeration, 1999. **22**: p. 194-204.
99. Dieng, A.O. and R.Z. Wang, *Literature review on solar adsorption technologies for ice-making and air-conditioning purposes and recent developments in solar technology.* Renewable & Sustainable energy reviews, 2001. **5**: p. 313-342.
100. Banker, N.D., K. Srinivasan, and M. Prasad, *Performance analysis of activated carbon + HFC-134a adsorption coolers.* Carbon, 2004. **42**: p. 117-127.
101. Cui, Q., et al., *Enviromentally benign working pairs for adsorption refrigeation.* Energy, 2005. **30**: p. 261-271.
102. Liu, Y. and K.C. Leong, *Numerical study of a novel cascading adsorption cycle.* International Journal of Refrigeration, 2006. **29**: p. 250-259.
103. San, J.-Y. and W.-M. Lin, *Comparison among three adsorption pairs for using as the working substances in multi-bed adsorption heat pump.* Applied Thermal Engineering, 2008. **28**: p. 988-977.
104. Schicktanz, M., P. HÃ¼genell, and S.K. Henninger, *Evaluation of methanol/activated carbons for thermally driven chillers, part II: The energy balance model.* International Journal of Refrigeration, 2012. **35**(3): p. 554-561.
105. Eun, T.-H., et al., *Enhancement of heat and mass transfer in silica-expanded graphite composite blocks for adsorption heat pumps. Part II. Cooling system using the composite blocksAmélioration du transfert de chaleur et de masse de blocs en matériaux composite graphite - silice expansé / dans les pompes à chaleur à adsorption : Partie II. Système de refroidissement utilisant des blocs en composite.* International Journal of Refrigeration, 2000. **23**(1): p. 74-81.

106. Demir, H., M. Mobedi, and S. Ülkü, *Effects of porosity on heat and mass transfer in a granular adsorbent bed.* International Communications in Heat and Mass Transfer, 2009. **36**(4): p. 372-377.
107. Glaznev, I.S. and Y.I. Aristov, *The effect of cycle boundary conditions and adsorbent grain size on the water sorption dynamics in adsorption chillers.* International Journal of Heat and Mass Transfer, 2010. **53**(9â€"10): p. 1893-1898.
108. Freni, A., et al., *Zeolite synthesised on copper foam for adsorption chillers: A mathematical model.* Microporous and Mesoporous Materials, 2009. **120**(3): p. 402-409.
109. Cacciola, G. and G. Restuccia, *Progress on adsorption heat pumps.* Heat Recovery Systems and CHP, 1994. **14**(4): p. 409-420.
110. Saha, B.B., A. Akisawa, and T. Kashiwagi, *Silica gel water advanced adsorption refrigeration cycle.* Energy, 1997. **22**(4): p. 437-447.
111. TatlIer, M. and A. Erdem-Senatalar, *The effects of thermal and mass diffusivities on the performance of adsorption heat pumps employing zeolite synthesized on metal supports.* Microporous and Mesoporous Materials, 1999. **28**(1): p. 195-203.
112. Restuccia, G., A. Freni, and G. Maggio, *A zeolite-coated bed for air conditioning adsorption systems: parametric study of heat and mass transfer by dynamic simulation.* Applied Thermal Engineering, 2002. **22**(6): p. 619-630.
113. Eun, T.-H., et al., *Enhancement of heat and mass transfer in silica-expanded graphite composite blocks for adsorption heat pumps. Part II. Cooling system using the composite blocks.* International Journal of Refrigeration, 2000. **23**(1): p. 74-81.
114. Kubota, M., et al., *Cooling output performance of a prototype adsorption heat pump with fin-type silica gel tube module.* Applied Thermal Engineering, 2008. **28**(2-3): p. 87-93.
115. Wang, L., D. Zhu, and Y. Tan, *Heat Transfer Enhancement on the Adsorber of Adsorption Heat Pump* Springer Netherlands, 1999. **5**: p. 279-286.
116. Restuccia, G. and G. Cacciola, *Performances of adsorption systems for ambient heating and air conditioning.* International Journal of Refrigeration, 1999. **22**(1): p. 18-26.
117. Waszkiewicz, S.D., M.J. Tierney, and H.S. Scott, *Development of coated, annular fins for adsorption chillers.* Applied Thermal Engineering, 2009. **29**(11-12): p. 2222-2227.
118. Ge, T.S., et al., *Experimental comparison and analysis on silica gel and polymer coated fin-tube heat exchangers.* Energy, 2010. **35**(7): p. 2893-2900.
119. Chang, K.-S., M.-T. Chen, and T.-W. Chung, *Effects of the thickness and particle size of silica gel on the heat and mass transfer performance of a silica gel-coated bed for air-conditioning adsorption systems.* Applied Thermal Engineering, 2005. **25**(14-15): p. 2330-2340.
120. Eun, T.-H., et al., *Enhancement of heat and mass transfer in silica-expanded graphite composite blocks for adsorption heat pumps: Part I. Characterization of the composite blocks.* International Journal of Refrigeration, 2000. **23**(1): p. 64-73.
121. Wang, L.W., et al., *Study of the performance of activated carbon-methanol adsorption systems concerning heat and mass transfer.* Applied Thermal Engineering, 2003. **23**(13): p. 1605-1617.
122. Wang, S.G., R.Z. Wang, and X.R. Li, *Research and development of consolidated adsorbent for adsorption systems.* Renewable Energy, 2005. **30**(9): p. 1425-1441.
123. Wang, S.G., et al., *Experimental Results and Analysis for Adsorption Ice-Making System with Consolidated Adsorbent.* Kluwer Academic Publishers, 2003. **9**: p. 349-358.

124. Hu, P., J.-J. Yao, and Z.-S. Chen, *Analysis for composite zeolite/foam aluminum-water mass recovery adsorption refrigeration system driven by engine exhaust heat.* Energy Conversion and Management, 2009. **50**(2): p. 255-261.
125. Bonaccorsi, L., et al., *Zeolite coated copper foams for heat pumping applications.* Microporous and Mesoporous Materials, 2006. **91**(1-3): p. 7-14.
126. Freni, A., et al. *Finite Element-Based Simulation of The Heat and Mass Transfer Process Through an Adsorbent Bed in an Adsorption Heat Pump/Chiller*. in *ASME-ATI-UIT, Conference on Thermal and Environmental Issues in Energy Systems*. 2010. Sorrento, Italy.
127. Voyiatzis, E., J.A. Palyvos, and N.-C. Markatos, *Heat-exchanger design and switching-frequency effects on the performance of a continuous type solar adsorption chiller.* Applied Energy, 2008. **85**(12): p. 1237-1250.
128. Boelman, E.C., B.B. Saha, and T. Kashiwagi, *Parametric study of a silica gel-water adsorption refrigeration cycle - the influence of thermal capacitance and heat exchanger UA-Values on cooling capacity, power density and COP.* ASHRAE Transaction, 1997. **103, Part 1**: p. 139-148.
129. Wang, X. and H.T. Chua, *Two bed silica gel-water adsorption chillers: An effectual lumped parameter model.* International Journal of Refrigeration, 2007. **30**(8): p. 1417-1426.
130. Saha, B.B., E.C. Boelman, and T. Kashiwagi, *computer simulation of a silica gel-water adsorption refrigeration cycle - the influence of operating conditions on cooling output and COP.* ASHRAE Transaction, 1995. **101**(part 2): p. 348-357.
131. Saha, B.B., E.C. Boelman, and T. Kashiwagi, *Computational analysis of an advanced adsorption-refrigeration cycle.* Energy, 1995. **20**(10): p. 983-994.
132. Akahira, A., et al., *Mass recovery adsorption refrigeration cycle--improving cooling capacity.* International Journal of Refrigeration, 2004. **27**(3): p. 225-234.
133. Khan, M.Z.I., et al., *Study on a re-heat two-stage adsorption chiller - The influence of thermal capacitance ratio, overall thermal conductance ratio and adsorbent mass on system performance.* Applied Thermal Engineering, 2007. **27**(10): p. 1677-1685.
134. Miyazaki, T. and A. Akisawa, *The influence of heat exchanger parameters on the optimum cycle time of adsorption chillers.* Applied Thermal Engineering, 2009. **29**(13): p. 2708-2717.
135. Miyazaki, T., et al., *A new cycle time allocation for enhancing the performance of two-bed adsorption chillers.* International Journal of Refrigeration, 2009. **32**(5): p. 846-853.
136. Uyun, A.S., et al., *Numerical analysis of an advanced three-bed mass recovery adsorption refrigeration cycle.* Applied Thermal Engineering, 2009. **29**(14-15): p. 2876-2884.
137. Cacciola, G., G. Restuccia, and G.H.W. van Benthem, *Influence of the adsorber heat exchanger design on the performance of the heat pump system.* Applied Thermal Engineering, 1999. **19**(3): p. 255-269.
138. Saha, B.B., et al., *A new generation cooling device employing CaCl2-in-silica gel-water system.* international Journal of Heat and Mass Transfer, 2009. **52**: p. 516-524.
139. Vasta, S., et al. *Simulation of a small size solar assisted adsorption air conditioning system for residential application*. in *Heat Powered Cycles*. 2009. Berlin.
140. Zhao, Y.L., E. Hu, and A. Blazewicz, *A non-uniform pressure and transient boundary condition based dynamic modeling of the adsorption process of an adsorption refrigeration tube.* Applied Energy, 2011. **90**(1): p. 280-287.

141. Zhao, Y., E. Hu, and A. Blazewicz, *Dynamic modelling of an activated carbonâ€“methanol adsorption refrigeration tube with considerations of interfacial convection and transient pressure process.* Applied Energy, 2012. **95**(0): p. 276-284.
142. Schicktanz, M. and T. Núñez, *Modelling of an adsorption chiller for dynamic system simulation.* International Journal of Refrigeration, 2009. **32**(4): p. 588-595.
143. Grisel, R.J.H., S.F. Smeding, and R.d. Boer, *Waste heat driven silica gel/water adsorption cooling in trigeneration.* Applied Thermal Engineering, 2010. **30**(8-9): p. 1039-1046.
144. Wang, X., et al., *Investigation on the isotherm of silica gel+water systems TG and volumetric methods.* Journal of Thermal Analysis and Calorimetry, 2004. **76**: p. 659-669.
145. Wang, X.L., H.T. Chua, and L.Z. Gao, *A thermogravimetric analyzer for condensable gas adsorption under subatospheric conditions.* Journal of Thermal Analysis and Calorimetry, 2007. **90**: p. 935-940.
146. Tso, C.P., Y.C. Cheng, and A.C.K. Lai, *An improved model for predicting performance of finned tube heat exchanger under frosting condition, with frost thickness variation along fin.* Applied Thermal Engineering, 2006. **26**(1): p. 111-120.
147. Holman, J.P., *Heat Transfer*1990: Library of Congress Cataloging
148. Zhu, D. and S. Wang, *Experimental investigation of contact resistance in adsorber of solar adsorption refrigeration.* Solar Energy, 2002. **73**(3): p. 177-185.
149. Incropera, F.P. and D.P. DeWitt, *Fundamentals of Heat and Mass Transfer*. 5 ed2001: Johns Wiley & Sons. 969.
150. Le, C.V., P.K. Bansal, and J.D. Tedford, *Three-zone system simulation model of a multiple-chiller plant.* Applied Thermal Engineering, 2004. **24**(14-15): p. 1995-2015.
151. Cengel, Y.A., *Heat Transfer*. Second Edition ed. Second Edition. Vol. 1. 2003: McGraw-Hill Higher Education. 932.
152. Premalatha, K. and A.M. Natarajan, *Hybride PSO and GA for Global Maximization.* International Journal of problems computation and mathimatics, 2009. **2**: p. 597-608.
153. *Genetic Algorithm and Direct Search toolbox for use with matlab*: The Mathworks.
154. Chang, W.S., C.C. Wang, and C.C. Shieh, *Experimental study of a solid adsorption cooling system using flat-tube heat exchangers as adsorption bed.* Applied Thermal Engineering, 2007. **27**(13): p. 2195-2199.
155. Wang, D.C., et al., *Study of a novel silica gelâ€“water adsorption chiller. Part II. Experimental study.* International Journal of Refrigeration, 2005. **28**(7): p. 1084-1091.
156. Saha, B.B., et al., *Study on an activated carbon fiberâ€“ethanol adsorption chiller: Part II â€“ performance evaluation.* International Journal of Refrigeration, 2007. **30**(1): p. 96-102.
157. Boer, R.d., S. Smeding, and S. Mola. *Silica gel-water adsorption cooling prototype system for mobile air conditioning*. in *Heat powered cycles*. 2009. Technische Universtat Berlin.
158. Xia, Z.Z., et al., *Development and comparison of two-bed silica gel-water adsorption chillers driven by low-grade heat source.* International Journal of Thermal Sciences, 2009. **48**(5): p. 1017-1025.
159. Critoph, R.E. and S.J. Metcalf, *Specific cooling power intensification limits in ammonia-carbon adsorption refrigeration systems.* Applied Thermal Engineering, 2004. **24**: p. 661-678.
160. Chen, C.J., et al., *Study on a silica gel-water adsorption chiller integrated with a closed wet cooling tower.* International Journal of Thermal Sciences. **49**(3): p. 611-620.

161. GrÃ¤ber, M., et al., *Determining the optimum cyclic operation of adsorption chillers by a direct method for periodic optimal control.* International Journal of Refrigeration, 2011. **34**(4): p. 902-913.
162. Aristov, Y.I., et al., *Reallocation of adsorption and desorption times for optimisation of cooling cycles.* International Journal of Refrigeration, 2010. **35**(3): p. 525-531.
163. Alam, K.C.A., et al., *A novel approach to determine optimum switching frequency of a conventional adsorption chiller.* Energy, 2003. **28**(10): p. 1021-1037.
164. Chamra, L.M. and P.J. Mago, *Modeling of condensation heat transfer of refrigerant mixture in micro-fin tubes.* international Journal of Heat and Mass Transfer, 2006. **49**(11-12): p. 1915-1921.
165. Khan, M.Z.I., et al., *Parametric study of a two-stage adsorption chiller using re-heatâ€"The effect of overall thermal conductance and adsorbent mass on system performance.* International Journal of Thermal Sciences, 2006. **45**(5): p. 511-519.
166. van Benthem, G.H.W., G. Cacciola, and G. Restuccia, *Regenerative adsorption heat pumps: Optimization of the design.* Heat Recovery Systems and CHP, 1995. **15**(6): p. 531-544.
167. Demir, H., M. Mobedi, and S. Ulku, *A review on adsorption heat pump:*

Problems and Solutions. Renewable & Sustainable energy reviews, 2008. **12**: p. 2381-2403.
168. Jakob, U. and W. Mittelbach, *Development and investigation of a compact silica gel/water adsorption chiller integrated in solar cooling systems*, in *VII Minsk International seminar*2008.
169. Schnabel, L., et al., *Adsorption kinetics of zeolite coatings directly crystallized on metal supports for heat pump applications (adsorption kinetics of zeolite coatings).* Applied Thermal Engineering, 2010. **30**(11-12): p. 1409-1416.
170. Demir, H., M. Mobedi, and S. Ülkü, *The use of metal piece additives to enhance heat transfer rate through an unconsolidated adsorbent bed.* International Journal of Refrigeration, 2010. **33**(4): p. 714-720.
171. Hamilton, R.l. and O.K. Crosser, *Thermal conductivity of hetrogeneous two-component systems.* Industrial and Engineering Chemistry Fundamentals, 1962. **1**: p. 187-191.
172. Rezk, A.R.M. and R.K. Al-Dadah, *Physical and operating conditions effects on silica gel/water adsorption chiller performance.* Applied Energy, 2012. **89**(1): p. 142-149.
173. Deng, S., *Sorbent tecjnology.* Encyclopedia of Chemical Processing, 2006. **DOI: 10.1081/E-ECHP-120007963**: p. 2825-2845.
174. Grant Glover, T., et al., *MOF-74 building unit has a direct impact on toxic gas adsorption.* Chemical Engineering Science, 2010. **In Press, Accepted Manuscript**.
175. Min Wang, Q., et al., *Metallo-organic molecular sieve for gas separation and purification.* Microporous and Mesoporous Materials, 2002. **55**(2): p. 217-230.
176. Kondo, A., et al., *Adsorption of water on three-dimensional pillared-layer metal organic frameworks.* Journal of Colloid and Interface Science, 2007. **314**(2): p. 422-426.
177. Guillou, N., F. Millange, and R.I. Walton, *Rapid and reversible formation of a crystalline hydrate of a metal-organic framework containing a tube of hydrogen-bonded water.* Chemical Communications, 2010. **47**(2): p. 713-715.
178. Chao, Z., *Preparation, characterization, ion exchange, and hydrogen absorption studies of some zinc*, in *School of Chemistry*2008, University of Birmingham: Birmingham. p. 79.

179. Li, S.L., et al., *Study on the adsorption isosteres of the composite adsorbent CaCl2 and expanded graphite.* Energy Conversion and Management, 2011. **52**(2): p. 1501-1506.
180. El-Sharkawy, I.I., et al., *A study on the kinetics of ethanol-activated carbon fiber: Theory and experiments.* International Journal of Heat and Mass Transfer, 2006. **49**(17-18): p. 3104-3110.
181. Aristov, Y.I., et al., *Kinetics of water adsorption on silica Fuji Davison RD.* Microporous and Mesoporous Materials, 2006. **96**(1-3): p. 65-71.
182. Aristov, Y.I., et al., *Kinetics of water sorption on SWS-1L (calcium chloride confined to mesoporous silica gel): Influence of grain size and temperature.* Chemical Engineering Science, 2006. **61**(5): p. 1453-1458.
183. Raymond, A. and S. Garimella, *Intraparticle Mass Transfer in Adsorption Heat Pumps: Limitations of the Linear Driving Force Approximation.* Journal of Heat Transfer, 2011. **133**(4): p. 042001-13.
184. Saha, B.B., et al., *Study on an activated carbon fiber-ethanol adsorption chiller: Part I - system description and modelling.* International Journal of Refrigeration, 2007. **30**(1): p. 86-95.
185. Ruthven, D.M., *Principles of adsorption and adsorption process*. First ed1984, New York: John Wiely & Sons.
186. Jeremias, F., et al., *MIL-100(Al, Fe) as water adsorbent for heat transforamationpurposes – a promising application.* J Materials Chemistry, 2012. **22**.
187. Akiyama, G., R. Matsuda, and S. Kitagawa, *Highly porous and stable coordination polymers as water sorption materials.* Chemistry letters, 2010. **39**: p. 360-361.
188. Horcajada, P., et al., *Synthesis and catalytic properties of MIL-100(Fe), an iron (III) carboxylate with large pores.* Chemical Communications (Cambridge), 2007: p. 2820-2822.
189. I.I.Elsharkawy, et al., *Experimental investigation on activated carbon-ethanol pair for solar powered adsorption cooling applications.* International Journal of Refrigeration, 2008. **31**: p. 1407-1413.
190. Lin, C.-I. and L.-H. Wang, *Rate equations and isotherms for two adsorption models.* Journal of the Chinese Institute of Chemical Engineers, 2008. **39**(6): p. 579-585.
191. Llano-Restrepo, M. and M.n.A. Mosquera, *Accurate correlation, thermochemistry, and structural interpretation of equilibrium adsorption isotherms of water vapor in zeolite 3A by means of a generalized statistical thermodynamic adsorption model.* Fluid Phase Equilibria, 2009. **283**(1â€"2): p. 73-88.
192. Stoeckli, F. and T. Jakubov, *Water adsorption in active carbons described by the Dubinin-Astakhov Equation.* J. CHEM. SOC. FARADAY TRANS, 1994. **90**((5)): p. 783-786.
193. Mahle, J.J., *An adsorption equilibrium model for Type 5 isotherms.* Carbon, 2002. **40**(15): p. 2753-2759.
194. Akpa, O.M. and E.I. Unuabonah, *Small-Sample Corrected Akaike Information Criterion: An appropriate statistical tool for ranking of adsorption isotherm models.* Desalination, 2011. **272**(1â€"3): p. 20-26.